



National Library
of Canada

Bibliothèque nationale
du Canada

Canadian Theses Service

Services des thèses canadiennes

Ottawa, Canada
K1A 0N4

CANADIAN THESES

THÈSES CANADIENNES

NOTICE

The quality of this microfiche is heavily dependent upon the quality of the original thesis submitted for microfilming. Every effort has been made to ensure the highest quality of reproduction possible.

If pages are missing, contact the university which granted the degree.

Some pages may have indistinct print especially if the original pages were typed with a poor typewriter ribbon or if the university sent us an inferior photocopy.

Previously copyrighted materials (journal articles, published tests, etc.) are not filmed.

Reproduction in full or in part of this film is governed by the Canadian Copyright Act, R.S.C. 1970, c. C-30.

**THIS DISSERTATION
HAS BEEN MICROFILMED
EXACTLY AS RECEIVED**

AVIS

La qualité de cette microfiche dépend grandement de la qualité de la thèse soumise au microfilmage. Nous avons tout fait pour assurer une qualité supérieure de reproduction.

S'il manque des pages, veuillez communiquer avec l'université qui a conféré le grade.

La qualité d'impression de certaines pages peut laisser à désirer, surtout si les pages originales ont été dactylographiées à l'aide d'un ruban usé ou si l'université nous a fait parvenir une photocopie de qualité inférieure.

Les documents qui font déjà l'objet d'un droit d'auteur (articles de revue, examens publiés, etc.) ne sont pas microfilmés.

La reproduction, même partielle, de ce microfilm est soumise à la Loi canadienne sur le droit d'auteur, SRC 1970, c. C-30.

**LA THÈSE A ÉTÉ
MICROFILMÉE TELLE QUE
NOUS L'AVONS REÇUE**

Photoelectrochemical and Photocatalytic behaviour of Thin
Porphyrin Films on Semiconductor Materials.

Andrew Martin Crouch

A Thesis
in
The Department
of
Chemistry

Presented in Partial Fulfillment of the Requirements
for the Degree of Doctor of Philosophy at
Concordia University
Montréal, Québec, Canada

August 1987

© Andrew Martin Crouch, 1987

Permission has been granted to the National Library of Canada to microfilm this thesis and to lend or sell copies of the film.

The author (copyright owner) has reserved other publication rights, and neither the thesis nor extensive extracts from it may be printed or otherwise reproduced without his/her written permission.

L'autorisation a été accordée à la Bibliothèque nationale du Canada de microfilmer cette thèse et de prêter ou de vendre des exemplaires du film.

L'auteur (titulaire du droit d'auteur) se réserve les autres droits de publication; ni la thèse ni de longs extraits de celle-ci ne doivent être imprimés ou autrement reproduits sans son autorisation écrite.

ISBN 0-315-37067-X

ABSTRACT

Photoelectrochemical and Photocatalytic behaviour of thin Porphyrin Films on Semiconductor materials.

Andrew Martin Crouch, Ph.D.
Concordia University, 1987.

The photoelectrochemical and photocatalytic processes of thin films of zinc tetraphenylporphyrin were studied on semiconductors in three stages.

- 1) as thin films modified by axial ligation.
- 2) as chromophores in ionically conductive polymer films.
- 3) as films on semiconductor particulates.

The effect of axial ligands such as pyridine, triphenylphosphine, triphenylarsine and poly(4 - vinylpyridine) on films of zinc tetraphenylporphyrin shows that flat band potentials are shifted by axial ligation and rates of the electron transfer for a redox couple like $\text{Fe}(\text{CN})_6^{3-/4-}$ are increased. The photophysical properties of zinc tetraphenylporphyrin are affected and the photoelectrochemical behaviour is dependent on the redox couple in solution and the film thickness. Photocurrent behaviour at transparent SnO_2 electrodes were explained by charge separation at the SnO_2 /film interface and the efficiency of energy transport to the interface.

Zinc tetraphenylporphyrin and its anionic analogue zinc tetraphenylporphyrin tetrasulphonate (ZnTPPS^{-4}) in a

pyridine containing ionic blend which have both hydrophilic and hydrophobic domains and which shows large ion retention and ion exchange capabilities shows that the photophysical properties of the chromophore are not adversely changed by the polymer host at suitable loadings. Chromophore concentration in films on SnO₂, ITO, TiO₂, CdS and CdSe could be increased without inducing serious resistance effects. Chromophores in the polymer matrix do not affect the charge carrying properties of the polymer significantly. Photoelectrochemical behaviour of the thin polymer films is explained by a mechanism of charge separation by the dye - pyridine complex of the polymer followed by charge trapping and eventual propagation by molecular ion states in the polymer. The mechanism requires the suitable "tuning" of semiconductor, polymer, chromophore and electrolyte energy levels.

Photocatalytic studies of thin polymer - chromophore films on TiO₂, CdS, CdSe semiconductor particulates show degradation of refractory waste material such as complexed cyanide in alkaline media. A direct relationship between the respective macro photoelectrode and the micro photocatalyst is observed.

ACKNOWLEDGEMENTS

I am indebted to a large number of individuals and groups who have helped in this endeavor, but despite the impossibility of giving credit to everyone, I would like to single out certain people or groups who have been especially instrumental in the completion of this work.

Dr. C.H. Langford for his guidance throughout my stay in Canada. His dedication to research and teaching will always be an inspiration to me.

The Peninsula Technikon for its dedication to staff development and for providing me with leave.

Mr. W.J. Evert for financial support at a critical stage of the work.

The Foundation for Research Development (CSIR) in South Africa for financial support which made the completion of this work possible.

My wife, Lynnette, for her love and support and for typing this script.

To my Family

TABLE OF CONTENTS

	PAGE
CHAPTER 1	
INTRODUCTION.	
1.0. Overview.	1
1.1. An overview of the porphyrins.	4
1.1.1. Ground state absorption properties.	6
1.1.2. Axial ligation to metalloporphyrins.	9
1.1.3. Redox process of metalloporphyrins.	12
1.1.4. Electron transfer processes of metalloporphyrins.	16
1.1.5. Photochemical and photophysical properties.	18
1.2. Chemically Modified Surfaces.	23
1.3. Polymer films on electrodes.	24
1.3.1. Methods of making films.	25
1.3.1.a). Formation from preformed polymers.	25
b). In situ formation from the monomer.	26
1.3.2. Redox polymers.	27
1.3.3. Ion exchange polymers.	28
1.3.4. Electronically conductive polymers.	29
1.3.5. Charge transport in electroactive polymer films.	30
1.3.6. Present and future applications of polymer modified electrodes.	34
1.4. Modified Semiconductors.	35
1.4.1. Sensitization of semiconductors.	40
1.4.2. Photocatalysis at particulate semiconducting surfaces.	42
CHAPTER 2.	
EXPERIMENTAL.	
2.1. Materials.	46
2.2. Preparation of complexes and polymers.	48
2.2.1. Preparation of zinc meso - tetra(4 - sulfonato phenyl) porphine.	48
2.2.2. Preparation of solutions of zinc tetraphenylporphyrin with axial ligands.	49
2.2.3. Preparation of poly(4-vinylpyridine) solutions.	49
2.2.4. Preparation of ZnTPP - PVP solution.	49
2.2.5. Preparation of Ionically conductive polymer.	50

	PAGE
2.2.6. Preparation of ZnTPPS - polymer blend solution.	51
2.3. Semiconducting photocatalysts.	51
2.3.1. Preparation of particulate photocatalyst.	51
2.3.2. Experimental conditions for photocatalysis.	52
2.3.3. Determination of cyanide in irradiated solutions.	53
2.4. Modified Electrodes; Preparation and Characterization.	53
2.4.1. Preparation of Gold electrodes.	53
2.4.2. Preparation of SnO ₂ electrodes.	54
2.4.3. Preparation of ITO electrodes.	55
2.4.4. Preparation of TiO ₂ electrodes.	56
2.4.5. Preparation of CdS and CdSe electrodes.	56
2.4.6. Film thickness measurements by profilometer and micrometer.	57
2.5. Electrochemical and Photoelectrochemical techniques.	
2.5.1. Electrochemical techniques.	61
2.5.2. Photoelectrochemical techniques.	64
2.6. Electronic Absorption Spectra.	66
2.7. Fluorescence measurements.	66
2.8. Flash Photolysis Studies.	66
2.8.1. Nanosecond Transient Absorption Spectroscopy.	66
2.8.2. Picosecond Flash Photolysis measurements.	67
2.8.3. Pulse Fluorescence measurements.	69
 CHAPTER 3.	
RESULTS AND DISCUSSION I.	
3.1. Electronic absorption spectra of porphyrins in solution.	70
3.2. Photoelectrochemical generation of intermediate porphyrin species in solution during bulk photolysis.	77
3.3. Electrochemistry and Spectroelectrochemistry of H ₂ TPP and ZnTPP solutions.	79
3.3.1. Electrochemistry of H ₂ TPP with pyridine.	79
3.3.2. Electrochemistry of ZnTPP with pyridine.	81
3.3.3. Electrochemistry of ZnTPP with Polyvinylpyridine.	85
3.3.4. Electrochemistry of ZnTPP with triphenylarsine and triphenylphosphine.	85

	PAGE
3.4. Absorption Spectroscopy and Electrochemistry on the porphyrin films.	89
3.4.1. Choice of redox couple and selection of experimental conditions for thin film electrochemistry.	89
3.4.2. Absorption spectra of porphyrin thin films on SnO ₂ electrodes.	91
3.4.3. Electrochemical effect of modifying the SnO ₂ surface with porphyrin and axially ligated porphyrin.	95
3.4.4. Heterogeneous electron transfer kinetics of Fe(CN) ₆ ^{3-/4-} at SnO ₂ and porphyrin modified electrodes.	98
3.4.5. Effect of porphyrin film thickness on dark electrochemistry.	106
3.4.6. Determination of flatband potentials of porphyrin films.	112
3.5. Photoelectrochemistry of ZnTPP and modified porphyrin thin films.	117
3.5.1. Photocurrent transient spectra.	117
3.5.2. Photocurrent action spectra of thin films.	119
3.5.3. Film thickness dependence of photocurrent.	122

CHAPTER 4.

RESULTS AND DISCUSSION II.

4.1. Electrochemical properties of the ionically conductive polymer blend.	125
4.1.1. Ion retention ability of polymer.	125
4.1.2. Apparent diffusion coefficients of ions in the polymer matrix.	127
4.1.3. Potential of pyridinium group in the polymer blend.	132
4.2. Solution Absorption Spectra and Electrochemistry of ZnTPPS-4.	132
4.2.1. Absorption spectra of H ₂ TPPS-4 and ZnTPPS-4.	132
4.2.2. Solution electrochemistry of ZnTPPS-4 in aqueous media.	133
4.3. Thin Film Absorption Spectra.	137
4.4. Dark electrochemistry of ZnTPPS-4-PVP-copolymer films on gold and different semiconducting surfaces.	137
4.4.1. Electrochemistry of SnO ₂ /ZnTPPS-4-PVP-copolymer electrodes.	137
4.4.2. Electrochemistry of ITO/ZnTPPS-4-PVP-copolymer electrodes.	145

	PAGE
4.4.3. Electrochemistry of Au/ZnTPPS-4-PVP-copolymer electrodes.	149
4.4.4. Electrochemistry of Ti/TiO ₂ /ZnTPPS-4-PVP-copolymer electrodes.	149
4.4.5. Electrochemistry and absorption spectra of ITO/CdS/ZnTPPS-4-PVP-copolymer electrodes.	152
4.4.6. Electrochemistry of ITO/CdSe/ZnTPPS-4-PVP-copolymer electrodes.	156
4.5. Photoelectrochemistry of ZnTPP - PVP - copolymer and ZnTPPS-4-PVP-copolymer films on gold and different semiconducting surfaces.	156
4.5.1. Transient photocurrent behaviour of thin porphyrin - polymer films.	156
4.5.2. Effect of white light intensity on photocurrent.	160
4.5.3. Photoaction spectra of thin polymer films.	160
4.5.4. Dependence of photocurrent on polymer film thickness and chromophore concentration.	162

CHAPTER 5.

RESULTS AND DISCUSSION III.

5.1. Fluorescence spectra of ZnTPP and ZnTPPS-4 in solution and in solid films.	167
5.1.1. Fluorescence maxima in solution and in films.	167
5.1.2. Fluorescence behaviour of ZnTPPS-4 on addition of PVP - copolymer.	170
5.2. Submicrosecond Transient Absorption Spectroscopy on ZnTPP, ZnTPP with axial ligands and ZnTPPS-4.	172
5.3. Picosecond Pulse Fluorescence on porphyrin solutions and films.	175
5.4. Picosecond Transient Absorption Spectroscopy of ZnTPP and ZnTPPS-4 solutions.	177

CHAPTER 6.

DISCUSSION IV AND CONCLUSION.

6.1. Redox properties and energetic considerations for ZnTPP films.	185
6.2. Effect of structure of pendant - group polymers: the electrochemical and photoelectrochemical consequences.	192

	PAGE
6.2.1. The role of the polymer.	192
6.2.2. Diffusion of counterions in the polymer.	193
6.2.3. Polymer band structure; A molecular - ion state approach.	194
6.3. Photochemical and electrochemical considerations, for dye - polymer films.	197
6.4. Catalytic effects of porphyrin films on different semiconductor surfaces.	203
6.5. Conclusions.	205
REFERENCES	207
ANNEX.	
Photochemical treatment of complexed cyanides by porphyrin-polymer coated semiconducting powders.	218

LIST OF FIGURES

	PAGE
CHAPTER 1	
1.1 Scheme for solar-energy conversion devices.	2
1.2 The "four orbital model".	7
1.3 Electron transfer processes of porphyrins.	17
1.4 Jablonski diagram for aromatic molecules with singlet ground-state.	19
1.5 Band model for semiconductors.	36
1.6 Energy position of valence and conduction bands for various semiconductors.	39
1.7 Redox processes at particulate semiconductor.	43
CHAPTER 2.	
2.1 Film thickness vs. porphyrin concentration plots for ZnTPP and ZnTPP - Pyridine films.	58
2.2 Film thickness vs. light absorbed for a dye-polymer film on SnO ₂ .	59
2.3 Film thickness vs. light absorbed for a ZnTPPS-4 - polymer film on ITO.	60
2.4 Schematic of the flow - through cell.	63
CHAPTER 3.	
3.1 Electronic Absorption Spectra of H ₂ TPP and ZnTPP in solution.	71
3.2 Absorption Spectra of ZnTPP and ZnTPP with axial ligands.	72

	PAGE
3.3 Absorption Spectrum of ZnTPP-PVP in CH ₂ Cl ₂ .	73
3.4 Absorption Spectra of ZnTPP with PPh ₃ as ligand.	75
3.5 Photochemically produced spectra of ZnTPP in solution.	78
3.6 Voltammograms of (A) background CH ₃ CN electrolyte and (B) H ₂ TPP in CH ₃ CN:CH ₂ Cl ₂ titrated with pyridine.	80
3.7 Voltammogram of ZnTPP in CH ₃ CN:CH ₂ Cl ₂ titrated with pyridine.	82
3.8 Visible spectra of ZnTPP titrated with pyridine.	83
3.9 Voltammogram of ZnTPP titrated with PVP..	86
3.10 Voltammogram of ZnTPP titrated with PPh ₃ .	87
3.11 Voltammogram of ZnTPP with triphenylarsine.	88
3.12 Variation of half wave potential with pH for Fe(CN) ₆ ^{3-/4-} on different surfaces.	90
3.13 Absorption Spectra of ZnTPP films on SnO ₂ .	92
3.14 Absorption Spectra of ZnTPP pyridine films on SnO ₂ .	93
3.15 Absorption Spectra of ZnTPP - PPh ₃ films on SnO ₂ .	94
3.16 Voltammogram of Fe(CN) ₆ ^{3-/4-} on (a) SnO ₂ (b) SnO ₂ /ZnTPP and (c) SnO ₂ /ZnTPP - Pyridine electrodes.	96
3.17 Voltammogram of Fe(CN) ₆ ^{3-/4-} on (a) SnO ₂ (b) SnO ₂ /ZnTPP-PPh ₃ and (c) SnO ₂ /ZnTPP - PVP electrodes.	97
3.18 Scan rate dependence of Fe(CN) ₆ ^{3-/4-} on	

	PAGE
SnO ₂ surface.	100
3.19 Variation of the rate constant with change in peak potential for the Fe(CN) ₆ ^{3-/4-} couple on SnO ₂ .	101
3.20 Variation of the rate constant with change in peak potential for the Fe(CN) ₆ ^{3-/4-} couple on SnO ₂ /ZnTPP - pyridine.	102
3.21 Peak current vs. scan rate dependence of Fe(CN) ₆ ^{3-/4-} on the different surfaces.	105
3.22 Variation of dark potentials with film thickness for different films.	111
3.23 Flat band determination from photovoltage for the film ZnTPP - pyridine on SnO ₂ .	113
3.24 Flat band determination of the film ZnTPP - PVP on SnO ₂ .	114
3.25 Photocurrent transients for some porphyrin films.	118
3.26 Photoaction spectrum vs. absorption spectrum for ZnTPP film on SnO ₂ .	120
3.27 Photocurrent vs. light absorbed for different films.	123
 CHAPTER 4.	
4.1 Voltammogram showing continuous scanning and leaching of Fe(CN) ₆ ^{3-/4-} from polymer film	126
4.2 Peak current vs. scan rate for ITO/PVP - copolymer	

	PAGE
electrode.	129
4.3 Schematic representation of polymer structure.	130
4.4 Absorption spectra of H ₂ TPPS-4 and ZnTPPS-4 in aqueous medium.	131
4.5 Voltammogram of ZnTPPS-4 in aqueous medium and titration with PVP - copolymer.	134
4.6 Absorption spectra of ZnTPP-PVP-copolymer on SnO ₂ electrode.	135
4.7 Absorption spectra of ZnTPPS-4-PVP-copolymer film on SnO ₂ surface.	136
4.8 Voltammograms of Fe(CN) ₆ ^{3-/4-} on SnO ₂ and SnO ₂ /Polymer surface.	138
4.9 Scan rate dependence of redox couple on SnO ₂ /ZnTPP- PVP-copolymer surface.	140
4.10 Anodic and cathodic dark currents vs. scan rate for the electrode SnO ₂ /ZnTPPS-4-PVP-copolymer.	141
4.11 Cottrell plot for the redox couple Fe(CN) ₆ ^{3-/4-} on the surface SnO ₂ /ZnTPPS-4-PVP-copolymer.	142
4.12 Voltammograms of redox couple on different ITO modified surfaces.	146
4.13 Electrochemistry of Au - electrodes.	150
4.14 Electrochemistry of Ti/TiO ₂ electrodes.	151
4.15 Absorption spectrum of CdS and CdS/ZnTPPS-4-PVP- copolymer electrode.	153
4.16 Voltammograms of Fe(CN) ₆ ^{3-/4-} on CdS and CdSe/ZnTPPS-4-PVP-copolymer electrodes.	155
4.17 Photocurrent transients of different electrodes.	157

	PAGE
4.18 Photocurrent dependence on white light intensity.	159
4.19 Absorption spectrum vs. photocurrent action spectrum for thin films of ZnTPPS-4-PVP-copolymer.	161
4.20 Photocurrent vs. film thickness for the ZnTPP-PVP-copolymer film on SnO ₂ .	163
4.21 Photocurrent vs. film thickness for the ZnTPPS-4-PVP-copolymer film on SnO ₂ and ITO.	164
 CHAPTER 5.	
5.1 Fluorescence maxima for ZnTPP in CH ₂ Cl ₂ and ZnTPP film on SnO ₂ .	168
5.2 Fluorescence spectra of "titration" of ZnTPPS-4 in CH ₃ OH with PVP - copolymer.	171
5.3 Transient absorption spectra for ZnTPPS-4 in CH ₃ OH after excitation with a 10 ns pulse at 590 nm.	173
5.4 Transient fluorescence spectrum of ZnTPP in Pyridine after excitation with a 30 ps pulse at 355 nm.	176
5.5 Transient absorption spectra for ZnTPP in CH ₂ Cl ₂ at different time delays.	178
5.6 Transient absorption spectra for ZnTPP in Pyridine at different time delays.	179
5.7 Transient absorption spectra for ZnTPPS-4 in CH ₃ OH at different time delays.	182
5.8 Transient absorption spectra for ZnTPPS-4-PVP-	

	PAGE
copolymer in CH_3OH at different time delays after excitation:	183
 CHAPTER 6.	
6.1 Latimer diagrams for ZnTPP and ZnTPPS-4.	186
6.2 Flat - band potentials of ZnTPP and axially ligated ZnTPP with respect to the SnO_2 conduction band.	187
6.3 Energy distributions of the donor and acceptor states in pendant polymer groups.	195
6.4 Energetic considerations of chromophores with respect to the semiconductor and polymer levels.	198
6.5 Schematic presentation of reaction mechanism in photoelectrochemical cell.	202
 ANNEX.	
7.1 Decay of ferricyanide in 0.01 M NaOH in the presence of different TiO_2 based photocatalysts.	220
7.2 Cyclic voltammograms of 2mM $\text{K}_3\text{Fe}(\text{CN})_6$ in 0.01 M NaOH before and after irradiation at a CdS/ZnTPPS-4-PVP-copolymer electrode.	224
7.3 Absorption spectra showing the decay of the visible bands of ferricyanide on irradiation.	225

TABLES.

PAGE

CHAPTER 1.

- | | | |
|------|--|----|
| 1.1. | Redox potentials for water soluble porphyrins. | 14 |
| 1.2. | Redox potentials for organic soluble porphyrins. | 15 |
| 1.3. | Photophysical properties of some metallo-porphyrins. | 21 |

CHAPTER 2.

- | | | |
|------|---------------------------------------|----|
| 2.1. | Supplier and Grade of compounds used. | 46 |
|------|---------------------------------------|----|

CHAPTER 3.

- | | | |
|------|--|-----|
| 3.1. | Rate constants of the $\text{Fe}(\text{CN})_6^{3-/4-}$ couple on different electrode surfaces. | 104 |
| 3.2. | Electrochemical properties of $\text{SnO}_2/\text{ZnTPP}$ electrodes. | 107 |
| 3.3. | Electrochemical properties of $\text{SnO}_2/\text{ZnTPP}$ -pyridine electrodes. | 108 |
| 3.4. | Electrochemical properties of $\text{SnO}_2/\text{ZnTPP}$ -triphenylarsine electrodes. | 109 |
| 3.5. | Electrochemical properties of $\text{SnO}_2/\text{ZnTPP}$ -PVP electrodes. | 110 |
| 3.6. | Flat band potentials for thin films on SnO_2 . | 115 |

CHAPTER 4.

- | | | |
|------|---|--|
| 4.1. | Dark electrochemistry of $\text{SnO}_2/\text{ZnTPPS-4-PVP}$ | |
|------|---|--|

copolymer electrode.	144
4.2. Dark electrochemistry of ITO/ZnTPPS-4-PVP-	PAGE
copolymer electrodes.	147
4.3. Photoelectrochemistry of CdS/ZnTPP-PVP-copolymer	
electrodes.	154

CHAPTER 5.

5.1. Fluorescence maxima for porphyrin solutions and	
thin films.	169
5.2. Photophysical data for ZnTPP, ZnTPPS-4 and	
thin films.	174

ANNEX.

7.1. Extent of degradation of ferricyanide in alkaline	
medium after 60 minutes.	222
7.2. Degradation of ferricyanide with TiO ₂ catalyst.	227
7.3. Degradation of ferricyanide with TiO ₂ /ZnTPPS-4-	
PVP-copolymer as catalyst.	227
7.4. Degradation of ferricyanide with CdS as	
catalyst.	228
7.5. Degradation of ferricyanide with CdS/ZnTPPS-4-	
PVP-copolymer as catalyst.	228
7.6. Degradation of ferricyanide with CdSe as	
catalyst.	229
7.7. Degradation of ferricyanide with CdSe/ZnTPPS-4-	
PVP-copolymer as catalyst.	229

CHAPTER 1**INTRODUCTION****1.0 OVERVIEW**

The development of systems capable of collecting and storing solar energy have enjoyed considerable interest by academia and industry (1, 2). In principle, it is an extremely important area of research since the total amount of solar energy that falls on the surface of the earth far outweighs our present and future energy demands. Devices that work at even a moderate efficiency will be considered of significance.

Many different approaches have been advocated, but the only system capable of the chemical collection and storage of solar energy on a practical scale is the natural photosynthetic process. This natural process is an extremely complex one, but mankind can learn a great deal from studying this system and in recent years numerous laboratory models have been constructed.

Two distinct types of solar energy conversion devices or systems have emerged over the years, i.e.;

- (a) Solar thermal conversion devices.
- (b) Solar photoconversion devices.

The first category principally uses the infrared region of the solar spectrum and the second category is based on the

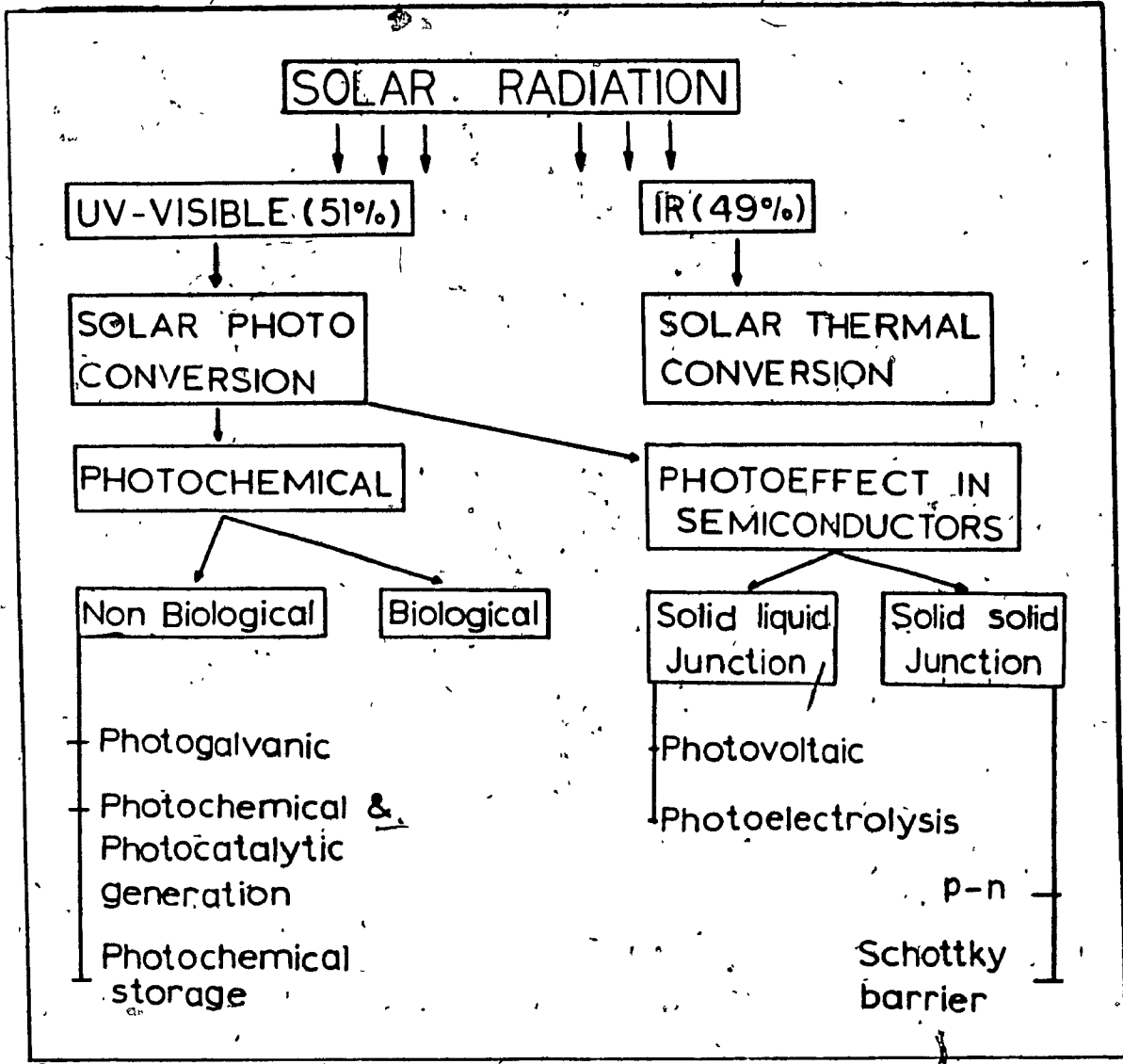


Figure 1.1. Schematic representation of major solar energy conversion devices:

visible - ultraviolet region. Figure 1.1 summarizes some of these devices.

The theme presented here will address mainly solar photoconversion, and in particular non - biological photoconversion i.e. photovoltaic, photogalvanic and / or photocatalytic processes. Some principles of these systems will be discussed below.

The term photovoltaic cell denotes a class of photoelectrochemical cells that can convert solar energy directly into electricity. In some cases it is possible to store solar energy as chemical energy. The overall power generation process can be divided into a number of steps i.e.

- (a) Absorption of photons in a chemical species (in the case presently in focus usually a dye molecule).
- (b) Formation of the charge carrying species.
- (c) Transfer of charge carriers to the electrode.

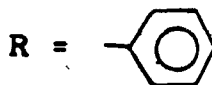
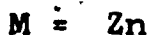
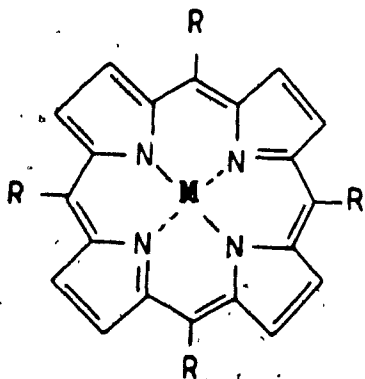
Photocatalysis denotes reactions activated by a system which on absorption of solar irradiation triggers a chemical reaction in an otherwise inert system. Although the photocatalyst participates in the reaction, it does not undergo a net chemical change. It acts merely as a shuttle for electron transfer reactions, resulting in an overall oxidation or reduction process. In both the photovoltaic and the photocatalytic process, the charge transferred to or from the electrode may be measurable in

the form of a current and voltage. The magnitude of the current or voltage is dependent on the photochemical and electrochemical properties of the substance involved.

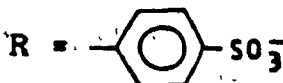
It is thus evident that not all materials will have desirable properties to be used in photoelectrochemical or photocatalytic processes, and frequently a combination of a number of materials is needed to give the properties sought. In this respect there is a growing interest to couple the photophysical, photochemical and redox properties of inorganic and organic dye molecules with large bandgap semiconductors. This thesis will deal with an aspect of that interest exploiting especially the properties of metalloporphyrins, pyridine based polymers and semiconductor materials such as SnO_2 , TiO_2 and CdS .

1.1 AN OVERVIEW OF THE PORPHYRINS.

The basic porphine skeleton (see below) lays the foundation for the construction of a variety of porphyrins, phlorins, chlorins and phthalocyanines.



ZnTPP



ZnTPPS⁻⁴

The synthesis of the symmetric porphyrins such as tetraphenylporphyrin (TPP) is well known (3) and a wide range of metal complexes have been reported (4,5,6,7).

The study of porphyrin chemistry is said to have begun as early as 1880 (7) and by 1964, up to 28 synthetic metalloporphyrins were listed (7). The porphyrins, in common with other macrocyclic ligands, have a central hole of essentially fixed size. In certain complexes, the metal is unable to fit into this hole (8) and lies out of the plane of the square planar ligand. For Zn porphyrin, X-ray crystallographic studies confirmed that the zinc atom is in the centre of the porphinato plane. (10). Most complexes of porphyrins are acid labile and undergo demetallation (3).

- The porphyrins and certain other unsaturated ligands (eg. bipyridyl) are distinguished by their delocalized pi systems. This pi system can overlap with metal d-orbitals to produce a moderately high ligand field (11). By acting as pi-acids back accepting pi density from complexed metals, the ligands can stabilize complexed metals in a lower oxidation state (12).

Porphyrins and metalloporphyrins are capable of collecting a considerable fraction of the solar spectrum. TPP can absorb about 46% of the energy available in the

solar spectrum (16) and although this value decreases for metalloporphyrins due to a hypsochromic shift caused by metal ion interaction with the porphyrin pi system, PdTPP can still absorb some 25% of the solar spectrum. Because of this high absorption in the visible region, the porphyrins appear to be attractive candidates as sensitizers. They also show good stability upon prolonged irradiation in aqueous solutions. Most porphyrins give relatively high triplet yields and form separated ion products when irradiated in the presence of electron donors or acceptors (16).

Apart from the above, porphyrins have the appropriate redox properties in both the ground and the excited state to be used as a sensitizer. The redox properties of the excited state will depend on the nature of the metal and the ligands. Significant changes in the potentials can occur from small changes in the composition of the ligands.

1.1.1 GROUND-STATE ABSORPTION PROPERTIES

The absorption spectra of many metal free and metalloporphyrins have been described in detail by a number of authors (13,14). As can be seen in figure 1.2, the fairly weak bands in the visible region are normally termed Q bands and the most intense band in the

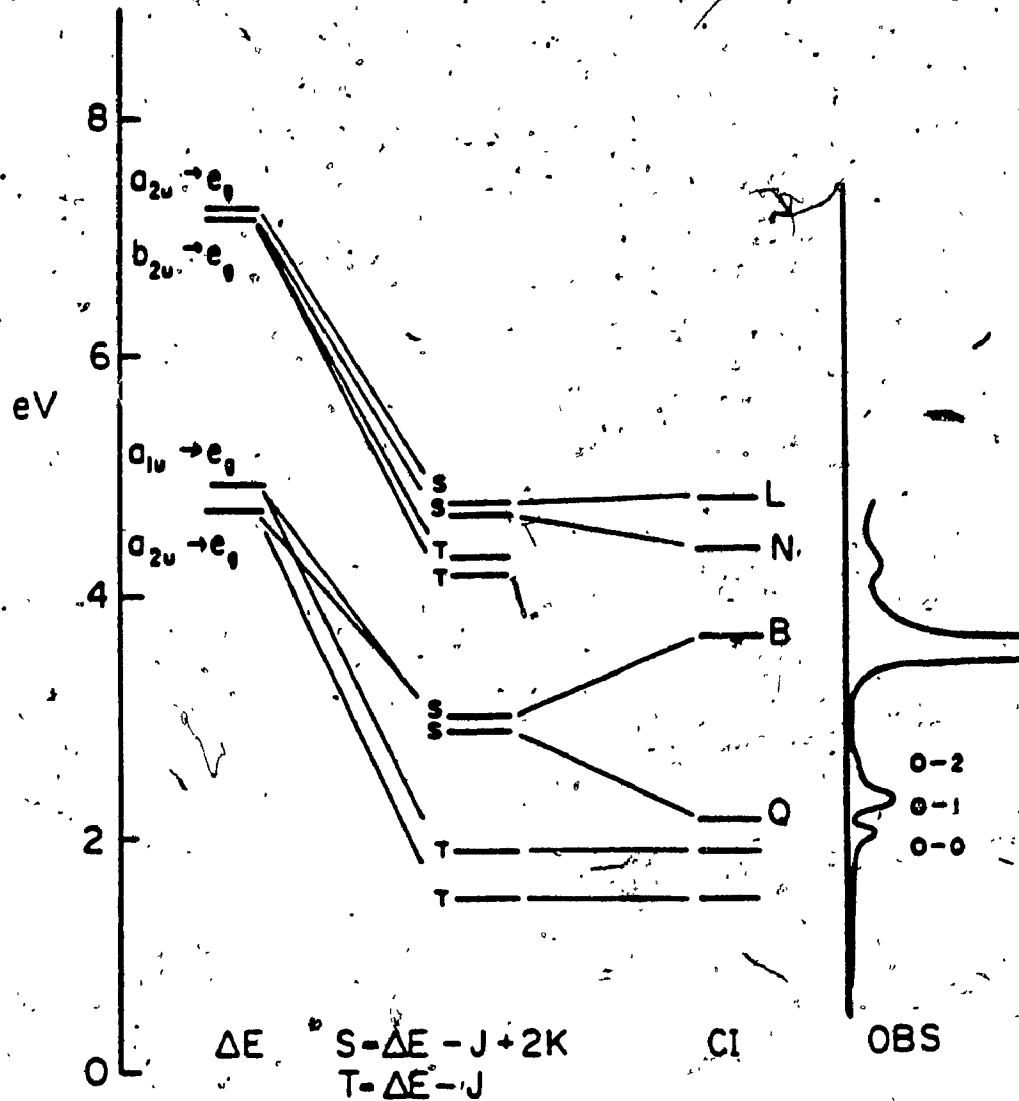


Figure 1.2. The "four orbital model" showing the origin of the Q and B band. (from ref. 14)

absorption spectrum is the B band. This band is the origin of the second singlet excited state and occurs normally around 410 - 420 nm. It is sometimes referred to as the Soret band. For the metalloporphyrin the Q region consists of two bands, the lowest (α) band is the origin of the first excited singlet and the second (β) band is a vibrational overtone. To the higher energy region of the Soret band, there are generally weaker bands termed the L, M and N bands. The origin of these transitions have been most successfully represented in the 4 - orbital model proposed by Gouterman (15). In fig 1.2 only the two highest occupied and two lowest unoccupied MO's are considered. In a molecule with D_{4h} symmetry (as in the case of zinc tetraphenylporphyrin), the Lowest Unoccupied Molecular Orbitals (LUMOs) are degenerate and of $e_g(ii)$ symmetry. The Highest Occupied Molecular Orbitals (HOMOs) are of a_{1u} and a_{2u} symmetry respectively. The a_{1u} and a_{2u} orbitals lie near in energy and electronic transitions from HOMOs to LUMOs would also lie very close in energy and would be expected to interact strongly. This interaction would give rise to lowering the energy of one transition and raising the energy of the other. The oscillator strengths for these two transitions should reinforce each other for the higher energy transition and cancel each other for the lower. This would give rise to a weakly allowed transition in the visible and an intense transition in the ultraviolet. This pattern is seen in nearly all metalloporphyrins. Both the energy and the

oscillator strength of the lowest energy absorption band depends upon the central metal ion and it has been shown (16,17) that for Zn and Pd, the interaction of the ligand with the metal is strong. This interaction is dependent on the size of the metal ion, the geometry of the metalloporphyrin and electrostatic and inductive effects.

The oxidation or reduction of porphyrin π rings to give cation or anion radicals dramatically alters the absorption spectrum. The reasonably well resolved visible (α and β) and UV (Soret) regions of the neutral porphyrin is replaced by a continuous broad absorption that extends from about 650nm. to well beyond 300nm., with a maximum absorbance in the Soret region at around 410nm. for the oxidized porphyrin (14). Reduced porphyrins have a characteristic band between 600 - 700nm.

1.1.2 AXIAL LIGATION TO METALLOPORPHYRINS

The dependence of the electronic spectrum of metalloporphyrins on the nature of their axial ligands has long been recognized as a natural reporter of their environment in the case of heme proteins (13, 22). The observation of a long wavelength soret band in the carbonyl complex of cytochrome P - 450 is an interesting example. The interpretation of changes in iron porphyrin spectra on axial ligation is important and a number of papers on model compounds have appeared (23).

The visible spectrum of a metalloporphyrin is strongly ligand dependent. Normally, three effects are observed on addition of axial ligands.

- 1) There is a red shift in the entire spectrum.
- 2) There is a change in the relative intensity of the α and β bands.
- 3) When the ligand is strongly electron donating, there is the appearance of a new band on the higher energy side of the Soret (B) band.

The relative degree of these effects will depend on the nature of the ligand i.e., its electron withdrawing or donating power, its size (steric effect) and the base strength. Unfortunately, the interpretation of the spectra of some axially ligated metalloporphyrins has not been straight forward because of complications introduced by partly filled d - orbitals of the metals and their oxidation states eg. in Ru, Os (24), Co (25). This has led to studies of metalloporphyrins where the central metal is unambiguously in a fixed oxidation state. Such metalloporphyrins are the class of zinc porphyrins which provide simpler systems than those of iron and a wide range of ligands can be studied (22).

The four coordinated zinc porphyrin will accept one axial ligand to form a five coordinate complex (22) which is similar to that of high spin iron (II) porphyrins. Although five coordination is preferred, a six coordinated complex of $(\text{THF})_2 \text{ZnTPP}$ has been reported (26) in which

the zinc atom occupies a position in the mean plane of the porphyrin ligand. Six-coordination is common for other metalloporphyrins such as Os and Ru (24, 26).

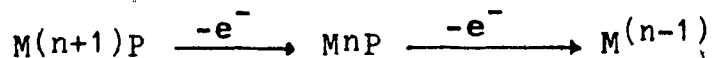
The effects of a variety of ligands on the visible spectrum of ZnTPP have been studied (22). These include the halogen anions and some nitrogenous bases such as pyridine. Ligand binding of substituted pyridines to Ni(II) and Zn(II) porphyrins have indicated a dependency of the strength of the complex on basicity of the ligand (28). Similar effects were observed for Co(II) porphyrins (25) and Cu(II) porphyrins (29)

Photochemical methods have been used to study ligand ejection from Ru porphyrins (23) and the equilibrium constants for phosphine dissociation from Ru porphyrins have been reported (27). The effect of axially coordinating pi - acid ligands on the photovoltaic properties of ZnTPP has been studied and the MCD spectra of the coordinated complexes have been reported (30). The axial ligands were found to stabilize the porphyrins with respect to "hole" energy. A recent study (31) reports the effect of axial ligation on the photoelectrochemical properties of ZnTPP. Axial ligation has also been exploited as a possible route to anchor porphyrins to polymer backbones to allow their use in heterogeneous catalysts (32).

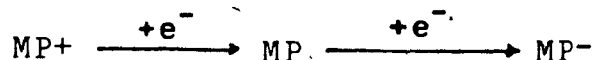
1.1.3 REDOX PROCESSES OF METALLOPORPHYRINS.

In general, the redox chemistry of metalloporphyrins (MP) can be divided into two major classifications.

(1) Systems where the redox process involves a change in formal oxidation number of the central metal ion.



(2) Systems where the redox process involves the porphyrin pi system.



The former are exemplified by many transition metal porphyrins, such as iron, cobalt and manganese (33, 34). Both oxidation and reduction processes can be brought about and the redox properties have been characterized by spectroscopic (13, 35, 36), electrochemical (34, 37), chemical (38, 39) and pulse radiolytic techniques (33, 40).

The latter class of compounds (of which chlorophyll is a member) has been studied by chemical (41, 42) and electrochemical (35, 36, 42) techniques. The products are the metalloporphyrin pi radical cations and anions respectively. The absorption spectra of the anions and cations have been characterized (35, 36, 42) and electron spin resonance (37, 43, 44) and magnetic circular dichroism spectra (MCD) (45) have been documented. MCD

spectroscopy and spectroelectrochemical techniques have been used with considerable success and a number of UV visible and MCD spectra of both cationic and anionic species of porphyrins have been reported (35, 36, 45).

Porphyrin electrochemical studies may be divided into two groups based on whether protic (especially aqueous) or aprotic solvents were used.

Since most porphyrins are at most slightly soluble in aqueous media, several water soluble porphyrin derivatives have been synthesized. Table 1.1 lists some water soluble porphyrins and their one electron reduction and oxidation potentials (35). For many of these metalloporphyrins, oxidation or reduction was not restricted to a single electron process and the formation of dianions and trianions could be resolved from cyclic voltammetry (33). The dications were more difficult to resolve from cyclic voltammetry since they are very reactive towards the solvent. The dianions are susceptible to protonation, with subsequent formation of phlorins and chlorins. From table 1.1 a comparison of the $E_{1/2}$ values for the different metalloporphyrins indicates that the difference in half wave potentials for the addition and removal of an electron is 2.2 ± 0.15 V. Most of the water soluble porphyrins seem to undergo extensive aggregation at moderate concentrations (34).

Redox chemistry of water insoluble metalloporphyrins

TABLE 1.1

REDOX POTENTIALS FOR VARIOUS ONE AND TWO ELECTRON OXIDATION AND REDUCTION OF WATER SOLUBLE PORPHYRINS.

Compound	Oxidation		Metal	Reduction	
	(2)	(1)		(1)	(2)
H ₂ TPPS	1.23	1.10		-1.06	-1.40
H ₂ TMPyP		>1.30		-0.23	-0.43
ZnTPPS	1.14	0.87		-1.16	
ZnTPPC	1.06	0.80		-1.16	
ZnTMPyP	1.34	1.18		-0.85	
PdTPPS		1.09		-1.04	-1.39
PdTMPyP		1.40		-0.63	
MnIII ₂ TPPS		1.11	-0.21		-1.07
MnIII ₂ TPPC		1.10	-0.23		-1.14
MnIII ₂ TMPyP		>1.30	+0.10		-0.76
CoIII ₂ TMPyP			-0.41		
CoIII ₂ TPPS			-0.82		

TABLE 1.2

REDOX POTENTIALS OF METALLOPORPHYRINS.

Compound	Oxidation		Metal		Reduction	
	(2)	(1)	Ox.	Red.	(1)	(2)
H ₂ TPP	1.28	0.95			-1.05	-1.47
H ₂ OEP	1.30	0.81			-1.46	-1.86
ZnTPP	1.03	0.71			-1.35	-1.80
ZnOEP	1.02	0.63			-1.65	
CdTPP	0.93	0.63	0.32	-0.82	-1.25	-1.70
CdOEP	1.04	0.55			-1.52	
FeTBP(Cl)		1.4	1.13			
FeOEP(Cl)			0.99			
MgTPP	0.86	0.54				
MgOEP	0.77	0.54				
MnIIIITPP(Cl)				-0.23	-1.38	-1.70
NiTPP	1.42	1.10	1.00	0.7	-1.5	
NiOEP		0.73	0.7		-1.5	
PbTPP	0.96	0.63			-1.10	-1.52
RuTPP(CO)	1.21	0.82				
RuTPP(Py) ₂		1.26	0.21			
V(IV)OEP	1.25	0.96			-1.25	-1.72

has been carried out in solvents such as dimethylformamide (DMF), dimethylsulfoxide (DMSO), methylene chloride and acetonitrile. Aggregation is eliminated or decreased by the use of these solvents. Protonation of the reduction products and decomposition of the oxidation products is also prevented. Relatively simple reversible redox processes can be observed. A number of cyclic voltammetric and polarographic studies have been carried out in this way (34, 41, 43) and the results of some of the studies are summarized in table 1.2.

1.1.4 ELECTRON TRANSFER PROCESSES OF METALLOPORPHYRINS

General considerations of mechanisms for electron transfer and studies of electron transfer rates have indicated that electron transfer can either take place via an axial encounter or peripheral encounter of the partners (46). These processes are presented in figure 1.3. The axial electron transfer processes require a substitution of the inner coordination sphere via an axial path. This can result in an axial bond cleavage process analogous to the "inner sphere" mechanism advocated for the reduction of $[Co^{III}Cl(NH_3)_5]^{2+}$ by $Cr^{II}(aq)^{2+}$ or an axial through-ligand mechanism analogous to the "outer sphere" process (47):

The peripheral electron transfer process can take place via π transfer or by β meso addition. π transfer is an

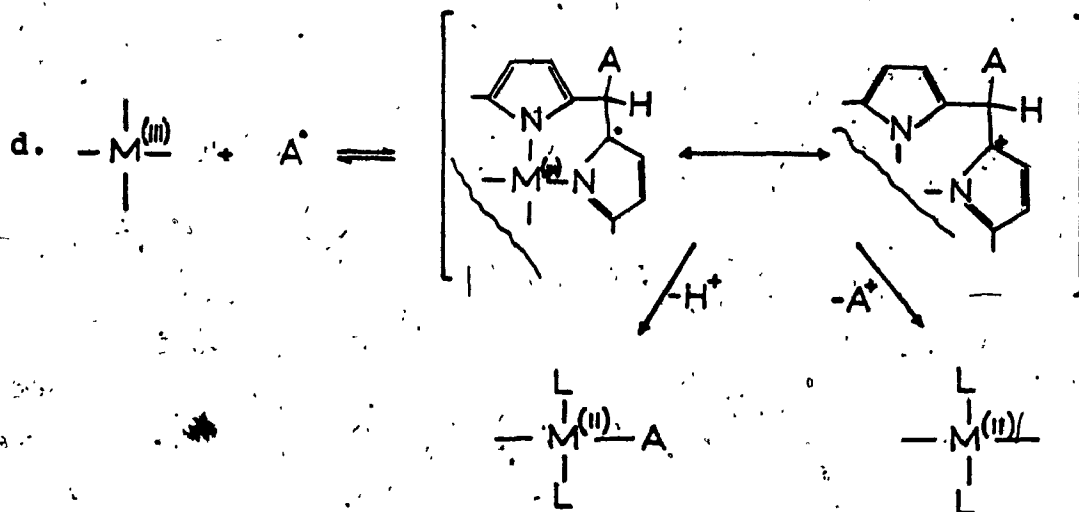
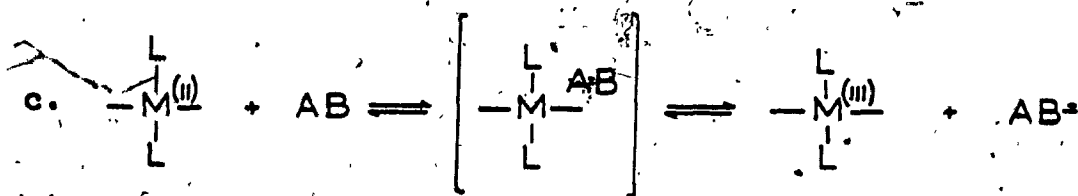
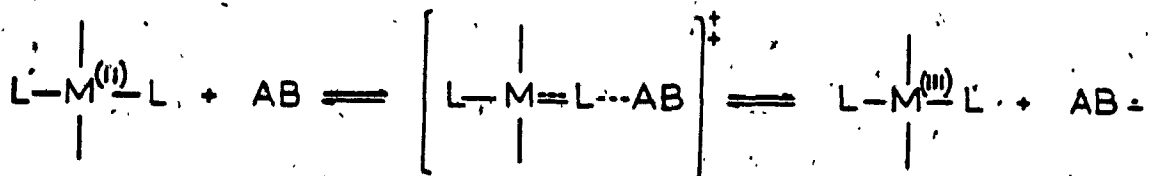
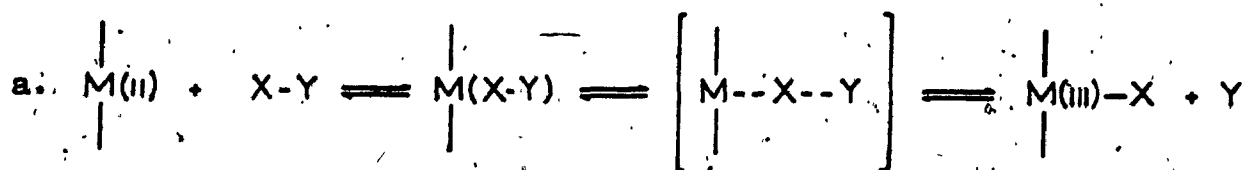


Figure 1.3. Electron transfer processes of porphyrins. (a) and (b) are axial encounters, (c) and (d) are peripheral encounters. (from ref. 46).

example of an "outer sphere" process and meso addition represents a group transfer to the periphery which, in many cases, can result in the formation of an isoporphyrin (48, 49; 50).

Since there is an extremely wide range of available metalloporphyrins, it is in principle possible to select a compound that possesses the exact redox potential required for a particular purpose, and within limits, this situation can be realised.

1.1.5 PHOTOCHEMICAL AND PHOTOPHYSICAL PROPERTIES

Figure 1.4 shows an energy level diagram that is applicable for the description of most aromatic molecules with singlet ground states. Excitation from the ground state S_0 to any singlet excited state S_x commonly leads to very fast radiationless decay to the lowest excited singlet S_1 in times $10^{-12} - 10^{-13}$ sec. From S_1 the molecule can emit fluorescence radiation $S_1 \rightarrow S_0$ with rate constant k_f , can radiationlessly decay $S_1 \rightarrow S_0$ with rate constant k_1 or can intersystem cross to the lowest triplet $S_1 \rightarrow T_1$ with rate constant k_2 . S_1 decays over times between 10^{-12} and 10^{-7} sec, after which, if the system is still excited, it exists in the triplet, T_1 . The molecule can emit phosphorescence radiation $T_1 \rightarrow S_0$ with rate constant k_p , can by a radiationless pathway decay $T_1 \rightarrow S_0$ with rate constant k_3 or can be reexcited to the first excited singlet $T_1 \rightarrow S_1$ with rate constant k_{-2} .

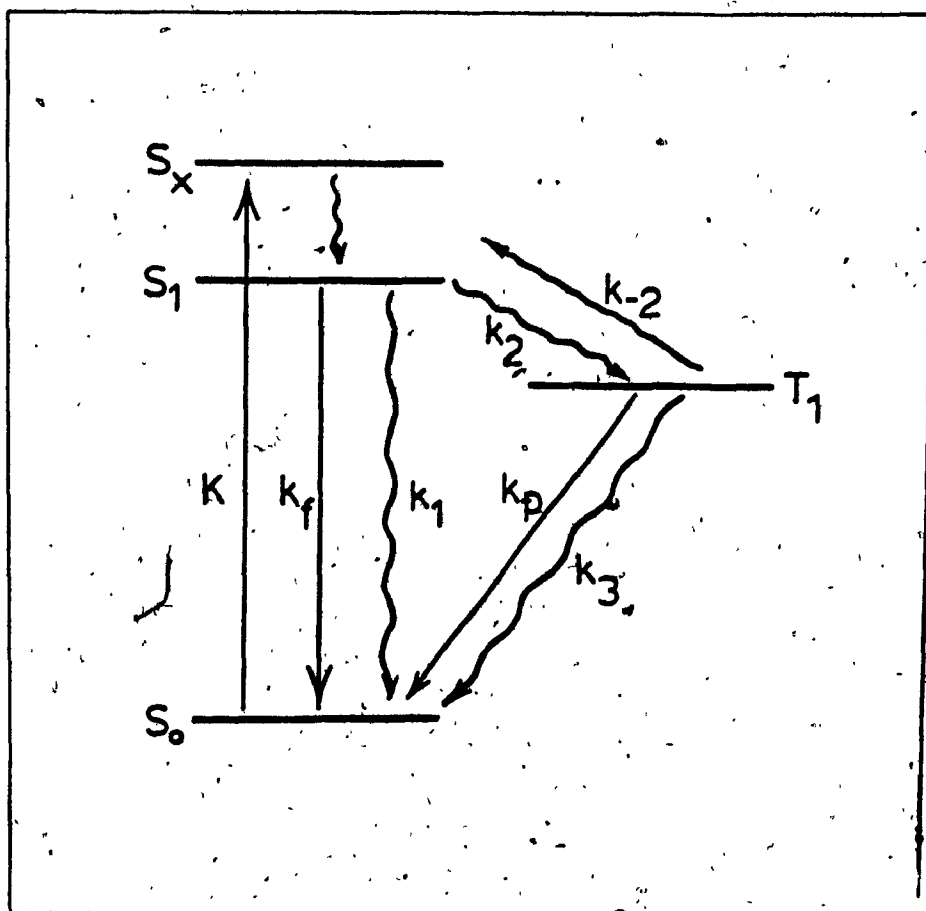


Figure 1.4. Energy level diagram applicable to molecules with a singlet ground state.

Repopulation of S_1 can lead to delayed fluorescence. This requires an input of energy to T_1 which could be thermal repopulation or triplet-triplet collisions. The observables of emission consist of spectra, lifetimes and quantum yields. In general the quantum yields for fluorescence, phosphorescence and the triplet yield can be expressed as

$$\Phi_f = k_f/k_f^*$$

$$\Phi_p = k_2 k_p / k_f^* (k_p + k_3)$$

$$\Phi_t = k_2 / k_f^*$$

$$t_f = 1/k_f^*$$

$$t_p = 1/(k_p + k_3)$$

The sharp and intense long wavelength electronic transitions and relatively long-lived excited states of most metalloporphyrins have been associated with $\pi-\pi^*$ states of the porphyrin macrocycle as described above. These states are little perturbed energetically by substitution of different metals, but the lifetimes and luminescence properties are strongly affected by different metals (16, 52, 53). Strong fluorescence has been observed for free-base and closed-shell metal complexes. Several open shell diamagnetic metal complexes have shown both fluorescence and phosphorescence in solution and some have shown emission only in rigid media at low temperature (52 - 57).

The intersystem crossing constant k_2 is expected to increase in the presence of heavy metals. Φ_f is expected

TABLE 1.3

PHOTOPHYSICAL PROPERTIES OF SOME METALLOPORPHYRINS

Porphyrin	Fluorescence (2980K)			Phosphorescence (2980K)		
	E_s	T_f /ns	ϕ_f	E_T	T_t /ms	ϕ_p
H ₂ TMPyP	1.18	5.3	0.011	1.42	0.165	<10 ⁻⁴
ZnTMPyP	1.96	1.3	0.020	1.61	1.31	<10 ⁻⁴
PdTMPyP	2.14		<10 ⁻⁴	1.79	0.144	0.006
H ₂ TPPS	1.90	10.4	0.080	1.42	0.420	<10 ⁻⁴
ZnTPPS	2.02	1.7	0.043	1.59	1.40	<10 ⁻⁴
PdTPPS	2.19		<10 ⁻⁴	1.76	0.35	0.007
ZnTPPC	2.00	1.8	0.037	1.75	1.30	<10 ⁻⁴
PdTPPC			<10 ⁻⁴		0.285	
H ₂ TPP	1.86	13.6	0.13	1.43	1.38	0.82
MgTPP	2.03	9.2	0.15	1.48	1.35	
ZnTPP	2.05	2.7	0.04	1.59	1.20	0.88
CdTPP	2.03			1.54	0.260	
HgTPP	1.92		<10 ⁻³	1.46	0.032	
AlTPP	2.07	5.1	0.11	1.61	1.140	
PdTPP	2.25			1.79	0.380	~1
PtTPP	2.31		<10 ⁻³	1.90		
CuTPP	2.13		<10 ⁻³	1.66		~1
ZnOEP	2.14	2.2	0.04	1.76		
SnOEP	2.15	0.5		1.79		0.8
CuOEP	2.19		<10 ⁻³	1.83	1	1.0
PdOEP	2.24		<10 ⁻³	1.88	0.3	1.0

to decrease. A very significant feature of porphyrins is the relatively small energy gap between the lowest excited singlet and triplet states. Table 1.3 presents a summary of the observed emission energies, quantum yields and lifetimes for the emissions for a variety of porphyrins (16). In general those are listed as metalloporphyrins soluble in protic and aprotic solvents.

Metalloporphyrins have been reported to undergo singlet - singlet energy transfer (53). This is especially important to the light - harvesting process in the photosynthetic apparatus (54). Most fluorescent porphyrins and metalloporphyrins are strongly quenched by ground state triplet oxygen and this has been suggested as a mechanism for superoxide formation. The long lived excited triplets (see table 1.3) of porphyrins are potentially excellent sensitizers for donation of triplet excitation and Harriman (58) has reported the photooxidation of metalloporphyrins in aqueous media in the presence of electron acceptors (59). Triplet excited states of porphyrins have also been used in energy transfer processes and ligand exchange (60, 61). In fact, in almost all cases where a porphyrin has been used to sensitize a photoredox reaction it is the excited triplet that is the active sensitizer. In this respect, the ideal sensitizer should have an appropriately long triplet lifetime coupled with favourable redox properties. On the basis of the properties mentioned, the class of zinc

tetraphenylporphyrins were chosen as "model" compounds for study in this thesis.

1.2 CHEMICALLY MODIFIED SURFACES.

Chemical modification of surfaces (and in particular electrodes) differs from traditional adsorption on surfaces. The most important difference is that it is a deliberate attempt to immobilise a chemical on an electrode surface so that the electrode afterwards displays the chemical, electrochemical, optical and other properties of the immobilized species. The immobilized chemicals are selected on the basis of known properties or on the basis of any desired property sought i.e. electron transfer centre, photosensitizer for a semiconductor electrode, corrosion inhibitor, or scavenger of trace elements for preconcentration. To a large extent the properties of the modified surface reflect those of the modifier molecule in a homogeneous solution, with the exception that it is confined to the electrode surface.

The most interesting and most studied immobilized species are those which are also electrochemically active. Some, such as the metalloporphyrins, may have other interesting properties such as electron transfer - mediator catalysts, and photosensitizing abilities other than their favourably,

electrochemical properties. They do not however have the desired ruggedness, but this could be overcome by immobilizing them on surfaces in polymers. Such a route has been taken in this thesis in immobilizing Zinc tetraphenylporphyrin via a polymer pendant group to different semiconducting surfaces.

1.3 POLYMER FILMS ON ELECTRODES.

The formation of polymer films on electrodes have been known and used for analytical purposes for some time (65). Electrochemically active polymer literature has been sparse and consequently polymer - modified electrode research has invented new, electroactive polymeric materials and other associated filming methods, to the point where electroactive polymers now represent an emerging class of important materials (62, 63, 66). Polymeric materials are unique because of the range of structural forms that can be synthesized and the way in which changes can be made in the structure and in a local or general way. They are however molecular materials and each polymer chain is its own entity. Within the individual polymer chains, the chemical units may or may not have a unique spatial arrangement. This will normally have a profound effect on the properties of the polymer. Electroactive polymers fall into three broad categories ie. Redox polymers, ionically conducting (ion exchange)

polymers and electronically conducting polymers. Modification of electrodes can take place with any one group of polymers or a combination of all three, depending on the properties sought.

Electroactive polymer films can be formed in a number of ways. Some polymers can be functionalized so that they form chemical bonds to the electrode surface (67, 68, 69, 70). This is normally achieved via a silane bridge. Other polymers have been applied to electrodes without consideration of any bonding. In this case bonding generally occurs by some poorly understood adsorptive process.

1.3.1 METHODS OF MAKING FILMS

The application of polymers to electrode surfaces can take place via two routes.

- a) From preformed polymers
- b) In situ film formation from the monomer.

1.3.1 a) Formation from preformed polymers.

(i) Spin coating

This is well known film forming technique and has been used for a number of preformed polymers (71, 72). It is normally used for modifying disk - type electrodes.

(ii) Dip coating

The electrode is normally exposed to a dilute solution of the polymer for a period of time, during which time an adsorbed polymer layer is formed (73, 74).

(iii) Drop evaporation

A few drops of the dissolved polymer are spread on the electrode and the solvent is allowed to evaporate. This sometimes gives rise to films with rough topology (63).

1.3.1 b) In situ formation from the monomer

(i) Electrochemical polymerization

A solution of the monomer is oxidized (as with pyrrole (75) or aniline (76, 77)), or reduced (78) to produce radicals which can yield polymer films. The films produced can be electroactive or non electroactive. Films produced in this way are not very thick, unless the polymer itself is redox active (79).

(ii) Organosilane Condensation.

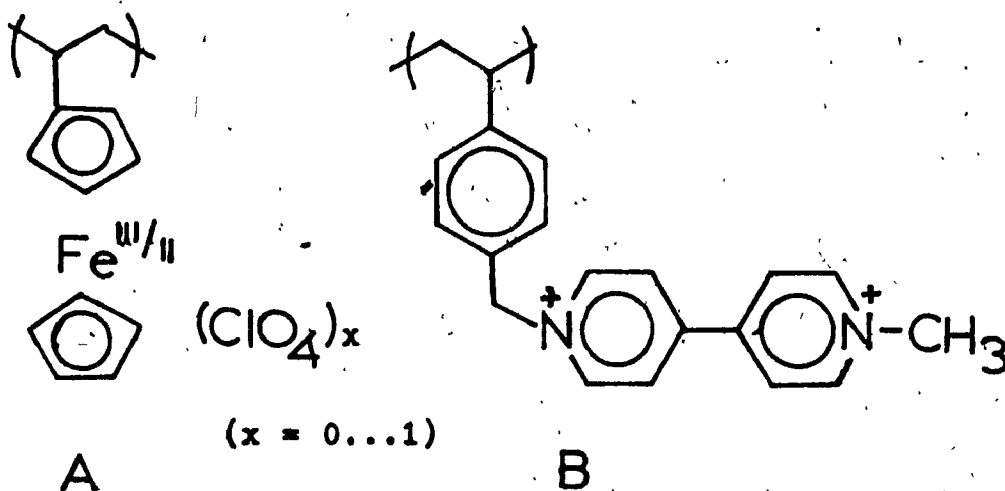
Organosilane reagents which are hydrolytically unstable can be polymerized under dip coating or drop evaporation. These techniques have been applied to ferrocene, viologen, (69) and quinone (68) derivatives.

(iii) Plasma polymerization

Monomers can be introduced into plasma discharges to deposit polymer films. Murray (62) used this procedure to form electroactive polymeric films from vinyl ferrocene. This is a chemically complex route to depositing films and is not commonly used.

1.3.2 REDOX POLYMERS

Redox polymers are synthesised straightforwardly by polymerization of the appropriate monomer. Monomers such as ferrocene, nitrostyrene and 4,4' bipyridinium (viologens) were incorporated into polymers in this way.



A synthetically more versatile approach is the attachment of the electroactive moiety as a pendant group to a suitably functionalized polymer such as

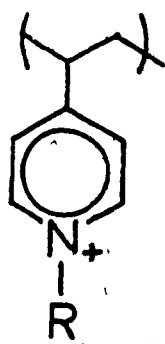
poly(vinylpyridine), poly(chloromethyl styrene) or poly(metacrylic acid) (80, 81, 81). Ferrocene (A), bipyridyl complexes (B) (83) and tetrathiofulvalenes have been synthesised in this way. Metalloporphyrins such as Fe(III)tetra(o - aminophenyl) porphyrin have been attached to poly (methacryl chloride) (85). Polymers prepared in this manner can be purified, fractionated and analytically characterized.

Another approach to forming redox polymers is to first form a film with the functionalized polymer and then attach the redox group afterwards. Anson and co - workers (84) have produced an interesting pendant metal complex redox polymer from poly(vinyl pyridine) and $\text{Fe}(\text{CN})_5(\text{OH}_2)^{3-}$. Such polymers have an inhomogeneous distribution of redox states and may be of little importance in some applications.

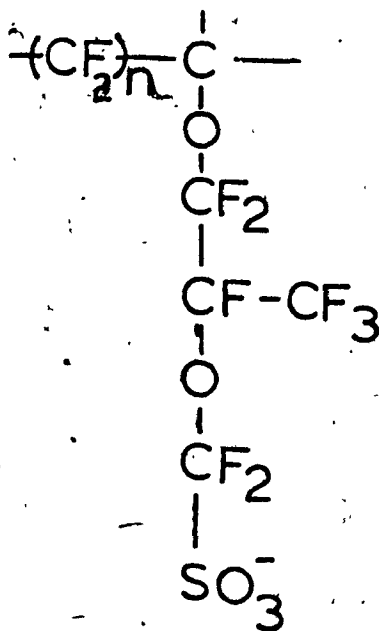
1.3.3 ION EXCHANGE POLYMERS.

Anson and Oyama (86) introduced a versatile strategy for confining redox species into polymer films by incorporating them into polyelectrolytes. The synthesis of these polyelectrolytes does not differ significantly from that of the traditional ion exchangers. Polymers synthesized included the quaternization of poly (4 vinyl pyridine) (A) and poly(chloromethyl styrene) by methyl iodide. These polymers incorporated counterions such as

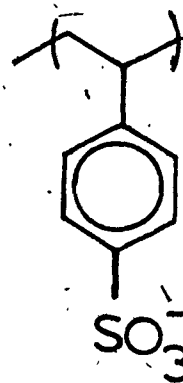
$\text{Fe}(\text{CN})_6^{3-}$, IrCl_6^{3-} , $\text{Mo}(\text{CN})_8^{4-}$ (87, 88, 89, 90). Several cationic complexes such as $\text{Os}(\text{bpy})_3^{3+}$, $\text{Ru}(\text{NH}_3)_6^{3+}$, $\text{Co}(\text{NH}_3)_6^{3+}$ have been incorporated into Nafion (B) (91, 92). $\text{Ru}(\text{NH}_3)_6^{3+}$ and $\text{Cr}(\text{bpy})_3^{3+}$ were studied in films of sulphonated poly styrene (C).



A.



B.



C.

The redox ion is normally incorporated by soaking the preformed film electrode in a dilute solution containing the ion. To avoid partitioning out of the ion into fresh electrolyte, the ion exchange partition coefficient should be large. The partition coefficients for large multiply charged ions are normally large.

1.3.4. ELECTRONICALLY CONDUCTIVE POLYMERS.

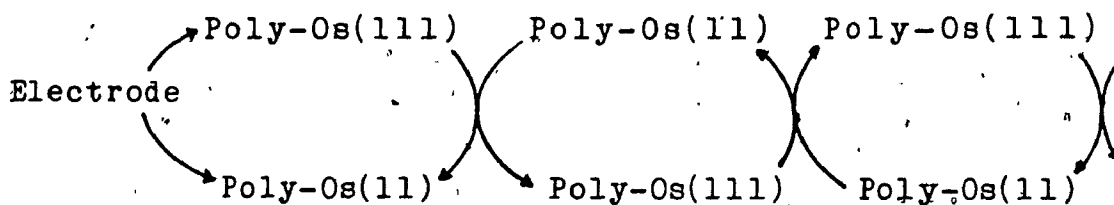
New organic polymeric materials with high electronic conductivities have been reported. These include polyacetylene, polythiazyl $(SN)_x$, polypyrrole (93, 94), polyacetylene (95), poly (p - phenylene) (96, 97) and polyaniline (98). Most of these materials are pi conjugated materials with delocalized electronic states. The conductive states are made by oxidative or reductive doping with chemical reagents such as the halogens and arsenic pentafluoride.

1.3.5. CHARGE TRANSPORT IN ELECTROACTIVE POLYMER FILMS.

The understanding of electrochemical reactivity of the films is important both fundamentally and for the design of polymer films for electrocatalysis and other uses. Electroactive polymers have characteristics which are similar to both of the classical components in electrochemistry; 1) the dense, highly conducting metal electrodes and, 2) the small freely diffusing ions and molecules in electrolyte solutions. Like metal electrodes, electroactive polymers can conduct electrons and can have some mechanical rigidity, but unlike metals, electroactive polymers are dynamic matrices which can accommodate the movement of various counterions. The overall transport mechanism in any one of the classes of polymers mentioned

previously is thus dependent on the physical and chemical properties of the polymer involved.

Electron site to site hopping is often the predominant mechanism of charge transport in redox polymers (86, 99, 100, 101) as in the example of poly Os(11/111)



This hopping resembles a diffusion process for which a wide variety of charge transport diffusion constants D_{ct} have been measured (99, 101). A transport process has also been shown to occur via actual diffusion of the redox species within the polymer (102). This creates a concentration gradient of the oxidized and reduced forms. Electroneutrality can be maintained by the presence of mobile counterions. In some instances, both diffusion and electron hopping were found to occur (103). Site concentration and distances between redox sites also play a major role in the transport mechanism. D_{ct} was found to be independent of the redox sites in the films at high quantities for ferrocene (81) and $\text{PyFe}(\text{CN})_5^{3-}$, (84), but began to decrease at low quantities. This decrease was attributed to the onset of limitation by the rate of electron transfer between adjacent sites of redox centres. Dahms (104) has given a relation of the rate of apparent charge diffusion by electron self - exchange as

$$D_{ct} = D_s + D_{ET} = D_s + k_{xd}^2 C / 4$$

where D_s = diffusion constant of the solute

d = distance between redox centres

C = concentration of redox species

D_{ET} = electron transfer between sites

Results of D_{ct} obtained as a function of concentration of redox species have found D_{ct} for $\text{Ru}(\text{bpy})_3^{2+}$ in Nafion films to be independent of concentration (103). This effect could be seen as an increased electrostatic cross-linking of the polymer at high loading of ionic redox couples.

Ion exchange films provide exceptions of their own in determining the overall transport. In - and out - partitioning between the polymer film and the electrolyte play a major role. Given the electrostatic nature of the in - partitioning process, one would expect stronger ion association between the more highly charged member of the ion couple and the polyionic sites. This can also give rise to formation of small aggregates (105). Other factors, such as association with hydrophobic interactions, can override ion association. In general, ions in ion exchange polymers are diffusion controlled and also characterized by a diffusion coefficient D_{app} . This apparent diffusion coefficient follows the same diffusion

laws as the diffusion constant for electrolyte, but contains the contributions of all the processes involved in charge propagation.

A potential step at a polymer film covered electrode can cause a current time decay which reflects the diffusional rate of the electrochemical charge. Under conditions where semi - infinite diffusion prevails, the decay of current from a large potential step (usually from where the redox species is oxidized to where it is reduced) should conform to the Cottrell equation (106)

$$i = nFAD_{app}^{1/2} C / \pi t^{1/2}$$

where C = concentration of the electroactive sites in the polymer.

A = electrode area.

D_{app} = apparent diffusion coefficient.

F = Faradays constant

i = the limiting current

Plots of i vs $t^{-1/2}$ can yield slopes from which the diffusion coefficient can be extracted if all the other parameters are known.

Numerous other methods have been employed to determine the apparent diffusion coefficient, including linear sweep and cyclic voltammetry at different scan rates and rotating disk voltammetry (63, 106). In cyclic voltammetry, the peak separation should be independent of film thickness if the resistance of the film is small. All these methods

measure an overall value for D_{app} and do not take polymer chain mobility into account. For most of the counterions used to date, D_{app} was measured as smaller than 10^{-8} cm/sec in the polymer films. Anson (89, 90) reported a polyelectrolyte which exhibited high ion retention and high diffusion coefficients. The high diffusion rates were attributed to the internal morphology of the film which consisted of segregated hydrophobic and hydrophilic domains.

Internal morphology also plays an important role in electronically conductive polymers. Although electronic conduction refers to electron transport through the polymer via a delocalized band structure, materials such as polyphenylene, polypyrrole and polyaniline (97, 98) have shown a strong relation between internal film morphology and conductivity. Breakdown in local structures can cause localized states which could give rise to electron traps which can seriously impair the charge-carrying properties of the polymer. This carrier trapping can also occur at phase boundaries. When the conductive polymer contains polar groups (ie. polyaniline), each dipole can act as an electron or "hole" trap. For most electronically conductive polymers, charge transfer can be reasonably explained in the language of semiconductor theory. Simon and Andre (97) have given an extensive account of this field.

1.3.6. PRESENT AND FUTURE APPLICATIONS OF POLYMER MODIFIED ELECTRODES.

The study of the transport of ions and electrons in electroactive polymers has been at the source of the development of a number of applications. These include modified electrode surfaces to act as preconcentration surfaces in analytical determinations, in microstructures such as array electrodes, microelectrodes for biological use, bi-layer electrodes and ion-gate electrodes. It has also opened the way to the field of macromolecular electronics (66).

1.4 MODIFIED SEMICONDUCTORS

Derivatization of electrodes, whether through monolayer or multilayer (polymer) modification has traditionally been attempted on highly conducting surfaces, usually metals. Semiconductor modification seemed a natural offshoot. This led electrochemists into the field of light-driven electrode reactions or photoelectrochemistry.

Semiconductors are solids which are different from metals in that their electronic properties can usually be described by the "band model". In the "band model", (figure 1.5), an electron is not associated with any one

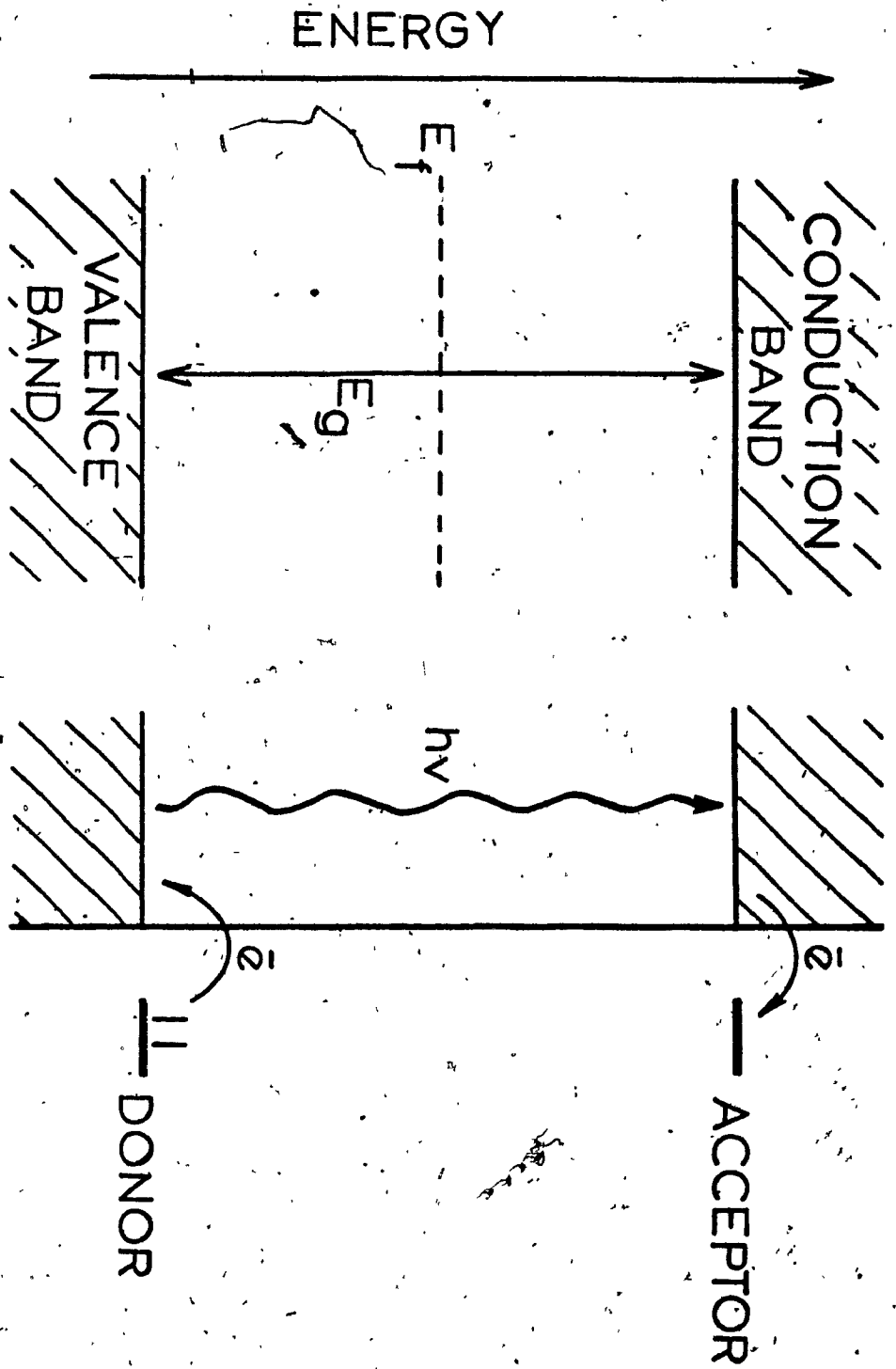


Figure 1.5. Schematic representation of the band model for intrinsic semiconductors.

particular molecule in the solid, but rather resides in "bands" which are formed from the overlap of closely packed orbitals in the solid (106, 107, 108). This gives rise to allowed and disallowed energies for electrons. Calculation (which is a complex process and outside the scope of this discussion) of the energy bands give rise to allowed energy bands separated by a forbidden gap. There is a filled band (valence band) and an empty band (conduction band). The bandgap is the minimum separation between the conduction band minimum and the valence band maximum. The Fermi level E_f is that energy where the probability of finding an electron is $1/2$. Semiconductors are defined as intrinsic (the number of electrons equals the number of "holes") or extrinsic ($n \neq p$) where n and p refer to the electrons or holes. Either electrons or holes can be mainly responsible for the conductivity of the semiconductor, in which case they are called majority carriers. If they make a small contribution to the conductivity they are termed minority carriers. The speed with which the majority carriers move through the bands i.e., the carrier mobility is important to the properties of the semiconductor. Semiconductors can either be p- or n-doped by introducing foreign atoms in the solid lattice. Electrons can be excited from the valence band to the conduction band, creating a vacancy (hole) in the valence band (see figure 1.5). This process of excitation could be thermal or via an external light source. If a

semiconductor which is in contact with an electrolyte at an interface (such as in photoelectrochemistry) is illuminated with light of energy greater than the bandgap, an electron from the valence band can be transferred to the conduction band. At the solid / liquid interface, electron transfer can either take place from the conduction band to the electrolyte, or from the electrolyte to an acceptor (hole) in the valence band. This process forms the basis of light induced electron transfer reactions at semiconductor surfaces (54, 108, 109). The excess charge does not remain at the surface, but is distributed in a space charge layer which forms an electric field, causing the bands to bend at the solid / liquid interface. The potential at which no excess charge exists (ie. no electric field) is called the flat - band potential E_{fb} .

A major problem in photoelectrochemistry, as in most photochemical reactions, is the very fast recombination of the primary products ie. the electron - hole pair. High recombination leads to low yields of photoproducts. To have higher yields of photoproducts, it is necessary to "tune" the position of the acceptor or donor states with respect to the valence or conduction band to give the most efficient yield for electron transfer. A number of contributions on this problem by Gerisher (110, 111), Bard (112), Wrighton (113) and Gratzel (114) for heterogeneous charge transfer have been documented. Surface states

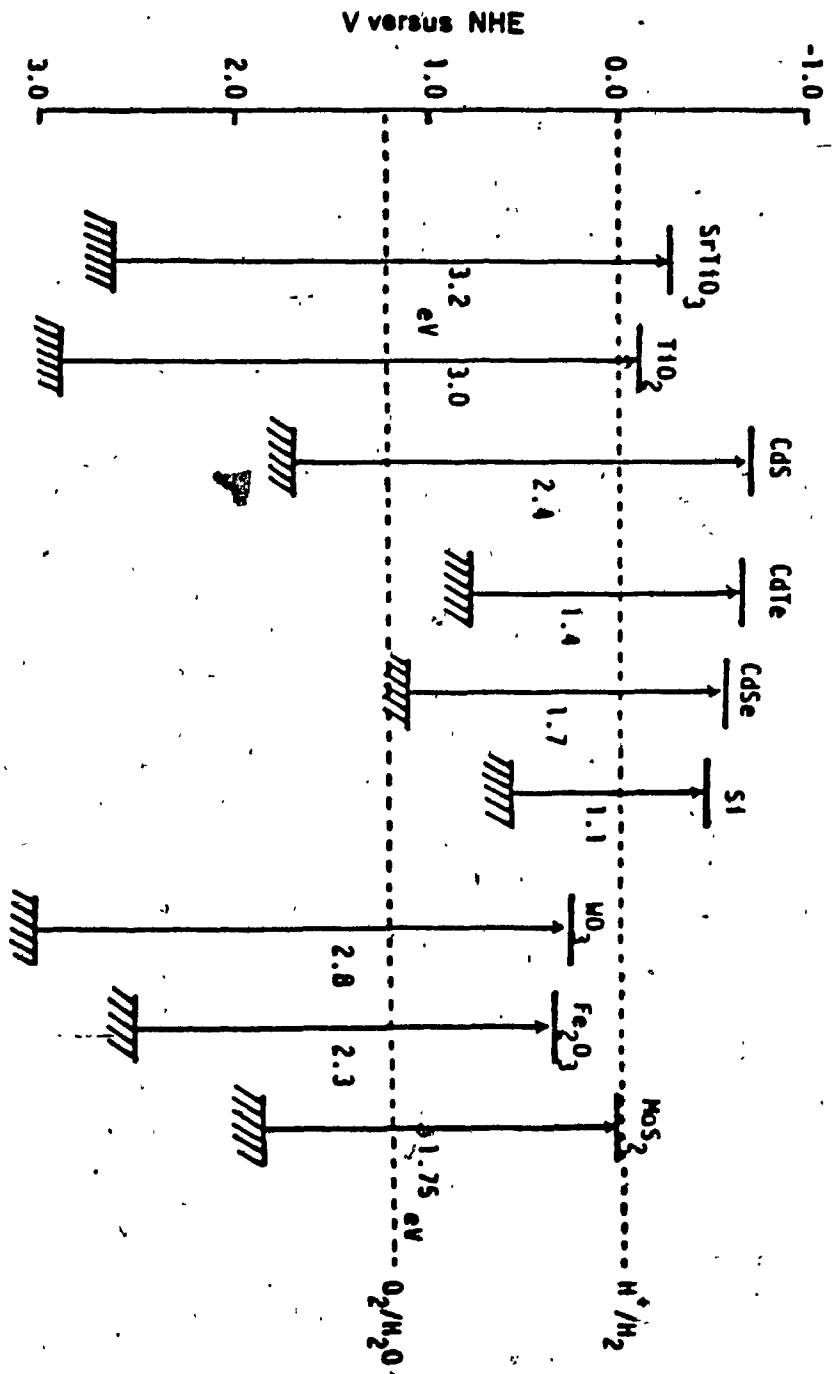


Figure 1.6. The energy positions of valence and conduction band edges for various semiconductors. (from ref. 1).

(energy states between the valence and conduction band) (111, 113) in most semiconductors also pose problems in that they can either act as recombination centres or as centres for reaction with the electrolyte.

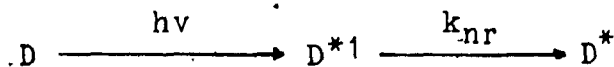
From the simple arguments put forward it is clear that a knowledge of the position of band edges is required in the selection of a suitable semiconductor for use as an electrode. Figure 1.6 gives an energy level diagram indicating the energy position of the conduction and valence bands for various semiconductors in aqueous solution (1). From the figure it is clear that one can distinguish between wide bandgap ($E_g > 2.5$ eV) and narrow bandgap ($E_g < 2.5$ eV) semiconductors. Most of the metal oxide semiconductors have relatively wide bandgaps and the other metal chalcogenides have narrow bandgaps. The narrow bandgap semiconductors are normally modified to prevent photoanodic corrosion processes from taking place (54, 62, 113). The wide bandgap semiconductors are modified for the purpose of sensitisation.

1.4.1 SENSITIZATION OF SEMICONDUCTORS

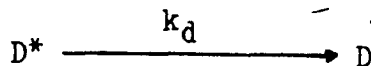
Oxide semiconductors with their relatively large bandgap absorb light only in the UV - region of the solar spectrum. The efficiency of the corresponding solar devices will be small. The sensitivity of these stable

metal oxide semiconductors can be extended to absorb visible light by using corresponding sensitizers. The semiconductor can be sensitized either by doping or by modification of its surface with a dye molecule. The latter approach has been a topic of extensive search (54, 63, 109). Sensitization of semiconductor electrodes by dyes have been mainly based on the redox properties of the dyes (115), but regardless of the dye used, the following sets of reactions must be considered in any analysis of dye sensitisation.

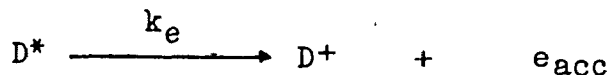
- 1) Absorption of light by the dye followed by non-radiative decay to the long-lived state D^* .



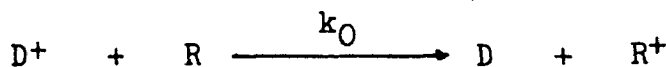
- 2) Decay of D^* to D by luminescence or some other parasitic process.



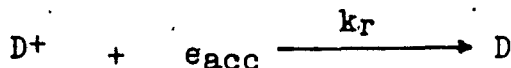
- 3) Injection of an electron from D^* into an acceptor.



- 4) Oxidation of a species R in solution by D^+ .



- 5) Recapture of an electron from the acceptor by D^+



If in reaction 3, the acceptor is an electrode such as n-SnO₂ or n-TiO₂, the corresponding sequence of reactions will give rise to an anodic photocurrent. The electrode at which the reaction takes place is known as a photoanode. An example is the anodic photocurrents obtained when Ru(bpy)₃²⁺ was adsorbed onto SnO₂ (116, 117). Excited molecules are only involved in the electron transfer process at the semiconductor electrode if they can reach the electrode within the duration of its lifetime. For dye molecules with low excited state lifetimes, molecules in the bulk of the dye film is not expected to contribute significantly to the electron transfer process (or the photocurrent). To obtain high efficiencies, the dye concentration at the surface must be increased, a dye with long lived excited states must be used, and/or conduction or charge transport within the film must be improved. The use of the favourable properties of porphyrins makes them ideal dyes for use in experiments involving sensitization. A more viable study of electron transfer and transport properties of porphyrins can be made when coupled to the versatile properties of polymers.

1.4.2. PHOTOCATALYSIS AT PARTICULATE SEMICONDUCTING SURFACES:

During the process of photocatalysis, the rate of a reaction is increased by the presence of an irradiated

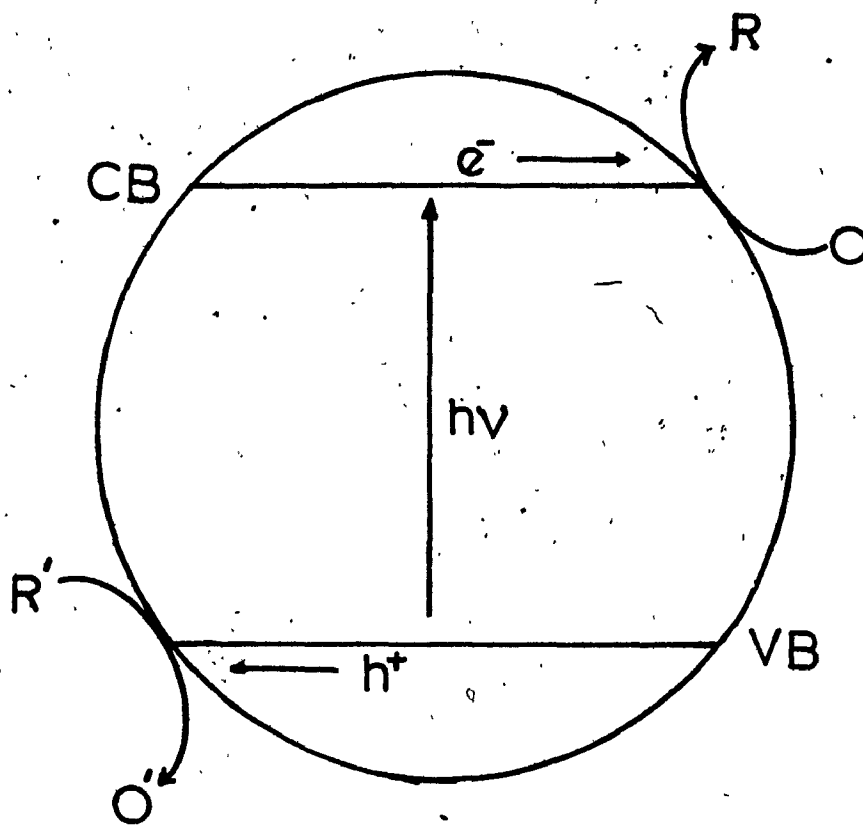


Figure 1.7. Schematic presentation of redox processes at an irradiated particulate semiconductor.

solid or solution. Photocatalysis can be classified into two groups i.e.; (a) dye molecules in a homogeneous or heterogeneous system, (b) semiconductors in a heterogeneous system. Sometimes a combination of a semiconductor and a dye is used; such as in the present case.

The photocatalytic nature of a particulate semiconductor is best described by the scheme in figure 1.7. Electrons and holes generated in the valence and conduction bands of the semiconductor can reduce or oxidize species adsorbed at the surface of the semiconductor. Charge separation of electrons and holes is achieved by band bending of the valence band and conduction band at the surface. Recombination of the photogenerated hole and electron causes reduced quantum yields. The electron or hole must also reach the surface within their lifetime to contribute to any reaction taking place at the surface. Electrical neutrality of the particle is dependent on the rate of the reduction or oxidation reactions at the surface. The scheme in figure 1.7 therefore resembles a photoelectrochemical cell.

For the photocatalytic process to be effective, the energy of the photogenerated electron must be higher than the species O at the surface. Similarly, the energy level of h^+ must be lower than that of the species R'. This will depend on the relative energy positions of the conduction and valence bands. The absence of intermediate states

within the bandgap (trap states) will enhance the process. Semiconductors such as TiO_2 and ZnO (109) have no deep lying energy states within the bandgap and are suited for use in photocatalysis. The photogenerated holes in these oxide semiconductors are related to the energy derived from the 2p orbitals of the oxygen anion lattice, whereas in oxides such as Fe_2O_3 and V_2O_3 , the photogenerated states are related to orbitals derived from the metal cation. The latter class of oxide semiconductors are practically inactive in photocatalysis.

CHAPTER 2

EXPERIMENTAL

2.1 MATERIALS

The commercially available starting materials were used without further purification unless stated otherwise. Table 2.1 is a list of these materials.

TABLE 2.1

Supplier and Grade of compounds used.

Compound	Supplier	Grade
Zinc(II) mesotetra-phenyl Porphyrin.	Strem Chemicals Inc.	Analytical
Meso-tetraphenyl-porphyrin	Strem Chemicals Inc.	Analytical
Pyridine	Anachemia	Reagents
Triphenylphosphine	Eastman	Reagent
Triphenylarsine	Kodak	Reagent
Pyrazine	Sigma Chem. Com.	Reagent
Poly(4 vinyl-pyridine - costyrene)	Aldrich	Reagent
Azobisisobutyronitrile	Chemical Dynamics	High purity
Benzyl Chloride	Fisher	Reagent

Chloromethylstyrene	Analychem Corp. LTD.	Reagent
Triethanolamine	Aldrich Chem Corp.	Analytical
Triethylamine	Aldrich Chem.	Analytical
Titanium foil	Aldrich Chem.	
Cadmium Sulfide	Fluka	High purity
Cadmium Selenide	Fluka	High purity
Cadmium Telluride	Fluka	High purity
Barbituric acid	Aldrich Chem.	Reagent
Chloromine T Hydrate	Aldrich Chem.	Reagent
Titanium tetrachloride	Aldrich Chem.	Reagent
Tetrasodium-meso-tetra(4-sulfonatophenyl) porphine	Strem Chem.	Analytical
Sodium Perchlorate	Anachemia	Purified
Sodium Cyanide	BDH Chemicals	Reagent

Other salts such as potassium chloride, ammonium chloride, Iodine were used as received. Common solvents such as methanol, tetrahydrofuran, ethanol, benzene, toluene and acetone were reagent grade and used without further purification. Solvents such as dichloromethane and acetonitrile were spectrograde and used as received. Dichloromethane obtained from the Concordia stock room was distilled and stored over molecular sieves prior to use. All acids eg. HCl, H₂SO₄ and bases eg. NaOH were used as obtained.

All water used was distilled and deionized. In synthetic as well as electrochemical work, the nitrogen used was of high quality.

Synthetic work was performed in normal laboratory glassware (Pyrex) and all subsequent purifications resulted in products which were dried in a vacuum oven at 60 °C.

Synthesized products were characterized by comparison to literature reports of their UV visible spectra and ion exchange capacity in the case of polymers. Chromatography or precipitation were used to purify compounds.

2.2 PREPARATION OF COMPLEXES, SOLUTIONS AND COPOLYMERS.

2.2.1 Preparation of Zinc meso - tetra (4 - sulfonato phenyl) porphine

0.7 g of tetra sodium - mesotetra(4 - sulfonatophenyl) porphine (12 - hydrate) (TPPS-4) was refluxed with Zn metal (which was etched with concentrated hydrochloric acid and washed thoroughly with distilled water) in distilled water for 24 hours. After cooling the solution was decanted from the excess Zn metal, the water evaporated and the dried product stored under vacuum at 60 °C for 24 hours. UV visible spectra of the dissolved dye (ZnTPPS-4) show complete conversion of TPPS-4 to ZnTPPS-4.

2.2.2. Preparation of solutions of Zinc tetraphenyl porphyrin with axial ligands

75 mg ZnTPP (0.11 m mol.) and 0.4 m mol of the dopant (triphenylphosphine, triphenylarsine, pyrazine) was dissolved in 10 ml of spectrograde methylene chloride. The mole ratio of dye to dopant in these solutions were typically 1:4. When pyridine was used as a dopant, pyridine was used as a solvent in place of CH_2Cl_2 .

2.2.3. Preparation of poly (4 vinylpyridine) solution (PVP)

A 1% solution of PVP was prepared in methylene chloride by dissolving 1 gram of PVP (10% costyrene) in 50 ml of CH_2Cl_2 . A 2% solution of PVP in methanol was prepared in a similar fashion.

2.2.4. Preparation of ZnTPP - PVP solution.

75 mg of ZnTPP was dissolved in 10 ml of solution

2.2.3. (1% PVP in methylene chloride)

2.2.5. Preparation of Ionically conductive Polymer

A 100 ml solution of benzene containing 3.166g of styrene, 18.374g of chloromethylstyrene and 0.5188g of 2,2' - azobis (isobutyronitrile) (AIBN) was degassed with highly pure nitrogen. The copolymerization process was then allowed to proceed for 24 hours in a 250 ml three necked round bottom flask under a blanket of nitrogen at 60 °C. The resulting random copolymer was isolated from the unreacted monomers by precipitating it with n - hexane. The precipitate was then redissolved in 100 ml of benzene and 13 ml of triethylamine was added. This solution was refluxed for 1.5 hours at 80 °C and then allowed to cool. 10 ml of triethanolamine was then added and refluxing was allowed to continue for an additional 90 min. The resulting copolymer was then precipitated by isopropanol and the light - yellow polymer was dried under vacuum at 30 °C for 24 hours. The composition of the polymer was established by infrared spectroscopy and the ion exchange capacity was determined by titration of the excess hydroxide. The ion capacity was found to be 0.7 meq/g. 2 grams of this polymer (further referred to as copolymer 1) was dissolved in 100 ml of methanol to give a working solution of effectively 2% copolymer.

2.2.6. Preparation of Zinc mesotetra (4 sulfonatophenyl) porphine - polymer blend solution (casting solution).

53.92 mg of ZnTPPS-4 dissolved in 10 ml of methanol was added to 10 ml of 2% PVP in methanol and 10 ml of 2% copolymer 1 in methanol. This solution gives an effective concentration of 1.65 mM ZnTPPS-4, 0.67% PVP and 0.67% copolymer 1 in methanol.

2.3 SEMICONDUCTOR PHOTOCATALYSIS.

2.3.1. Preparation of particulate photocatalysts.

The semiconducting powders TiO_2 (anatase), CdS, CdSe, CdTe and Fe_2O_3 were used as received from the manufactures. Each type of powder was of the highest purity commercially available. Each type of semiconductor powder was modified in the following way. 1.00g of powder was added to a beaker containing 5 ml of the casting solution containing ZnTPPS-4, PVP and copolymer 1. 50 ml of methanol (spectrograde) was added. The suspensions were then sonicated to allow equal distribution of the particles in the dye - polymer solution. Sonication was continued until the suspensions were completely dry. The dried catalysts which adhered to the sides of the beaker were scrapped off with a spatula. The effective loading of

dye - polymer on the semiconducting powders were between 0.75 - 0.85% (w/w). The physical appearance of the particulate catalysts ranged from green - yellow for the TiO_2 particles to yellow for the CdS particles. Further drying of the catalysts was effected in a vacuum oven at 30 °C for 24 hours.

2.3.2. Experimental conditions for photocatalysis.

The photocatalysts were irradiated as 0.2% slurries in a 100 cm³ three-necked round bottom flask. The test solution was either a 70 ppm. $K_3Fe(CN)_6$ in 0.1 M NaOH or a 90 ppm $K_3Fe(CN)_6$ in 0.01 M NaOH. Typically 50 cm³ of this solution was used. The illumination source was a 75 watt Xe lamp and the light beam was passed through a 5 cm water filter to remove IR and a 400 nm cutoff filter to remove UV light, respectively. The focal point of the beam was c. 1 cm inside the solution slurry. The incident radiation at the focal point was 200 mW/cm² as measured by a Coherent power meter. The flask was equipped with a water condenser and the slurry was stirred continuously during irradiation. At certain time intervals 1.5 ml samples were taken with a syringe. The samples were filtered through a no. 1 Whatman filter paper to remove the catalyst and then testing proceeded. Standards were treated in a similar fashion:

2.3.3. Determination of cyanide in the irradiated solutions.

The free cyanide concentration in the solutions were determined by the standard ASTM D 2036 method for cyanide. This involves mixing 1 ml of the filtered sample with 3 ml of phosphate buffer at pH 7.0, followed by the addition of 0.4 ml of a 1% chloramine T solution. 1.0 ml of a pyridine-barbituric acid solution (15 g barbituric acid, 75 ml pyridine and 15 ml concentrated HCl in a 250 ml volumetric flask) is added immediately. The solution is diluted to 10 ml in a volumetric flask. A period of 8 min. is allowed to elapse for the red color to develop. The absorbance of the solutions are measured at 578 nm in a spectrophotometer. The concentration of the samples are obtained from a calibration curve for cyanide obtained in the same way.

2.4 MODIFIED ELECTRODES; PREPARATION AND CHARACTERIZATION.

2.4.1. Preparation of Gold electrodes

Gold electrodes were made by sputtering gold from a gold source under vacuum (E - 5100 Polaron Eq. LTD) onto a microscope slide which has previously been etched with 0.1

M HCl, washed with distilled water and subsequently ethanol and allowed to dry.

The thin films of gold on the electrode were 10 nm thick. The optical transmittance was determined by UV - Visible spectroscopy and found to be between 85 - 95%. Modification of the gold electrodes was performed by placing the slide on a levelled glass plate at a temperature of 60 °C. A few drops of the casing solution of either the polymer blend or the polymer blend with ZnTPPS-4 were dropped onto the surface of the slide. The fluid was then carefully spread to cover one - half of the slide. The electrode and the area around it was then covered with an inverted 2.5 liter glass beaker to allow slow evaporation of the solvent and also to prevent atmospheric dust particles from contaminating the electrode. Evaporation of the solvent normally took between 6 - 9 hours depending on the amount of solvent. The dried films were then characterized by optical spectroscopy and their thickness determined by profilometry.

2.4.2. Preparation of SnO₂ disks

The SnO₂ electrodes were cut as disks with an i.d of 25 mm from n - doped NESA glass obtained from the O.H. Johns Co. These electrodes typically have a resistance of 15 - 25 sq⁻¹. Before use or modification they were cleaned with 1:1 HCl: HNO₃, rinsed with distilled water and

stored in absolute ethanol.

Thin films of porphyrin were cast onto the SnO₂ electrodes from solutions of the porphyrin in either methylene chloride or pyridine. Casting was accomplished on a spin coating device which allowed rotation at variable speeds under a blanket of nitrogen. During spinning, the electrode disk was held in place by vacuum suction. A typical operation involved placing the dried disk on the spin - coating platform while applying a vacuum via a water aspirator. The surface of the electrode is then flooded with a solution of the desired porphyrin. The electrode is covered with an inverted buchner funnel which is connected to a nitrogen stream. The rotation is initiated and continued for 10 - 20 seconds. Thin films of variable thickness could be prepared depending on rotation rate and solvent volatility. Characterization of the surfaces include direct optical measurements on the films which were correlated with solution optical measurements after washing the dye off the electrode. The films also appear smooth and completely uniform in scanning electron micrographs (Hitachi 520 Scanning Electron Microscope). No crystals of > 20 um were apparent.

2.4.3. Preparation of I T O electrodes

Indium doped tin oxide (ITO) conductive films on glass were cut as 5 x 1.5 cm strips from a plate obtained

from Applied films Lab Inc. The resistances of these electrodes were typically 70 - 80 Ω sq⁻¹. These electrodes were soaked in 0.1 M HCl for 5 min, washed with distilled water and stored in absolute ethanol until prior to use.

The electrodes were modified in the same way as the Au electrodes ie. by drop evaporation of the polymer film. Film characterization was the same.

2.4.4. Preparation of TiO₂ electrodes

Titanium strips (1 cm x 5 cm) were cut from titanium foil obtained from Aldrich. These strips were etched with concentrated HCl and washed thoroughly with distilled water. TiCl₄ was slowly dropped on one face of the wet titanium strip and the TiCl₄ allowed to evaporate. The electrode was then annealed in a furnace at 550 °C for 1 hour. After cooling, the white TiO₂ electrodes were stored in a dust free container until further modification. Modification of the TiO₂ electrodes were the same as that of the ITO and Au electrodes.

2.4.5. Preparation of the CdS and CdSe electrodes

CdS electrodes were a kind gift from Dr J.P. Dodolet at INRS Energie. The electrodes consisted of a thin film of CdS electrodeposited on an ITO electrode (118, 119). These electrodes were characterized by their optical

spectra. They were modified by drop evaporation in the same way as the ITO and Au electrodes.

CdSe electrodes were a kind gift from Dr M. Lawrence. The electrodes were prepared by vapour deposition of Cd and Se on an ITO electrode. Modification of the CdSe electrodes were similar to that of the ITO.

2.4.6. Film thickness measurements by Profilometer and Micrometer.

The thickness of the thin porphyrin films and the polymer loaded films on the optically transparent electrodes were determined by mechanical surface profile measurements using the Talysurf Taylor - Hobson Step Profilometer, or by a hand - held micrometer (Mitutoyo). Films of different thickness of ZnTPP and axially ligated porphyrin were prepared on SnO_2 electrodes by spin coating as described in section 2.4.2. Films of different thickness of ZnTPPS-4 in polymer blend (section 2.2.6.) were prepared on ITO, SnO_2 , CdS and Au electrodes by drop evaporating a known amount (0.1 ml to 2 ml) of casting solution on the electrode. The thickness of these films were then determined as well as the optical absorbance of the films. In this way a calibration curve could be constructed relating the film thickness for a certain polymer film with the optical absorbance. Figure 2.1 is a plot of the film thickness curves of ZnTPP and ZnTPP-

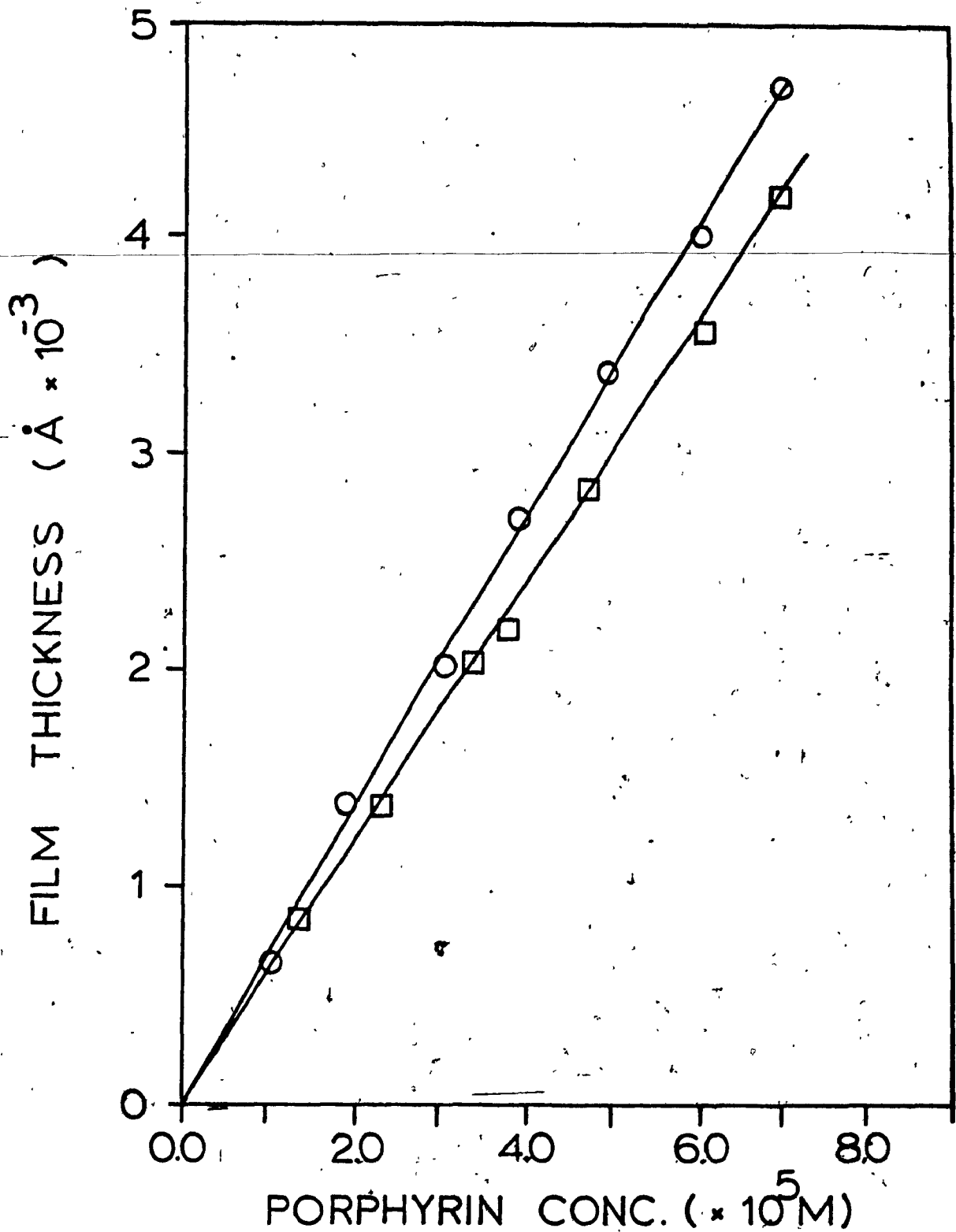


Figure 2.1. Film thickness vs. porphyrin concentration for ZnTPP (○) and ZnTPP-pyridine (□) films on SnO_2 electrodes.

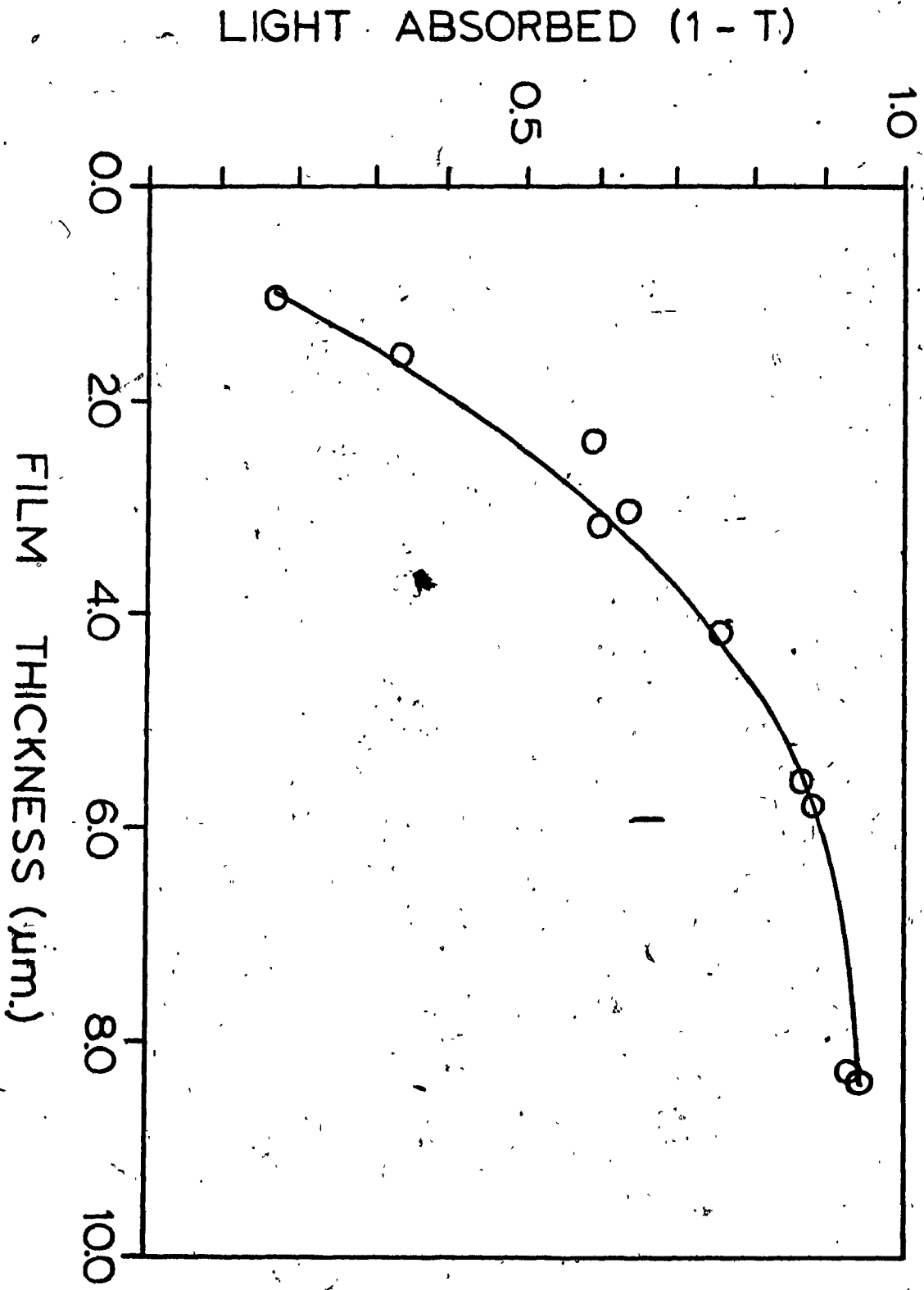


Figure 2.2. Film thickness vs. light absorbed for a dye-polymer film on SnO_2 . The dye is ZnTPPS^{4-} and the polymer is PVP-copolymer.



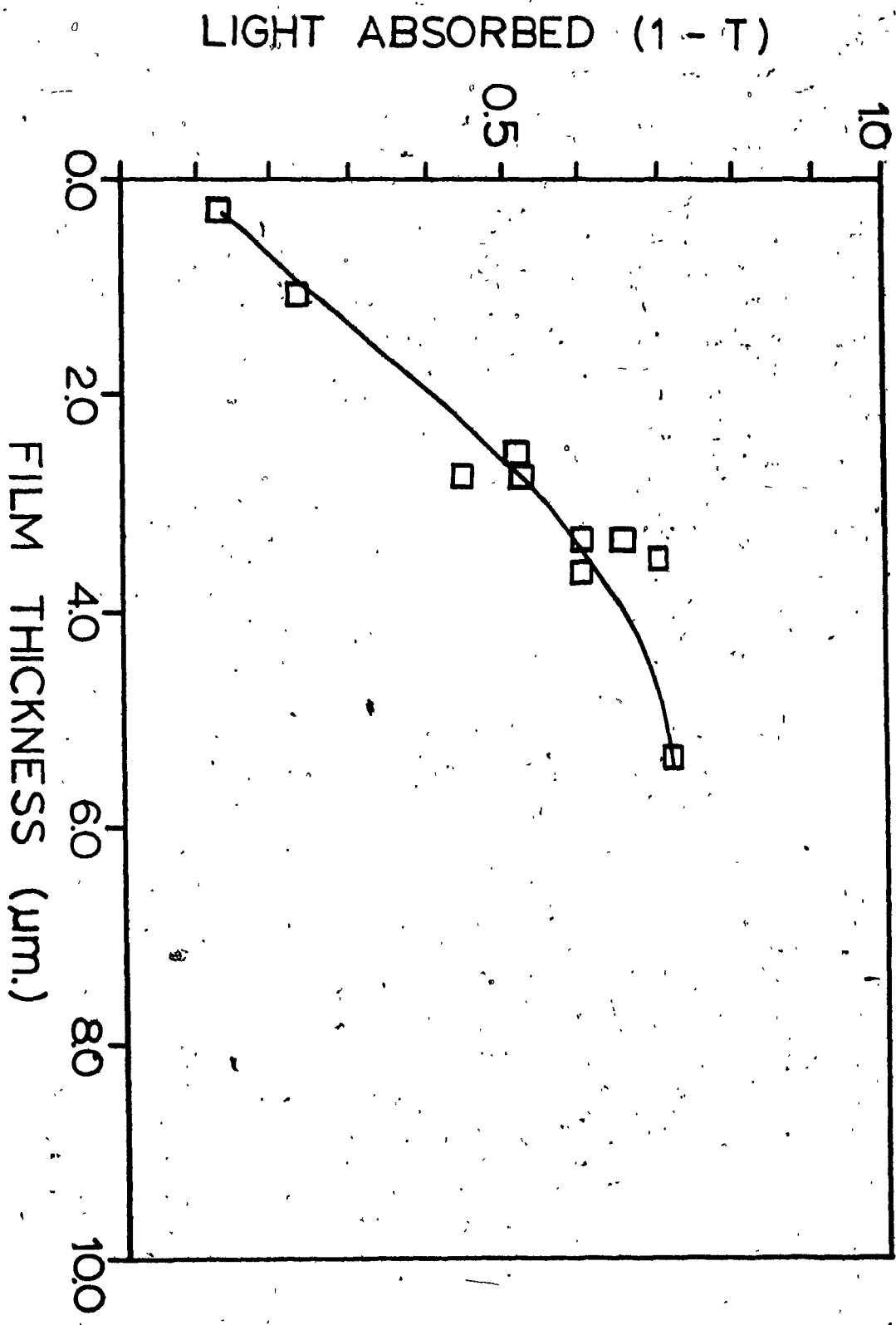


Figure 2.3. Film thickness vs. light absorbed for a film of ZnTPPS-4-PVP-copolymer on Indium Tin Oxide (ITO) electrodes.

pyridine on SnO_2 . Figures 2.2 and 2.3 are plots for ZnTPPS-4 - PVP - copolymer films on SnO_2 and ITO respectively.

Film thickness of only PVP - copolymer show no big difference from those loaded with dye.

The amount of ZnTPP on the SnO_2 electrodes were determined by washing the dye off the electrode, dissolving it in a known amount of methylenechloride and taking its optical absorbance. The amount of dye in the polymer film was directly determined from the optical absorbance of the film and the known extinction coefficient of the dye in the polymer.

2.5 . ELECTROCHEMICAL AND PHOTOELECTROCHEMICAL TECHNIQUES

2.5.1. Electrochemical Techniques

Aqueous and non - aqueous solution electrochemical experiments were performed with a Metrohm 506 Polaricord which was used to control the potentials, a Metrohm 616 VA Scanner to vary the potentials and generate a triangular wave function. Voltages were also digitally monitored with a Keithley Model 616 electrometer. Voltammograms were recorded on an X - Y recorder (Hewlett

Packard or Phillips PM8143). Voltammetric measurements were made in a conventional 3 electrode arrangement where in all cases the counter electrode was a Pt - wire electrode. The reference electrode was either a Ag/AgCl (Sat KCl) with a glass frit or a saturated calomel electrode for aqueous electrolytes or a Ag/Ag⁺ (0.1M AgClO₄) for non aqueous electrolytes. The working electrode varied from a Pt plate electrode to any of the modified electrodes mentioned in the previous sections. All measurements were performed at room temperature, unless otherwise stated. All measurements were done in either a conventional Metrohm Polarographic Cell which was modified to accommodate the ITO working electrodes or a Teflon flow - through cell with three chambers to accommodate the working, reference and auxiliary electrode. The Teflon flow - through cell was only used with the SnO₂ disk electrodes. The cell was connected to a peristaltic pump and an outside solvent reservoir which was equipped to deaerate solvents.

Before mounting the SnO₂ disks in the Teflon cell, the dye at the periphery of the disks were wiped clean with a methylene chloride wet tissue to ensure efficient contact between the SnO₂ and the brass ring contact in the teflon chamber. The SnO₂ optically transparent electrode was then tightly pressed against a silicone rubber O - ring serving as a seal, preventing electrolyte from coming in contact with the brass ring on the outer periphery. Figure 2.4 is

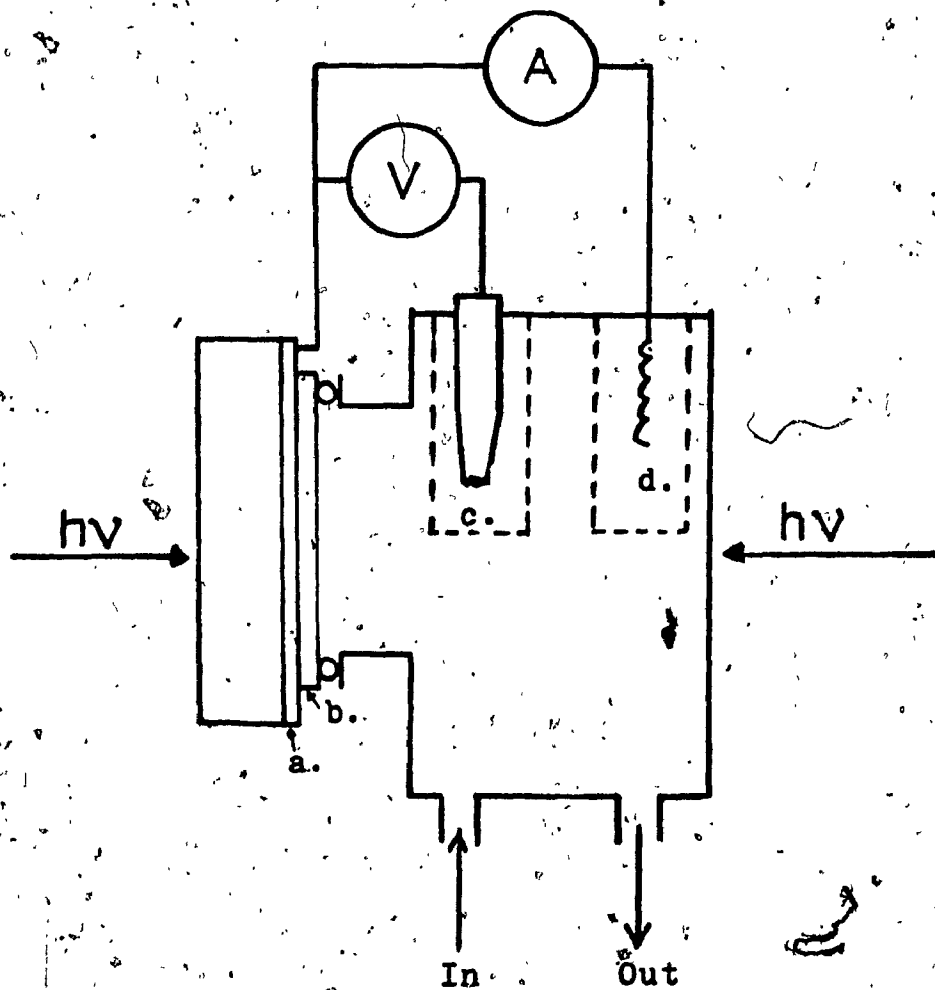


Figure 2.4. Schematic representation of the flow-through cell. (a) The SnO_2 electrode (b) Thin porphyrin film, (c) Reference electrode, (d) Counter electrode.

a schematic illustration of the flow - through cell.

The other modified electrode electrochemistry done in the conventional cell could be performed after a 1 cm² area of modified surface was isolated on the electrode by covering the other areas of the electrode with a resistive epoxy varnish to prevent the underlying surface from making contact with the electrolyte.

Thin film electrochemical measurements were performed with the same equipment as that used for the homogeneous measurements.

Most of the aqueous electrochemistry was performed with 1.0 M KCl as the background electrolyte, unless otherwise stated. The non - aqueous electrochemistry was performed in spectrograde acetonitrile or methylene chloride using sodium perchlorate, tetraethylammonium perchlorate or tetrabutylammonium perchlorate as the background electrolyte.

Chronoamperometric measurements were performed using the same equipment. Usually the X - Y recorder was used as a Y - t recorder or a strip chart recorder was used to record the chronoamperograms. The potential was usually stepped manually between + 0.4 V and - 0.4 V vs Ag/AgCl sat. KCl.

2.5.2. Photoelectrochemical Techniques

Photoelectrochemical studies were performed with the same cells and apparatus as that used in electrochemical studies. The light sources employed were a 300 W tungsten

halogen lamp from a Kodak slide projector, or an Ar ion laser. (Spectra - Physics) coupled to a dye laser (Coherent) using Rhodamine 6 G as the dye. For the White light illumination, the beam was passed through a 5 cm water cell to remove IR irradiation and a 400 nm cutoff filter (Ealing) to remove UV irradiation. The beam was collimated with a convex lens to illuminate the working electrode area. White light illumination was adjusted to 100 mW/cm^2 by using a Variac coupled to the Kodak slide projector. The power meter used to calibrate the light was a Coherent Power Meter.

Photocurrents were measured between the working and auxiliary electrodes, displayed on a Kiethley Model 177 multimeter and recorded on a strip chart recorder (Fisher). All photocurrents were measured under hydrodynamic conditions. Photocurrents measured with the teflon flow - through cell showed no difference between front (through the SnO_2 electrode) or back (through the electrolyte) illumination.

Photoaction spectra were obtained by mounting the electrochemical cell in a Faraday cage. Illumination was from a Xe lamp fitted with a motor driven Bausch and Lomb monochromator. The photocurrents under monochromatic light were measured with a Kiethley Model 616 electrometer and recorded on a strip chart recorder. The action spectra were normalized for light intensity and photon flux of the lamp.

2.6. ELECTRONIC ABSORPTION SPECTRA

All solution and solid state absorption spectra were taken with a Perkin Elmer 552 or a HP 8452A UV - Vis Diode Array Spectrophotometer. All solution spectra were taken with quartz cells with a pathlength of 1 cm or 2mm. Solid state spectra were recorded on the respective optically transparent electrode by mounting the electrode in front of the spectrophotometer cell holder. In all cases the background was corrected with the appropriate blank.

2.7. FLUORESCENCE MEASUREMENTS

Solution and solid state fluorescence measurements were performed with a Perkin Elmer MPF 44 B spectrofluorimeter. Solid state measurements required a special sample holder which allows the incident light beam to impinge at 30° to the surface of the sample.

2.8. FLASH PHOTOLYSIS STUDIES

2.8.1. Nanosecond Transient Absorption Spectroscopy

Transient absorption flash photolysis experiments were performed using a dye laser (Model DL 2100 C) with a coaxial flash lamp (Model DL 15). The flash lamp as well as the dye solution was cooled with tap water. The dye

solution (50 μm Rhodamine 590 in methanol), was circulated through the inner tube of the lamp and was excited by the discharge of the lamp surrounding it. The flash beam and monitoring beam passed at right angles through a quartz photolysis cell. The monitoring beam was from a 250 W Xenon lamp (Ealing). The photodetector system consisted of a grating monochromator and a photomultiplier (high gain). The output from the photomultiplier was displayed on a storage oscilloscope (Tektronix 7633) or on a computer (Danesh XT).

All samples were thoroughly degassed for periods of 40 - 60 min. with purified Ar before use.

2.8.2. Picosecond Flash Photolysis Measurements.

Picosecond Flash Photolysis experiments were performed in the Canadian Centre for Picosecond Flash Photolysis located at Concordia University. This system employs as excitation source a Quantel YG 402G Neodymium-doped YAG (Yttrium - Aluminum - Garnet) laser with a fundamental output at 1064 nm with 30 ps pulses at a maximum rate of 10 p ps. The fundamental frequency could be frequency doubled to 532 nm by passing through a KDP type 1 crystal. By passing the 532 nm pulse and the fundamental pulse of 1064 nm through a KDP type 11 crystal produces the third harmonic at 355 nm by frequency mixing. The 355 nm pulse was used as the excitation beam in these experiments. Frequency mixing does not convert all the

light of fundamental frequency and this unconverted light is focused into a Raman active fluid (50% D₂O in H₂O v/v). This results in the generation of a transient birefringence which produces a Stokes and anti - Stokes Raman effect. It results in the production of a continuum of white light (400 nm to 600 nm) with a pulse width similar to that of the excitation beam. The continuum of white light is split by a beam splitter, one beam going to the sample to act as probe beam. The other beam is used as a reference.

Light transmitted by an excited sample is detected by a multichannel photodiode arrangement and fed into a microprocessor where the necessary data manipulation is performed.

The probe beam can be delayed between 0 - 10 ns. after excitation of the sample. The sample is contained in a quartz cell with a path length of 2 mm. For each experimental delay period, a set of data consist of four excitation shots, one for the blank and three for the sample.

The transient absorption spectra are presented as the average absorbance change between the blank and the sample and were thus recorded as difference spectra. All samples for picosecond transient spectroscopy were prepared on the day the experiments were performed.

2.8.3 Pulse fluorescence measurements.

Fluorescence decay on both solutions and on solids were monitored using the same picosecond system as outlined in section 2.8.2., with the exception that a streak camera (Hamamatsu) with a resolution of 10 ps was added to detect the fluorescence traces. Glass filters and interference filters were placed before the entrance slit of the streak camera to reject the scattered probe pulse of 355 nm. For more exact measurements a monochromator was inserted between the streak camera and the sample to allow time resolved fluorescence measurements at a single wavelength. The output of the streak camera was recorded on a Temporal Analyser (a rapid electronic readout system for video images). The output of the temporal analyser was recorded on a strip chart recorder.

Samples for the fluorescence measurements were prepared freshly on the day of the experiments. Solid state films were cast on an optically transparent slide 1 cm. x 5 cm.

CHAPTER 3

RESULTS AND DISCUSSION I.

ELECTROCHEMISTRY AND PHOTOELECTROCHEMISTRY OF THIN PORPHYRIN FILMS ON SnO_2 ELECTRODES.

The first approach in using porphyrin molecules as sensitizers involved the study of the interaction of porphyrins with single molecules, preferably those that can ligate axially to the zinc metal of the porphyrin. This chapter depicts the spectroscopic, kinetic, electrochemical, and photoelectrochemical effects observed in thin films of zinc tetraphenylporphyrin modified with axial ligands. This study was motivated by the model of porphyrin "doping" discussed in reference (30).

3.1. ELECTRONIC ABSORPTION SPECTRA IN SOLUTION.

Fig 3.1 is the absorption spectrum of tetraphenylporphyrin (H_2TPP) and zinc tetraphenylporphyrin (ZnTPP) in methylenechloride. The H_2TPP has four major peaks in the visible region, all of which can be assigned as transitions explained by the 4 - orbital model in section (1.1.1). When a metal such as zinc is inserted in the porphyrin "hole", there is a major change in the intensity of the peaks in the visible region. The α and β bands which are characteristic for

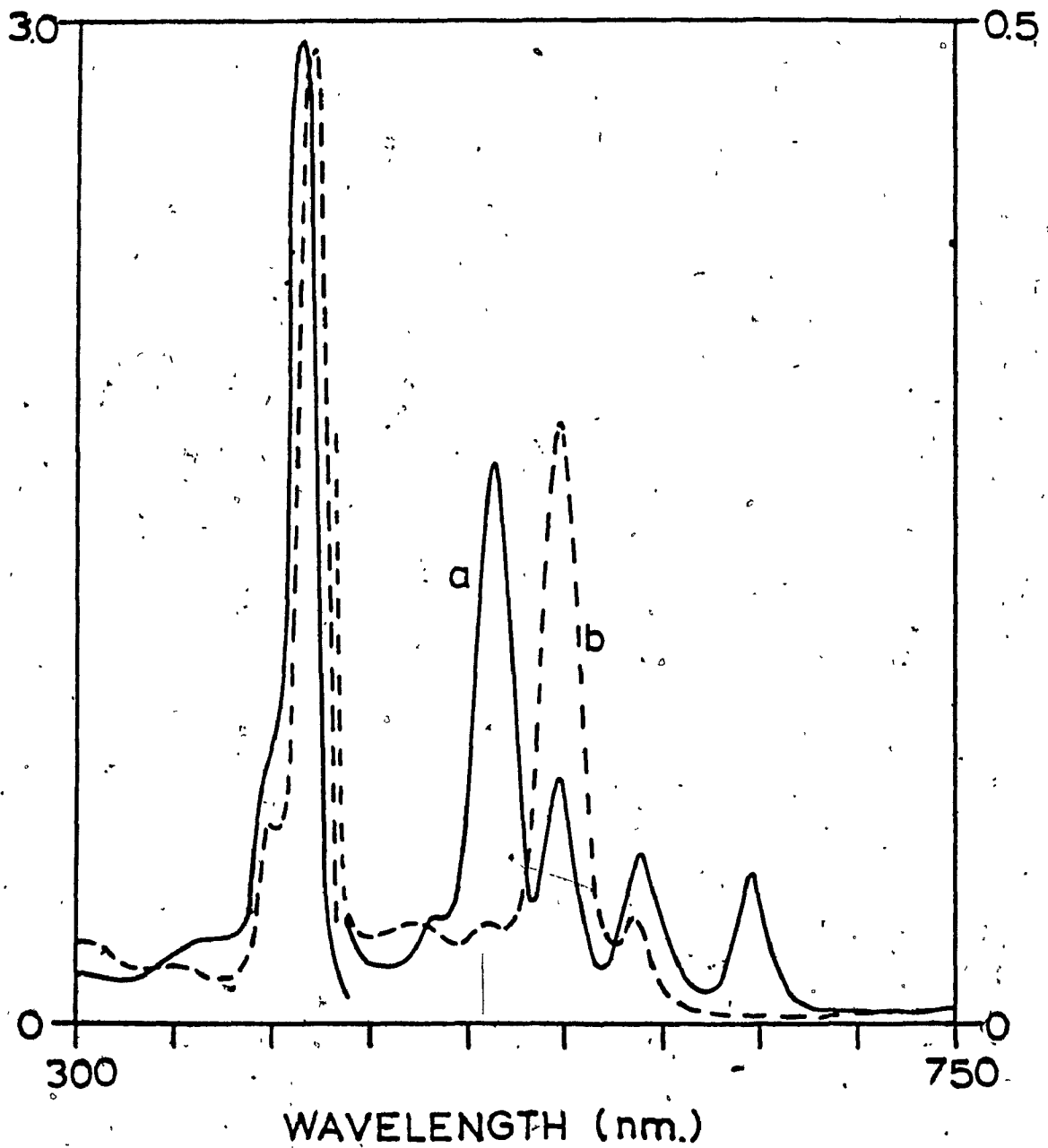


Figure 3.1. Electronic absorption spectra of (a) H₂TPP and (b) ZnTPP in CH₂Cl₂.

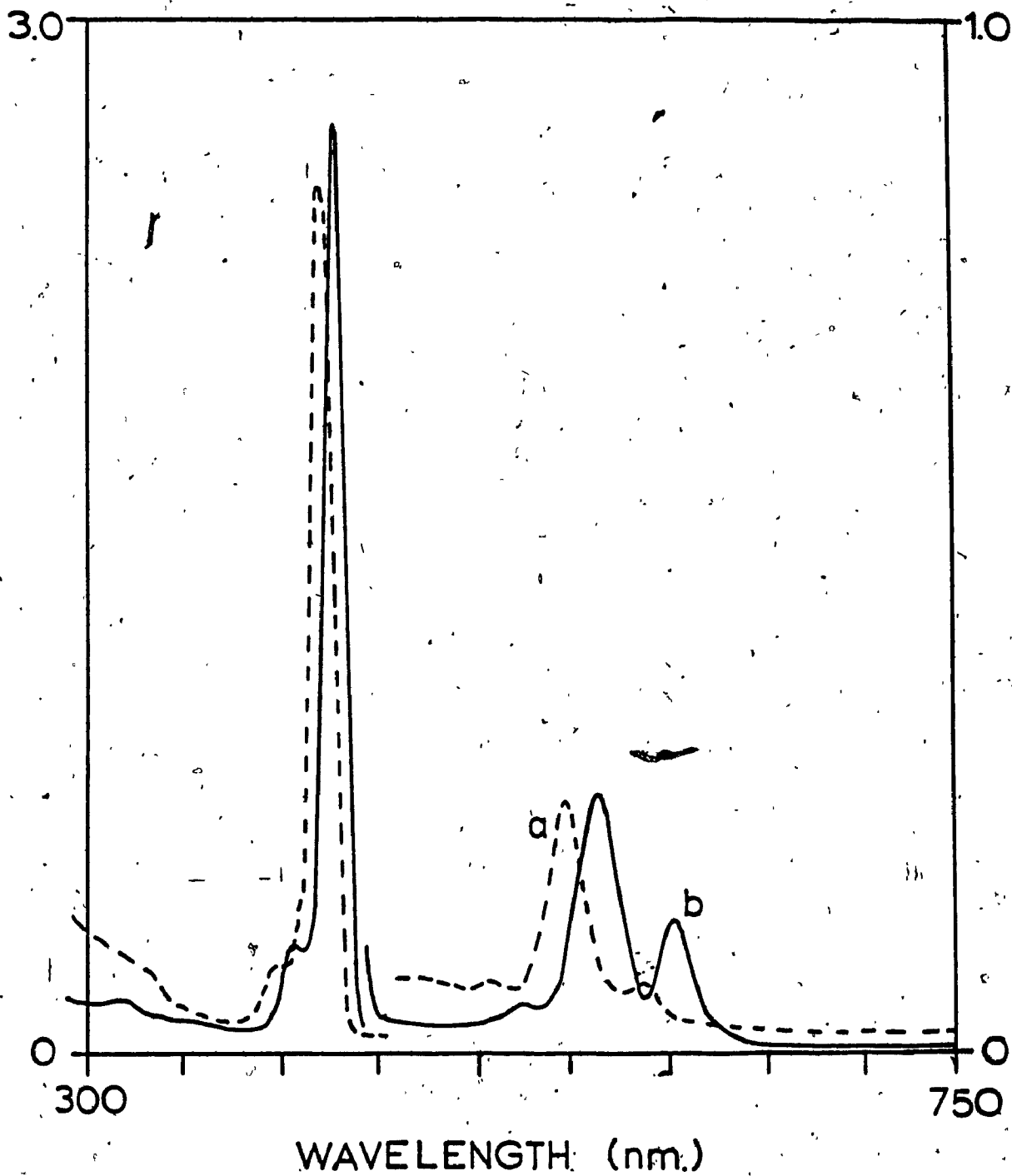


Figure 3.2. Absorption spectra of (a) ZnTPP in CH_2Cl_2 and (b) ZnTPP with different axial ligands in CH_2Cl_2 .

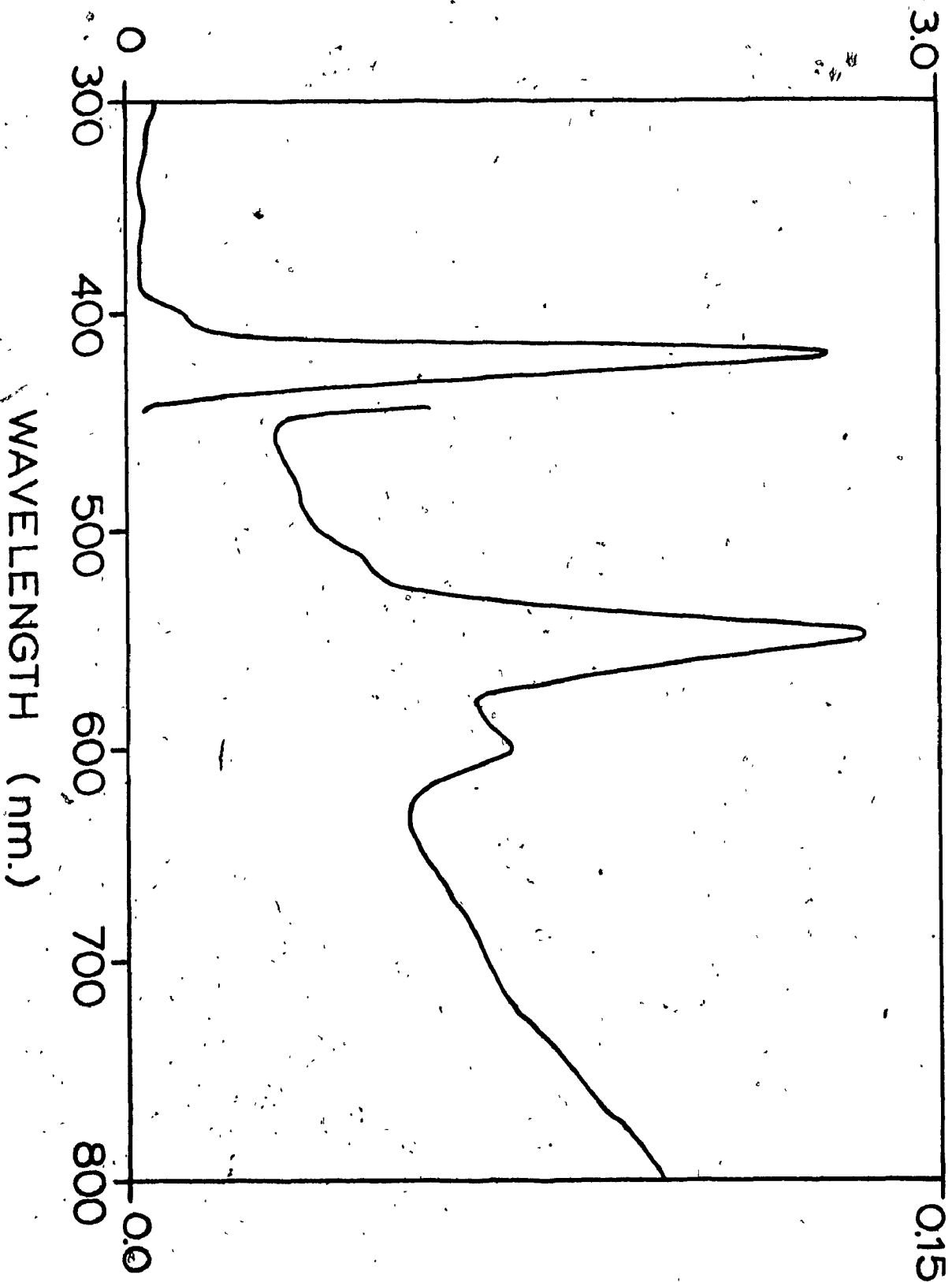


Figure 3.3. Electronic absorption spectrum of ZnTPP with poly(4-vinylpyridine) in CH₂Cl₂.

"normal" metalloporphyrin are evident in the figure.

On addition of bases such as pyridine, triphenylphosphine, triphenylarsine or polyvinylpyridine which can axially ligate to the ZnTPP, there is a major change in the position and the relative intensities of the α and β bands in the visible spectrum of ZnTPP. Fig 3.2 shows the changes that occur when ZnTPP is dissolved in pyridine. The axially ligated pyridine causes the α and β bands to shift bathochromically by 12 nm. The relative ratio of β/α decreases from 6:1 to 2:1. This change in ratio of the β/α bands has been correlated with the charge and polarizability of the axial ligand and its ability to transfer charge to the porphyrin ring (22). The ligands triphenylphosphine (TPhP), triphenylarsine (TPA) and polyvinylpyridine (PVP) causes a similar effect when added to the ZnTPP in methylenechloride.

The extent of the bathochromic shift is in the order TPhP > pyridine > TPA > PVP. In all cases the shift of the α and β bands did not exceed 15 nm and the effect seen in fig 3.2 can be taken to be representative for all these ligands.

Poly(vinyl pyridine) as a ligand does not follow the same simple behaviour in its absorption spectrum. Fig 3.3 shows a strong underlying absorption which peaks well into the near infrared region. This absorption can be attributed to either light scattering due to the polymer or absorption by the polymer.

There is also a general red shift in the Soret band on

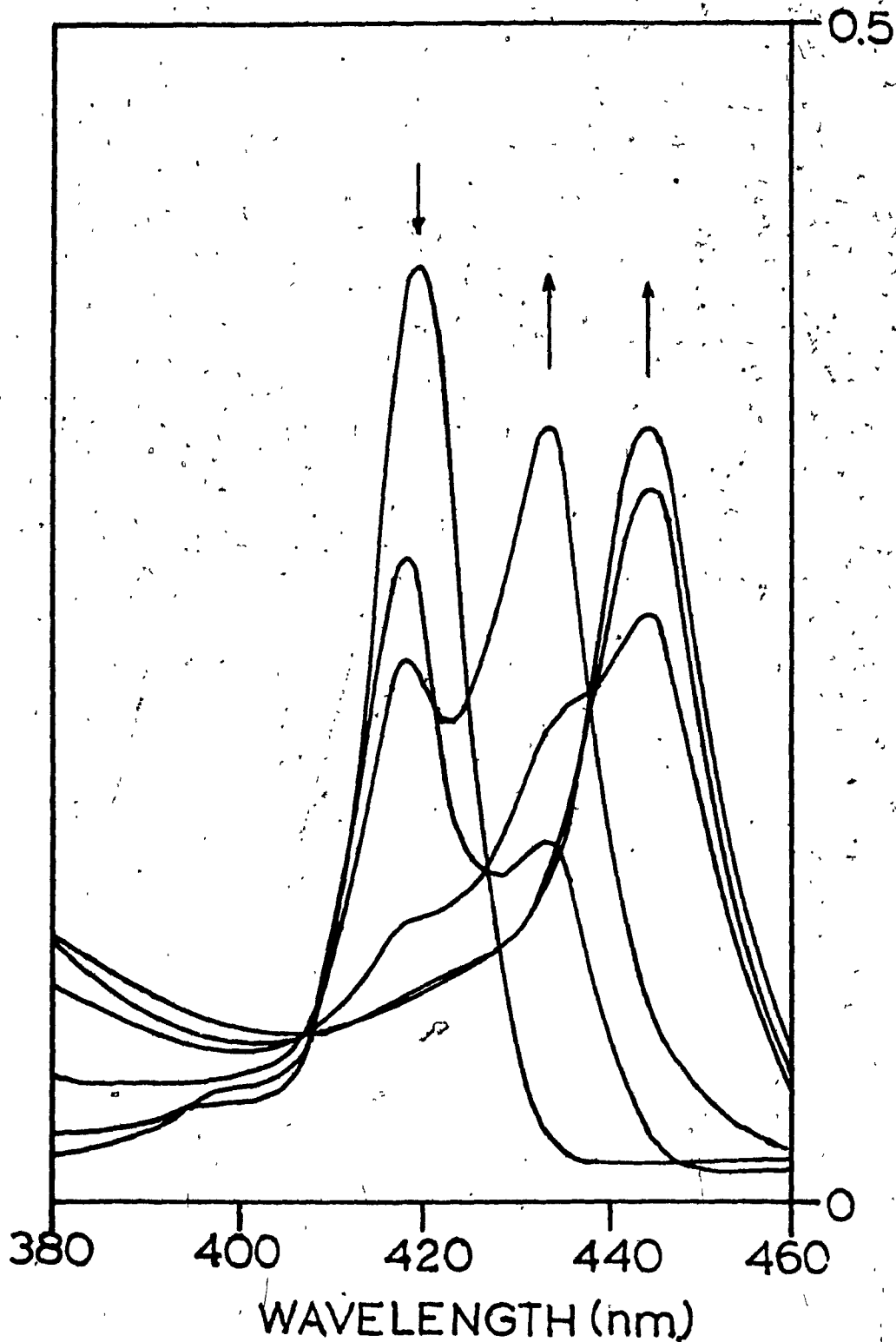
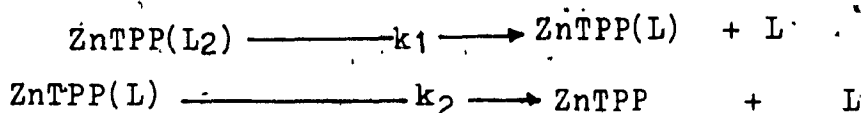


Figure 3.4. Spectrophotometric titration of 0.44 μM ZnTPP in CH_2Cl_2 with 9.0 mM triphenylphosphine in CH_2Cl_2 .

addition of axial ligands. The extent of the red shift will depend on whether the porphyrin is 5 - coordinated or 6 - coordinated. Fig 3.4 shows the spectrophotometric titration of 4.42×10^{-7} M ZnTPP in methylene chloride with 9.0×10^{-3} M PPh₃. The peak maxima are at 419, 433 and 444 nm respectively with isosbestic points at 425 nm and 437 nm. These correspond to the reactions.



For sufficiently dilute solutions of porphyrin ($<10^{-6}$ M) the six coordinate complexes dissociate completely. At high ligand concentration (>0.2 M), the limiting spectrum of the six coordinated species is formed. The data in figure 3.4 can be fitted to the equations

$$\log \frac{[\text{ZnTPP(L}_2\text{)}]}{[\text{ZnTPP(L)}]} = \log(\text{L}) - \log k_1$$

$$\text{and } \log \frac{[\text{ZnTPP(L)}]}{[\text{ZnTPP}]} = \log(\text{L}) - \log k_2$$

by using $(A - A_0)/(A - A)$ to calculate the concentration ratios. Values of k_1 and k_2 calculated for the ligand triphenylphosphine correspond to 0.989 and 0.939 M⁻¹ respectively. Comparing this to the k_{eq} for pyridine as a ligand ($k = 6900 \text{ M}^{-1}$) (22), the large value obtained for triphenylphosphine has been attributed to its lower

basicity, but the factors affecting axial ligation to metalloporphyrins are many and complex.

3.2. PHOTOELECTROCHEMICAL GENERATION OF INTERMEDIATE PORPHYRIN SPECIES IN SOLUTION DURING PHOTOLYSIS.

Figure 3.5 (A) presents the absorption spectra obtained on bulk photolysis of 2.0×10^{-5} M solutions of ZnTPP in CH_2Cl_2 . Tetraethylammonium perchlorate (0.40 M) was used as the electrolyte. The cell arrangement was such that the photolysis took place in a two-compartment cell using the porphyrin dissolved in CH_2Cl_2 with a Pt wire electrode as one half cell and a solution of $\text{Fe}(\text{CN})_6^{3-/4-}$ as the other half cell with another Pt electrode. The two half cells were joined by a salt bridge containing 0.4 M tetraethylammonium perchloride (TEAP) in CH_2Cl_2 . Only the porphyrin half cell was photolysed with white light from a 300 W tungsten halogen lamp. Photolysis was under short circuit conditions.

Bulk photolysis shows the appearance of an isoporphyrin type species (characterized by the strong absorption at 460 nm) after only a few minutes of irradiation. There is also loss of absorption in the Soret band and the Q band in the visible region. The increased absorption at 750 nm with time indicated a concomitant generation of a cationic type porphyrin species. In figure 3.5 (B), where the photolysis half cell contains 4×10^{-5} M pyridine,

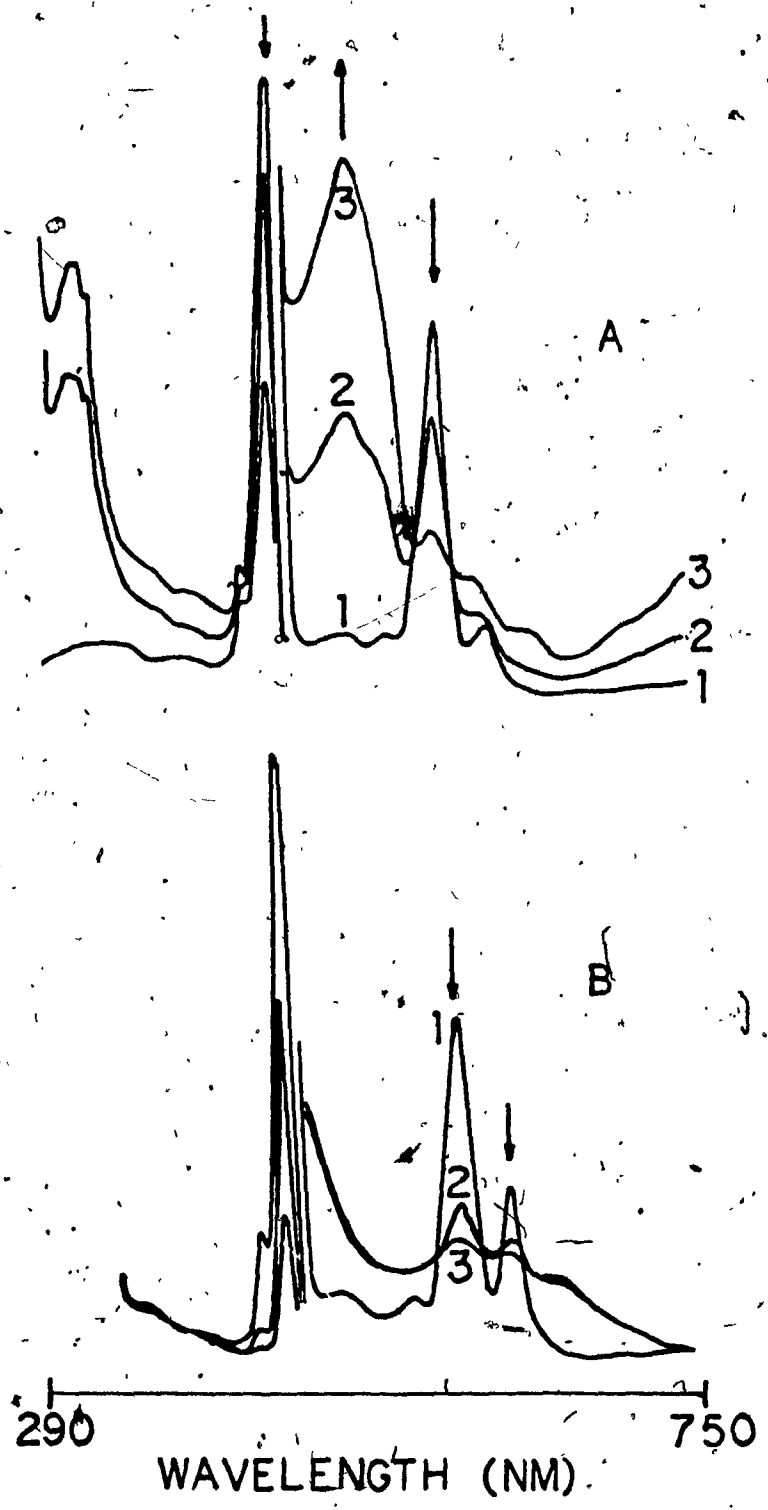


Figure 3.5. Absorption spectra of photolysed solutions in CH₂Cl₂.
(A) ZnTPP at (1) t = 0 min. (2) t = 5 min. and (3) t = 20 min.
(B) ZnTPP in pyridine at (1) t = 0 min. (2) t = 20 min. and (3) t = 120 min.

spectroscopic changes are only observed after a longer period of irradiation. The general change in the original spectrum of ZnTPP is the same i.e. decrease in the Soret, Q and α, β bands. This is followed by the growth of an almost featureless broad absorption in the visible spectrum between 450 nm and 750 nm, and a shoulder on the Soret band between 420 and 450 nm. This spectrum has been identified as the cation radical of the axially ligated porphyrin (33). Similar observations were made for the ligands triphenylphosphine and triphenylarsine.

3.3 ELECTROCHEMISTRY AND SPECTROELECTROCHEMISTRY OF TETRAPHENYLPORPHYRIN AND ZnTPP SOLUTIONS.

3.3.1. Electrochemistry of H_2 TPP with Pyridine.

The experimental conditions were as described in section 2.5.1. Figure 3.6 (A) shows a voltammetric scan at 100 mV/s for the background electrolyte used i.e. 0.1 M NaOCl₄ in the mixed solvent CH₃CN:CH₂Cl₂ (50:50). The working electrode was a Pt plate electrode with a total area of 2 cm². Figure 3.6 (B) is the electrochemical titration of 31.7 mg/50 ml of H₂TPP in the background electrolyte. Titration was with aliquots of a 5% pyridine solution in CH₃CN. The positions of the first (0.65 V) and second (0.84 V) reversible oxidations for H₂TPP is confirmed and corresponds well with the literature values in table 1.2. On addition of pyridine, the second reduction peak at 0.78

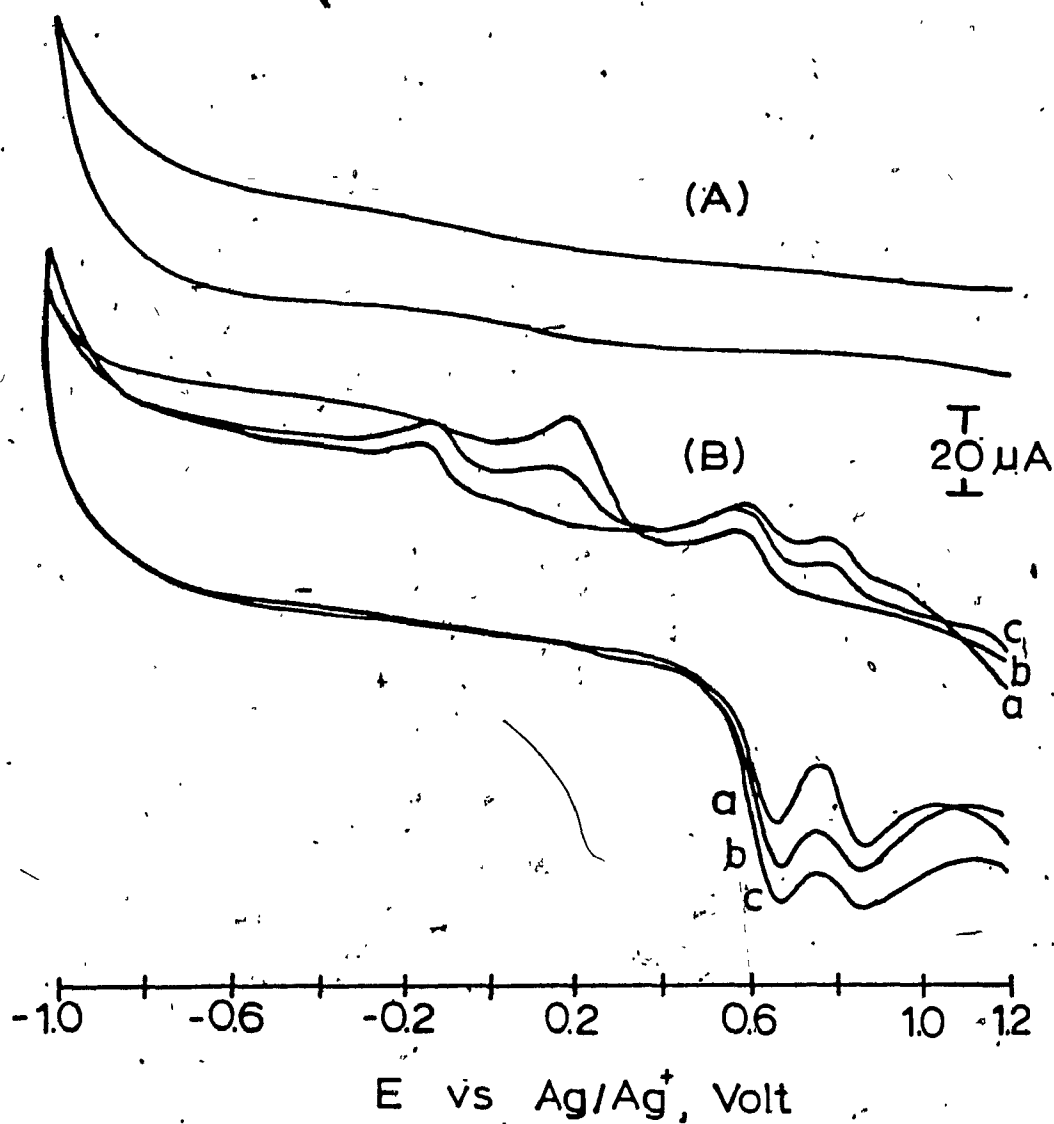


Figure 3.6. Voltammograms of (A) background electrolyte (CH_3CN) and (B) $31.7 \text{ mg}/50 \text{ ml}$ H_2TPP in $\text{CH}_3\text{CN}:\text{CH}_2\text{Cl}_2$ titrated with 10 ul portions of a 5% pyridine solution in CH_3CN . The background electrolyte was 0.1 M NaOCl_4 .

V vs Ag/Ag⁺ disappears with the corresponding formation of a reduction peak at 0.17 V vs Ag/Ag⁺. The oxidation peak currents for both oxidations increase on addition of pyridine. Since no metal site is present for the pyridine to bind to, the origin of the reduction peak at 0.17 V must be associated with a ring substituted porphyrin. Further evidence for this will be seen in the next section.

3.3.2. Electrochemistry of ZnTPP with Pyridine.

Figure 3.7 shows the electrochemical "titration" of 75.1 mg ZnTPP in 50 ml of 0.1 M NaOCl₄ in 50:50 CH₃CN:CH₂Cl₂ with 10% pyridine in CH₃CN. The experimental conditions are the same as that in section 3.3.1. In the absence of pyridine the voltammogram show two quasireversible peaks with E_{1/2} at 0.4 V and 0.75 V vs Ag/Ag⁺. These correspond to the first and second oxidation potentials of the porphyrin and agree well with values listed in table 1.2. As pyridine is added, the two anodic peaks remain observable, but the corresponding reduction peaks at 0.36 and 0.71 V progressively disappear rendering the oxidations irreversible. A new irreversible peak appears near 1.0 V and a reduction peak develops at -0.08 V. Integration of the new reduction feature at -0.08 V indicates that the number of coulombs passed equals the sum of the charge for the two electron oxidation within

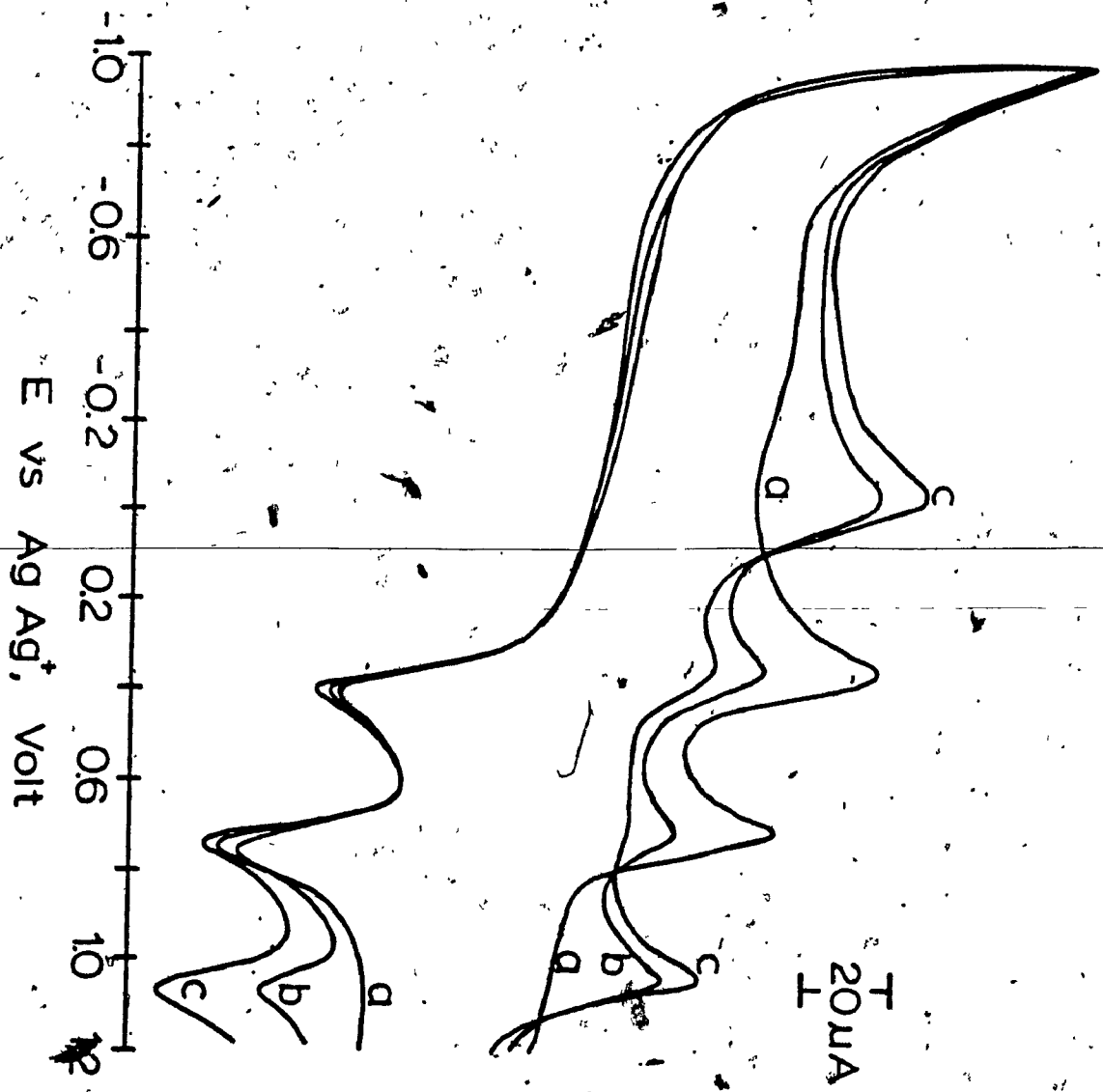


Figure 3.7. Cyclic voltammograms of 75 mg/50 ml of 0.1 M NaOCl₄ in CH₃CN:CH₂Cl₂ titrated with pyridine (5% in CH₃CN) in increments of (a) 0, (b) 10, (c) 30 ul each.

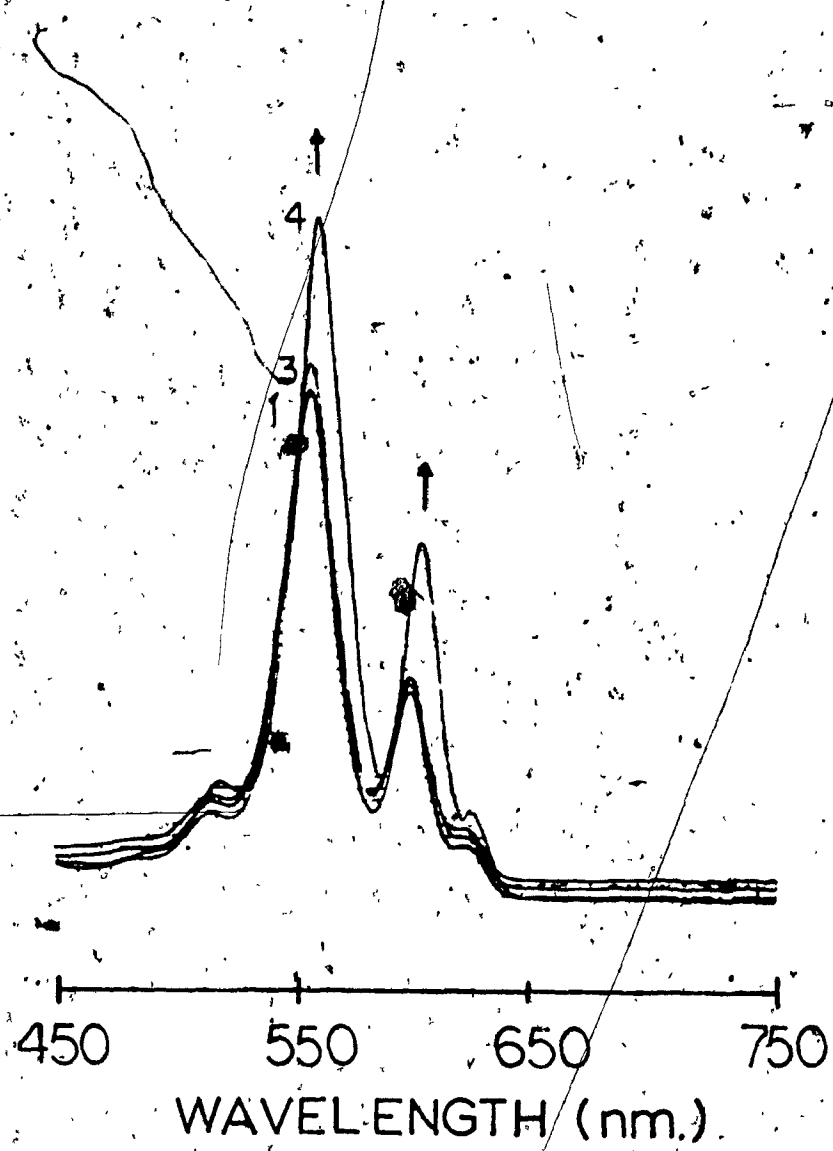


Figure 3.8. Visible absorption spectra of ZnTPP during titration with pyridine. Curves 1 - 3 correspond to the concentrations in figure 3.7. Curve 4 is the spectrum with a slight excess of pyridine.

6.9%. When a slight excess of pyridine over porphyrin is reached, axial ligation of the pyridine to the zinc of the porphyrin takes place as can be seen in spectrum 4 of figure 3.8. This spectrum coincides with voltammogram (C) in figure 3.7. On addition of more pyridine (ie. $> [ZnTPP]$), the reversible peak at 1.0 V declines again accompanied by reduction of the peak at -0.08 V. In fact, with a large excess of pyridine, the voltammogram becomes featureless and resembles the voltammogram of the background electrolyte.

The reversible peak at 1.0 V can be assigned to a ring substituted porphyrin. Ring substitution of the porphyrin only occurs after formation of the very reactive dication species (46, 47). This substituted pyridinium - porphyrin dication can create a cationic site on the quarternized pyridine nitrogen and releases a proton to the solution. This effectively reduces the porphyrin ring and accounts for the absence of reduction waves and the introduction of a new reversible wave at 1.0 V. This new wave may be seen as an analog to the one electron oxidation of the parent porphyrin near 0.36 V. The reduction wave near -0.08 V lie within the reduction region of a quarternized pyridine, which can initiate the two electron reduction in an electrochemical - chemical (EC) mechanism.

The featureless voltammogram obtained at high pyridine concentration can be attributed either to pyridine adsorption on the electrode or to the fact that axial

ligation of the porphyrin reduces the rate of the electron transfer. The titration of H_2TPP in section 3.3.1 seem to follow the same pattern, except that the reversible anodic peaks, at +1.0 V could not be observed clearly since it is shifted outside the measureable potential range.

3.3.3. Electrochemistry of ZnTPP with Polyvinylpyridine (PVP).

Figure 3.9 represents the titration of 40 mg ZnTPP/50 ml of 0.1 M $NaOCl_4$ in 50:50 $CH_3CN:CH_2Cl_2$ with aliquats of a 1% PVP solution in CH_2Cl_2 . (b) and (c) are voltammograms after the addition of 30 ul and 50 ul of PVP respectively. The feature observed for the titration with pyridine is not as evident, but one must keep in mind that the polymer contains a large number of pyridine groups on a single backbone and it is not possible to introduce a nucleophile at the porphyrin periphery without simultaneously putting pyridine groups in favourable positions for axial ligation. The voltammogram at large excess of PVP (not shown) resembles that at large pyridine concentration.

3.3.4. Electrochemistry of ZnTPP with triphenylarsine and triphenylphosphine.

Figures 3.10 and 3.11 are voltammograms for "titrations" similar to those in section 3.3.2 employing

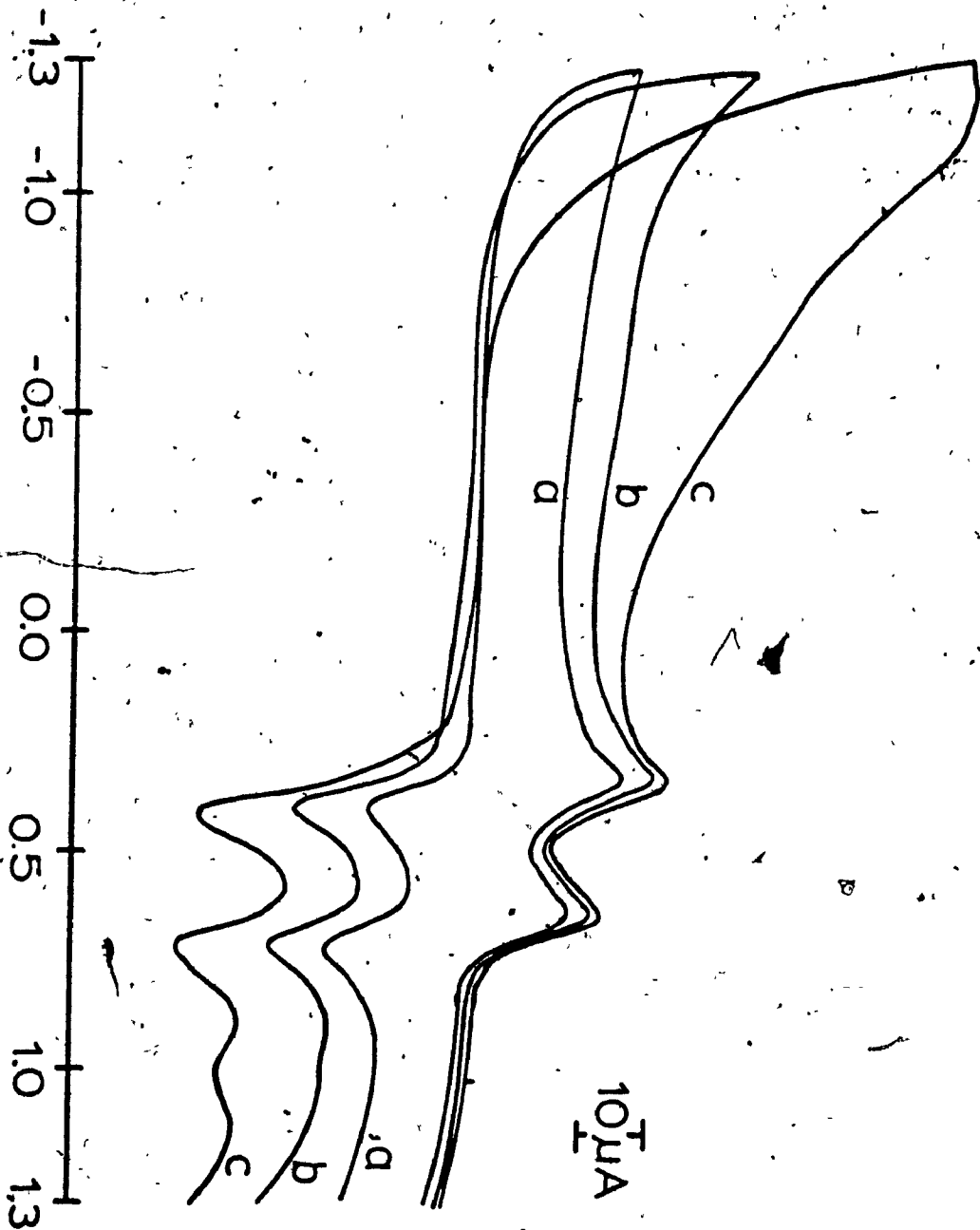


Figure 3.9. Cyclic voltammogram of ZnTPP in CH₂Cl₂:CH₃CN titrated with 2% PVP in CH₂Cl₂ in increments of (a) 0, (b) 10 and (c) 50 μl. Conditions are the same as in figure 3.7.

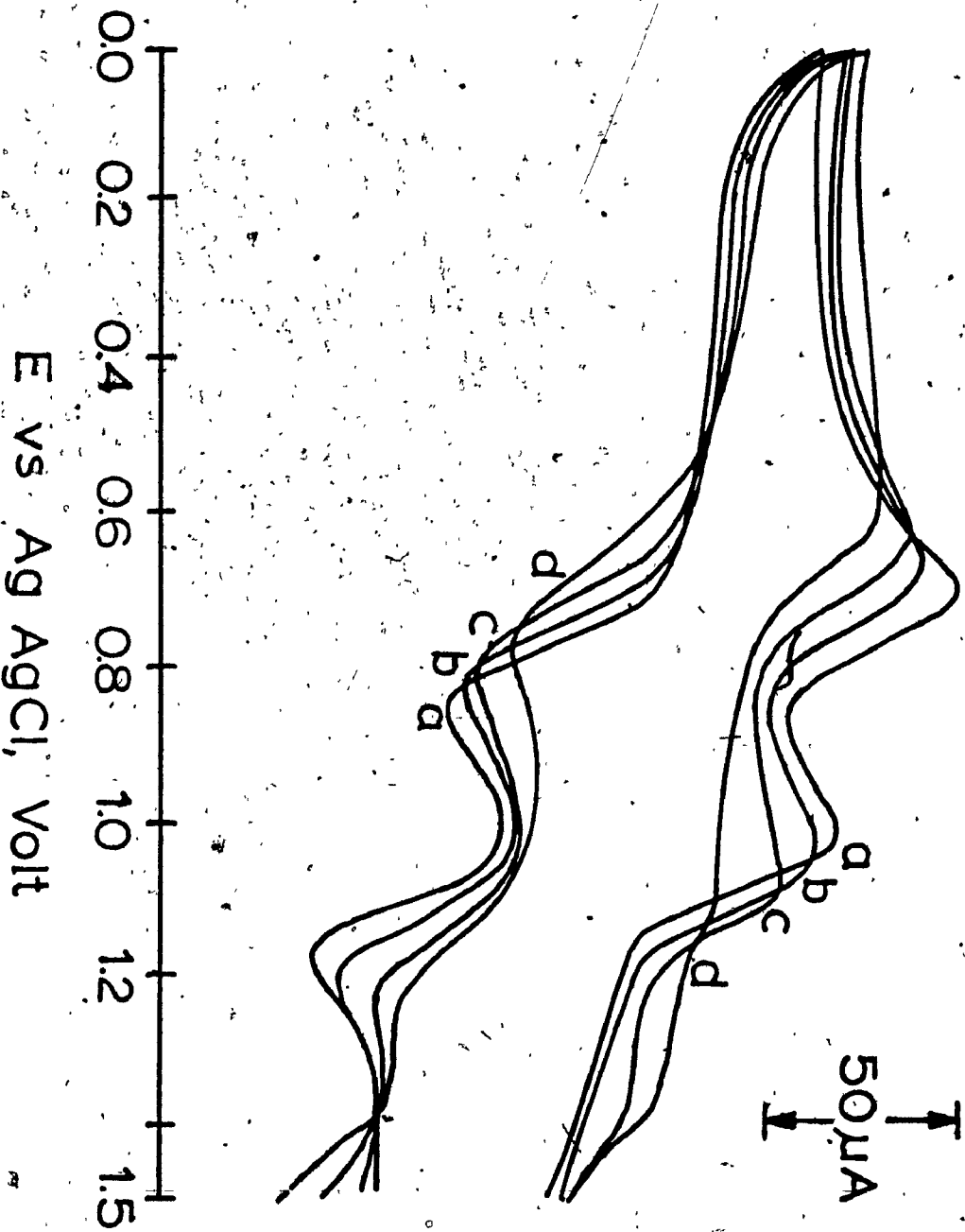


Figure 3.10. Voltammogram of ZnPP in CH_2Cl_2 titrated with 2% triphenylphosphine solution in CH_2Cl_2 . (a), (b), (c) and (d) correspond to aliquots of 0, 10, 30 and 70 μ L, respectively.

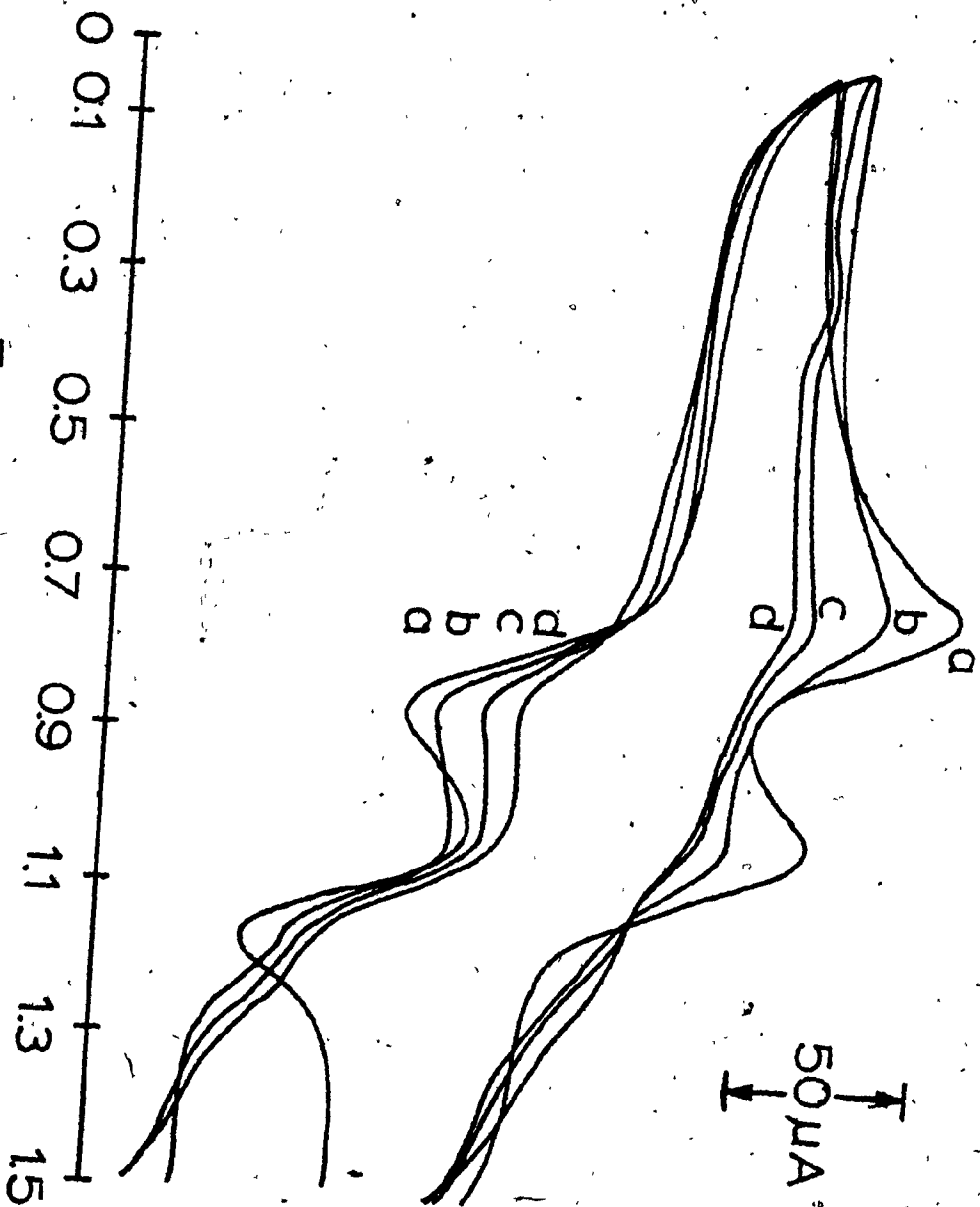


Figure 3.11. Cyclic voltammogram of ZnTPP in CH₂Cl₂ titrated with triphenylarsine in increments of (a) 0, (b) 10, (c) 30 and (d) 50 μl.

triphenylphosphine and triphenylarsine as ligands. The general picture is not as clear as in the pyridine case, but it hints towards a similar interpretation with reduced rates of electron transfer. This is plausible given the lower basicity of triphenylphosphine and triphenylarsine and its greater tendency to ligate axially.

3.4. ABSORPTION SPECTRA AND ELECTROCHEMISTRY OF THIN PORPHYRIN FILMS.

3.4.1. Choice of redox couple and selection of experimental conditions for thin film electrochemistry.

Characterization of thin film modified electrodes are traditionally performed in non - aqueous solvents like acetonitrile. Due to the solubility of the porphyrin films under study in organic solvents, a suitable aqueous redox couple had to be chosen to evaluate the properties of the thin porphyrin films on SnO₂ semiconductor electrodes. Thin semiconducting SnO₂ films on glass have been used as indicator electrodes in various investigations (120). The oxide surface is very sensitive to pH and the kinetics of electron transfer of a simple redox couple like Fe(CN)₆^{3-/4-} can be adversely influenced as seen in figure 3.12. The E_{1/2} of the redox couple Fe(CN)₆^{3-/4-} shifts from anodic to cathodic and back to anodic as the pH is varied between 1 and 13. The E_{1/2} reaches a maximum cathodic value at pH 5. The shift in E_{1/2} with pH can be attributed to protonation

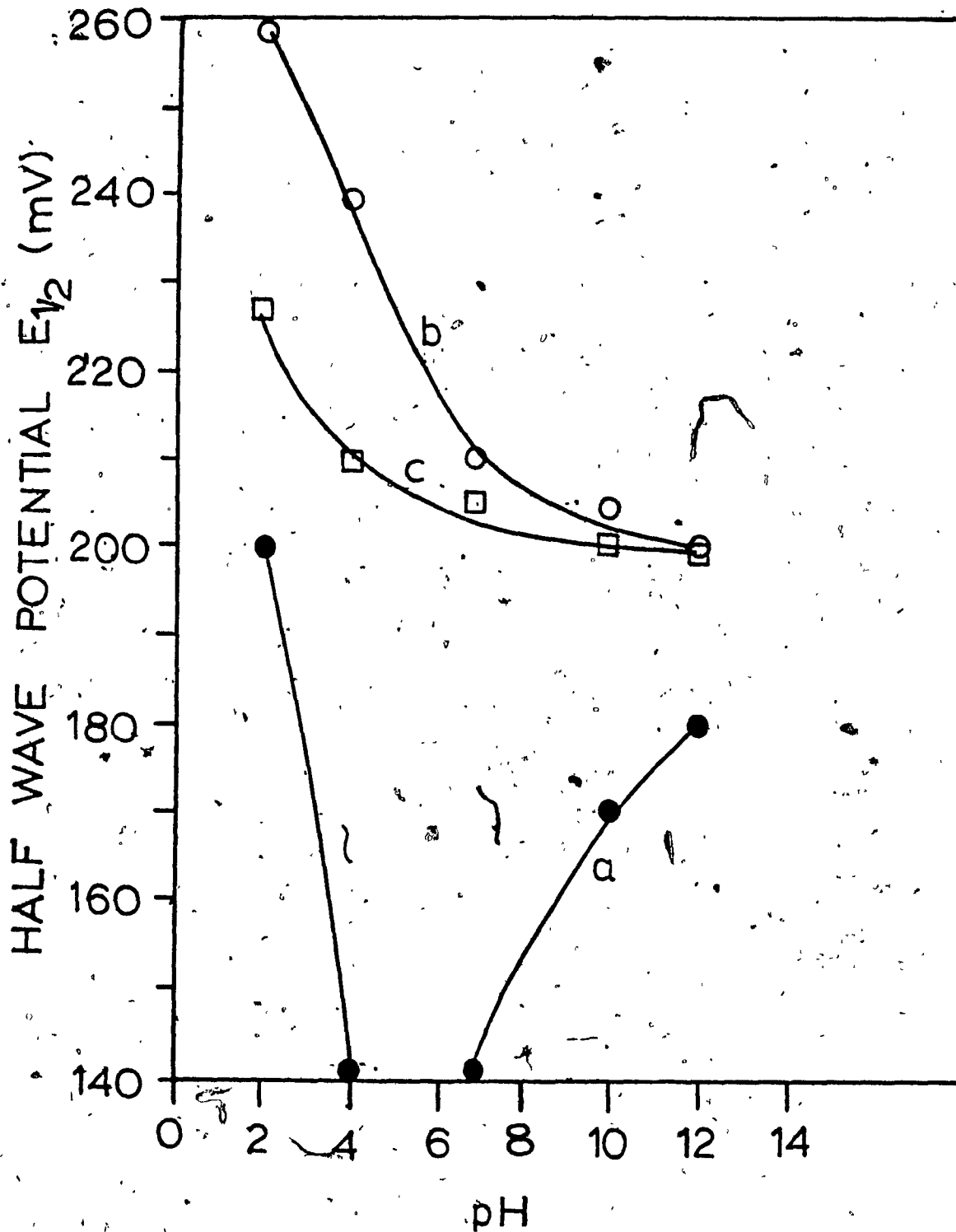


Figure 3.12. Variation of the half wave potential with pH for the couple $\text{Fe}(\text{CN})_6^{3-/4-}$ at the surface of (a) SnO_2 (b) $\text{SnO}_2/\text{ZnTPP-pyridine}$ and (c) Pt.

of the oxide surface. Protonation of $\text{Fe}(\text{CN})_6^{3-/4-}$ can also take place. The variation of the $E_{1/2}$ vs pH curve for $\text{Fe}(\text{CN})_6^{3-/4-}$ on the surfaces Pt (c) and $\text{SnO}_2 / \text{ZnTPP}$ - pyridine (b) are less complex. The anodic shift at low pH for the curve can readily be attributed to protonation effects on the $\text{Fe}(\text{CN})_6^{3-/4-}$ couple.

To be able to evaluate the properties of the porphyrin thin films effectively, the $\text{Fe}(\text{CN})_6^{3-/4-}$ couple in 1 M KCl at pH 7.0 was thus chosen as a working solution for all subsequent experiments, unless otherwise stated.

3.4.2. Absorption spectra of porphyrin thin films on SnO_2 electrodes.

Figures 3.13(a), 3.14(a) and 3.15(a) shows the absorption spectra obtained of thin films of ZnTPP, ZnTPP - pyridine and ZnTPP - triphenylphosphine spin coated onto SnO_2 electrodes. Electrode preparation was performed as outlined in section 2.4.2 and spectra on the disks were obtained as described in section 2.6. The absorption spectra of the porphyrin and modified porphyrin films have the same general features as their respective solution counterparts (section 3.1). The distinct α , β and soret bands are observed. Two significant differences are evident, 1) there is a significant red shift of the entire spectrum in a condensed phase and 2) peak broadening of the soret band accompanied by a large underlying

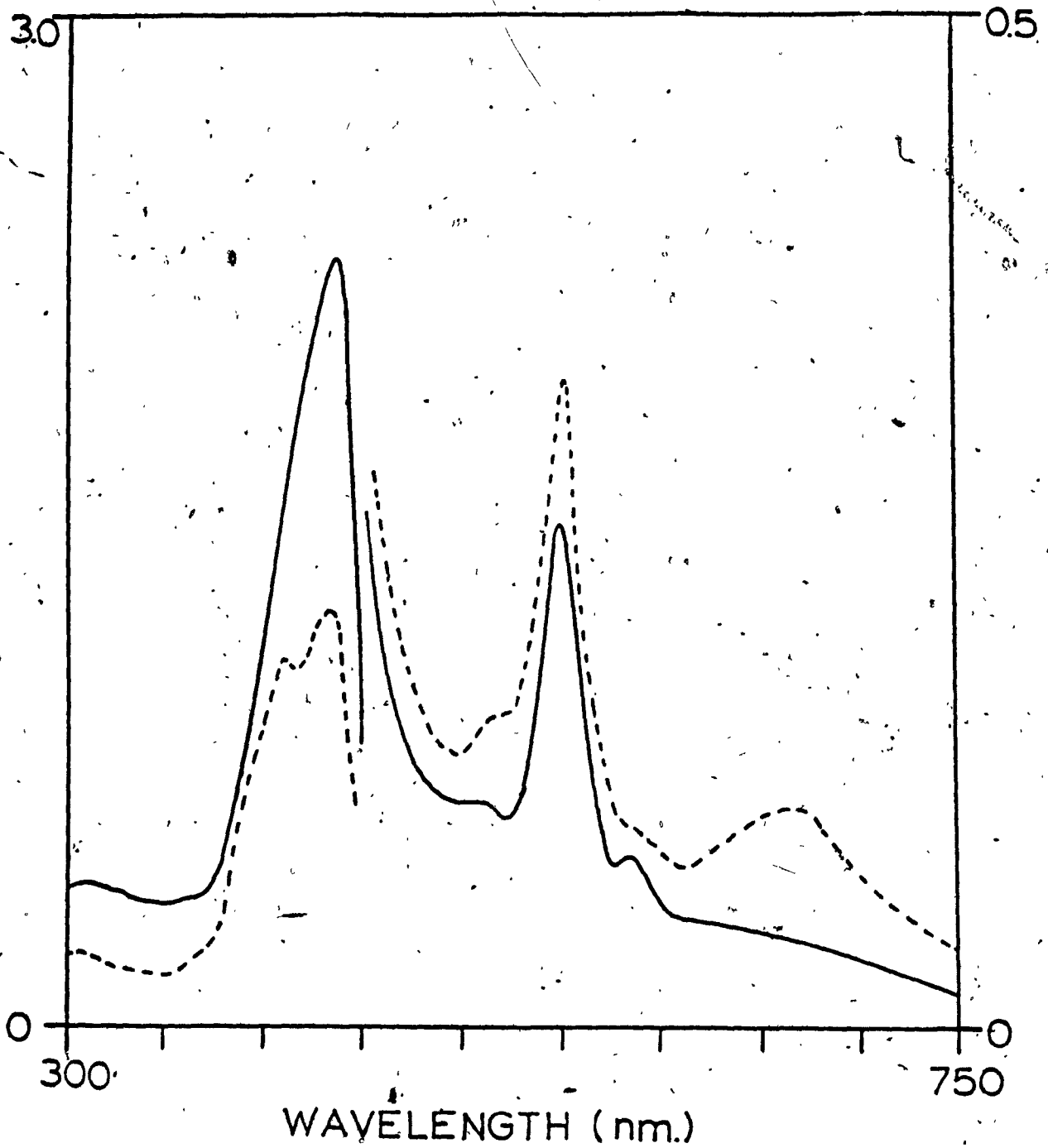


Figure 3.13. Absorption spectrum of ZnTPP films on SnO₂ electrodes (a) before and (b) after electrochemical measurements with the ferri/ferrocyanide couple.

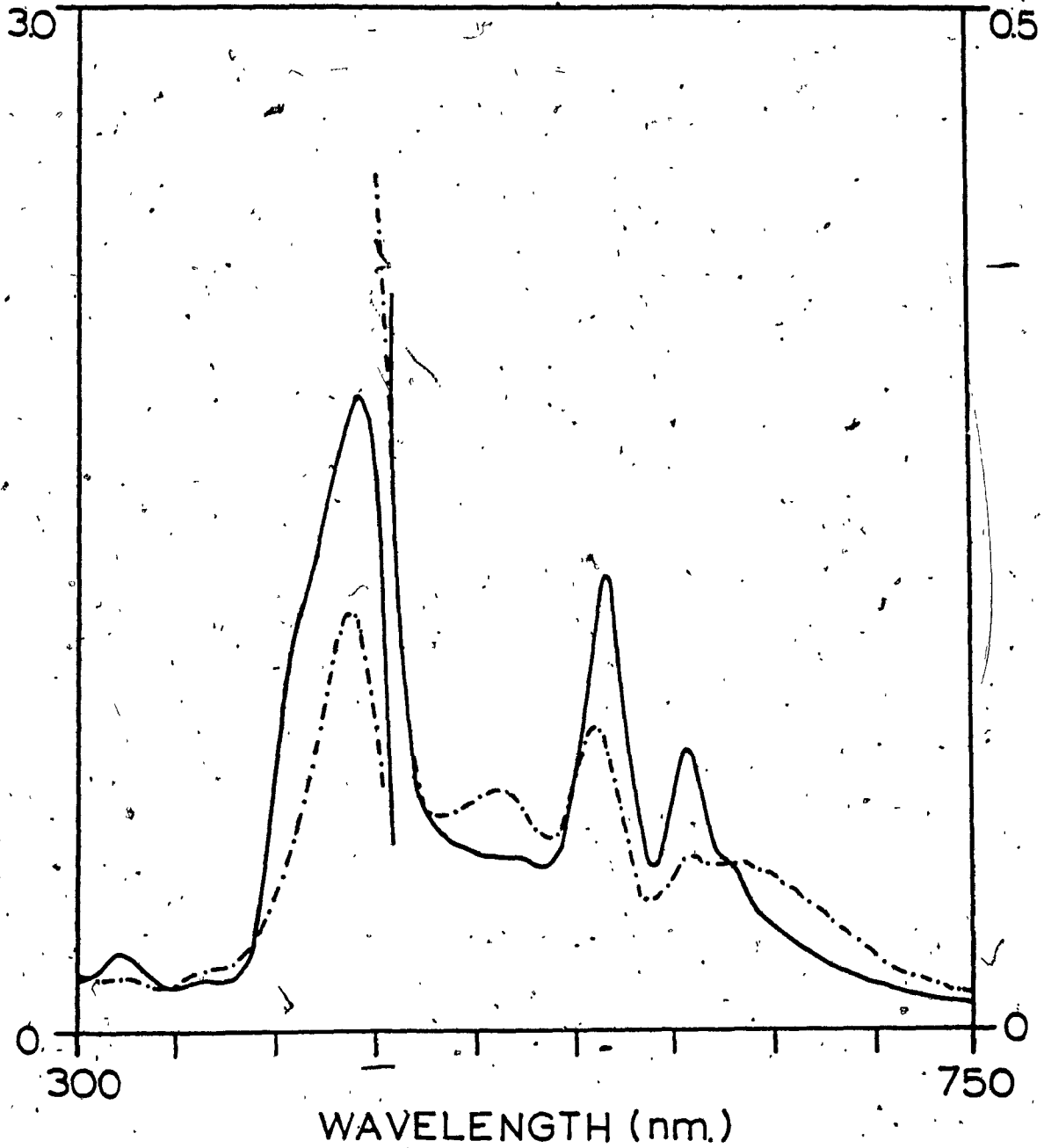


Figure 3.14. Absorption spectra of ZnTPP-pyridine films on SnO₂ electrodes before (a) and (after (b) electrochemistry with the ferri/ferrocyanide couple.

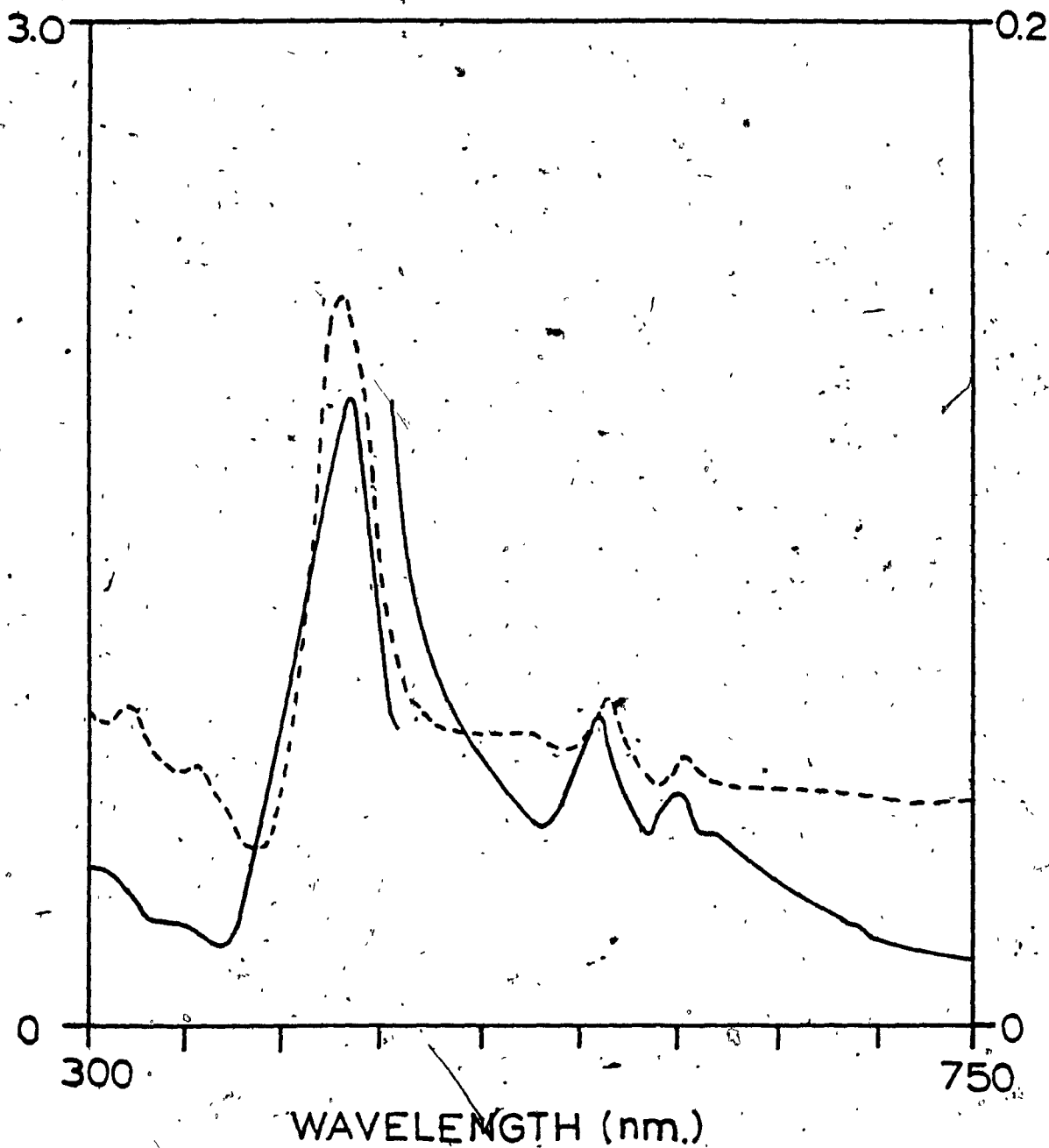


Figure 3.15. Absorption spectra of ZnTPP-triphenylphosphine films on SnO₂ electrodes before (a) and after (b) electrochemistry with the ferri/ferrocyanide redox couple.

absorption in the visible region between 450 nm and 750 nm. The latter can be explained by the effect of scattering or adsorption of the first few monolayers of porphyrin on the SnO₂ surface. The changes occurring in the spectrum after electrochemistry and photoelectrochemistry will be more fully treated in section 3.5.2.

3.4.3. Electrochemical effect of modifying the SnO₂ surface with porphyrin and axially ligated porphyrin.

Figures 3.16 and 3.17 shows the current voltage relationships of 2mM Fe(CN)₆^{3-/4-} in 1.0 M KCl, when in contact with the different surfaces. Experimental conditions are as outlined in section 2.5.1. In figure 3.16(a), the Fe(CN)₆^{3-/4-} couple shows quasireversible behaviour when in contact with bare SnO₂ with a difference between E_p^c and E_p^a as 270 mV. When the SnO₂ electrode is modified with ZnTPP, there is a dramatic decrease in anodic and cathodic peak currents and peak broadening is observed as in 3.16(b). The ΔE is difficult to estimate but is > 300 mV. On modifying the SnO₂ electrode with ZnTPP - pyridine, voltammogram (c) is obtained. The quasireversible behaviour of the Fe(CN)₆^{3-/4-} couple seen in (a) and (b) is replaced by a reversible voltammogram (E = 105 mV) and anodic and cathodic peak currents which are slightly higher than those on the SnO₂ surface. This behaviour of the SnO₂ / ZnTPP - pyridine electrode suggest

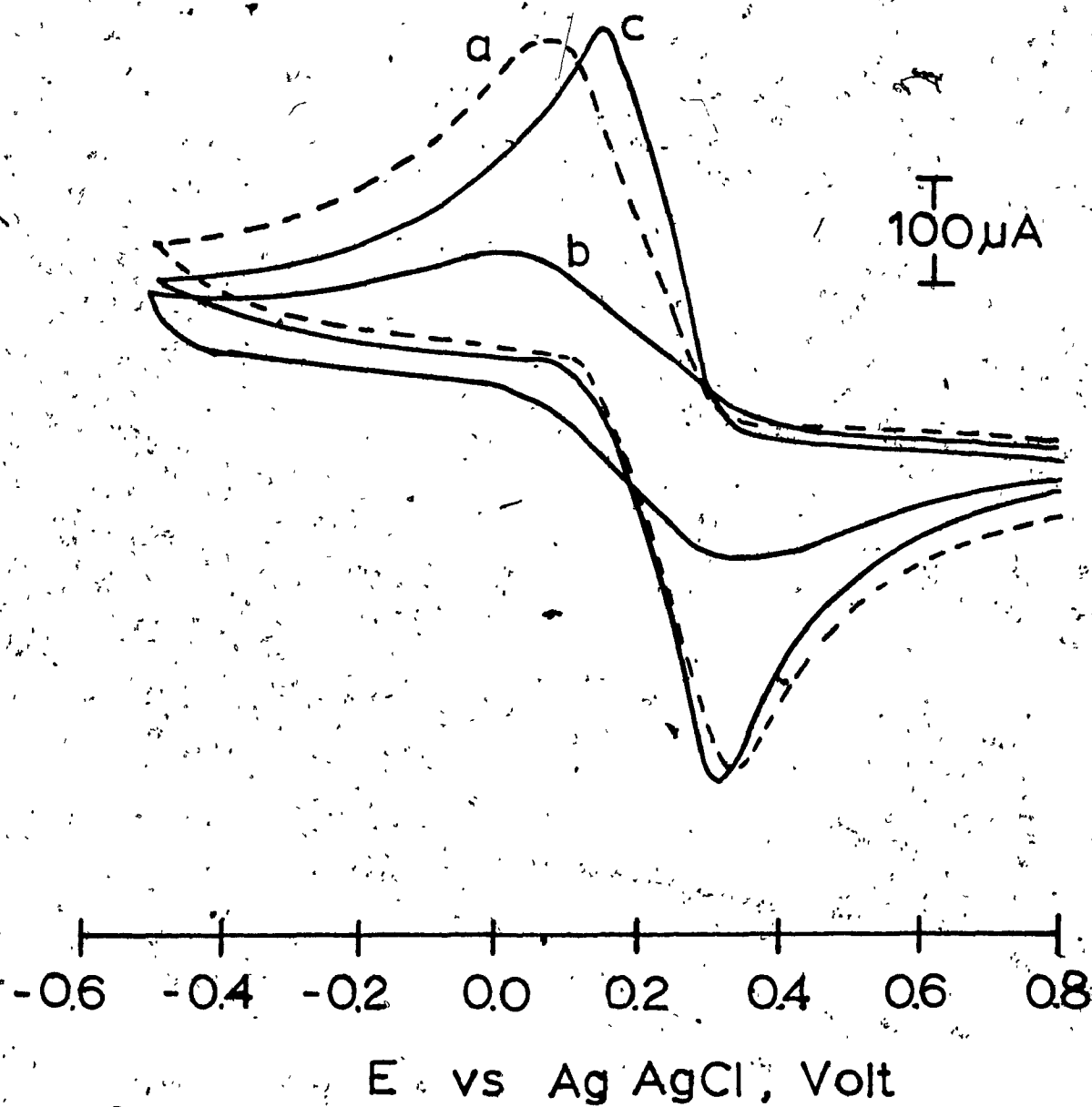


Figure 3.16. Voltammogram of $\text{Fe}(\text{CN})_6^{3-/4-}$ on (a) SnO_2 (b) $\text{SnO}_2/\text{ZnTPP}$ and (c) $\text{SnO}_2/\text{ZnTPP}$ -pyridine electrodes.

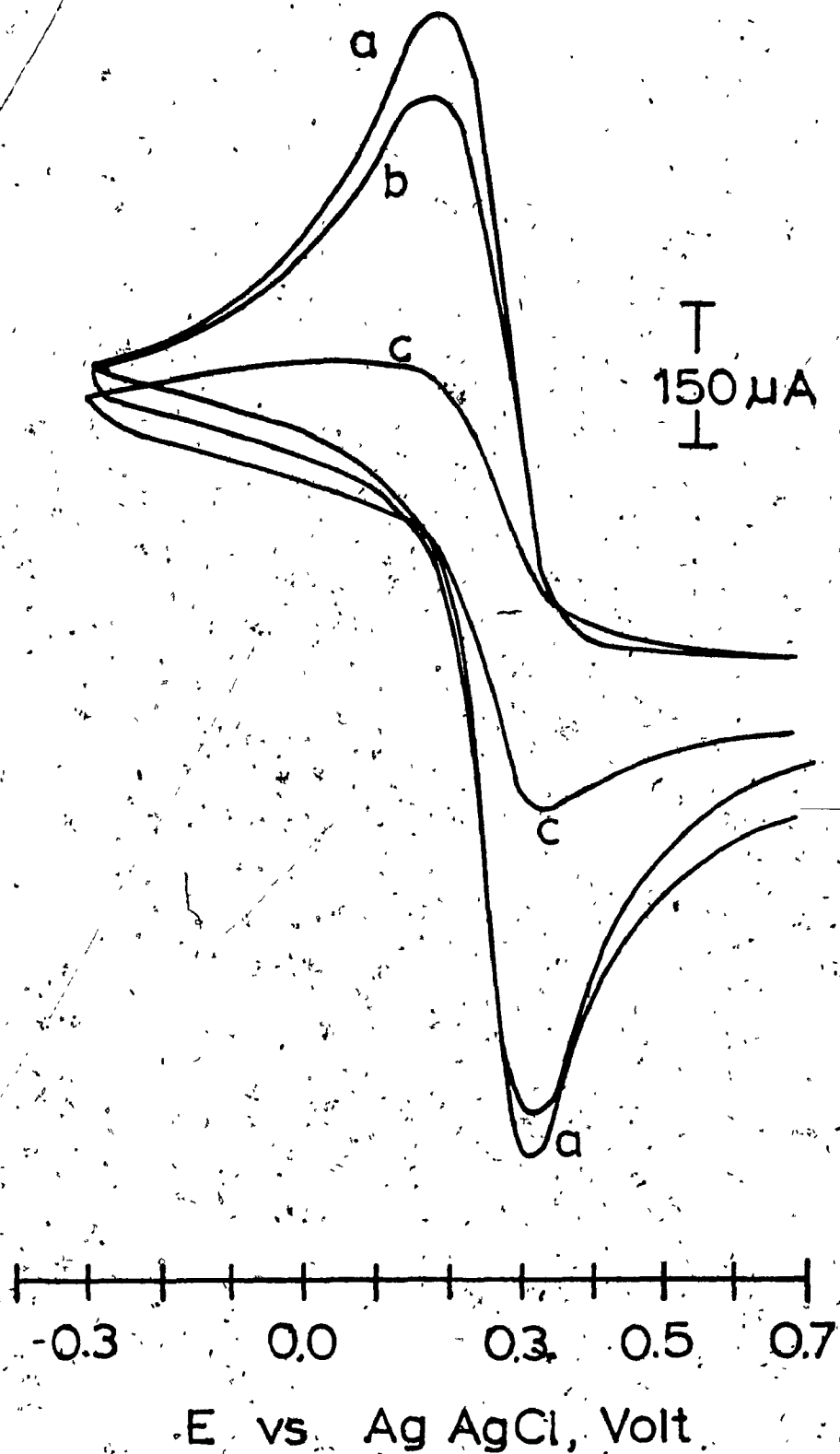


Figure 3.17. Voltammogram of $\text{Fe}(\text{CN})_6^{3-/4-}$ on (a) SnO_2 , (b) $\text{SnO}_2/\text{ZnTPP}$ -Triphenylphosphine and (c) $\text{SnO}_2/\text{ZnTPP}$ -PVP electrodes.

enhanced catalytic effects. The large peak broadening observed for (b) is due to the increased resistivity of the ZnTPP coating in SnO₂ electrode.

In figure 3.17, similar effects are observed as that for SnO₂ / ZnTPP - triphenylphosphine and SnO₂ / ZnTPP - PVP.

3.4.4. Heterogeneous electron transfer kinetics of Fe(CN)₆^{3-/4-} at SnO₂ and ZnTPP modified electrodes.

The electron transfer rate of the Fe(CN)₆^{3-/4-} couple on a Pt surface is well known and it follows simple quasi-reversible kinetics. To understand all factors involved in producing the change in voltammograms with surface modification, it is necessary to determine the electron transfer rate of Fe(CN)₆^{3-/4-} on each modified surface and to compare it with the rate of the couple on Pt.

This heterogeneous rate constant for electron transfer can be calculated from cyclic voltammetric studies. The potential dependence of the rate constant for a forward electron transfer $k(E)$, is given by the conventional expression (106).

$$k(E) = k_s \exp [(\alpha_a n F / RT)(E - E^0)] \quad 3.3$$

where E is the electrode potential, α_a = the transfer coefficient, n the number of electrons and E^0 the standard potential.

The solution of a system of differential equations by

Nicholson and Shain (119) predicts a current peak at the applied voltage as

$$E_p = E^0 + (RT/\alpha_a nF)(0.78 + \ln(D\alpha_a nFv/RT))^{1/2} - \ln k_s \quad 3.4.$$

Algebraic rearrangement of equation 3.4 followed by comparison with equation 3.3 gives equations 3.5 and 3.6.

$$k_s \exp[(\alpha_a nF/RT)(E_p - E^0)] = 2.18[D\alpha_a nFv/RT]^{1/2} \quad 3.5.$$

$$k(E_p) = 2.18(D\alpha_a nFv/RT)^{1/2} \quad 3.6.$$

For a totally reversible process, the electron transfer rate constant at the peak potential $k(E_p)$ is directly related to the sweep rate v . From eqns 3.3 and 3.6, then;

$$k_s = 2.18[D\alpha_a nFv/RT]^{1/2} \exp[(\alpha_a nF/RT)(E - E_p)] \quad 3.7.$$

By substituting for all the constants, assuming the same approximations for α_a as in (122) and D as in (123) i.e. $nF/RT = 39.2$ mole eq^{-1} volt $^{-1}$, $\alpha = 0.25$, $D_{ox}/D_{red} = 1/1.21$, an equation is obtained which is dependent only on the heterogeneous rate constant, the scan rate, and the difference between the cathodic and anodic peak potential.

$$k_s = 1.7197 \times 10^{-2} v^{1/2} \exp[-2.45 \Delta E] \quad 3.8.$$

where $\Delta E = E_p^c - E_p^a$, the difference between the cathodic

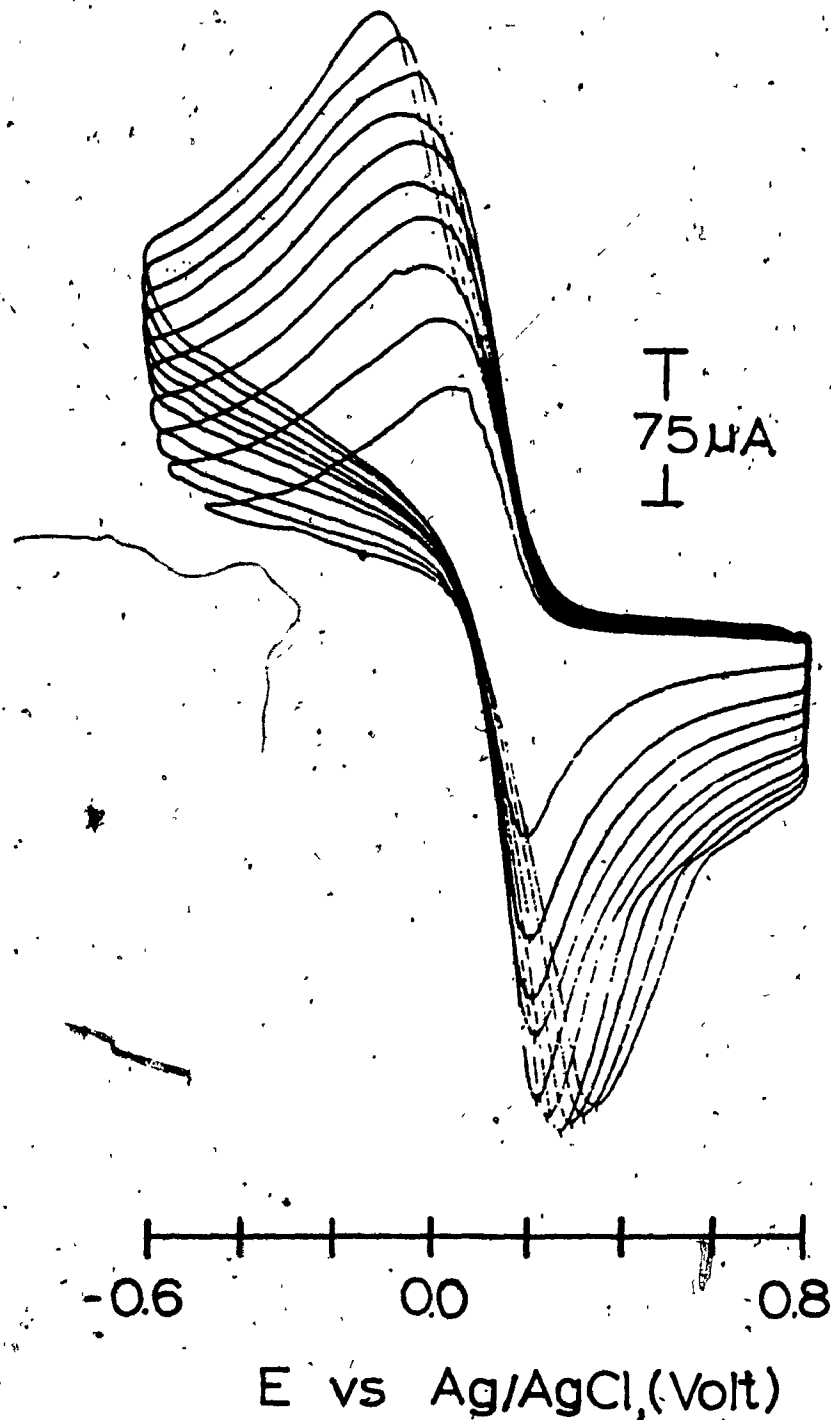


Figure 3.18. Voltammograms for the $\text{Fe}(\text{CN})_6^{3-/4-}$ couple at SnO_2 electrode. Scan rates vary from 1 mV/s to 100 mV/s.

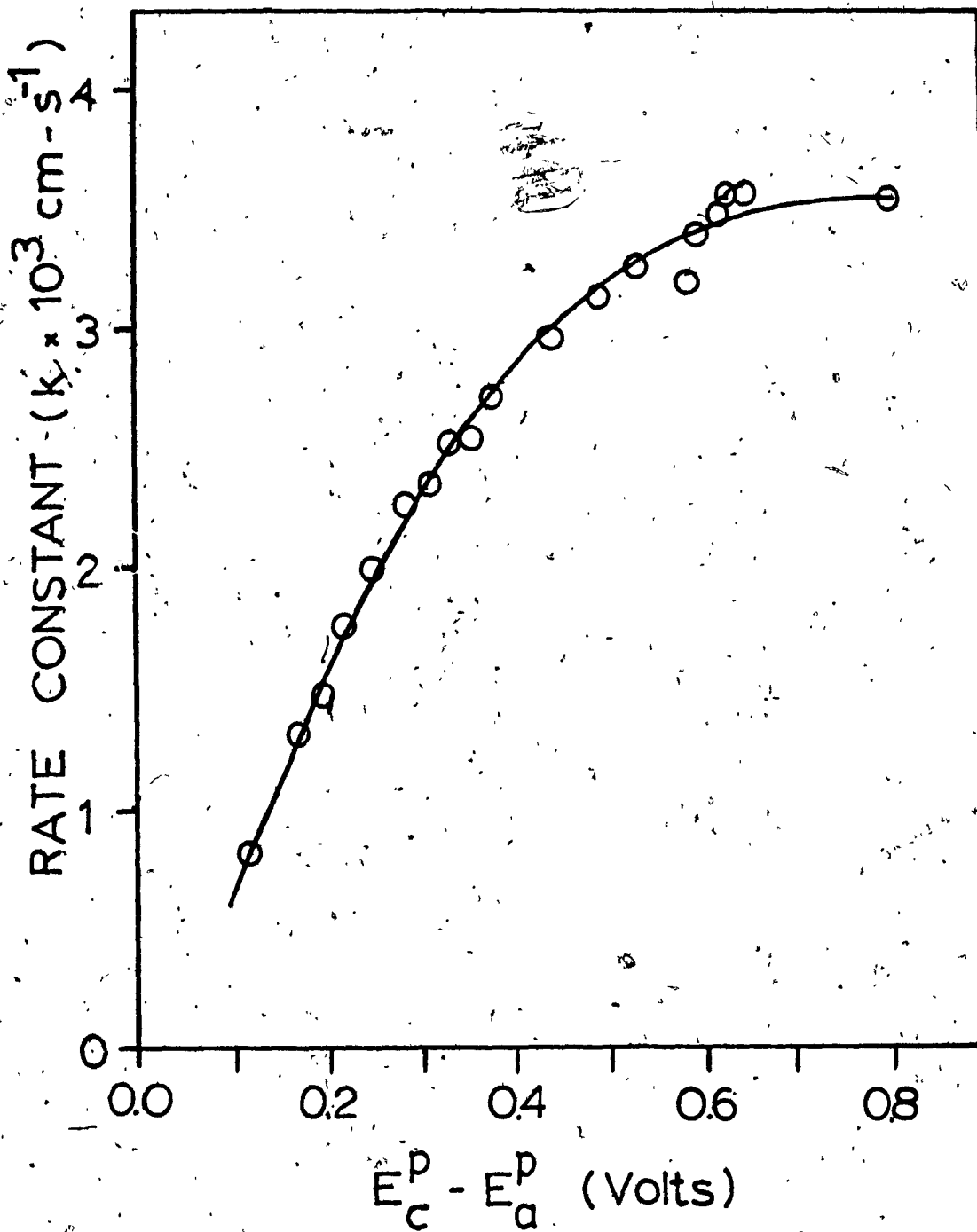


Figure 3.19. Variation of the rate constant with change in peak potential for the $\text{Fe}(\text{CN})_6^{3-/4-}$ couple on SnO_2 .

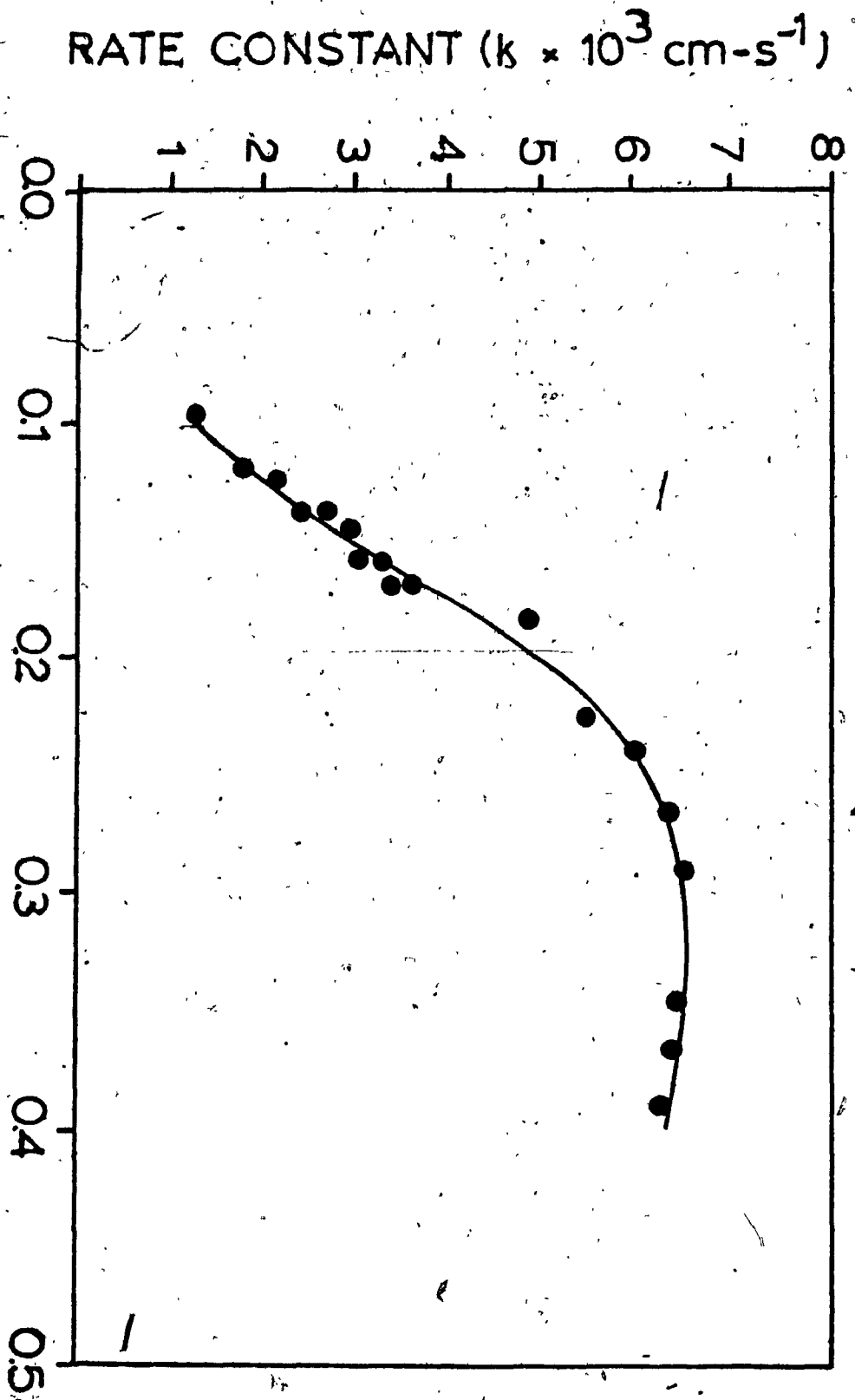


Figure 3.20. Variation of the rate constant with change in peak potential for the $\text{Fe}(\text{CN})_6^{3-/4-}$ couple on $\text{SnO}_2/\text{ZnTPP}$ -pyridine surface.

and anodic peak potentials. For very large sweep rates, the k_s becomes independent of ΔE and this represents the limiting k_s for that reaction.

Figure 3.18 depicts the voltammograms observed for the $\text{Fe}(\text{CN})_6^{3-}/4-$ couple in 1.0 M KCl on varying the scan rate between 1mV/sec and 100 mV/s at the SnO_2 electrode. Similar scans were done for all the other modified electrodes and figure 3.18 can be taken as representative. The ΔE and the peak currents increase with increasing scan rate for all the electrodes. At sufficiently high scan rates (>1000 mV/s), the peak currents and ΔE does not change further, signifying that the limiting rate of electron transfer has been reached. At these high scan rates, the rate of change in the potential exceeds the rate of the electron transfer and no changes in the voltammograms are observed.

By using eqn. 3.8, the value of k_s can be calculated at each scan rate. Figures 3.19 and 3.20 are shown as plots of the rate constant k_s vs the peak separation for the different scan rates. Figure 3.19 is for the same SnO_2 electrode used in Figure 3.18 and figure 3.20 is for a $\text{SnO}_2/\text{ZnTPP}$ - pyridine electrode. The limiting behaviour observed for the value of k_s in each figure represents the heterogeneous electron transfer rate constant of $\text{Fe}(\text{CN})_6^{3-}/4-$ at that surface. For SnO_2 , k_s is 3.53×10^{-3} cm/s and for $\text{SnO}_2/\text{ZnTPP}$ - pyridine, k_s is 6.5×10^{-3} cm/s. Results for other electrodes obtained in a similar fashion are summarized in table 3.1. The reversible

TABLE 3.1

Rate constants of the $\text{Fe}(\text{CN})_6^{3-/4-}$ couple on the different electrode surfaces.

Electrode	Rate constant $10^3 \text{ks} / \text{cm s}^{-1}$	Corrected rate constant
Pt	10.20	
SnO_2	3.53	
$\text{SnO}_2\text{-ZnTPP}$	5.46	9.10 (260)
$\text{SnO}_2\text{-ZnTPP-Pyridine}$	6.5	11.80 (154)
$\text{SnO}_2\text{-ZnTPP-Triphenylarsine}$	5.0	11.90 (148)

() = anodic and cathodic peak potential difference at "zero" thickness.

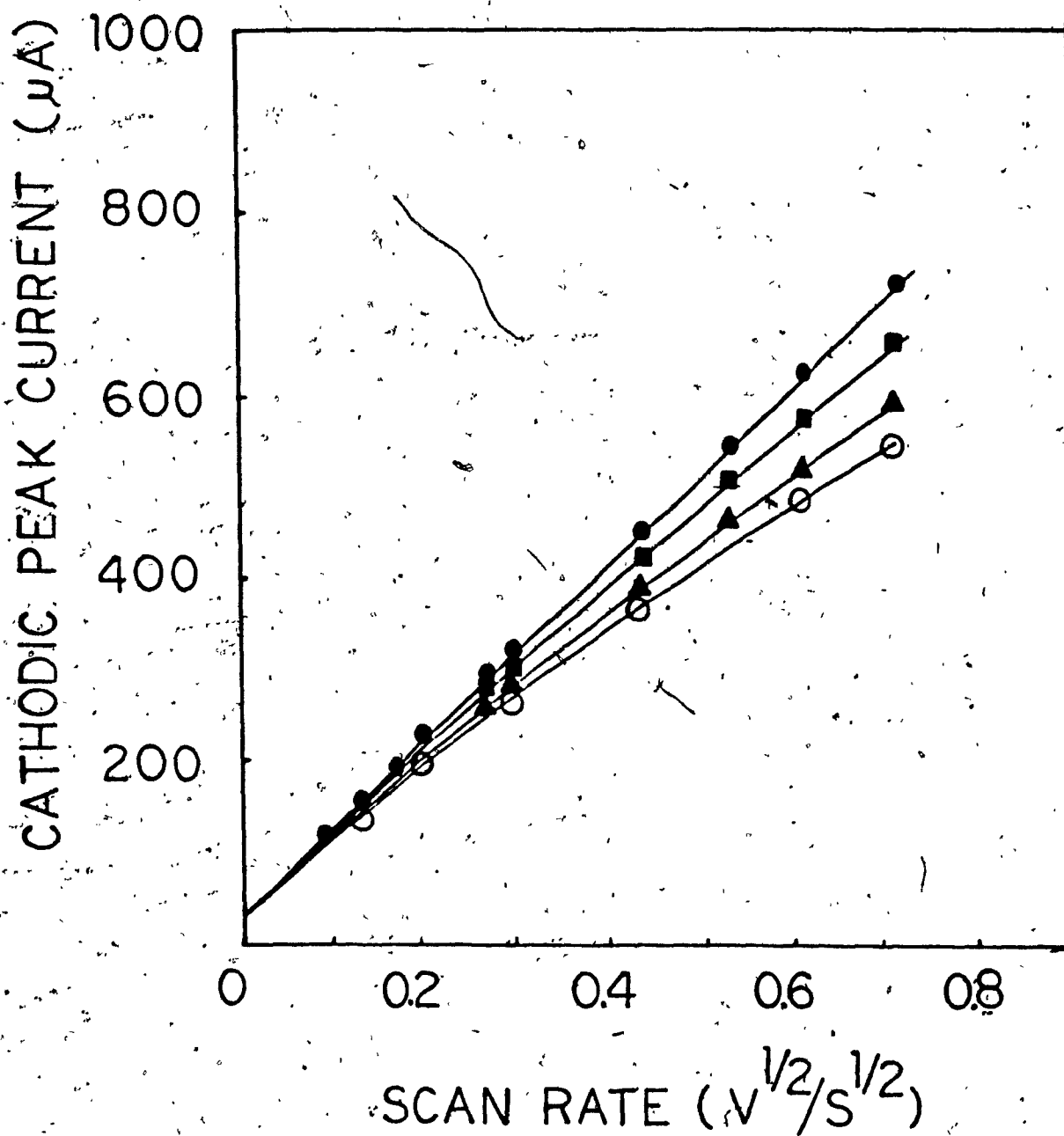


Figure 3.21. Peak current vs. scan rate dependence of $\text{Fe}(\text{CN})_6^{3-}$ on different surfaces.

(a) SnO_2 (b) $\text{SnO}_2/\text{ZnTPP}$ -pyridine (c) $\text{SnO}_2/\text{ZnTPP}$ -triphenylphosphine and (d) $\text{SnO}_2/\text{ZnTPP}$.

electron transfer rate on the Pt surface was confirmed. Values for the porphyrin modified electrodes show higher rates than on the base SnO₂ surface, but lower rates than on Pt. The lower values of k_s for the porphyrin modified electrodes compared to Pt can be attributed to resistive effects of the porphyrin thin films. When a correction is made for the thickness of the porphyrin film, the rate constants obtained are in good agreement with that obtained on the Pt surface. This indicates a catalytic effect on modification of the SnO₂ surface with porphyrins.

The plots of peak current vs the scan rate $V^{1/2}$ for the modified surfaces are shown in figure 3.21. The slopes of the curves are all linear showing that the reaction of Fe(CN)₆^{3-/4-} obey the Randles - Sevcik equation (106). Apparent diffusion coefficients obtained from these plots are all within the experimental limit of the diffusion coefficient for Fe(CN)₆^{3-/4-} in aqueous solution and an ionic strength of 1.0 M KCl. The values for D_{red} calculated are between 0.5 and 1 x 10⁻⁵ cm²/sec.

3.4.5. Effect of porphyrin film thickness on dark electrochemistry.

Tables 3.2, 3.3, 3.4 and 3.5 summarize the results of the electrochemical effect of varying the thickness of the porphyrin film on the SnO₂ electrode. In all cases, the

TABLE 3.2

ELECTROCHEMICAL PROPERTIES OF $\text{SnO}_2/\text{ZnTPP}$ ELECTRODES

No	Porphyrin conc. $\text{mol dm}^{-3} \times 10^5$	Film thickness A	Light absorbed (1 - T)	E_c , mV	E_a , mV	E, mV	i_c , μA	i_a , μA	J_{ph} , μA
1	0.15	100	0.067	50	310	260	370	390	0.40
2	0.20	130	0.088	40	340	300	350	340	0.65
3	0.55	360	0.224	0	340	340	330	300	1.40
4	0.70	470	0.276	-15	340	355	320	266	1.60
5	0.75	510	0.292	-25	360	385	318	260	1.75
6	2.05	1400	0.620	-175	385	560	252	105	3.75
7	2.40	1620	0.676	-200	395	595	265	70	3.80

TABLE 3.3

ELECTROCHEMICAL PROPERTIES OF $\text{SnO}_2/\text{ZnTPP-PYRIDINE}$ ELECTRODES.

No. Porphyrin conc'n. mol dm ⁻³ x 10 ⁵	Film thick. A	Light abs. (I-T)	E _c mV	E _a mV	E _{ic} mV	i _a uA	i _{ph} uA		
1	0.25	170	0.149	130	315	185	375	400	2.30
2	0.30	200	0.168	115	310	195	430	470	2.30
3	0.40	260	0.224	100	325	225	481	506	2.30
4	0.50	340	0.276	115	330	215	206	200	2.35
5	0.55	370	0.308	120	335	215	125	88	2.40
6	0.70	470	0.354	100	335	235	163	156	4.35
7	2.50	1690	0.743		>315				2.55

TABLE 3.4.

Electrochemical properties of SnO₂/ZnTPP - Triphenylarsine electrodes

Electrode Number	Porphyrin conc. mol/dm ³ 10 ⁵	Light absorbed (1-T)	E _c mV	E _a mV	E mV	I _c μA	I _a μA	Photo-current μA
1	1.00	0.437	130	340	210	395	395	0.65
2	1.30	0.527	190	320	130	430	440	0.75
3	1.40	0.553	180	330	150	450	460	0.95
4	2.60	0.776	180	320	140	395	425	0.75
5	2.70	0.789	150	320	170	376	442	0.80
6	2.75	0.795	160	330	170	328	370	0.80
7	4.50	0.925	150	320	170	---	---	0.75

TABLE 3.5.

Electrochemical properties of SnO₂/ZnTPP-PVP electrodes.

Electrode number	Porphyrin conc. mol/dm ³ 10 ⁵	Light absorbed (1-T)	E _c mV	E _a mV	E mV	I _c μA	I _a μA	Photo-current μA
1	0.40	0.127	-	-	-	-	-	0.61
2	0.45	0.141	165	330	165	20.8	18.8	0.70
3	0.49	0.153	180	335	155	50.8	48.5	0.80
4	1.33	0.360	135	350	215	67.3	61.5	0.66
5	0.29	0.029	160	320	160	50.0	44.0	0.50
6	1.42	0.380	160	360	200	37.5	36.3	1.09
7	14.6	0.993	-	-	-	-	-	1.60
8	11.96	0.982	185	300	115	1.4	2.1	1.58
9	16.8	0.997	175	315	140	5.6	5.6	1.72

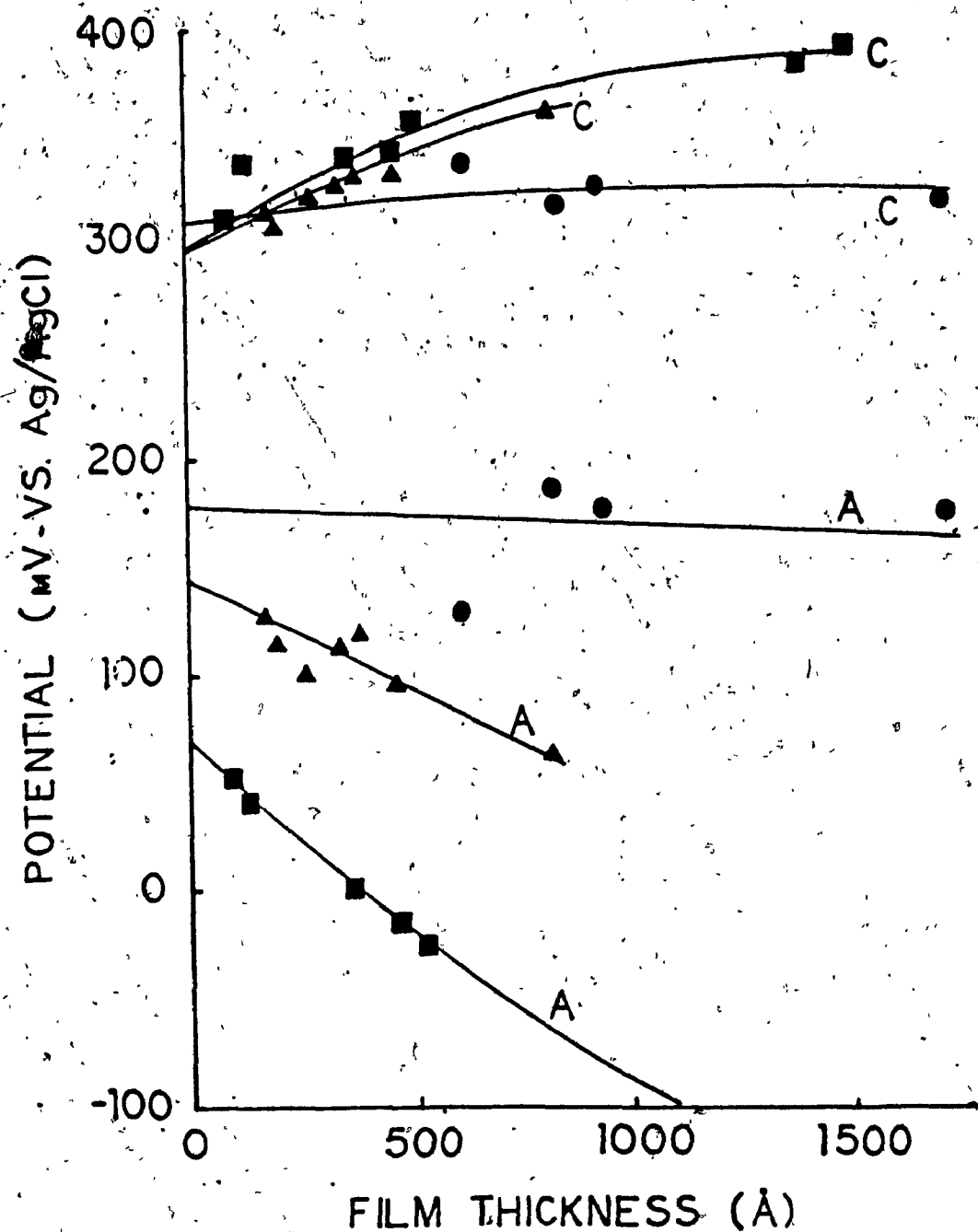


Figure 3.22. Variation of dark potentials with film thickness for the electrodes (■) ZnTPP, (▲) ZnTPP-pyridine, (●) ZnTPP-triphenylphosphine. (A) = anodic and (C) = cathodic.

effect is such that considerable peak broadening occurs in the voltammogram as the porphyrin film thickness increase. There is also a general decrease in both the anodic and cathodic peak currents. For the electrodes SnO₂/ZnTPP in table 3.2, the shift of cathodic and anodic peak potentials are larger than for the other modified electrodes in tables 3.3 and 3.4. Figure 3.22 shows the variation of dark potentials with film thickness for the different electrodes. The large peak separation and lower currents with increasing film thickness is attributed to the increase in resistance of the film with increase in film thickness. This is not surprising since the organic porphyrin molecule is more of an insulator than a conductor. The porphyrins have been described (97) as molecular semiconductors with low carrier mobilities.

3.4.6. Determination of flat - band potentials of porphyrin films.

An explanation of the dark currents and photocurrent behaviour of the porphyrin thin films require a knowledge of the position of the flat band potential of these films. The flat band potential can be estimated by the photopotentials developed by these films with the dark potentials of a series of electrolytes as in (30), or the photovoltage for a particular film can be observed with applied potential. This latter method has been successfully applied for determination of flat band

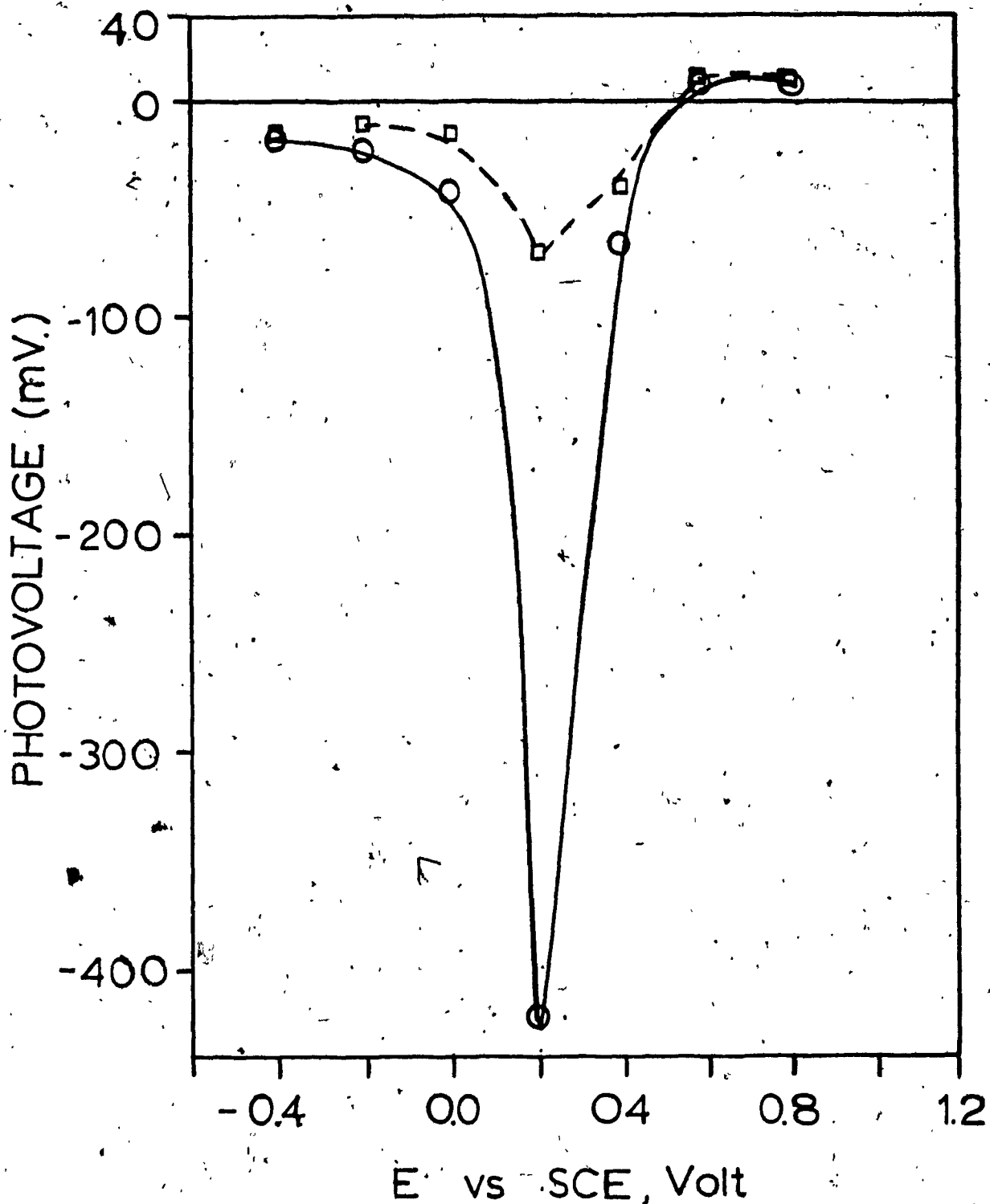


Figure 3.23. Flat band determination from photovoltage for the film ZnTPP-pyridine on SnO₂.

(---) 1.0 M KCl as electrolyte

(—) 2.0 mM Fe(CN)₆^{3-/4-} in 1.0 M KCl as electrolyte.

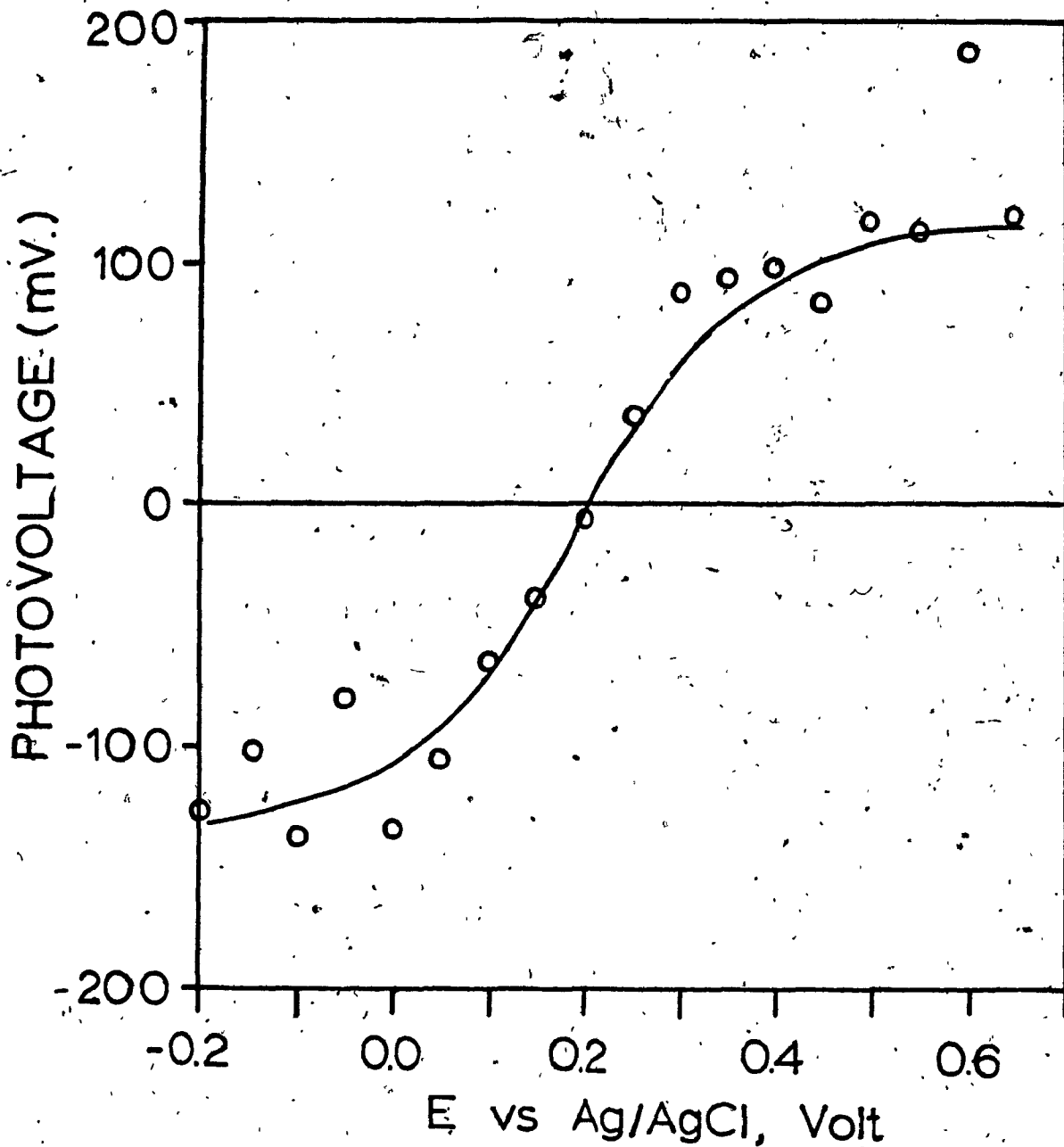


Figure 3.24. Variation of dark potentials with photovoltage for the film ZnTPP-PVP on SnO_2 . The electrolyte was 0.1 M ~~N~~rophenol in phosphate buffer at pH 7.0.

TABLE 3.6

FLAT BAND POTENTIALS	
Electrode System or Redox Couple	E/V vs SHE
Conduction Band SnO ₂	-0.20
ZnTPP	+0.80
ZnTPP - Pyridine	+0.54
ZnTPP - Triphenylarsine	+0.44
ZnTPP - Polyvinylpyridine	+0.40
Fe(CN) ₆ ^{3-/4-} (in 1.0 M KCl, pH 7.0)	+0.53
Nitrophenol (in 1.0 M acetate buffer, pH 7.0)	+0.30

potentials in semiconductors (130) and in thin porphyrin films (125). Figure 3.23 illustrates the steady - state photovoltage vs. potential curves for the $\text{SnO}_2/\text{ZnTPP}$ -pyridine electrode in aqueous electrolyte solutions. In the presence of background electrolyte only (1.0 M KCl) as in curve (a), only small photovoltages are observed over the potential range -0.4 V to +0.8 V vs SCE. This occurs under irradiation of the $\text{ZnTPP}/\text{SnO}_2$ -pyridine interface with white light from the tungsten - halogen lamp under conditions described in section 2.5.2. The onset potential (where the photovoltage - potential curve cuts the zero photovoltage axis) of +0.53 V is taken as the E_{fb} of the film. When a redox couple such as $\text{Fe}(\text{CN})_6^{3-}/4-$ is added to the background electrolyte (curve b), the photovoltages increases sharply over the potential range, but the onset potential of +0.53 V is unaffected. Similar observations were made for all the other films tested and the results of flat band determinations are summarized in table 3.6. The flat band potential is also unaffected by the use of other redox couples, except for methylviologen. Figure 3.24 shows the onset potential of +0.2 V vs Ag/AgCl for the $\text{SnO}_2/\text{ZnTPP}$ - PVP electrode in nitrophenol (1.0 M acetate buffer pH 7.0) to be the same as that observed in $\text{Fe}(\text{CN})_6^{3-}/4-$. The values in table 3.24 shows that the flat band potential is shifted more cathodic with respect to the ZnTPP film E_{fb} on addition of axial ligands to the ZnTPP . The effect is most pronounced for the ZnTPP - PVP

film. The fact that the PVP is not a simple ligand, but a multifunctional chain might play a role. The effects of polymer solid state on the flat band potential will be more closely evaluated in chapter 6.

3.5. PHOTOELECTROCHEMISTRY OF ZnTPP AND MODIFIED PORPHYRIN FILMS.

3.5.1. Photocurrent transient spectra.

Figure 3.25 represents the photocurrent transient spectra for the porphyrin thin films at close circuit. The experimental conditions are described in section 2.5.2. Irradiation took place with white light from the tungsten - halogen lamp at a power of 100 mW. Irradiation was through the SnO_2 glass but no difference was observed in the transients when irradiation was through the electrolyte solution. The photocurrent profile in figure 3.25 (a) is typical for the films modified with ZnTPP, ZnTPP - pyridine, and ZnTPP - triphenylarsine. It is characterized by an initial fast rise followed by a fast decay to reach a steady state under irradiation. On switching off the light, the process is reversed. This is associated with capacitive charging and discharging effects in the film (126). Irradiation of the porphyrin thin film causes electron-hole pairs. Accumulation and depletion of holes at the porphyrin /electrolyte interface is responsible for the capacitive effects

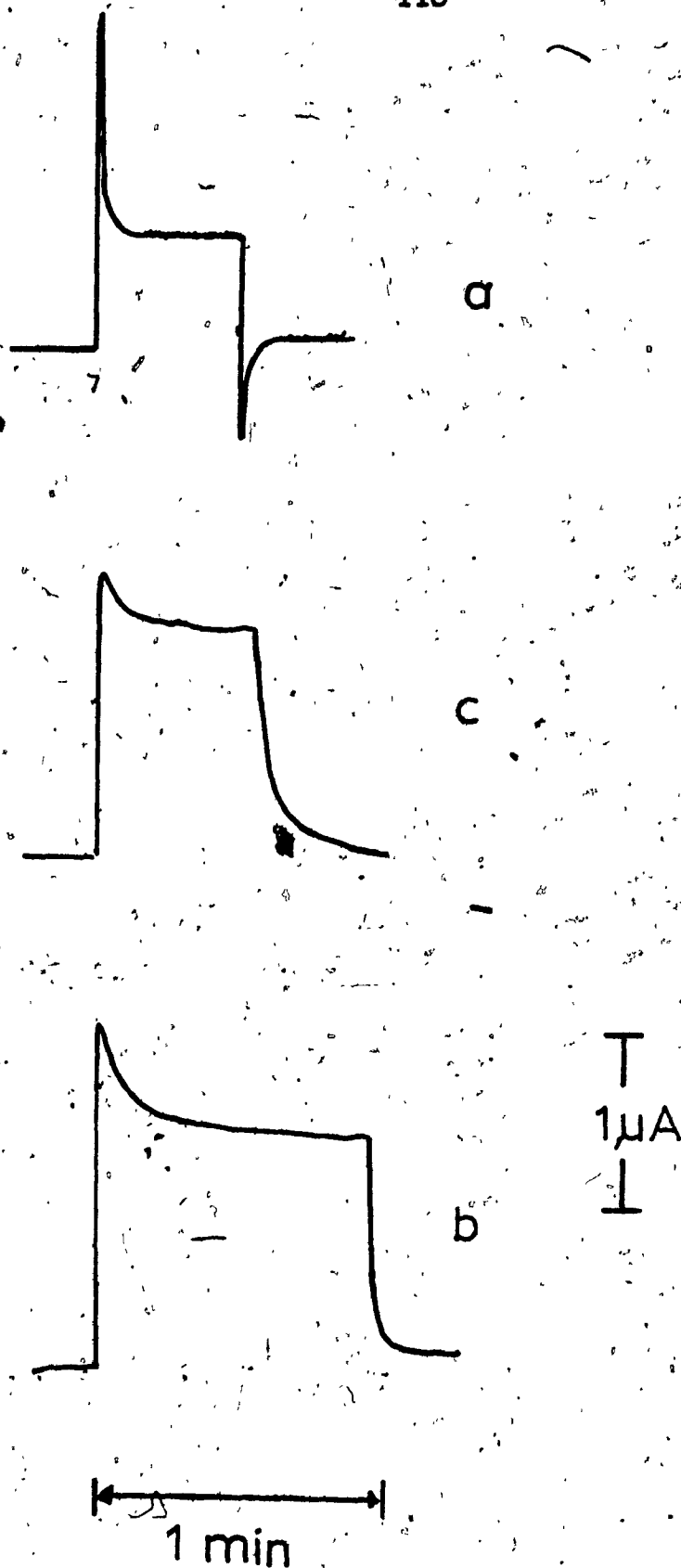


Figure 3.25. Photocurrent transients for some porphyrin films. (a) ZnTPP, (b) ZnTPP-PVP in $\text{Fe}(\text{CN})_6^{3-/4-}$ and (c) ZnTPP-PVP in nitrophenol.

observed. It should be observed that the discharge under irradiated conditions are larger than in the dark. Gerischer (126) showed that the capacitive discharge can be avoided by introducing a redox couple such as I^-/I_3^- which can react rapidly with the photogenerated holes. In all cases similar to figure 3.25 (a), the photocurrents were of a cathodic nature when the redox couple in solution was $Fe(CN)_6^{3-/4-}$. This indicates that under irradiation an electron is transferred from the porphyrin film to the electrolyte in solution. The photocurrent transients for the ZnTPP - PVP film in $Fe(CN)_6^{3-/4-}$ (figure 3.25b) show the same photocurrent discharge on irradiation. The capacitive discharge is slower. In the dark no reverse discharge takes place, rather a slow relaxation of the photocurrent. This slow relaxation is associated with charge trapping in the PVP moiety of the film (127, 128). The photocurrent changes from cathodic to anodic when the electrolyte is changed from $Fe(CN)_6^{3-/4-}$ to nitrophenol.

3.5.2. Photocurrent action spectra and absorption spectra of thin films.

Figure 3.26 shows the photoaction spectrum of the $SnO_2/ZnTPP$ electrode. The measurements of action spectra were carried out for all the porphyrin thin films, and figure 3.26 is representative. The photocurrent action

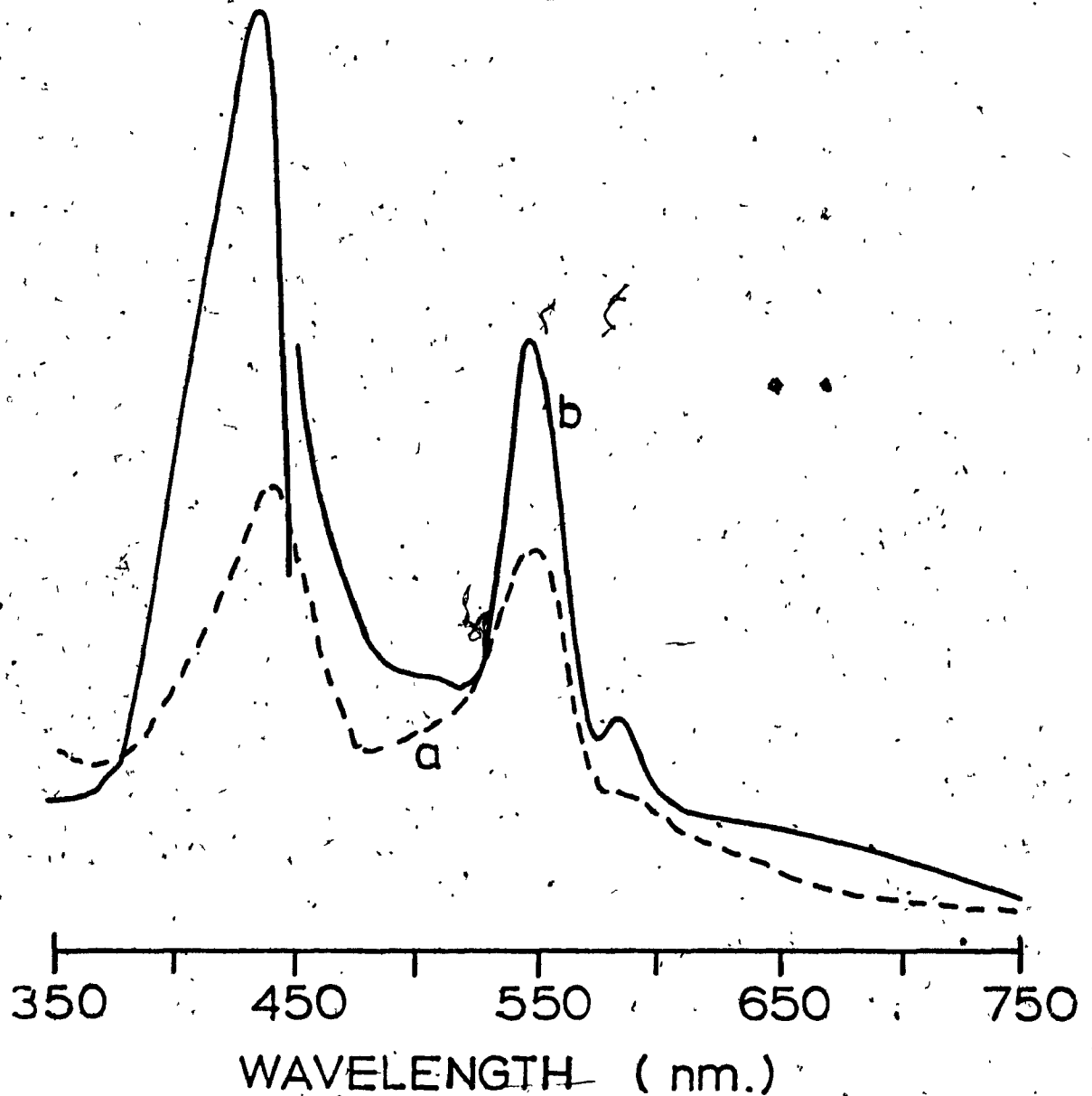


Figure 3.26. Photoaction spectrum (a) vs. the absorption spectrum (b) for a ZnTPP film on SnO_2 . The electrolyte was 2 mM $\text{Fe}(\text{CN})_6^{3-/4-}$ in 1.0 M KCl.

shows that the origin of the photogenerated charge is the porphyrin excited states since in all cases the photoaction spectrum follows the electronic absorption spectrum. The photoaction spectrum for the ZnTPP - PVP film is similar to that obtained by Kido and Langford (32).

The absorption spectrum of the thin films after photoelectrochemistry (figures 3.13, 3.14 and 3.15) show significant changes in the spectra. For the $\text{SnO}_2/\text{ZnTPP}$ electrode (figure 3.13(b)) the two significant changes which occur is a decrease in the soret band and the development of a new band with a peak at 660 nm. The band at 660 nm has been associated with the diacid form of the demetallated porphyrin (13), but it does not seem to play a role in the photogeneration process. The appearance of a shoulder on the soret band at 408 nm indicates the formation of a cationic species. This is a reversible change.

In figure 3.14 (b), the spectrum of the $\text{SnO}_2/\text{ZnTPP}$ - pyridine electrode after photoelectrochemistry show decreases in the, and soret bands with the appearance of peaks at 510 nm and 660 nm. Again this hints at the formation of cationic type species together with isoporphyrin like species (35, 36). Figure 3.15 (b), the spectrum for $\text{SnO}_2/\text{ZnTPP}$ - triphenylphosphine, shows a broad absorption in the visible region which is associated with the cationic porphyrin radical species.

3.5.3. Dependence of Photocurrent on film thickness.

An evaluation of the film thickness is important in determining the charge carrying mechanism in the porphyrin films. Axial ligation of ZnTPP changes the bulk solid state properties of the film as can be seen from a film thickness profile of the photocurrent in figure 3.27. The film thickness parameter is represented here as the amount of light absorbed by these films at the band of the absorption spectrum. All measurements depicted in figure 3.27 are taken at closed circuit and in contact with 2mM $\text{Fe}(\text{CN})_6^{3-/4-}$ in 1.0 M KCl as redox solution.

The photocurrent profile increases linearly with film thickness for the ZnTPP film (a). This linear increase reach a plateau and eventually decrease again for very thick film. Only films which fall within a range between 100 Å - 2000 Å are represented on the graph. The decrease of photocurrents at large film thickness is associated with resistance effects and filtering effects.

For the ZnTPP - pyridine films, an initial linear rise is obtained at low thickness which quickly reaches a plateau. The observation of photocurrents with very thick films (> 5000 Å) are similar to that observed for ZnTPP films.

The ZnTPP - PVP films (c) generally gives lower photocurrents than either the ZnTPP or ZnTPP - pyridine films. The films ZnTPP - triphenylphosphine and ZnTPP -

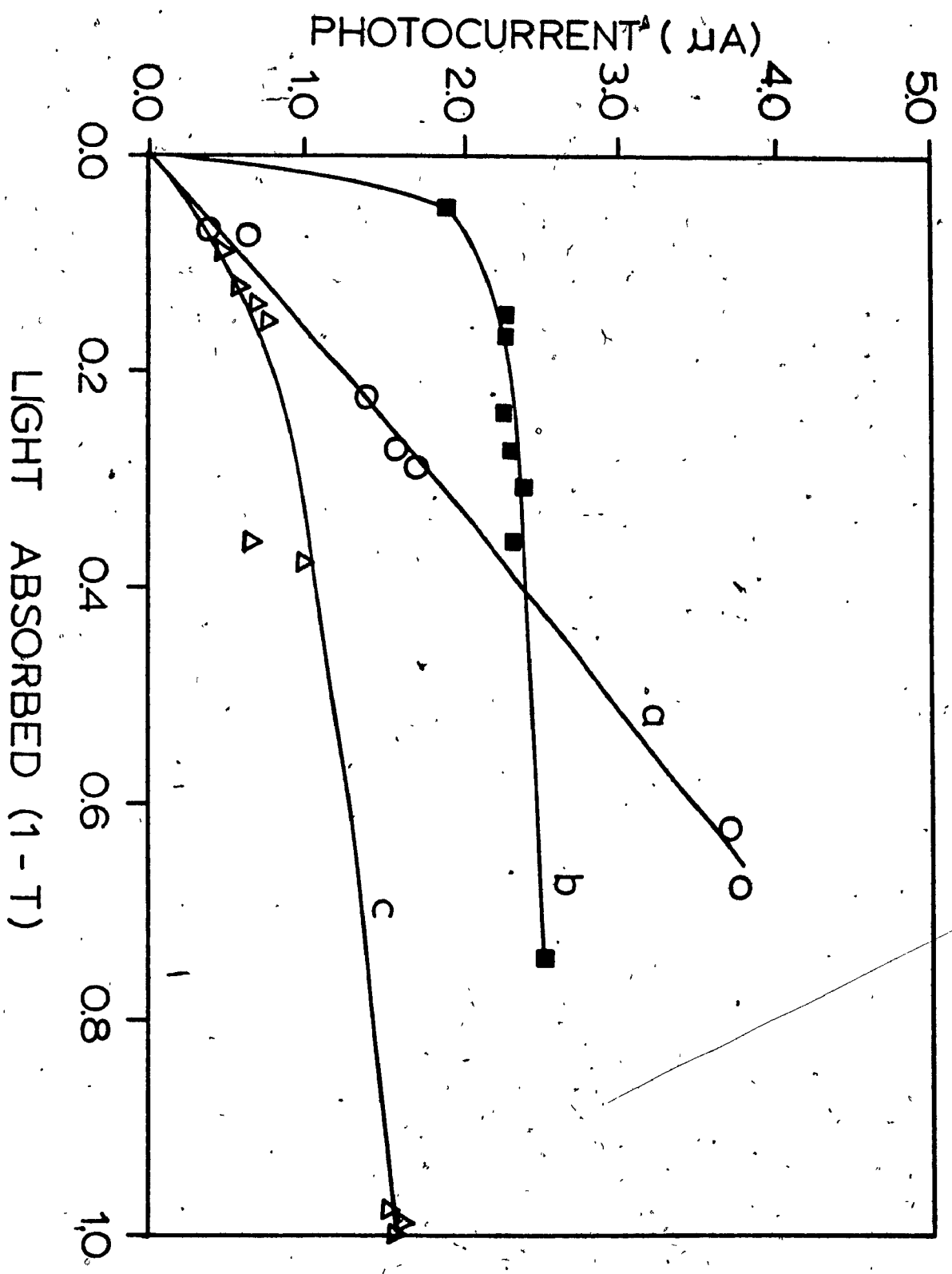


Figure 3.27. Photocurrent vs. Light absorbed for films of (a) ZnTPP, (b) ZnTPP-pyridine and (c) ZnTPP-PVP on SnO₂.

triphenylarsine gives profiles similar to that of ZnTPP +
PVP and is not represented on the graph.

CHAPTER 4.

RESULTS AND DISCUSSION II.

ELECTROCHEMISTRY AND PHOTOELECTROCHEMISTRY OF PORPHYRIN-POLYMER MODIFIED ELECTRODES.

Porphyrin fragility and the increasing resistance of thick films allows sensitization of wide bandgap SnO₂ only to a certain limit. To overcome this limit and to increase the ruggedness of the porphyrin, it is necessary to imbed the porphyrin dye into a suitable polymer matrix. Such a polymer matrix should allow a high capacity for and not largely change the physical properties of the porphyrin. It should also allow efficient transfer of charge throughout the polymer matrix.

The results in this chapter reports the interaction of porphyrin with an ionically conductive polymer.

4.1. ELECTROCHEMICAL PROPERTIES OF THE IONICALLY CONDUCTIVE POLYMER BLEND.**4.1.1. Ion retention ability of polymer.**

The copolymer described in section 2.2.5. was blended in a 1:1 ratio with PVP costyrene from 2% solutions of the polymer in methanol. This blend, which is 1% in PVP and 1% in copolymer was used to modify a SnO₂ electrode.

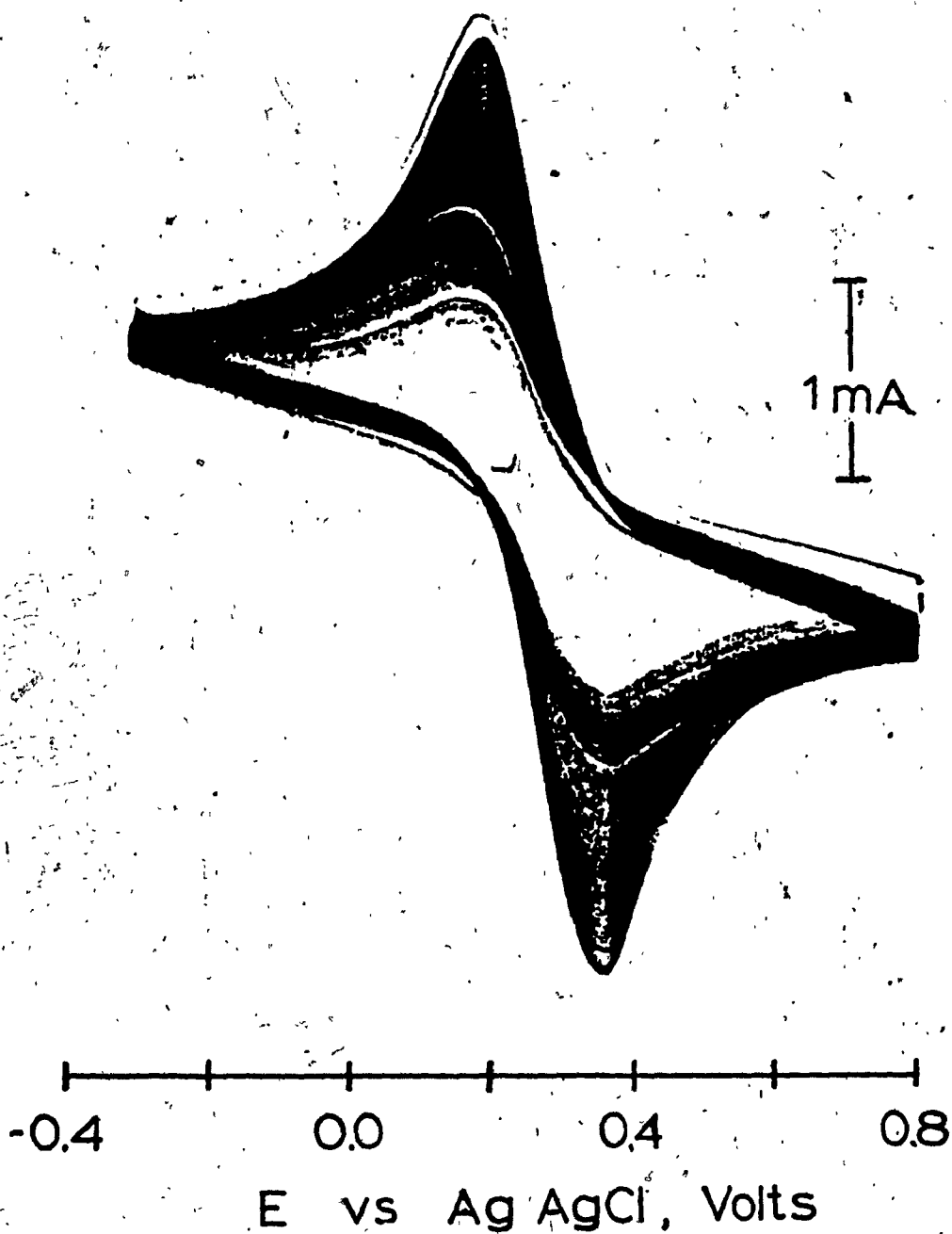


Figure 4.1. Voltammograms of continuous scanning showing leaching of $\text{Fe}(\text{CN})_6^{3-/4-}$ from the polymer film on SnO_2 . The electrolyte was 1.0 M KCl.

Modification was accomplished by drop evaporation as described in section 2.4.1. This electrode was left in a solution of 2mM $\text{Fe}(\text{CN})_6^{3-/4-}$ in 1.0 M KCl for 24 hours to allow ion exchange of the $\text{Fe}(\text{CN})_6^{3-/4-}$ into the film. The electrode was mounted in the flow through cell in contact with 1.0 M KCl as the electrolyte. Cyclic voltammetry shows that a considerable amount of $\text{Fe}(\text{CN})_6^{3-/4-}$ has been preconcentrated in the film (figure 4.1). Continuous scanning for a period of 4 hours shows that out-partitioning of the counterion $\text{Fe}(\text{CN})_6^{3-/4-}$ from the polymer film is a gradual process and reaches a limit of 46%. This high ion retention behaviour of the polymer blend corresponds with that reported by Anson (89, 90) for a similar blend on glassy carbon electrodes. This property of the polymer is advantageous since it can serve as a source of preconcentration of anionically changed dye molecules such as ZnTPPS-4.

4.1.2. Apparent diffusion coefficients of ions in the polymer thin films.

The significance of large diffusion coefficients for reactants which are confined within an electrode coating has been extensively reviewed in section 1.3.5.

In principle, apparent diffusion coefficients can be calculated from potential step chronocoulometry or linear sweep voltammetry at different scan rates.

Chronocoulometric measurements were employed by stepping the potential between +0.4 V and -0.4 V vs Ag/AgCl. The apparent diffusion coefficients obtained from Cottrell plots for three polymer electrodes are summarized in Table 4.1. The values of D_{app} for $Fe(CN)_6^{3-/4-}$ vary between 1.1×10^{-7} and $3 \times 10^{-7} \text{ cm}^2 \text{ s}^{-1}$. These values obtained are one order of magnitude smaller than those obtained by Anson (90) and two orders of magnitude smaller than the diffusion coefficient of $Fe(CN)_6^{3-}$ or $Fe(CN)_6^{4-}$ in solution (123).

Plots of peak current vs scan rate for electrode 1P in Table 4.1 indicates that linearity is obtained for scan rates up to 600 mV/s. (figure 4.2). This is observed when the bulk electrolyte is 2mM $Fe(CN)_6^{3-/4-}$ in 1.0 M KCl.

These composite coatings, despite the fact that they can retain ions efficiently, also shows low barriers for the diffusion of counterions. These two properties have been explained by the copolymer structure (figure 4.3 A) which is primarily responsible for the electrostatic binding of the counterions since the PVP portion (figure 4.3 B) cannot bind counterions unless it is extensively protonated (which is not the case in this experiment). Anson (90) showed that the cationic quaternary ammonium group retains its charge at all pH's and is the most likely site of exchange of anions.

The high retention values as well as the higher than normal diffusion coefficients have been linked to the internal morphology of the films. There is a discrete

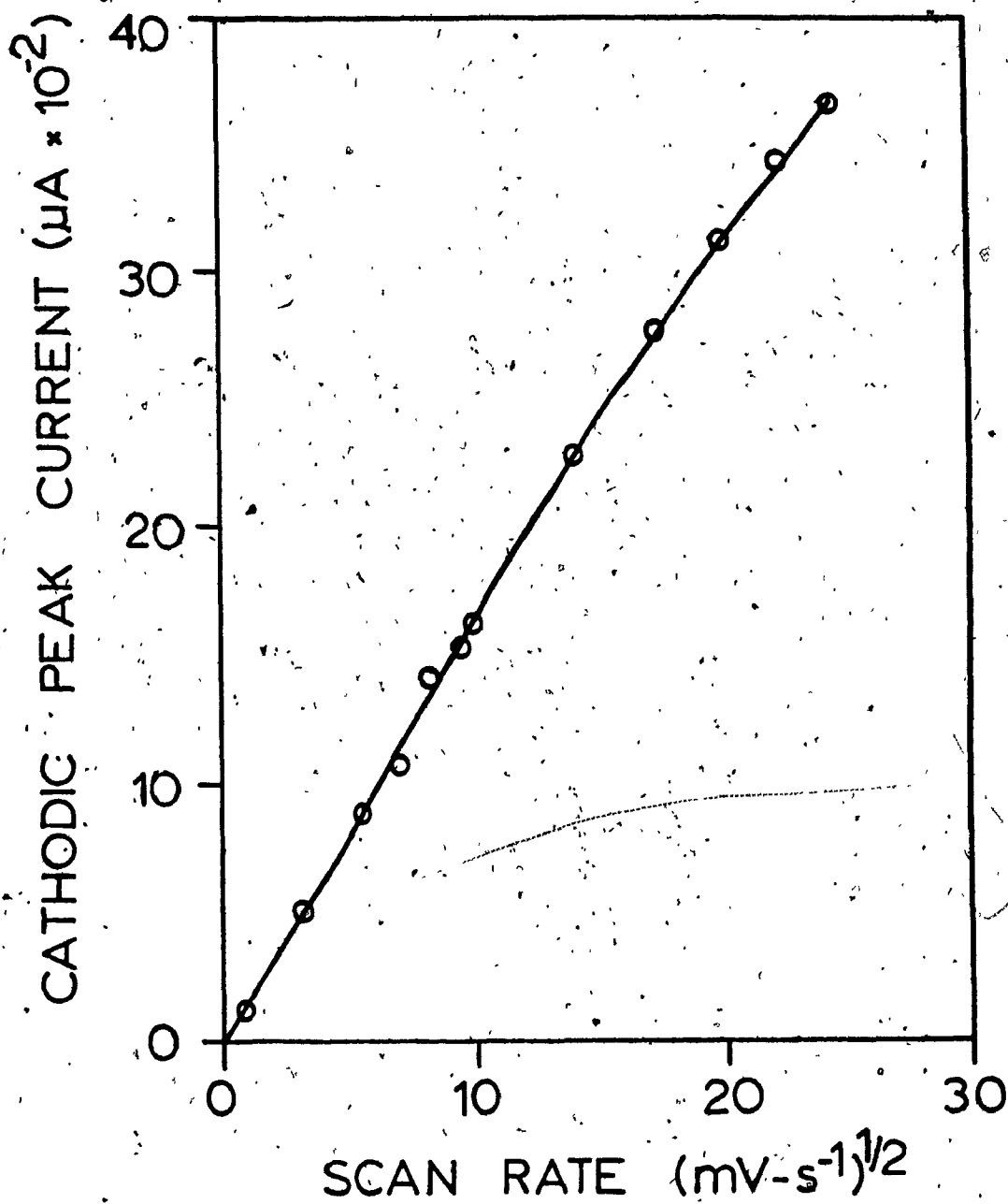
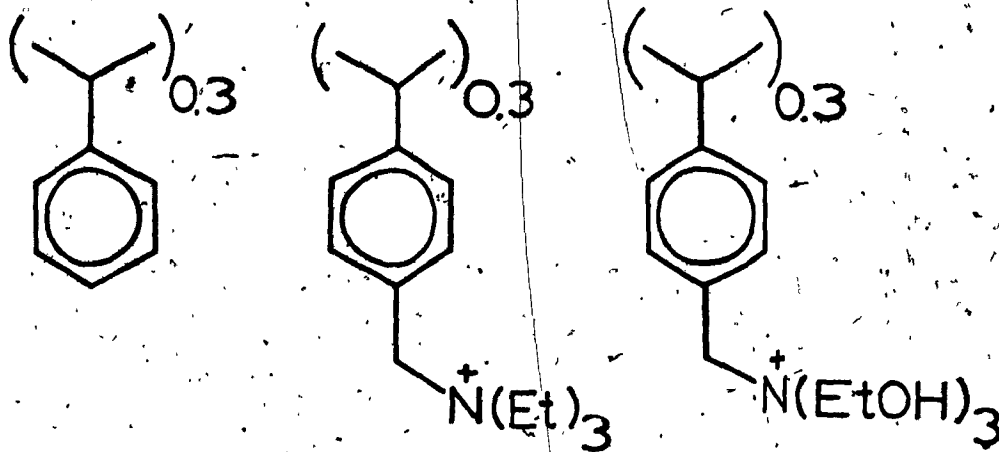
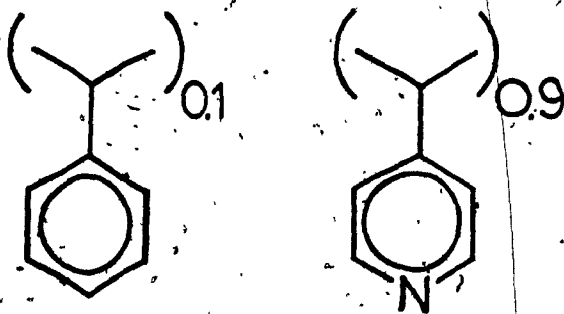


Figure 4.2. Cathodic peak current vs. scan rate for the ferri/ferrocyanide couple at a ITO/PVP-copolymer electrode.



A



B

Figure 4.3. Schematic representation of the polymer structure. (A) the copolymer and (B) poly(4-vinylpyridine) 10% costyrene.

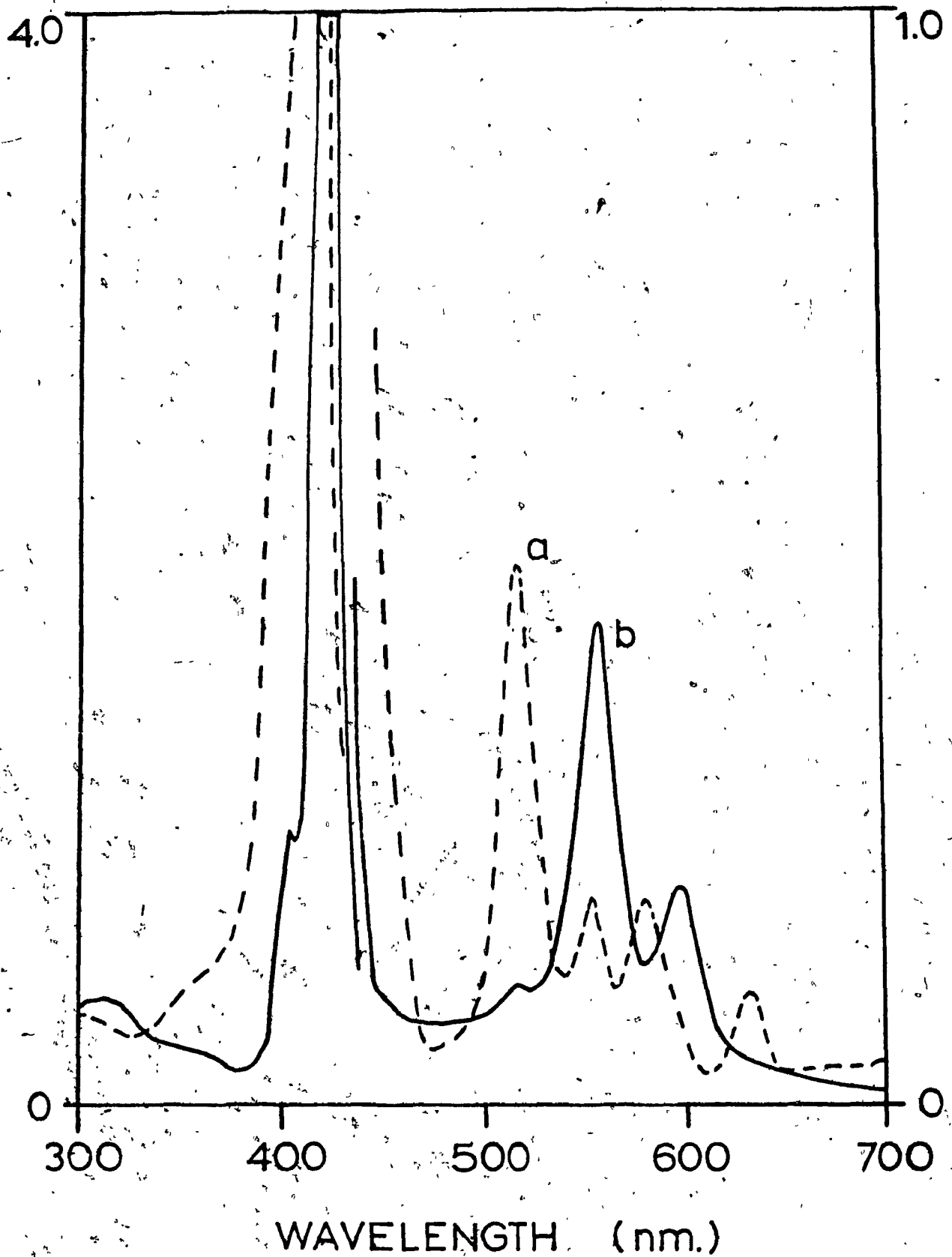


Figure 4.4. Absorption spectra of H₂TPPS and ZnTPPS in aqueous medium. (a) H₂TPPS and (b) ZnTPPS.

segregation between the hydrophobic and hydrophilic domains of the polymer. This property is important when chromophores are imbedded in this polymer blend.

4.1.3. Potential of pyridinium group in the polymer blend.

When the composite polymer film on SnO_2 is electrochemically scanned in 1.0 M KCl, no electrochemical activity other than the reduction of the pyridine group in the polymer is observed. This is shown in figure 4.8(a). The value calculated at the peak height was found to be -0.51 V vs Ag/AgCl.

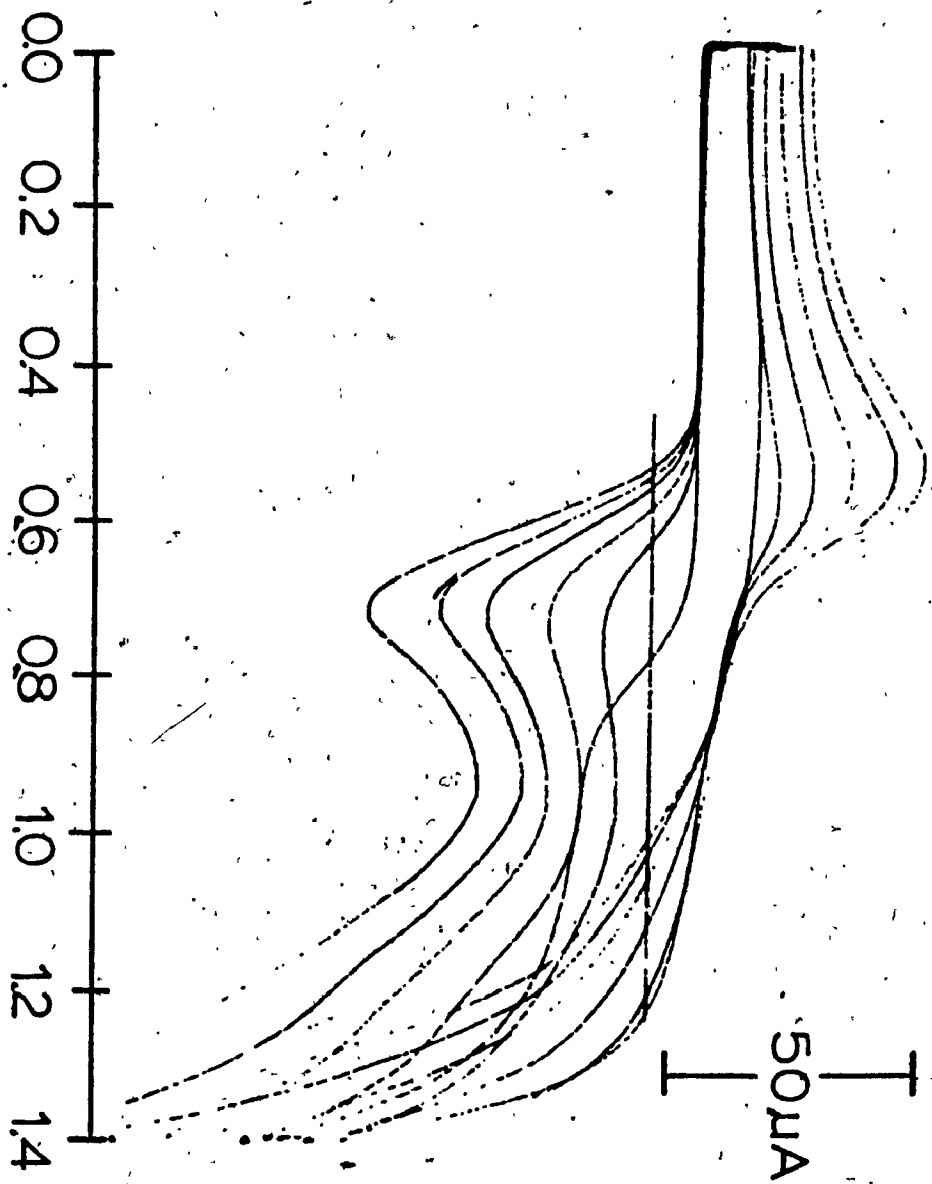
4.2. SOLUTION ABSORPTION SPECTRA AND ELECTROCHEMISTRY OF ZINC TETRAPHENYLPORPHYRIN-TETRASULPHONATE (ZnTPPS-4).

4.2.1. Absorption spectra of $\text{H}_2\text{TPPS-4}$ and ZnTPPS-4.

The absorption spectra of $\text{H}_2\text{TPPS-4}$ and ZnTPPS-4 in H_2O are shown in figure 4.4(a) and (b) respectively. The spectral interpretation is the same as that of the neutral analogs described in section 3.1.

4.2.2. Solution electrochemistry of ZnTPPS-4 in aqueous media.

Figure 4.5 shows the "titration" of ZnTPPS-4 in aqueous medium with 1.0 M KCl as the background electrolyte with a 1% solution of PVP: copolymer blend in methanol. The initial scan shows the first reversible oxidation reduction peak with $E_{1/2}$ at 0.62 V vs Ag/AgCl to correspond to the literature value cited in Table 1.1. The second ring oxidation could not be determined efficiently due to the electrochemical window of the aqueous electrolyte. Titration of this electrochemical solution with 0.1 ml portions of the polymer blend shows a decrease in the peak current of the first reversible oxidation reduction. With an excess of polymer blend the first oxidation - reduction peak disappears completely with the appearance of a broad irreversible oxidation peak at 0.95 V vs Ag/AgCl. The reduction in the C V peaks is attributed to the slower diffusion of polymer bound porphyrin. The binding of the ZnTPPS-4 to the PVP moiety of the polymer is demonstrated by the absorption spectrum of the solution taken at each step in the titration. Extensive binding takes place between the cationic sites of the copolymer and the anionic sites of the porphyrin. The porphyrin is essentially immobilised by these interactions and at large polymer concentration it does not show any heterogeneous electroactivity. This binding and redistribution of the ZnTPPS-4 in the polymer will be



E vs Ag/AgCl, Volt

Figure 4.5. Voltammograms of ZnTPPS-4 in aqueous medium titrated with aliquots of a 2% PVP-copolymer solution in methanol.

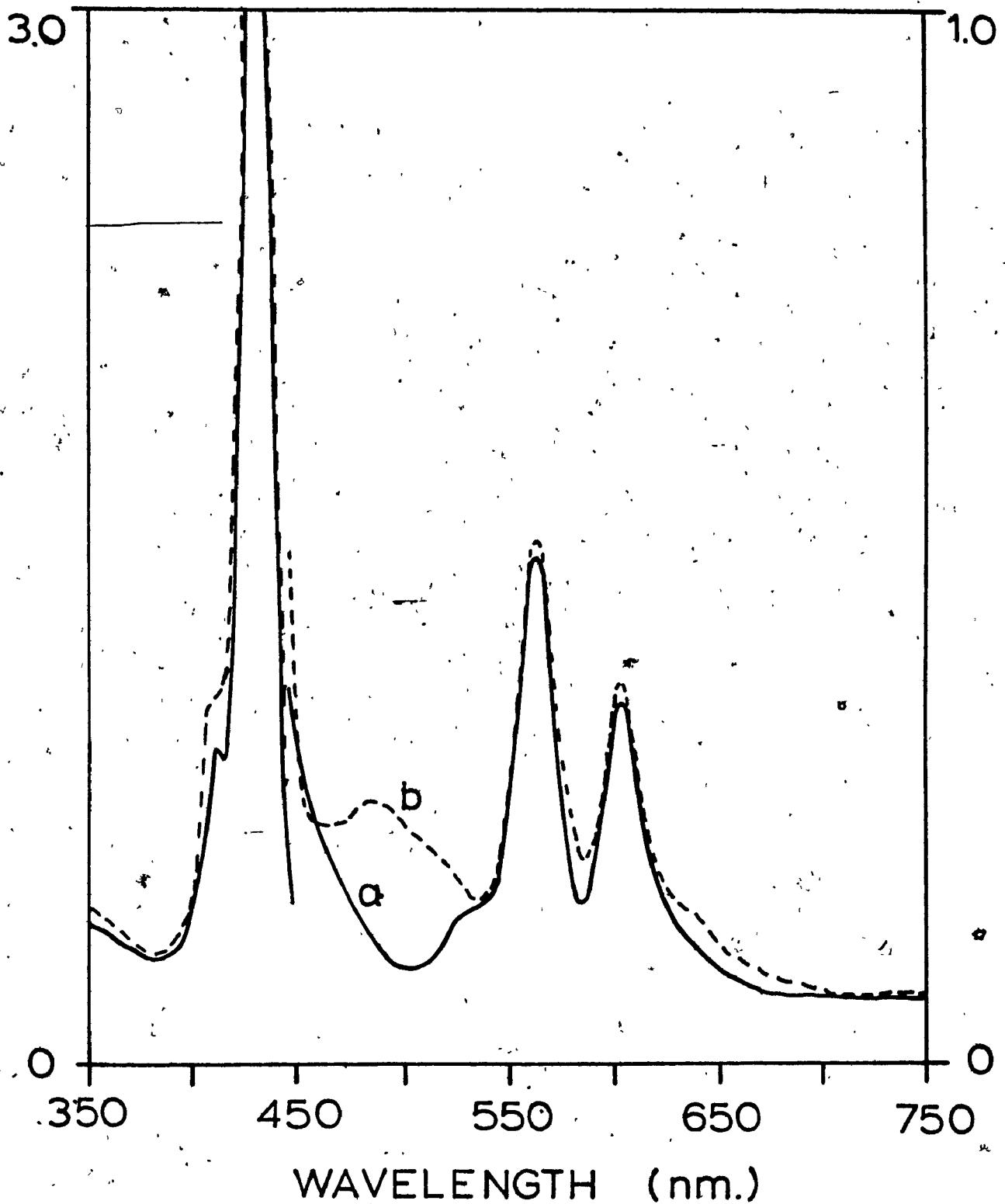


Figure 4.6. Absorption spectra of ZnTPP-PVP-copolymer on SnO₂ before (a) and after (b) electrochemistry with the Fe(CN)₆^{3-/4-} couple.

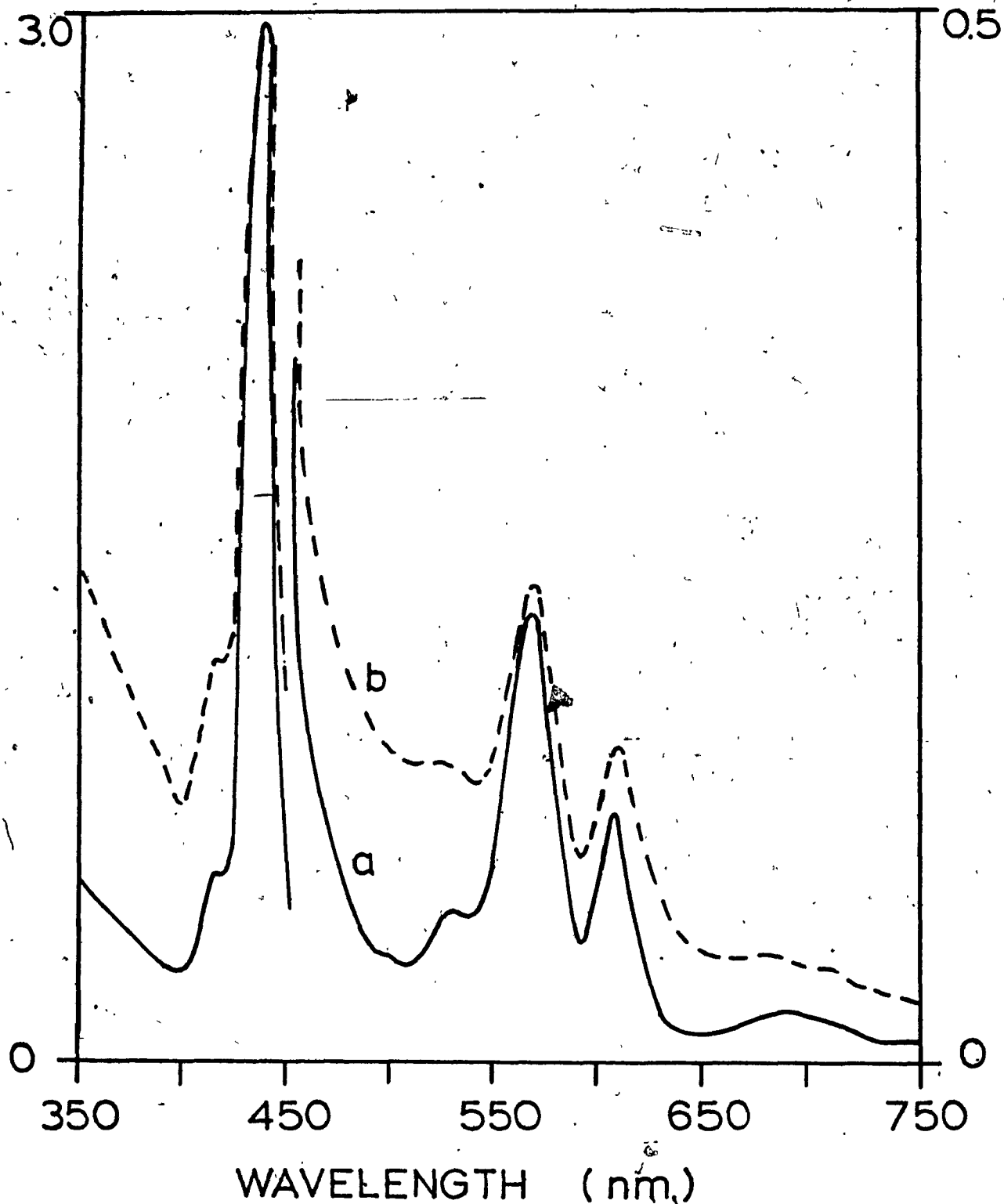


Figure 4.7. Absorption spectra of ZnTPPS⁴⁻-PVP-copolymer films before (a) and after (b) electrochemistry with the Fe(CN)₆^{3-/4-} couple.

further demonstrated in fluorescence studies in chapter 5.

4.3. THIN FILM ABSORPTION SPECTRA.

Absorption spectrum of $\text{SnO}_2/\text{ZnTPP}$ - PVP - copolymer and $\text{SnO}_2/\text{ZnTPPS-4}$ - PVP copolymer.

Figure 4.6 (a) presents the absorption spectrum of ZnTPP in the polymer PVP - copolymer as a film on SnO_2 . The ZnTPP is axially ligated to the pyridine of the PVP component of the polymer as can be seen from the relative intensities of the π and σ bands. The absorption peaks are not as broad as observed for the ZnTPP in PVP only, but there is still some degree of an underlying broad absorption in the visible region of the spectrum. Figure 4.7(a) shows the absorption spectrum of the anionic form of ZnTPP i.e. ZnTPPS-4, which is red - shifted by 8nm. Assignment of the bands are parallel to those described in section 1.1.1.

4.4. DARK ELECTROCHEMISTRY OF $\text{ZnTPPS-4-PVP-COPOLYMER}$ FILMS ON GOLD AND DIFFERENT SEMICONDUCTING SURFACES.

4.4.1. Electrochemistry of $\text{SnO}_2/\text{ZnTPPS-4-PVP-copolymer}$ electrodes.

Figure 4.8(a) represents the voltammogram of a film of PVP

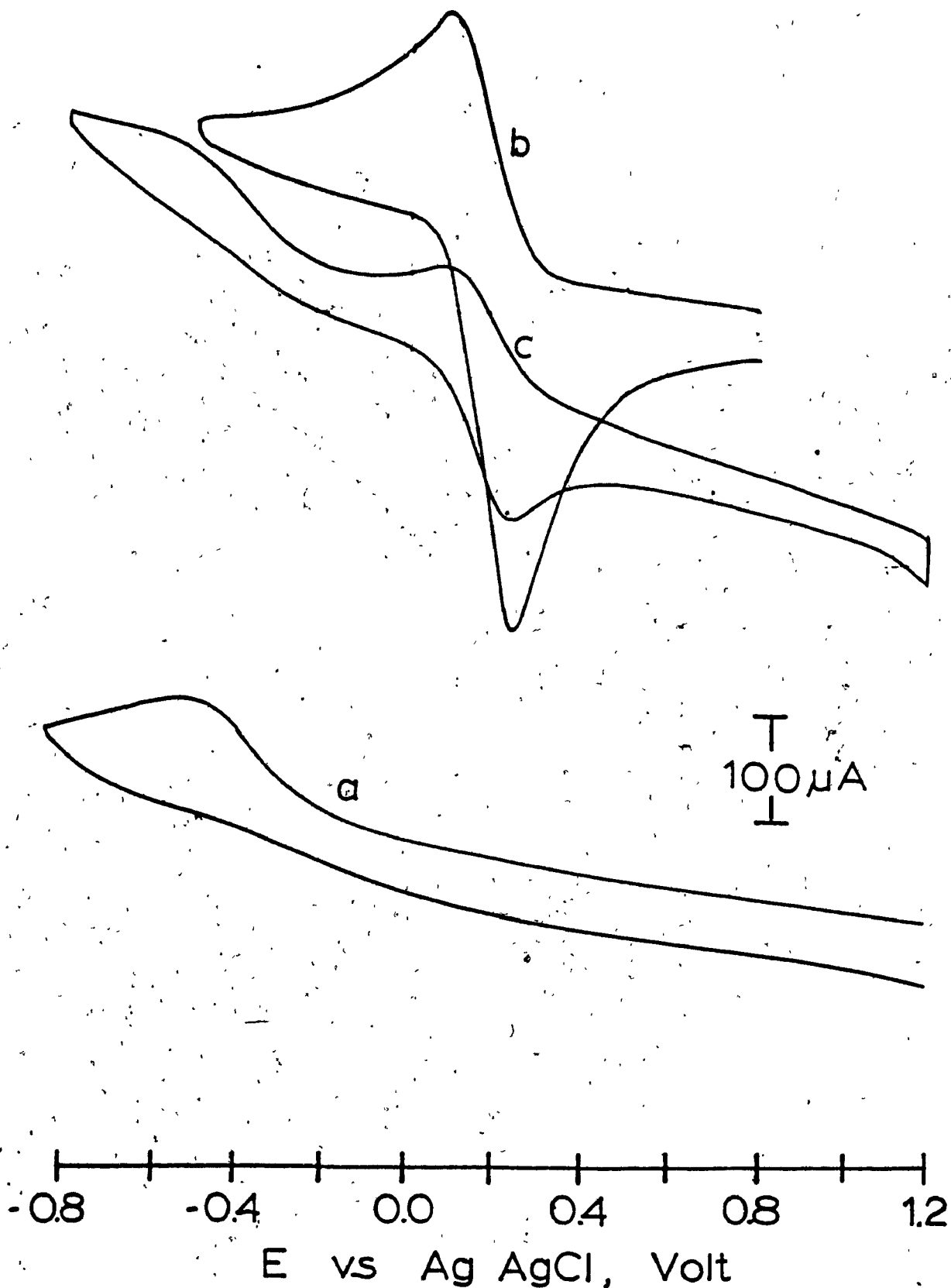


Figure 4.8. (a) Voltammogram of PVP-copolymer film on SnO_2 in 1.0 M KCl. (b) The same film in 2 mM $\text{Fe}(\text{CN})_6^{3-/4-}$ and thereafter in 1.0 M KCl (c).

- copolymer on SnO_2 in 1.0 M KCl (see section 4.1.3.). If a chromophore is incorporated into the polymer as in section 2.2.6 and a film is formed on an SnO_2 electrode to give a $\text{SnO}_2/\text{ZnTPPS-4} - \text{PVP} - \text{copolymer}$ electrode, this film shows no electrochemical activity for the ZnTPPS-4 if scanned in a solution of 2.0 mM $\text{Fe}(\text{CN})_6^{3-/4-}$ in 1.0 M KCl (figure 4.8(b)). The peak current of the voltammogram is also significantly lower than the peak current obtained in a film of comparable thickness, but with no chromophore imbedded in it. This signifies a lower preconcentration of $\text{Fe}(\text{CN})_6^{3-/4-}$ in the film in the presence of chromophore. This is understandable since the chromophore ZnTPPS-4 can compete for the cationic electrostatic binding sites of the copolymer.

The voltammogram of $\text{Fe}(\text{CN})_6^{3-/4-}$ is quasi-reversible, showing that incorporation of the chromophore did not change the kinetics of charge transport through the film significantly. If this electrode is transferred to a flow-through cell with only the background electrolyte present ie. 1.0 M KCl, the voltammogram obtained on scanning the potential is represented in figure 4.8(c). The reversible peaks of the $\text{Fe}(\text{CN})_6^{3-/4-}$ couple is still obtained, but at a reduced current. The area under the anodic and cathodic peaks will represent the concentration of $\text{Fe}(\text{CN})_6^{3-/4-}$ retained in the film. The broad reduction peak of the pyridine groups are also present, although these could not be clearly observed when the film was in

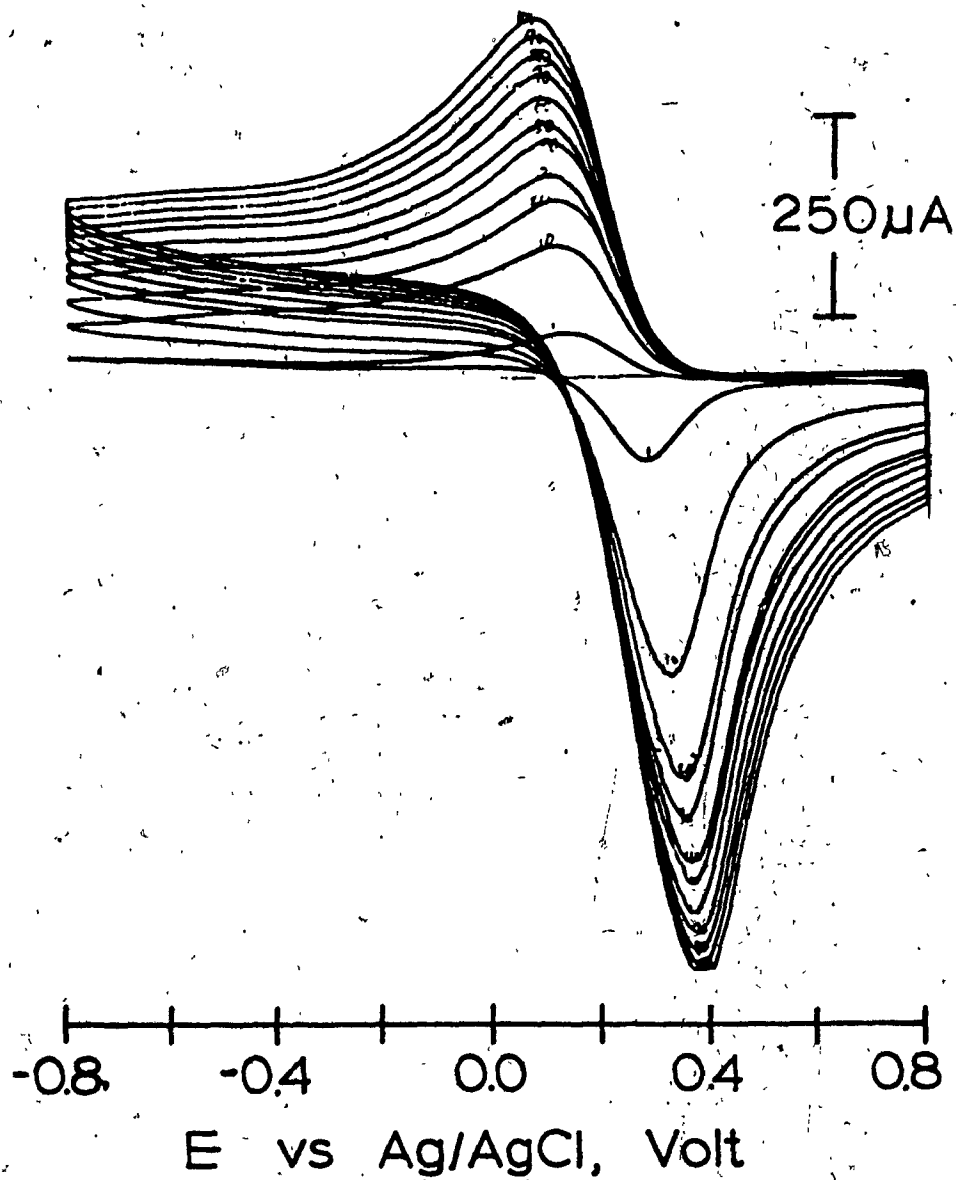


Figure 4.9. Voltammograms at different scan rates for the $\text{Fe}(\text{CN})_6^{3-/4-}$ couple on $\text{SnO}_2/\text{ZnTPPS}^{-4}$ -PVP-copolymer. Scan rate is varied from 1 mV/s to 100 mV/s.

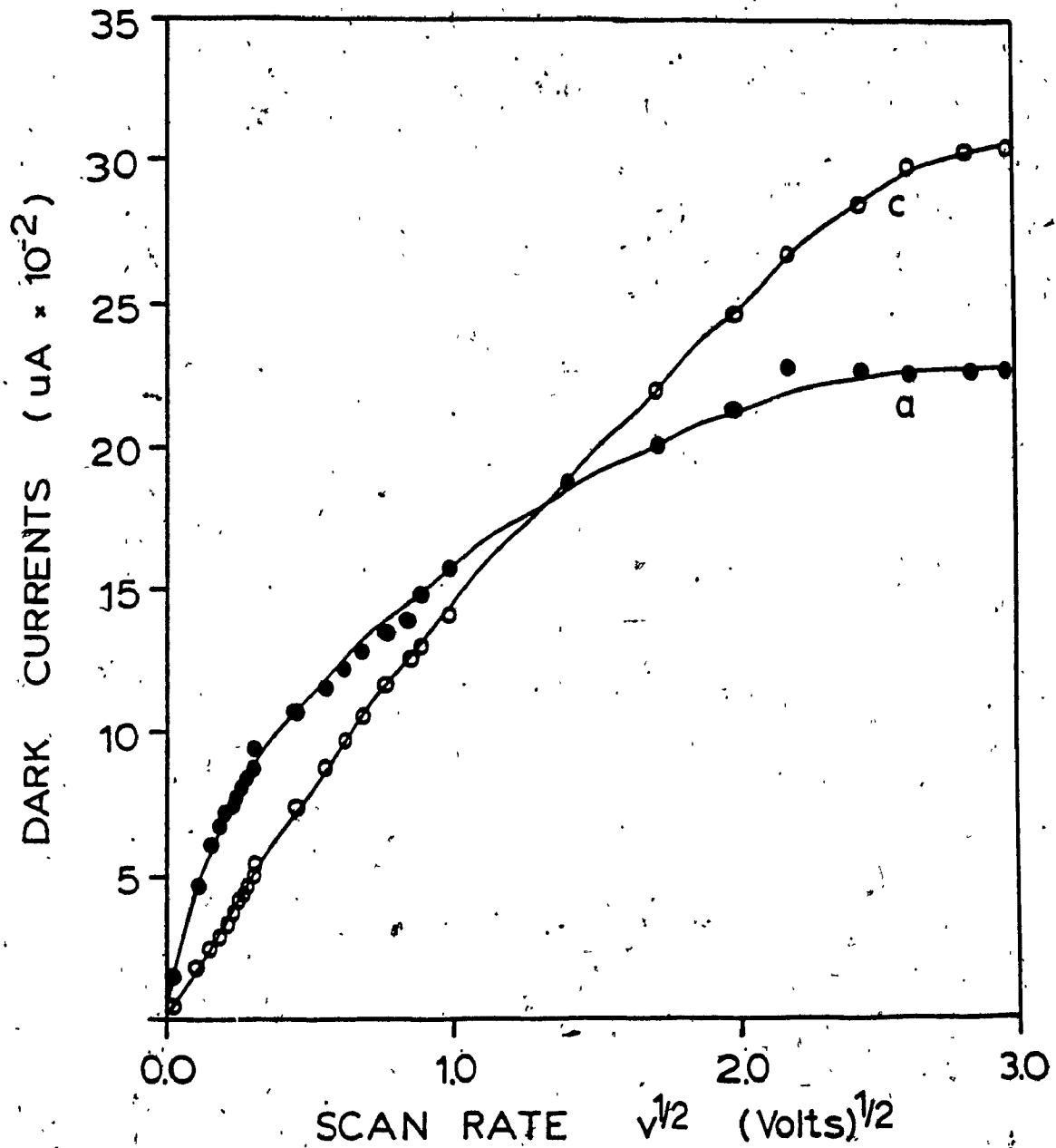


Figure 4.10. Anodic and cathodic dark currents vs. scan rate for the electrode $\text{SnO}_2/\text{ZnTPPS}^{-4}$ -PVP-copolymer. Electrode the same as for figure 4.9.

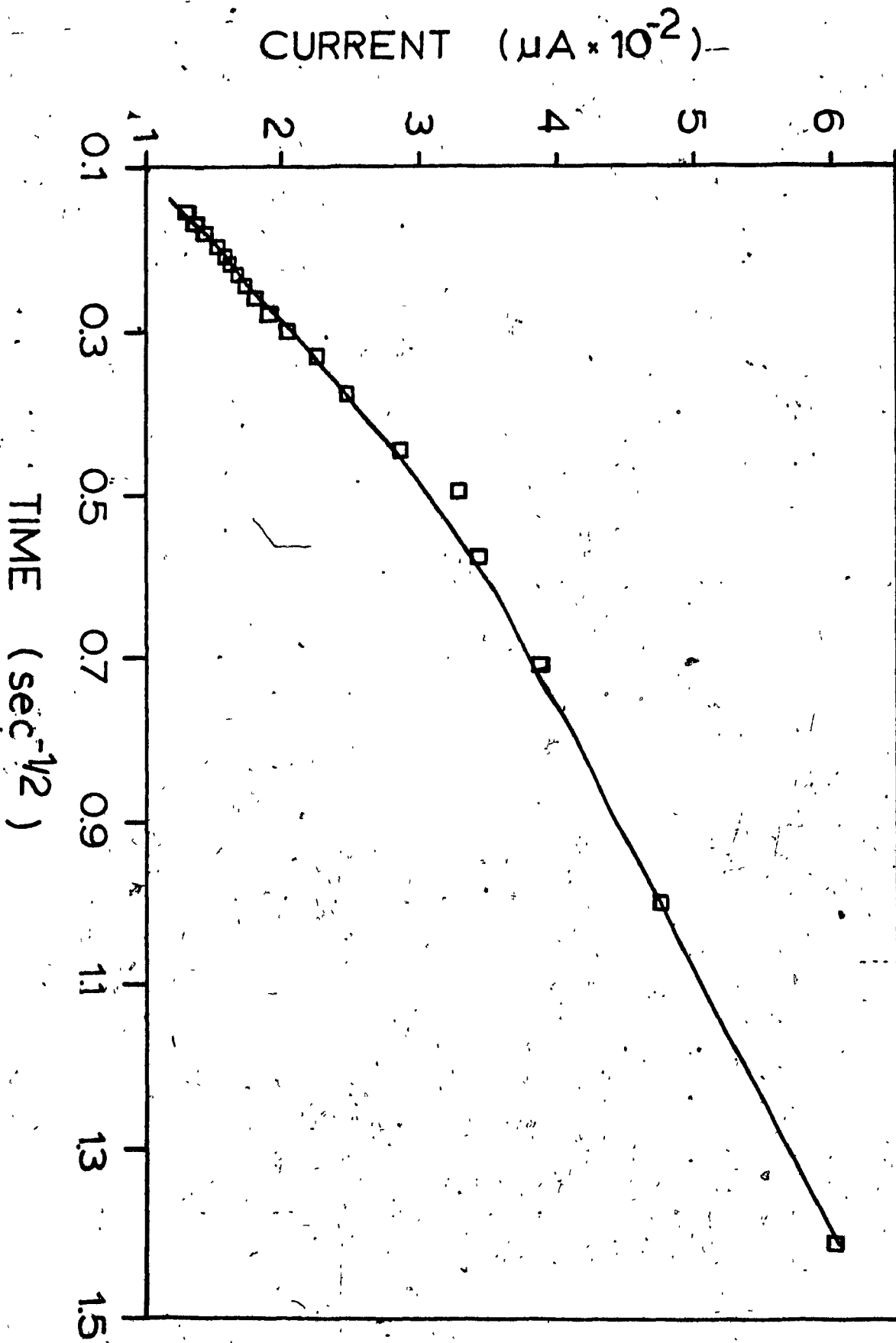


Figure 4.11. Plot of cathodic peak currents vs. time for the electrode in Figure 4.9. The potential was stepped between +0.4V and -0.4V.

an electrolyte containing a redox couple, even if the potential was varied past that reduction range.

By varying the scan rate of the potential for the ZnTPPS-4 - PVP - copolymer film in the redox couple (figure 4.9) and by plotting the peak potentials vs the square root of the scan rate, (figure 4.10) one observes that the slope for the cathodic peak remains independent of scan rate at lower scan rates, but becomes scan rate dependent at higher scan rates. This signifies diffusion controlled conditions for the reduction of $\text{Fe}(\text{CN})_6^{3-}$ to $\text{Fe}(\text{CN})_6^{4-}$. For the anodic reaction, the peak current vs scan rate shows that deviation from linearity occurs at relatively low scan rates. For the reaction $\text{Fe}(\text{CN})_6^{4-}$ to $\text{Fe}(\text{CN})_6^{3-}$ in the film, processes other than diffusion are contributing to the charge transport process. The apparent diffusion coefficient for $\text{Fe}(\text{CN})_6^{3-}$ in the polymer films were also determined for a series of films of different thickness. The potential in the chronoamperometric experiments were stepped between +0.4 V and -0.4 V vs Ag/AgCl. Figure 4.11 shows a Cottrell plot for electrode 10P. This Cottrell plot is typical for all the other electrodes. The other electrochemical data for SnO_2 modified electrodes are summarized in Table 4.1. The Cottrell plot in figure 4.11 shows a curve with two distinct slopes. These two slopes are more distinct for the thicker films (11P and 12P) and signifies the involvement of two diffusional processes, one slower and one faster. The values of diffusion coefficients reported in Table 4.1 only shows

TABLE 4.1.

Dark electrochemistry of $\text{SnO}_2/\text{ZnPPS-4-PVP-copolymer}$.

Electrode	E_c mV	E_a mV	i_c uA	i_a uA	Thickness um.	$i_{ph.}$ uA	$D_{app.}$ cm ² /s
			10^{-2}	10^{-2}			10^{-7}
1P	180	360	19.6	17.8	2.0	-	2.1
2P	-	-	-	-	4.1	-	1.1
3P	-	-	-	-	5.2	-	3.0
4P	90	230	3.3	5.6	4.3	10.0	-
5P	70	270	2.9	5.3	4.7	6.2	-
6P	90	220	4.3	6.4	4.0	13.5	-
7P	55	170	4.0	7.8	1.9	1.5	-
8P	35	210	4.4	8.1	8.0	15.0	-
9P	50	170	4.0	7.6	5.1	11.5	-
10P	20	270	3.7	10.5	8.1	15.0	1.1
11P	30	200	7.0	14.8	12.0	6.2	0.51
12P	40	200	8.0	16.0	15.0	3.0	0.29
13P	230	310	3.4	4.0	1.0	1.3	0.32
14P	70	450	6.1	3.7	1.2	0.8	0.42
16P	70	210	3.2	5.6	2.0	1.7	0.49
19P	-60	290	7.2	6.1	2.2	1.7	0.91
20P	30	310	5.8	3.4	2.3	1.5	0.21

the value for the faster process. The values of apparent diffusion coefficient D_{app} were found to compare with those films which does not have chromophore incorporated, but there was no definite sequence in D_{app} and the thickness of the film. In general the values for D_{app} varied between 1×10^{-7} and 2×10^{-8} cm^2s^{-1} for these films. No reasonable explanation can be offered for this trend of D_{app} with thickness. It does indicate that film properties depend on details of preparation.

The variation of the dark peak potentials with thickness show that there is a general anodic shift in potential with thin films, but the peak potential remains relatively constant in films thicker than 4 μm . The peak current generally increases with film thickness with a higher increase observed in the anodic peak than in the cathodic peak. The increase in peak current shows a higher incorporation of $\text{Fe}(\text{CN})_6^{3-/4-}$ with thicker films. In all cases the ratio of chromophore to polymer were the same.

4.4.2. Electrochemistry of ITO/ZnTPPS-4 - PVP copolymer.

Figure 4.12(a) shows the voltammogram of the $\text{Fe}(\text{CN})_6^{3-/4-}$ couple at the surface of an indium doped tin oxide electrode. The reaction is irreversible as observed by the broad, widely separated peaks. This is due to the high resistance of the ITO conductive glass. If the electrode

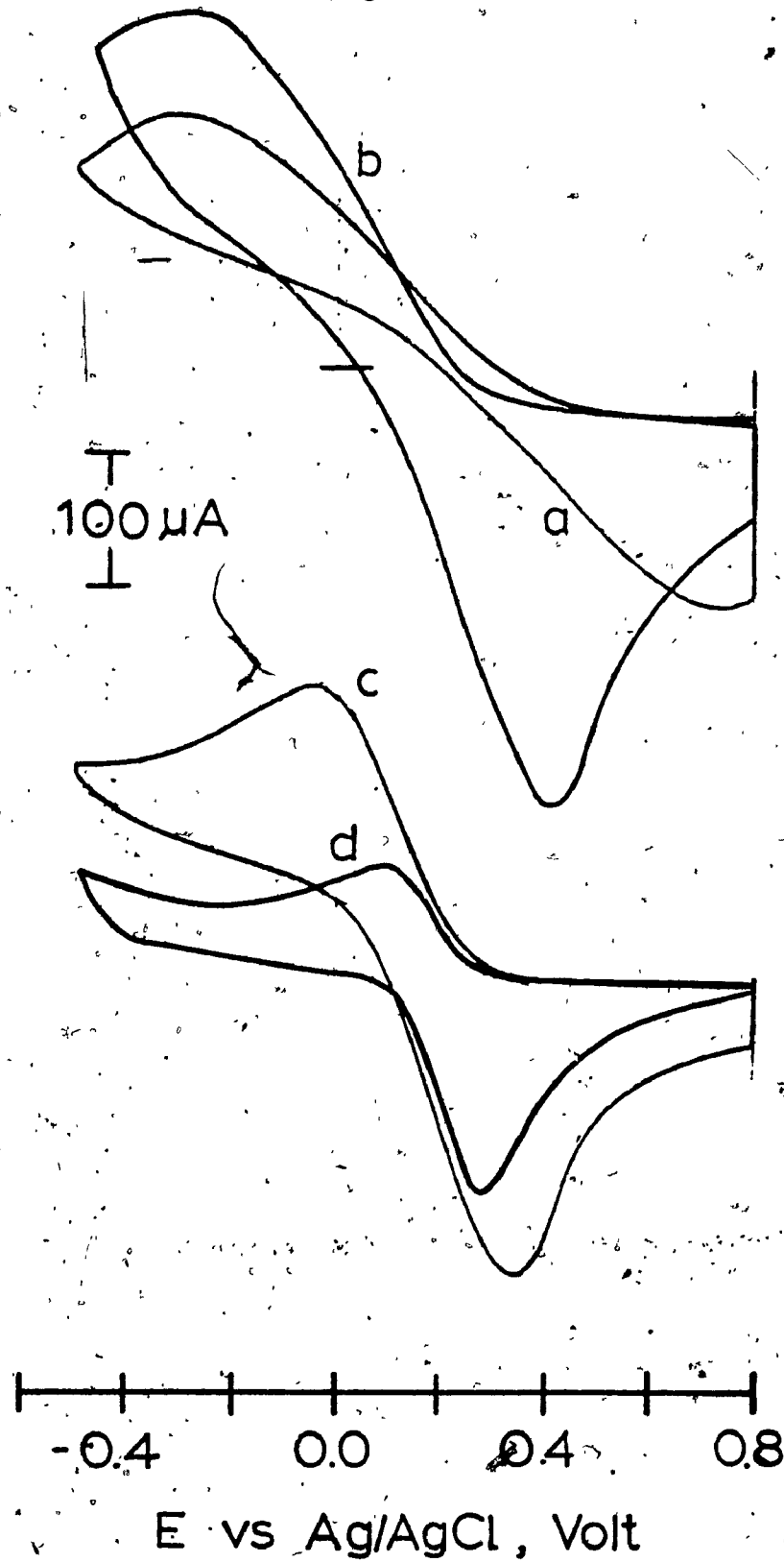


Figure 4.12. Voltammograms of $\text{Fe}(\text{CN})_6^{3-/4-}$ at different surfaces. (a) at ITO, (b) ITO/PVP-copolymer (c) ITO/ZnTPPS-PVP-copolymer and (d) Voltammogram of ITO/ZnTPPS-PVP-copolymer film containing $\text{Fe}(\text{CN})_6^{3-/4-}$ scanned in background electrolyte.

TABLE 4.2

DARK ELECTROCHEMISTRY OF ITO/ZnTPPS-4 - PVP - COPOLYMER.

	E_c	E_a	i_c	i_a	Thickness	i_{ph}
	mV	mV	μA	μA	μm	μA
			$\times 10^{-2}$	$\times 10^{-2}$		
A8					4.30	10.
A9					3.80	8.3
A10	-100	370	0.76	0.37	4.50	11.5
A11	- 15	300	1.09	1.21	1.20	2.0
A12	- 20	270	1.21	1.13	0.85	1.0
A13	- 10	300	0.88	1.29	1.75	2.2
A14	- 50	350	1.65	2.17	1.75	2.4
A15	- 90	350	1.17	1.45	2.80	7.4
A16					1.80	2.8
A17	- 60	350	1.7	2.20	3.90	9.4
A18	- 50	350	1.5	2.01	3.90	6.8

is modified with a PVP - copolymer film, some preconcentration of $\text{Fe}(\text{CN})_6^{3-/4-}$ occurs in the film and the voltammogram becomes more reversible (figure 4. 12(b), but is still the voltammogram of a quasi - reversible reaction.

When a film of ZnTPPS-4 - PVP - copolymer is cast onto the ITO electrode, the voltammetry observed for the ferri - ferro cyanide couple on this surface changes to an almost reversible wave (c).

The ZnTPPS-4 chromophore in the polymer matrix thus supplies a catalytic environment for increased kinetics for the electron transfer of the $\text{Fe}(\text{CN})_6^{3-/4-}$ couple. When this same electrode was placed in the background electrolyte (1.0 M KCl), voltammogram (d) was observed. The peak currents are reduced, but the $\text{Fe}(\text{CN})_6^{3-/4-}$ in the thin film shows an almost reversible voltammogram.

Table 4.2 summarizes the results of the ZnTPPS-4 - PVP - copolymer at different thickness on the ITO surface. In general, the $E_{1/2}$ values for the $\text{Fe}(\text{CN})_6^{3-/4-}$ couple is more anodic on the ITO surface compared to the SnO_2 surface. Generally, peak currents and peak positions follow the same trend as that observed for the SnO_2 electrodes. Peak currents are generally lower for the films on ITO compared to similar thickness on SnO_2 . Again this can be attributed to the higher resistance of the ITO film.

4.4.3. Electrochemistry of Au/ZnTPPS-4 - PVP - copolymer electrodes.

Dark electrochemistry on Au and modified Au electrodes shown in figure 4.13 show that rates of electron transfer at these surfaces are largely reduced. In (a), the voltammogram of the $\text{Fe}(\text{CN})_6^{3-/4-}$ couple on naked Au, a quasi reversible wave is seen. On modifying the Au electrode with PVP - copolymer, the voltammogram for the redox couple shows no recognizable peaks as seen in (b). Modification of the Au surface with ZnTPPS-4 - PVP - copolymer does not change the voltammogram in such a way that waves for $\text{Fe}(\text{CN})_6^{3-/4-}$ could be observed. Sluggish kinetics of the $\text{Fe}(\text{CN})_6^{3-/4-}$ couple at the Au surface should promote closer interaction between the chromophore and the redox counter-ion, especially in photoelectrochemical experiments where the back reactions can reduce quantum efficiencies for the electron transfer processes.

4.4.4. Electrochemistry of Ti/TiO₂/ZnTPPS-4 - PVP - copolymer electrode.

The TiO₂ layer formed on the Ti plate as in section 2.4.4. is essentially an insulating film. The dark electrochemistry with the redox couple $\text{Fe}(\text{CN})_6^{3-/4-}$ does not show any identifiable peaks as seen in figure 4.14(a).

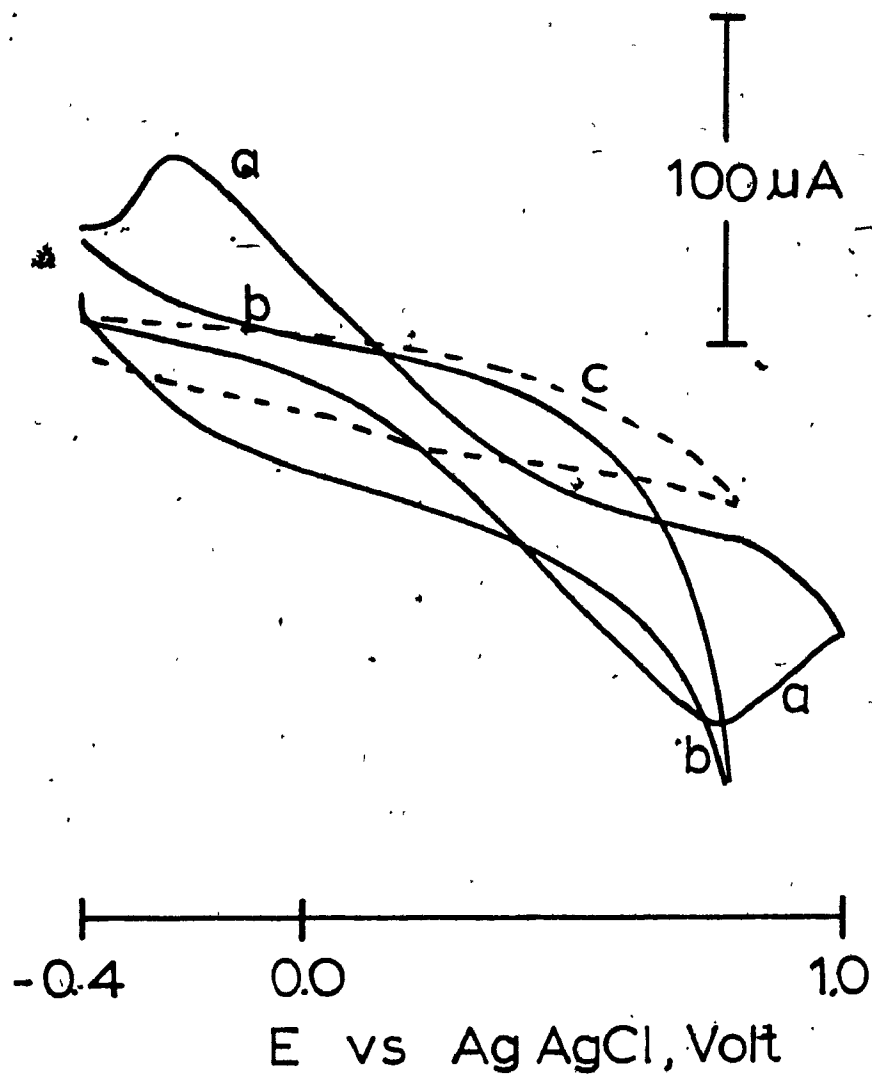


Figure 4.13. Voltammograms of the ferro/ferricyanide couple at different surfaces.
(a) Au surface, (b) Au/PVP-copolymer and
(c) Au/ZnTPPS-PVP-copolymer.

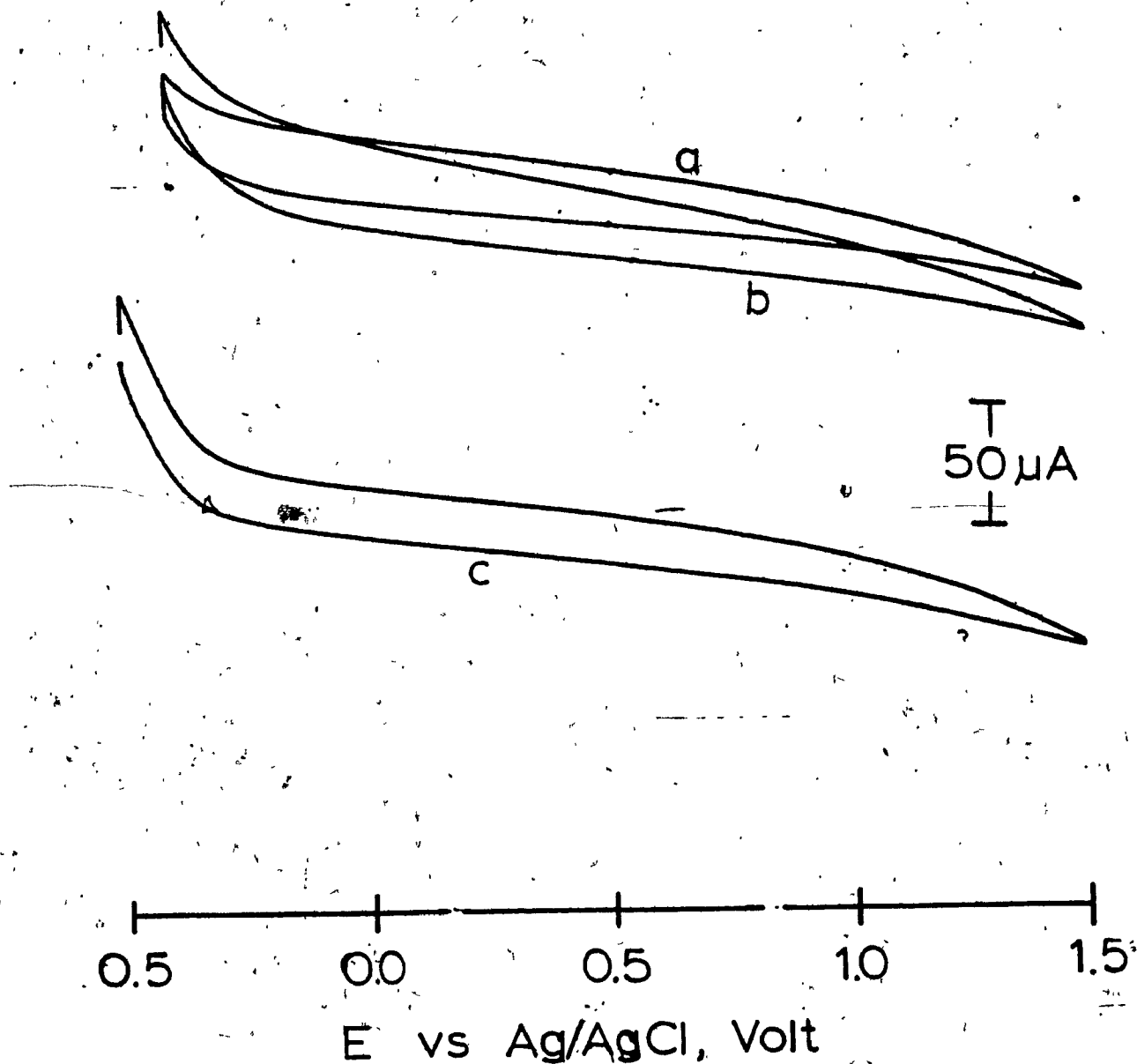


Figure 4.14. Voltammograms of the $\text{Fe}(\text{CN})_6^{3-/4-}$ couple at different surfaces. (a) TiO_2 , (b) TiO_2/PVP -copolymer and (c) $\text{TiO}_2/\text{ZnTPPS-PVP}$ -copolymer.

Modifying the TiO_2 surface with PVP - copolymer (figure 4.14(b)) or with ZnTPP - PVP - copolymer (figure 4.14(c)) does not change the voltammogram.

4.4.5. Electrochemistry and absorption spectra of ITO/CdS/ZnTPPS-4 - PVP - copolymer electrodes.

Thin films of CdS electrodeposited on ITO electrodes were transparent enough to allow spectral characterization by absorption spectroscopy. Figure 4.15(a) shows the absorption spectrum of CdS electrode A27. The onset of absorption at 500nm corresponds to the band gap of n doped CdS at 2.45 eV. Modification of this electrode with a film of ZnTPPS-4 - PVP - copolymer with a thickness of 2 μm shows the absorption spectrum of ZnTPPS-4 - PVP - copolymer superimposed on that of CdS (figure 4.15(b)).

Figure 4.16(a) shows the voltammogram of the redox couple $\text{Fe}(\text{CN})_6^{3-}/4-$ in contact with this surface. Identifiable waves for the reduction and reoxidation of $\text{Fe}(\text{CN})_6^{3-}/4-$ are observed, but there is an additional quasi-reversible wave in the voltammogram with an oxidation peak at +0.45 V vs Ag/AgCl. This peak has been associated with the formation of a $\text{CdFe}(\text{CN})_6^{2-}/1-$ overlayer (128).

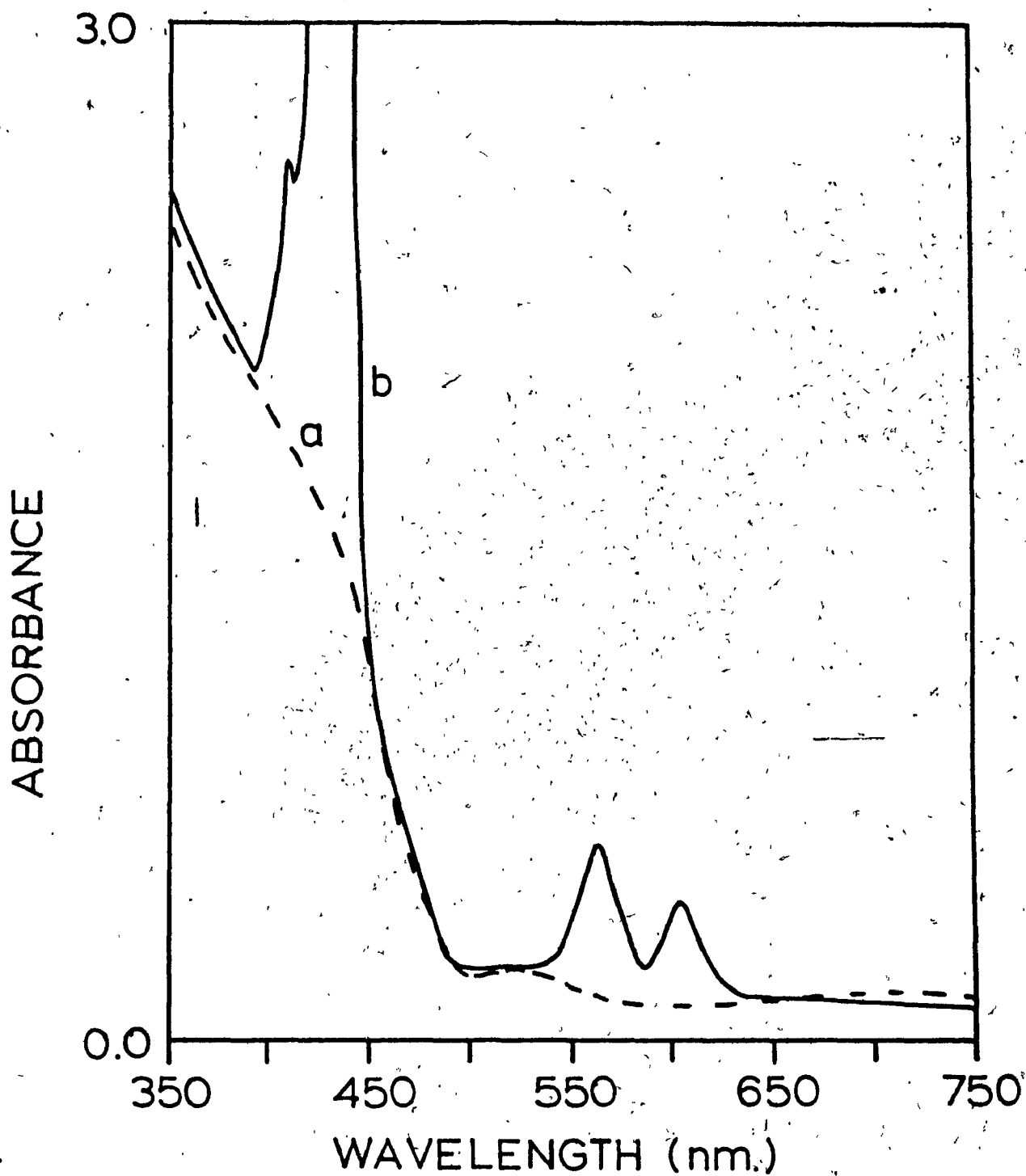


Figure 4.15. Absorption spectra of (a) a CdS film and (b) a CdS/ZnTPPS-PVP-copolymer film on ITO.

TABLE 4.3

PHOTOELECTROCHEMISTRY OF CDS/ZnTPPS - PVP - COPOLYMER.

Electrode	Thickness μm	Photovoltage volt	Photocurrent μA
A26	1.55		
A27	1.95	0.43	190
A28	1.75	0.72	133
A29	2.65	0.74	90
A30	2.75	0.70	108

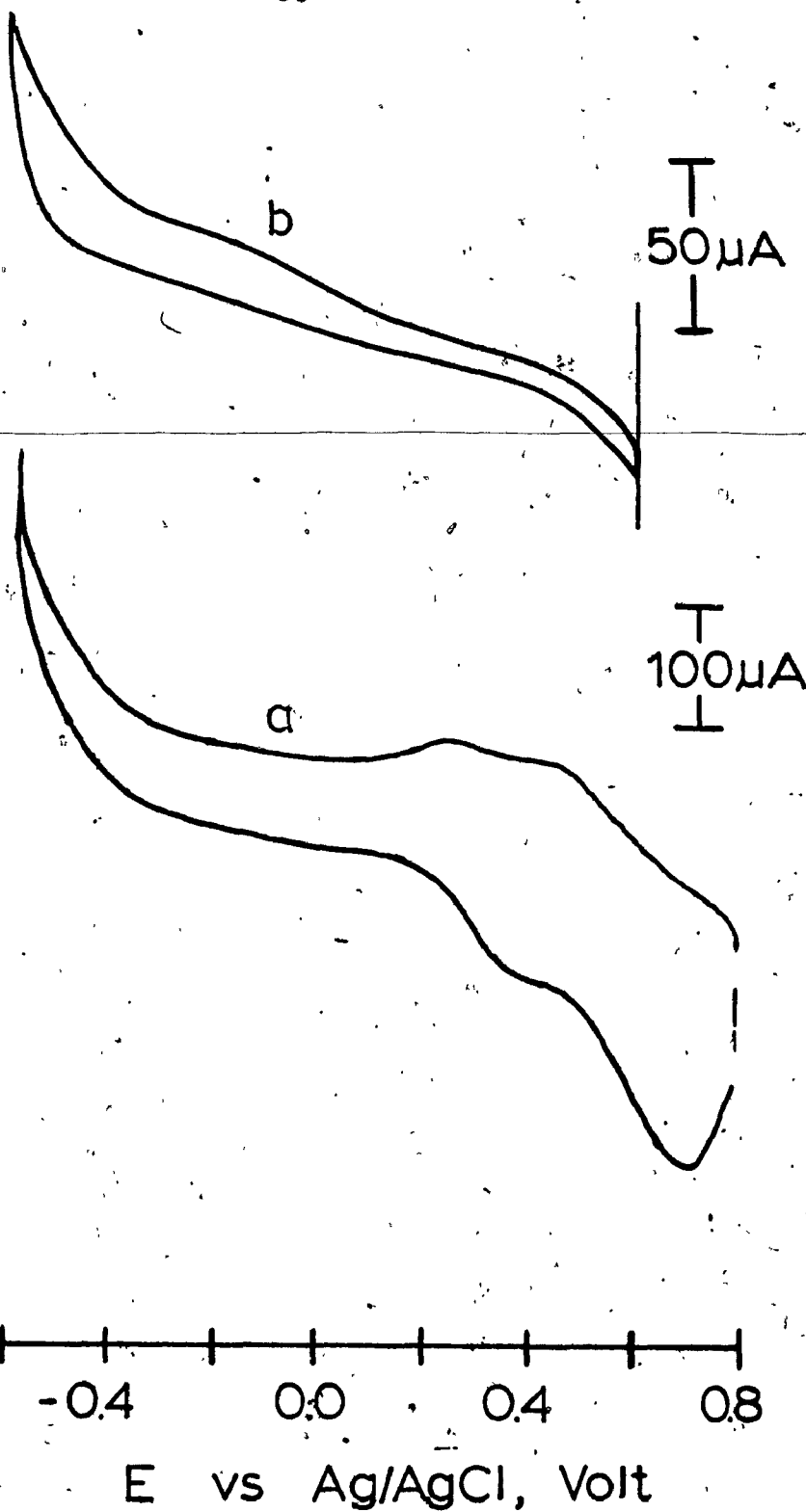


Figure 4.16. Voltammograms of $\text{Fe}(\text{CN})_6^{3-/4-}$ on (a) CdS/ZnTPPS-PVP-copolymer and (b) CdSe/ZnTPPS-PVP-copolymer electrodes.

4.4.6. Electrochemistry of ITO/CdSe/ZnTPPS-4-PVP-copolymer electrode.

The formation of n - type CdSe electrodes on ITO substrates leaves the CdSe overlayer as an insulating layer on the ITO. The electrochemistry for an electrode ITO/CdSe/ZnTPPS-4-PVP-copolymer is shown in figure 4.16(b) with the redox couple $\text{Fe}(\text{CN})_6^{3-}/4-$. The $\text{Fe}(\text{CN})_6^{3-}/4-$ wave cannot be seen, but extension of the potential scan to the anodic region shows an irreversible peak at +0.7 V which can again be assigned to the oxidation of the $\text{CdFe}(\text{CN})_6^{2-}/1-$ complex as seen for the CdS electrodes.

4.5. PHOTOELECTROCHEMISTRY OF ZnTPP-PVP-COPOLYMER AND ZnTPPS-4-PVP-COPOLYMER FILMS ON GOLD AND DIFFERENT SEMICONDUCTING SURFACES.

4.5.1. Transient photocurrent behaviour of thin porphyrin - polymer films.

The photocurrent transient spectra for the film ZnTPPS-4 - PVP - copolymer on different surfaces and in contact with the redox couple $\text{Fe}(\text{CN})_6^{3-}/4-$ are shown in figure 4.17. All the photocurrents were measured at short circuit between the working and the auxiliary electrode. (a) and (b) are the photocurrent transients for the film on SnO₂ and ITO electrodes respectively. These transients show an

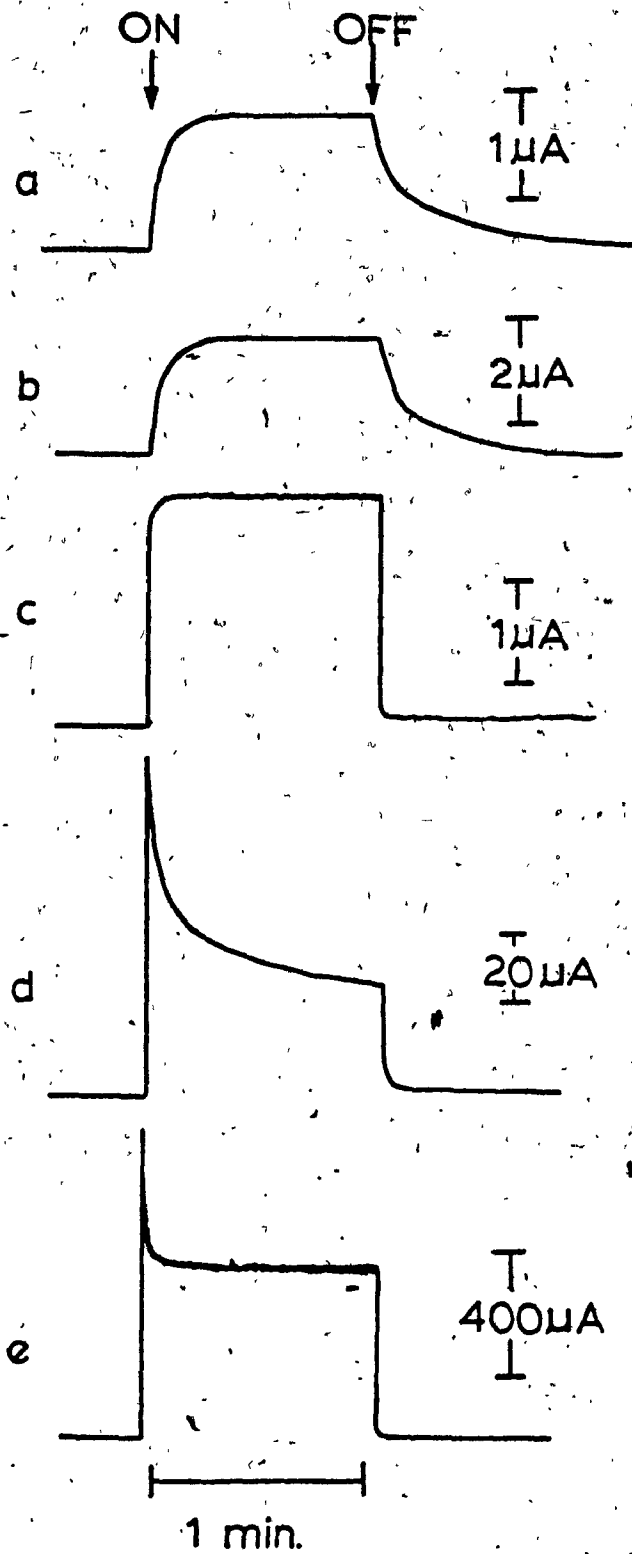


Figure 4.17. Photocurrent transients of different electrodes. (a) SnO_2/X , (b) ITO/X , (c) Au/X , (d) CdS/X and (e) CdSe/X where $\text{X} = \text{ZnTPPS-PVP-copolymer}$.

initial slow rise during the first 20 sec. of irradiation with white light from a tungsten - halogen lamp at 100 mW/cm², followed by the reaching of a steady state.

This steady state photocurrent can be maintained for periods longer than 4 hours before photocurrent drift sets in. The photocurrent is maintained only under continuous stirring of the electrolyte mixture. On switching off the light a slow decay process of the photocurrent takes place. The rate of this decay process is dependent on the time of irradiation. For irradiation of periods up to 5 minutes, the decay process is similar to that shown in figure 4.17(a) and (b). For longer periods of illumination, the decay process in the dark also becomes slower. This slow rise and decay processes have been associated with charge trapping within the polymer matrix. It has also been attributed to the formation of blocking contacts between the polymer film and the SnO₂ or ITO substrate. More will be said concerning the mechanism in Chapter 6. The spectra in (c), (d) and (e) are those of the film on Au, CdS and CdSe respectively. The fast response on Au seems to suggest that the previous slow response on SnO₂ and ITO were due to non-ohmic contact, but one should also keep in mind that the reversibility of the redox couple with the host surface might play a role. For CdS and CdSe modified electrodes, the photocurrent response represents those of the photogenerated charge in the narrow bandgap semiconductor rather than that of the

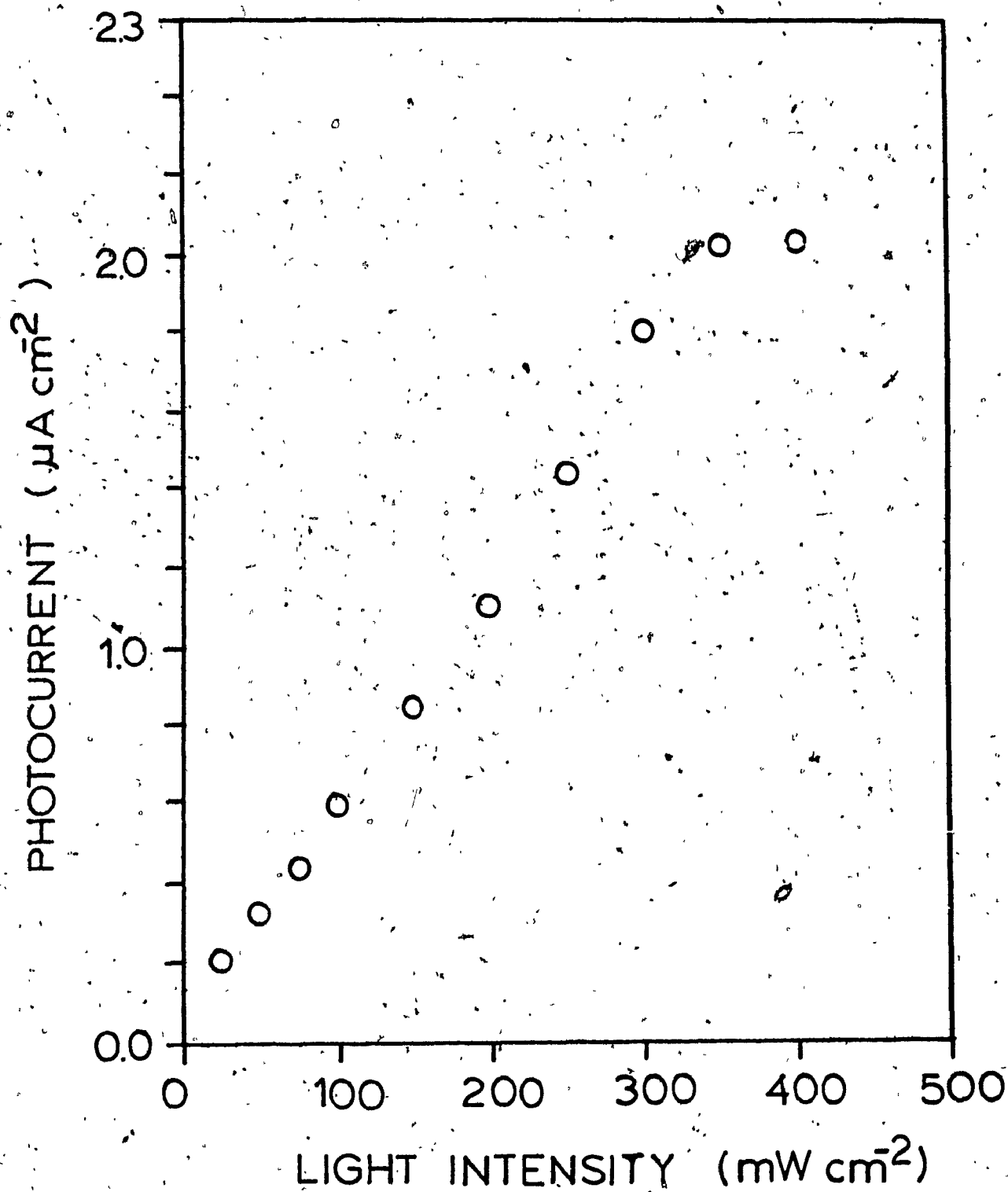


Figure 4.18. Photocurrent dependence vs. white light intensity for an electrode ITO/ZnTPPS-PVP-copolymer.

observed are similar to those observed for the thin porphyrin films in SnO₂ described in section 3.5.1.

4.5.2. Effect of white light intensity on photocurrent.

The photocurrent variation with the white light intensity for a thin film of ZnTPPS-4 - PVP - copolymer on ITO is shown in figure 4.18. The photocurrent increases linearly with increasing intensity up to a limit of 375 mW after which a saturation point is reached. At low photon flux, the photocurrent transients resemble a capacitive discharge effect. At higher intensities, this effect is reduced since not only chromophores at the interface are excited, but also chromophores in the bulk. This linear relationship shows that photocurrent generation is related to the cross section of chromophores which are excited throughout the bulk of the polymer film.

4.5.3. Photoaction spectra of thin polymer films.

The origin of the photocurrents in these thin films are seen to be from the lowest singlet excited state of the ZnTPPS-4 as exemplified in figure 4.19. The photoaction spectrum follows the absorption spectrum closely in the Q region of the spectrum. The peak in the action spectrum at 458 nm can be attributed to a contribution from the complex formed between Fe(CN)₆^{3-/4-} and pyridine. These

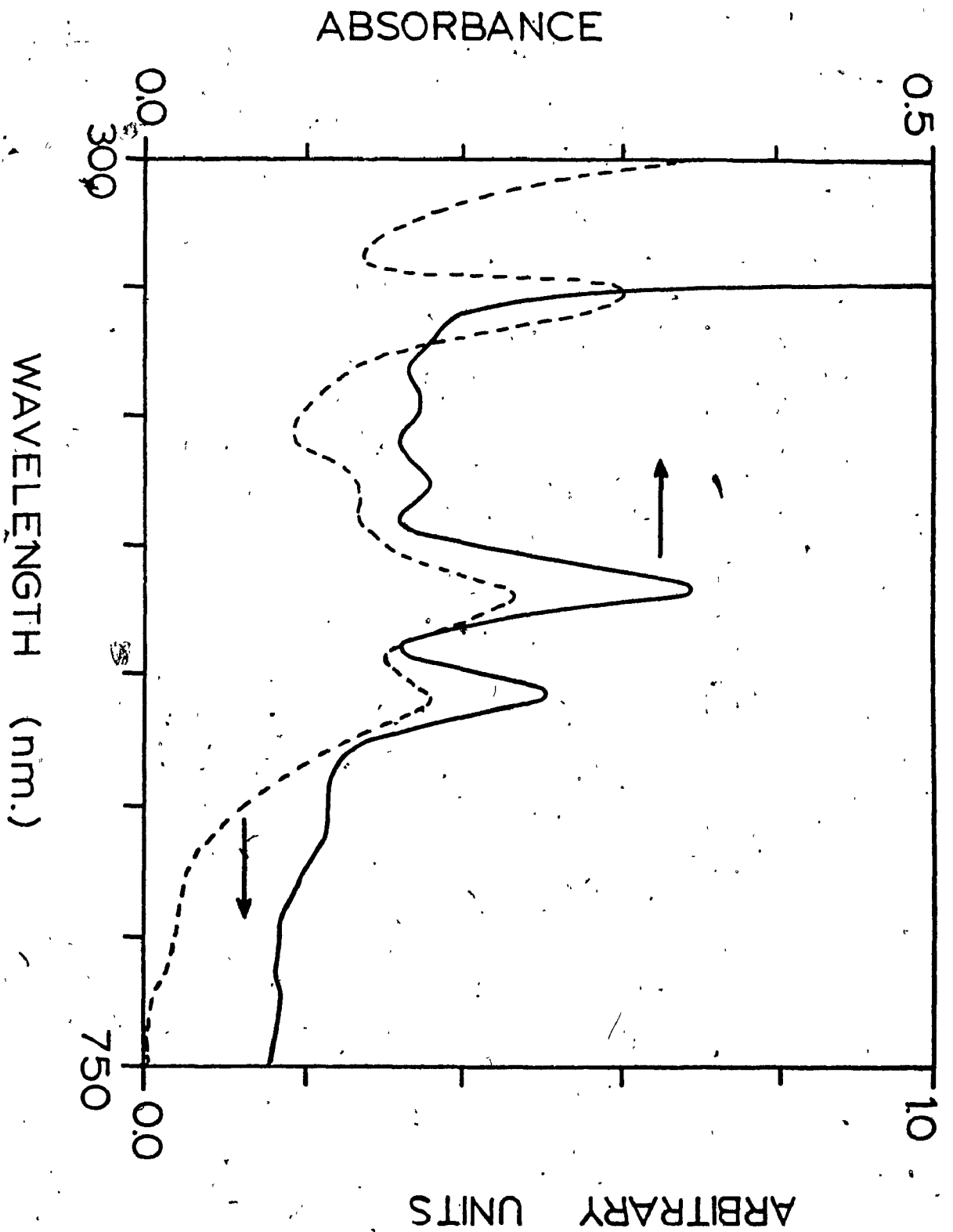


Figure 4.19. Absorption spectrum (—) vs. photocurrent action spectrum (---) for a thin film of ZnTPPS-PVP-Copolymer on ITO.

complexes have been shown to have a charge transfer band which is red-shifted with respect to the $\text{Fe}(\text{CN})_6^{3-}$ band at 420 nm. Significant filtering of the light also occurs since irradiation of the electrode surface takes place through the solution and only light of wavelengths greater than 420 nm reaches the electrode surface. This could account for not observing large photocurrent contributions from light with wavelengths similar to that of the Soret band.

4.5.4. Dependence of photocurrent on polymer film thickness and chromophore concentration.

Film thickness is a good measure of the extent to which the polymer film can be used to increase the photon absorption per cm^2 . Thicker films were earlier found (section 3.5.3.) to be the limiting factor in that although the chromophore concentration is increased, the thicker films poses barriers for conduction of the photoexcited species. With polymer films, a wide range of film thicknesses could be studied easily, but the work reported here concentrates on films with a maximum thickness of 20 μm . Films thicker than 20 μm showed irregularities in their surface structure. Figure 4.20 shows the photocurrent - thickness profile for films consisting of ZnTPP - PVP - copolymer on SnO_2 electrodes. Photoelectrochemical conditions are the same as those discussed earlier in section 2.5.2. The photocurrent

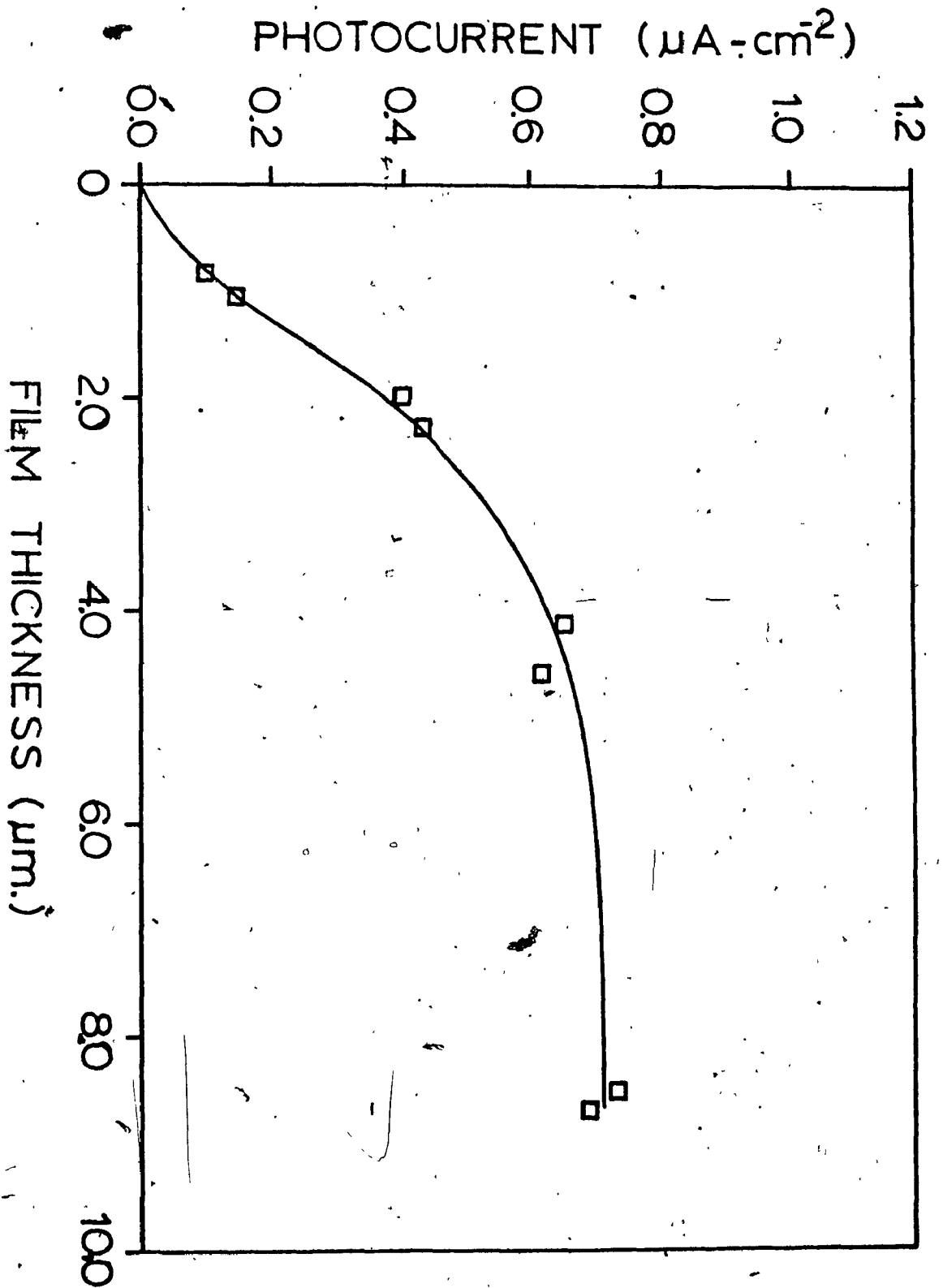


Figure 4.20. Photocurrent vs. film thickness for the ZnTPP-PVP-copolymer film on SnO₂.

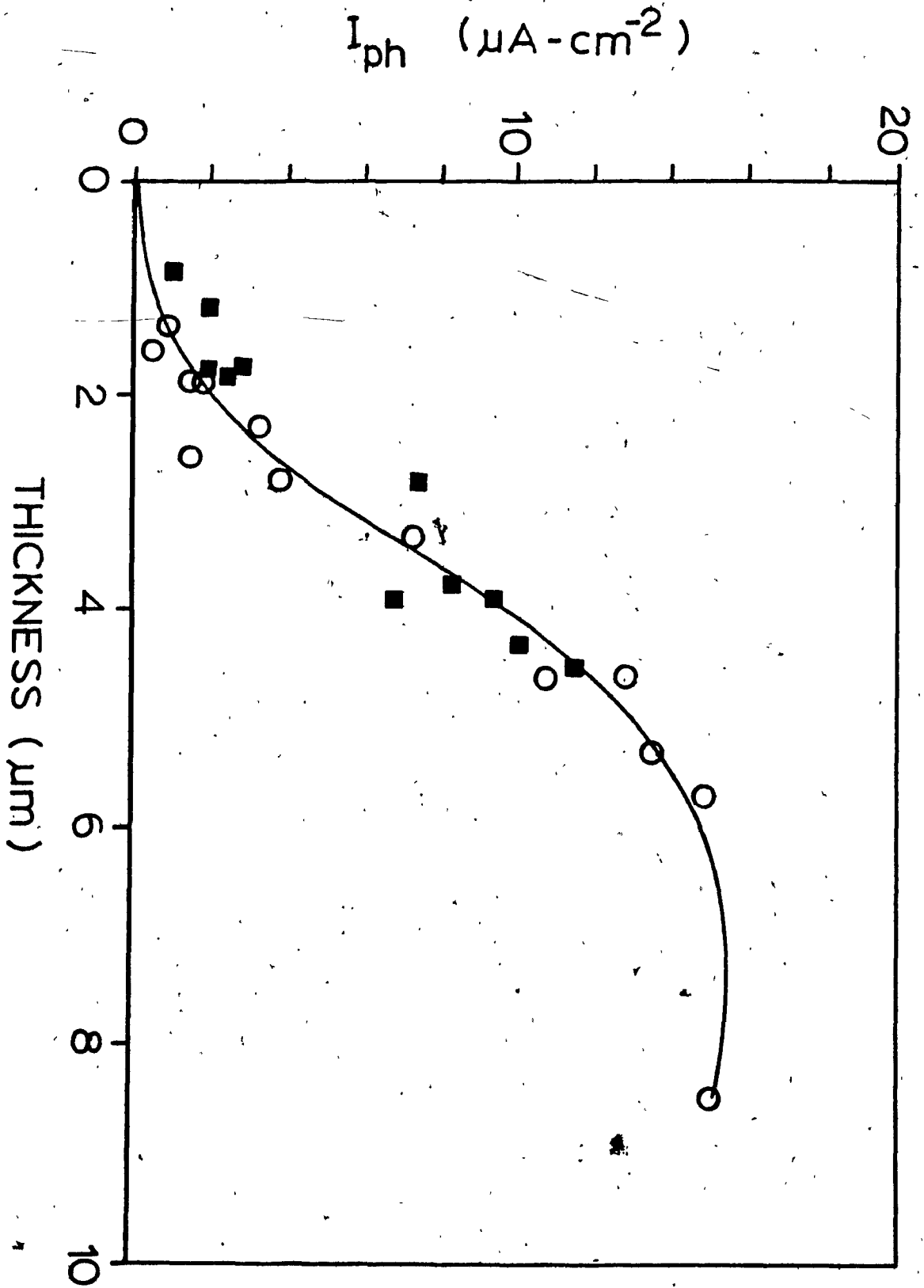


Figure 4.21. Photocurrent vs. film thickness for the ZnTPPS-PVP-copolymer film on SnO₂ (O) and on ITO (■).

profile for this chromophore in the polymer blend does not differ significantly from those of the ZnTPP in PVP. The addition of a conductive copolymer did not change the photocurrent characteristics. A plateau in photocurrent is reached with a film of 5 μm thick. The anionic analogue of ZnTPP, ZnTPPS-4 shows a much higher photocurrent response over the same film thickness range when films consisting of ZnTPPS-4 - PVP - copolymer are irradiated on SnO_2 and ITO surfaces (see figure 4.21). This difference in photocurrent for the different chromophores can be attributed to the electrochemical and photophysical behaviour of the chromophores and also the conformation they assume in the polymer matrix. A detailed discussion of this will follow in chapter 6.

The increase in the photocurrent for the ZnTPPS-4 - PVP - copolymer also reaches a plateau for films $> 7 \mu\text{m}$ after which the photocurrent steadily decreases for very thick films. The linear relationship of photocurrent vs thickness does not hold at thin films either (see figure 4.20 and 4.21). The photocurrent increases only after a certain film thickness ($\sim 1 \mu\text{m}$) is reached.

Table 4.3 summarized the photoelectrochemical data for the ZnTPPS-4 - PVP - copolymer films on CdS electrodes. The photocurrents are less than that observed for a naked CdS electrode ($\sim 230 \mu\text{A}$), suggesting that the quantum efficiency of the thin chromophore - polymer film is less than that of the underlying semiconductor and that the

film acts as a filter. The thin porphyrin - polymer film increases the photovoltage properties of the CdS electrodes significantly.

CHAPTER 5.

RESULTS AND DISCUSSION III.

PHOTOPHYSICS AND PHOTOCHEMISTRY OF PORPHYRIN SOLUTIONS AND FILMS.

The study of the photochemistry and the photophysics of porphyrin molecules is important in understanding the ability of the porphyrin excited states to undergo electron transfer reactions and in understanding the primary photoprocess in the polymer thin films. This chapter will be concerned with determining energy position of excited states, lifetimes of excited states and the detection of intermediates in the photoprocess.

5.1. FLUORESCENCE SPECTRA OF ZnTPP AND ZnTPPS-4 IN SOLUTION AND IN SOLID FILMS.

5.1.1. Fluorescence maxima in solution and in films.

The emission maxima for the porphyrins ZnTPP and ZnTPPS⁻⁴ in solution and as solid films are summarized in table 5.1. Illustrated in figure 5.1 are the emission maxima for ZnTPP in CH₂Cl₂ (a) and for a ZnTPP film (b) on SnO₂. The emission spectra of the solid differs from that in solution in that the bands are generally red - shifted. The solution spectra also shows the changes observed in

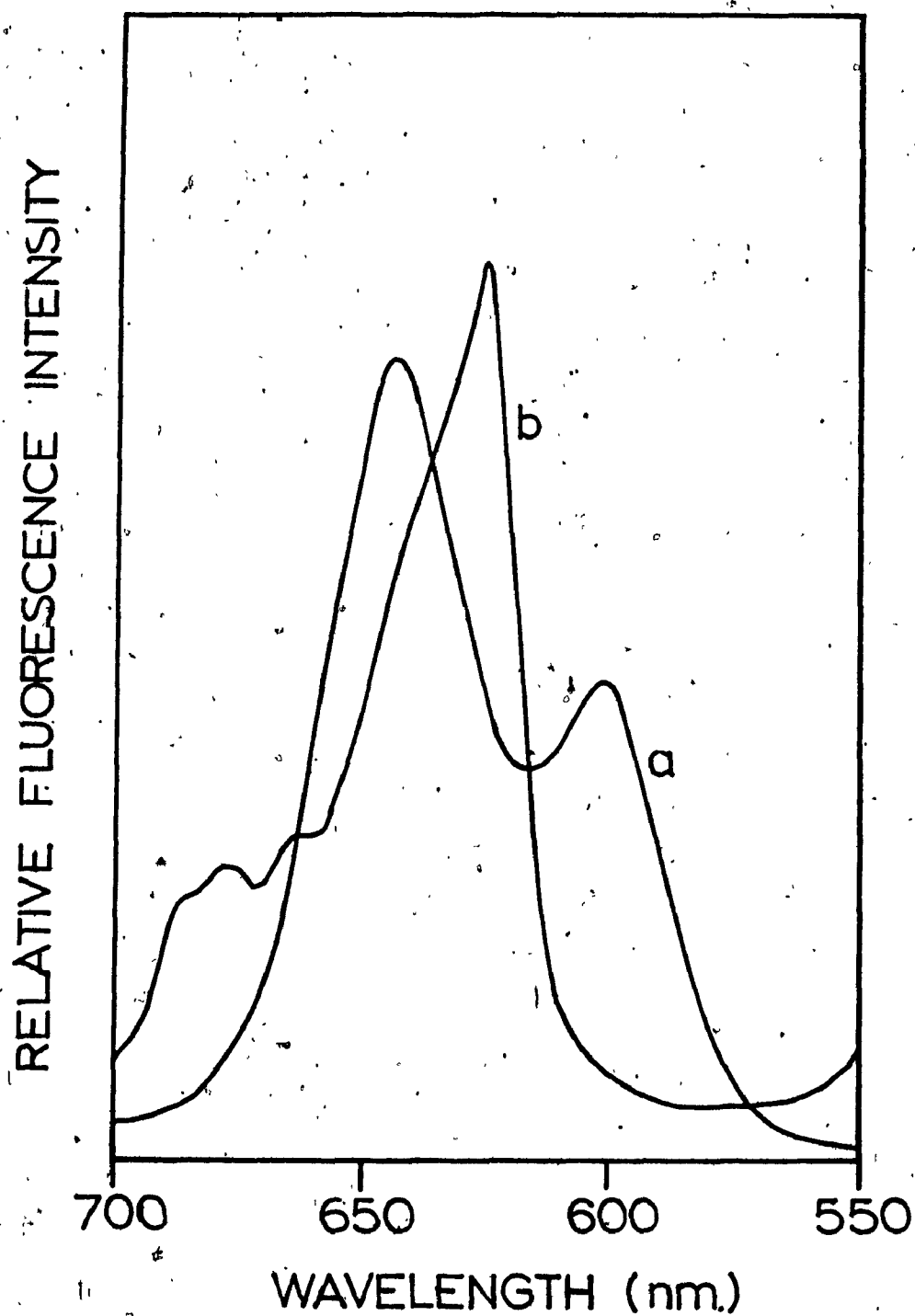


Figure 5.1. Fluorescence maxima for (a) ZnTPP in CH_2Cl_2 and (b) as a thin film of ZnTPP on SnO_2 .

TABLE 5.1

FLUORESCENCE MAXIMA FOR PORPHYRIN SOLUTIONS AND PORPHYRIN THIN FILMS ON SnO₂ ELECTRODES.

	Fluorescence Maxima	
	Solution nm	Film nm
ZnTPP in CH ₂ Cl ₂	603, 645	626, 663, 678
ZnTPP in Pyridine	618, 663	628, 695
ZnTPP - Triphenylphosphine	618, 663	618, 655
ZnTPP - Triphenylarsine	603, 647	615, 655
ZnTPP - PVP	606, 655	628, 647
ZnTPPS-4 in CH ₃ OH	606, 656	
ZnTPPS-4 - PVP - copolymer	608, 658	616, 670

the spectra of ZnTPP with the different ligands discussed in chapter 3. The lowest energy band for each case was used to determine the lowest excited singlet state of the porphyrin.

5.1.2. Fluorescence behaviour of ZnTPPS-4 on addition of PVP - copolymer.

The effect of "titrating" a 5 μ m solution of ZnTPPS-4 in CH_3OH with aliquots of a 1% PVP - copolymer solution in CH_3OH is shown in figure 5.2. The fluorescence bands of the ZnTPPS-4 is shown by (a). Curves (b); (c), (d) and (e) shows the fluorescence after 5, 10, 50 μ l and an excess of the PVP - copolymer solution has been added.

The fluorescence is first quenched (curves (b) and (c)) and after a certain concentration of polymer it recovers again (curves (d) and (e)). The quenching and recovery coincides with a decrease and a subsequent increase in the lifetime of the fluorescence. It is associated with the ability of the polymer to aggregate the ZnTPPS-4 at low concentration, but as more polymer is added, there is a distribution of the ZnTPPS-4 over separated polymer sites. Aggregation of the ZnTPPS-4 decreases its fluorescence lifetime significantly, a property which is common family (16).

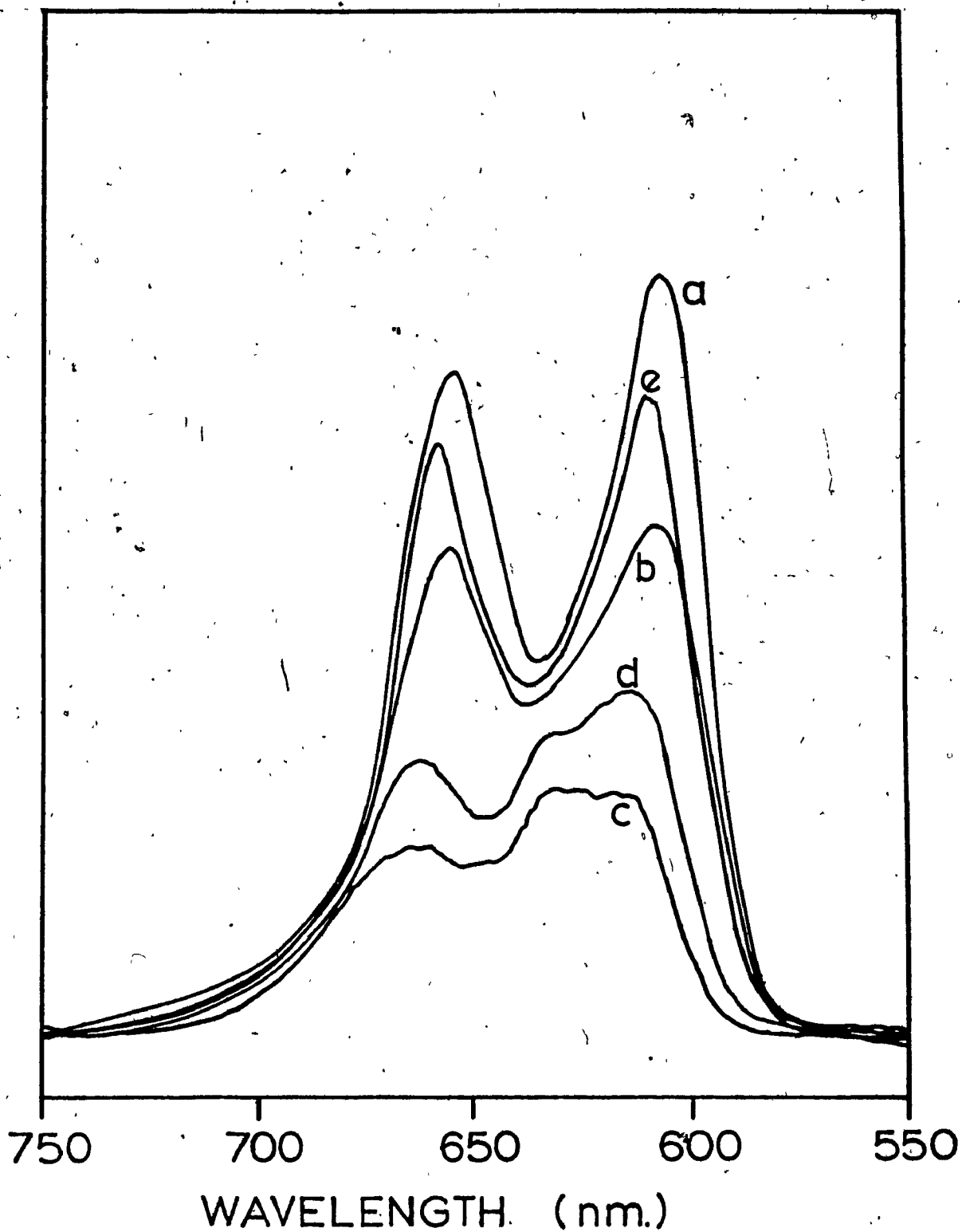


Figure 5.2. Fluorescence spectra of the titration of ZnTPPS⁻⁴ in CH₃OH with increments of a 1% PVP-copolymer solution. Addition of (a) 0, (b) 5 μ l, (c) 10 μ l, (d) 50 μ l and (e) an excess.

5.2. SUBMICROSECOND TRANSIENT ABSORPTION SPECTROSCOPY ON ZnTPP, ZnTPP WITH AXIAL LIGANDS AND ZnTPPS-4.

Nanosecond transient absorption measurements were performed as outlined in section 2.8.1. All samples were thoroughly degassed with Ar for periods of 40 - 60 min. Transient decay was followed at the wavelength of triplet-triplet (T - T) absorption for the porphyrins, which was generally between 450nm and 480nm. Figure 5.3 shows the transient observed after exciting a solution of ZnTPP-4 in methanol with a 20 ns pulse at 590 nm. The lifetime of the triplet excited state was calculated from the $\ln A$ vs time plot. Lifetimes for triplet states for ZnTPP and ZnTPPS-4 in the different media are recorded in table 5.2. In all cases except for the porphyrins in polymers, the kinetics were simple first order and the rate constant could be extracted from the $\ln -$ plot. For the cases of the polymers, the figures presented represents the faster of the kinetic processes involved. From table 5.2 it is seen that the presence of ligands such as pyridine increases the triplet lifetime of the chromophore - ligand complex. The pyridine based polymers have a similar effect on the triplet lifetime of ZnTPP and ZnTPPS-4.

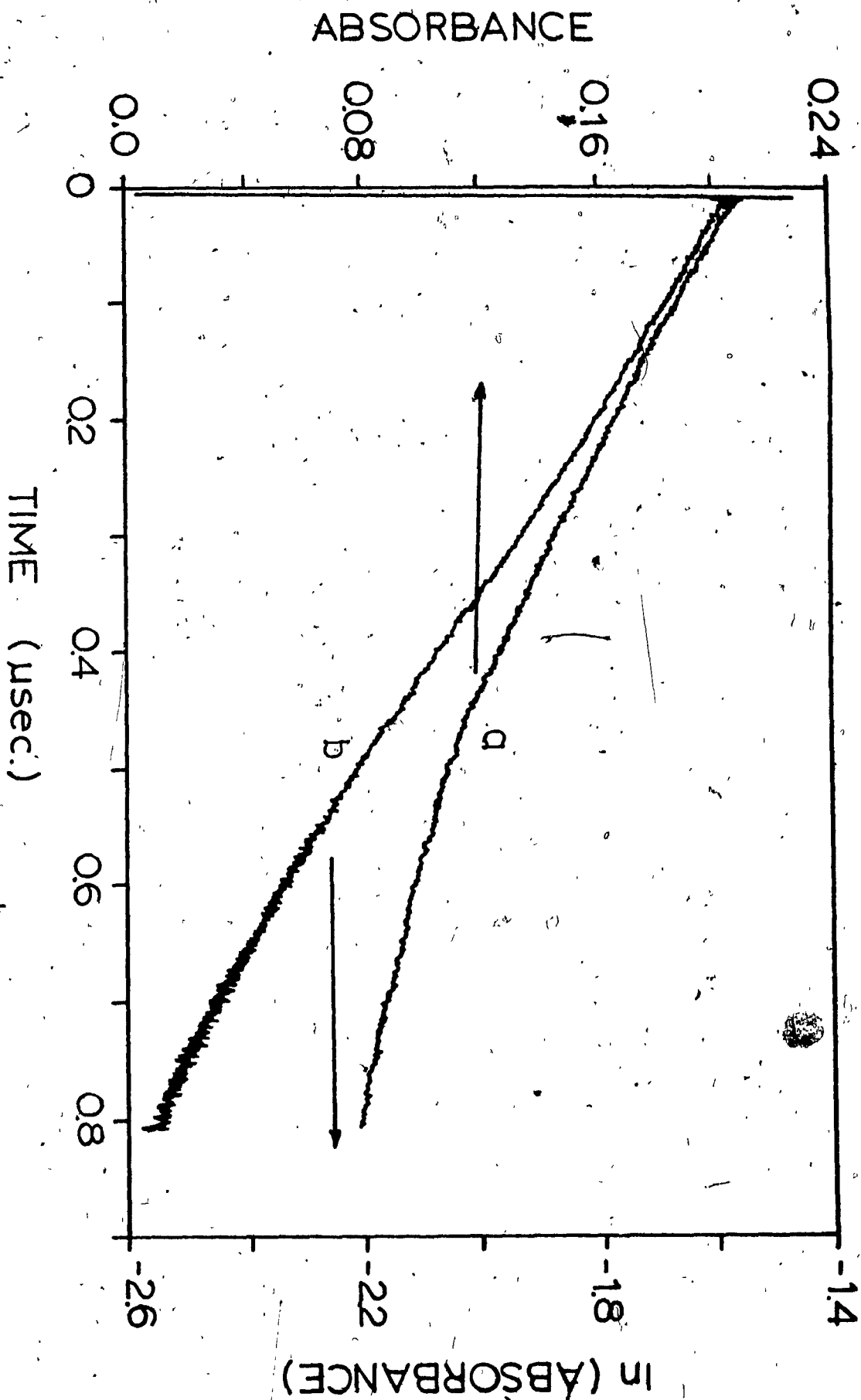


Figure 5.3. (a) Transient absorption spectrum for $ZnTPPS^{-4}$ in CH_3OH after excitation with a 10 ns. pulse at 590 nm.
(b) A ln. plot of (a).

TABLE 5.2

PHOTOPHYSICS OF PORPHYRIN AND PHTHALOCYAMINE DYES.

	Fluorescence		T-Tabs. decay	
	Singlet λ , nm	τ_s nsec.	Triplet λ , nm	τ_T usec.
ZnTPP in MeCl ₂	645	1.87	470	583
ZnTPP in Pyridine	663	1.48	470	200.2
ZnTPP in PVP	645	1.54	470	318
ZnTPPS in Methanol	656	2.18	460	785
ZnTPPS in PVP-copol(excess)	656	7.67	460	2180
ZnTPPS in PVP-copol(at Q1)	656	0.29		
ZnTPPS in PVP-copol film	>600	0.33		

5.3. PICOSECOND PULSE FLUORESCENCE ON PORPHYRIN SOLUTIONS AND FILMS.

Time resolved fluorescence measurements were taken in the Canadian Centre for Picosecond Flash Photolysis. A typical transient fluorescence decay is presented in figure 5.4 for the system ZnTPP in pyridine after excitation of the sample with a 30 ps pulse at 355nm. The \ln plot shows a first order relationship. Table 5.2 summarizes the fluorescence lifetimes for ZnTPP, ZnTPP with axial ligands, ZnTPPS-4 and ZnTPPS-4 - PVP - copolymer. The fluorescence lifetime of ZnTPPS-4 - PVP - copolymer as a thin film on ITO glass is also listed. A comparison of ZnTPP, ZnTPP - pyridine and ZnTPP - PVP shows that the singlet lifetime of the chromophore is just slightly reduced on addition of axial ligand. The ZnTPPS-4 system however shows that the presence of excess polymer increases the singlet lifetime almost 3.5X. The singlet lifetime which corresponds to conditions where aggregation takes place (figure 5.2(c)) is also reported in table 5.2. The lifetime is much shorter than that of the parent chromophore ZnTPPS-4 in CH_3OH and shows that aggregation is responsible for the quenching process observed in figure 5.2. This lifetime is of the same order as that observed for the thin film of ZnTPPS-4-PVP-copolymer on ITO. Conditions in the film should correspond to a situation where the chromophores are sufficiently

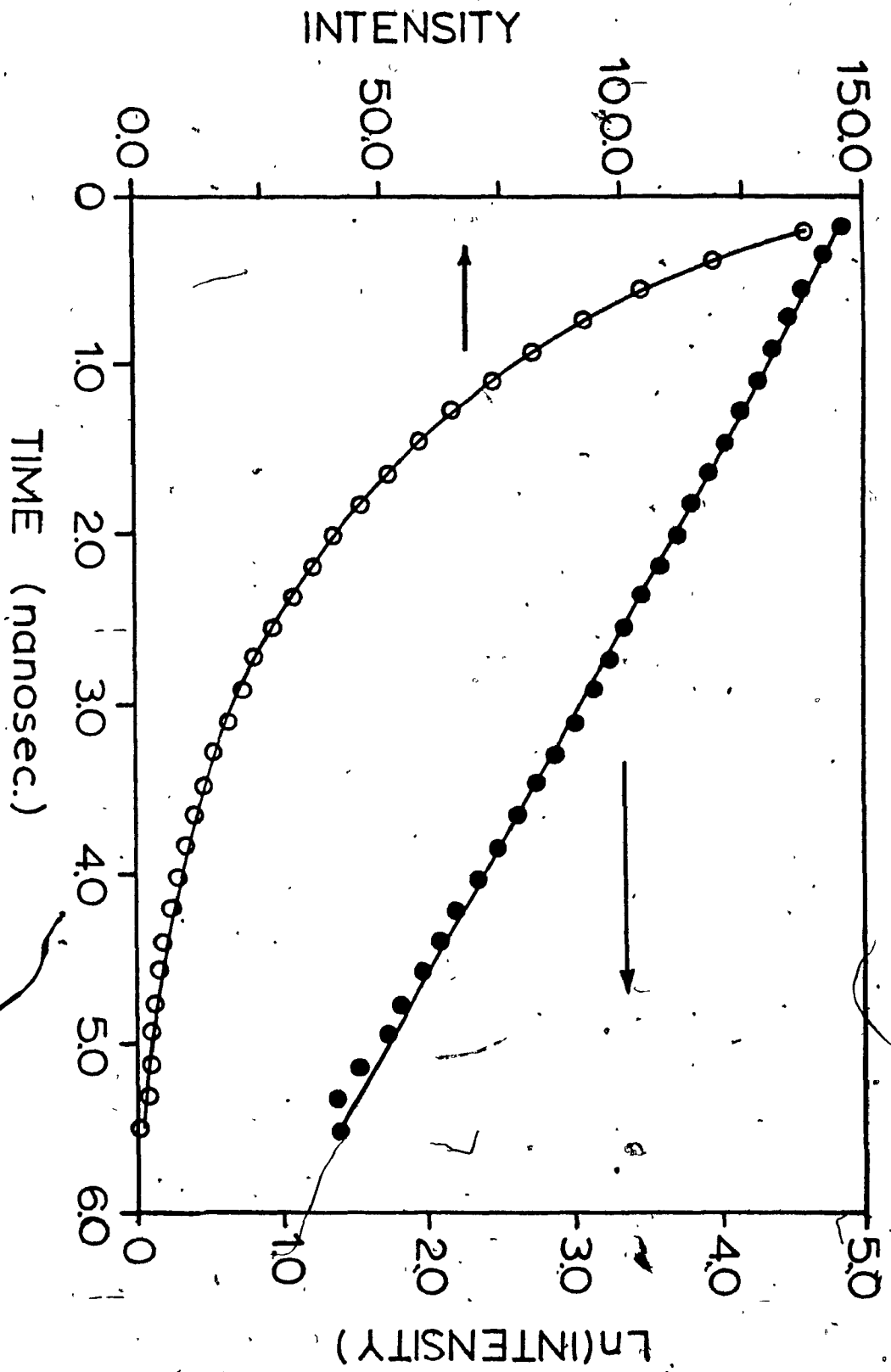


Figure 5.4. Transient fluorescence spectrum of ZnTPP in pyridine after excitation with a 30 ps. pulse at 355nm (O). The ln. plot of the transient decay (●).

close together for the quenching process to take place.

5.4. PICOSECOND TRANSIENT ABSORPTION SPECTROSCOPY OF ZnTPP AND ZnTPPS-4 SOLUTIONS.

Figure 5.6 shows the difference spectra of a 0.8 μM solution of ZnTPP in CH_2Cl_2 at different time decays after excitation with a 30 ps pulse at 355 nm. The experimental conditions were as described in section 2.8.2. The features of the spectrum at 50 ps after excitation are such that it shows a strong absorption in the region 450 - 530 nm with a peak at 460 nm. There is also some absorption at wavelengths > 575 nm. The spectrum shows bleaching at 548 nm which corresponds to bleaching of the ground state of the porphyrin. At longer time delays after excitation, the only notable change in the spectrum is the slight recovery of the ground state bleaching and a minimal increase in the absorption to the red. The spectra are difficult to assign as either singlet or triplet spectra since the excited state absorption of the singlet and triplet $\pi - \pi^*$ states of the porphyrin are expected to overlap strongly, but the triplet states absorb slightly more to the red (130). The small changes that occur in the spectrum in the region 450 - 520 nm between 0 ps and 10 ns suggest that the singlet and triplet strongly overlap. The singlet excited state lifetime under the same experimental conditions were measured as 1.87 ns, indicating that the persistence of the 460 nm band even after 3 ns can be

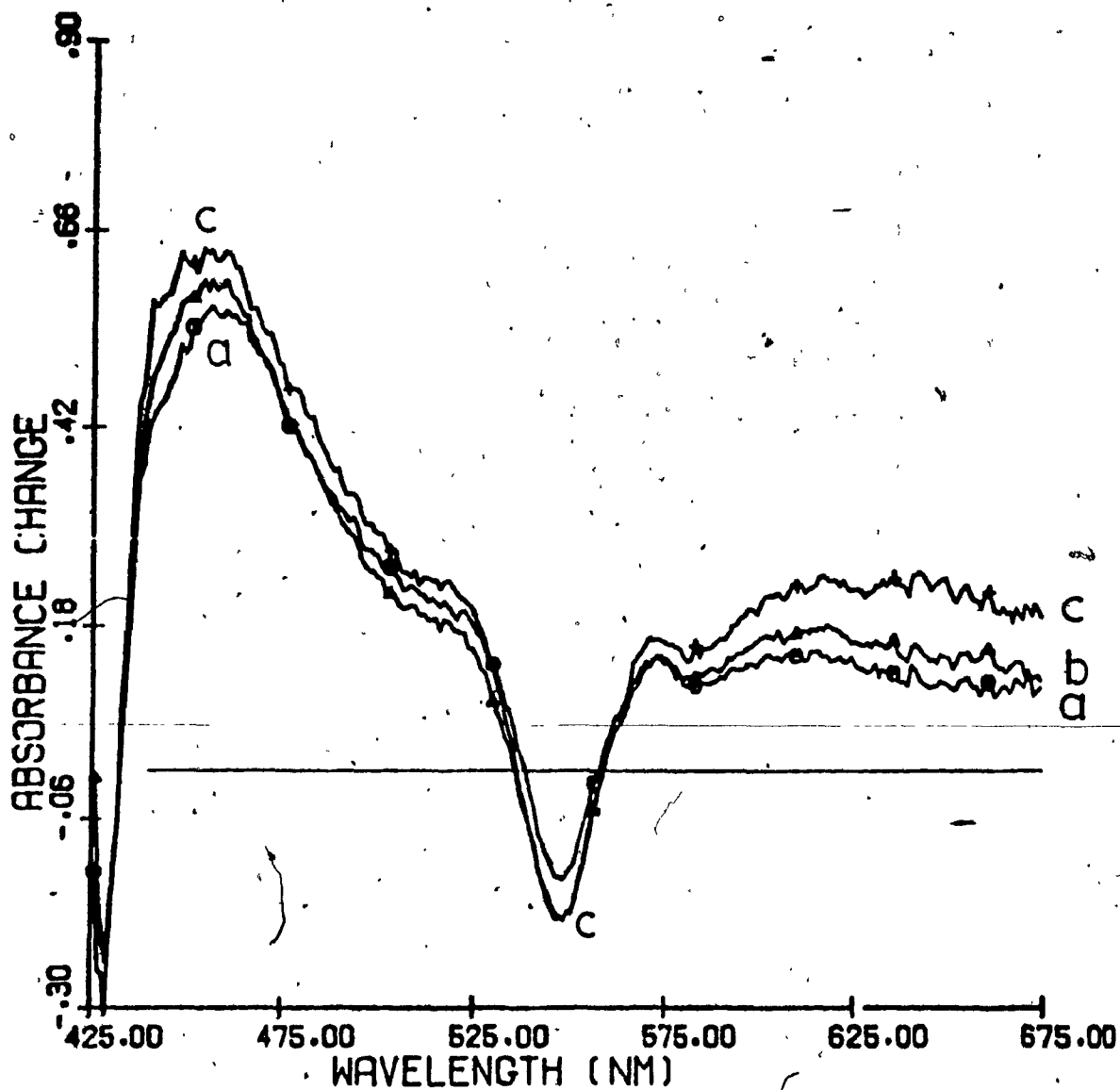


Figure 5.5. Transient absorption spectra for ZnTPP in CH₂Cl₂ at (a) 20 ps., (b) 1 ns. and (c) 10 ns. after excitation with a 30 ps. pulse at 355nm.

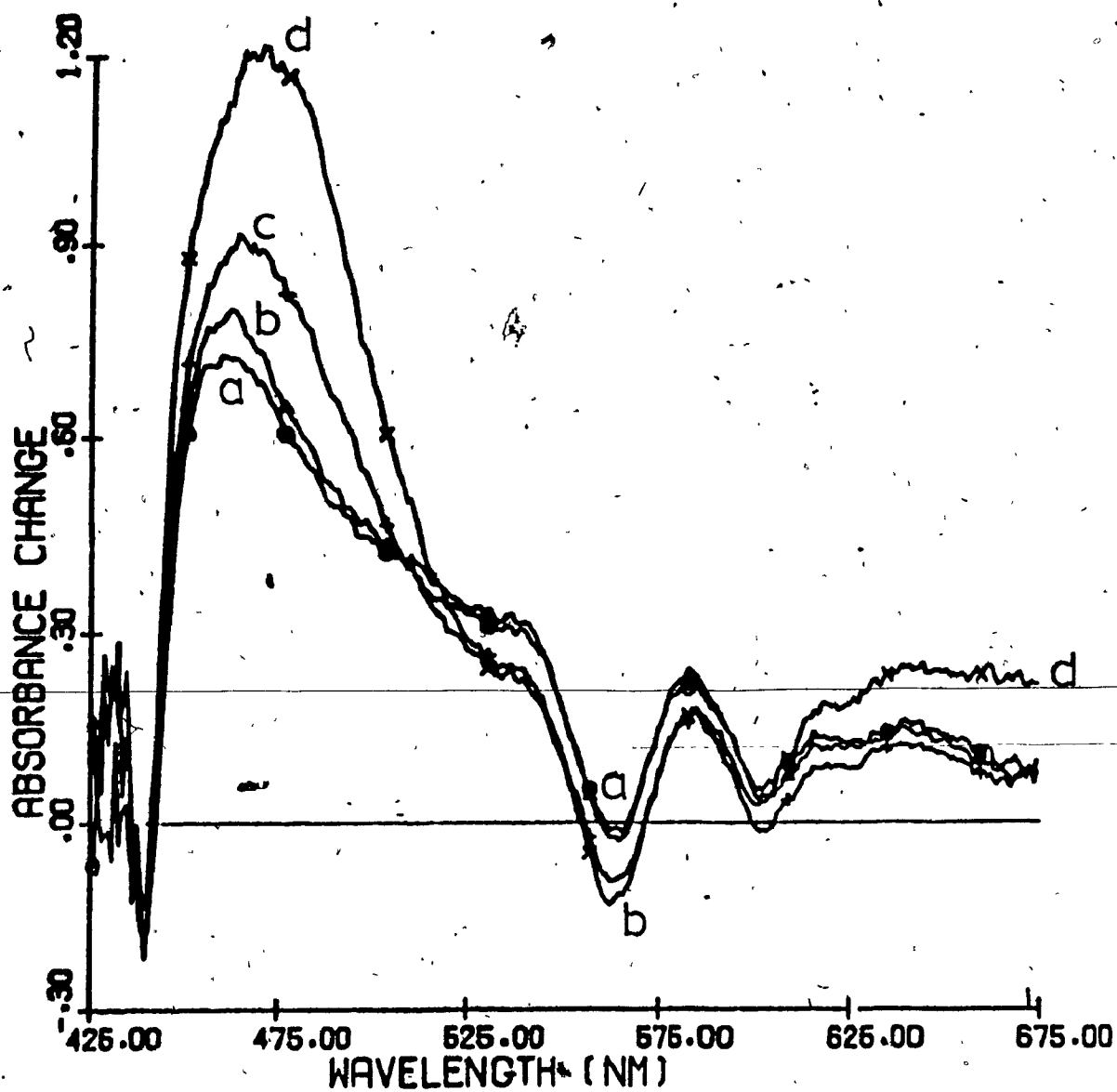
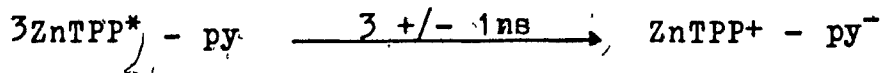
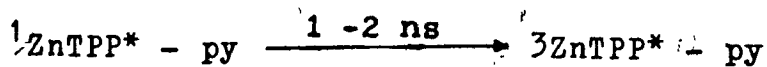
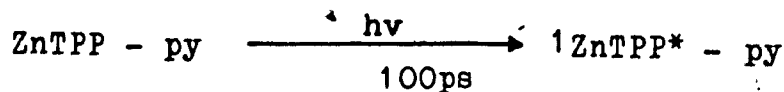


Figure 5.6. Transient absorption spectra for ZnTPP in pyridine at (a) 20 ps, (b) 50 ps, (c) 1 ns and (d) 10 ns after excitation with a 30 ps pulse at 355nm.

attributed to triplet absorption. The contribution to changes in the spectrum from photoelectron transfer from the singlet to the solvent is not excluded, since precedents do exist for the Cd and Hg analogs (130). This may also contribute to the absorption growth in the red of the spectrum.

The spectral changes in figure 5.6 are more revealing. This figure represents the spectra of ZnTPP in pyridine over a time range of 10ns. It has been shown earlier (section 3.1) that ZnTPP in this solvent exists as the bis-pyridine species. During the first 50ps there is some growth of the 450 - 500nm region which is associated with passage of the pulse. The subsequent growth of the 470nm band and the shift to the red of this band after 3ns coincides with the formation of an isosbestic point at about 506nm. There is also continuous growth in absorbance in the red and no indication of recovery of the ground state bleaching at 564nm. The growth of the absorbance peak at 475nm and the broad absorbance in the red are the signature of the pyridine coordinated radical cation of the ZnTPP (35, 131). The changes in the blue corresponds to similar changes observed in the reaction of a water soluble ZnTPPS-4 with nitrobenzene (132). The 10 ns spectrum in figure 5.6 can thus be assigned to as the charge transfer state ZnTPP+py⁻.

The development of this state will correspond to the reactions



The yield of this charge transfer state was estimated from the ground state bleaching after 10ns to be approximately 0.5.

Spectra for ZnTPP - PVP in methylene chloride suggests the formation of a similar charge transfer state, but this will take place at sufficiently high polymer concentrations. Experiments were performed only at low PVP concentration.

The spectra for ZnTPPS-4 in CH_3OH shown in figure 5.7 show slight changes, but it can be reasonably interpreted in the same way as the spectra for ZnTPP in CH_2Cl_2 . The coordinating solvent CH_3OH have the same effect on the blue region of the spectrum as that of pyridine in that the broad peak is slightly red shifted.

The spectra for ZnTPPS-4 - PVP - copolymer in methanol, shown in figure 5.8 resembles that of the spectra of ZnTPP in pyridine. These spectra were taken in situations, where a large excess of PVP - copolymer was present. The assignment is the same as that for the ZnTPP - py case. This suggest that the primary process in the photoelectrochemical films is the formation of this charge

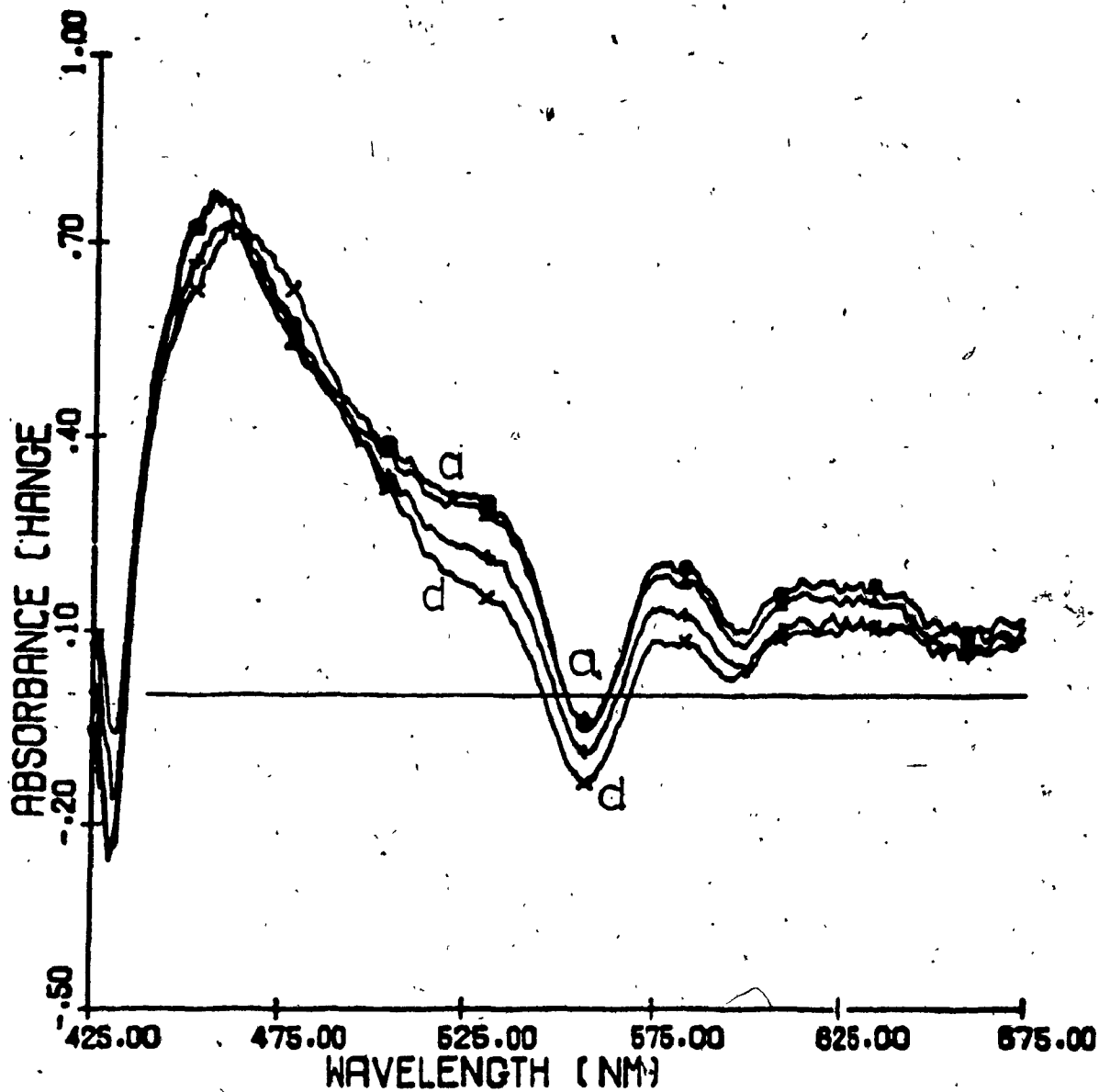


Figure 5.7. Transient absorption spectra for ZnTPPS⁻⁴ in CH₃OH at (a) 50 ps, (b) 100 ps, (c) 1 ns, and (d) 10 ns, after excitation with a 30 ps. pulse at 355nm.

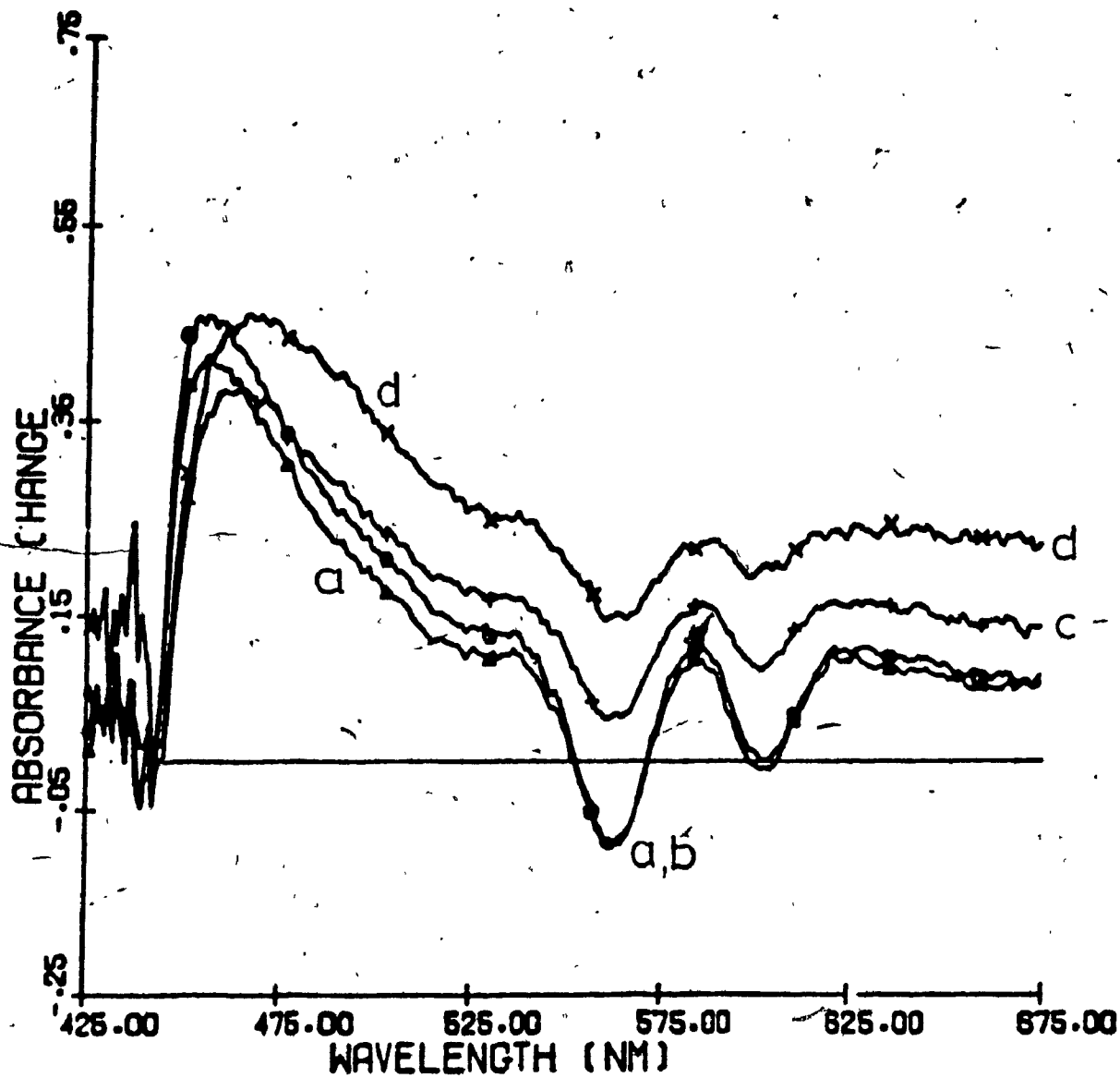


Figure 5.8. Transient absorption spectra of ZnTPPS⁴⁻-PVP-copolymer at (a) 50 ps, (b) 100 ps, (c) 1 ns and (d) 10 ns. after excitation with a 30 ps. pulse at 355 nm.

transfer state. The subsequent fate of the separated "ion - pair" forms the basis of a model to try to explain the photoelectrochemical and photocatalytic behaviour of the porphyrin - polymer films.

CHAPTER 6

DISCUSSION IV AND CONCLUSION

6.1. REDOX PROPERTIES AND ENERGETIC CONSIDERATIONS FOR ZnTPP FILMS.

Figure 6.1 presents the redox properties of the ground and excited states of ZnTPP and ZnTPPS⁻⁴ in solution. All the values recorded are based on the experimental values obtained here, except for the values of the reduction potentials, which were taken from tables 1.1 and 1.2. All these values are reported with respect to the NHE.

In order that semiconductors can be sensitized by dye molecules to produce photocurrents, excited electrons or "holes" from the dyes must be injected into the semiconductor. Charge transfer from dyes depends on the relative positions of the energies of the dye and semiconductor. The conduction band edge of the SnO₂ semiconductor lies between the ground and excited state of the ZnTPP as seen from figure 6.2. This figure presents the relative energy positions of ZnTPP and ZnTPP with different axial ligands. Also presented in the figure are the relative positions of the redox couples Fe(CN)₆^{3-/4-} and nitrophenol.

The thin porphyrin films on the SnO₂ semiconductor have been shown (97) to be p - type semiconductors with low carrier mobility. If a porphyrin film (whose Fermi level

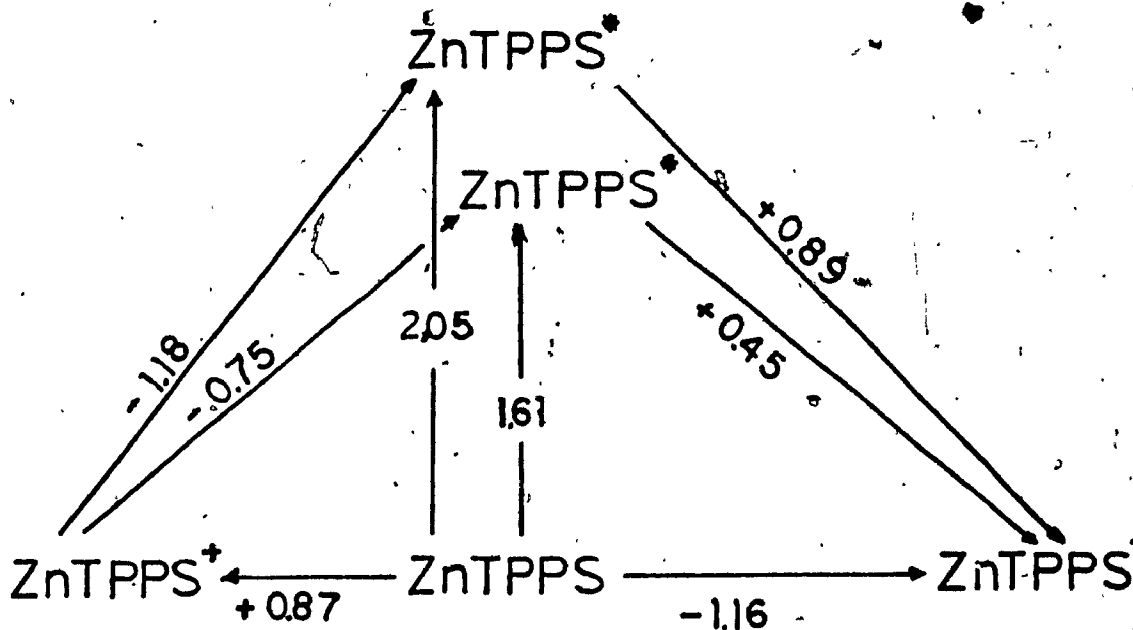
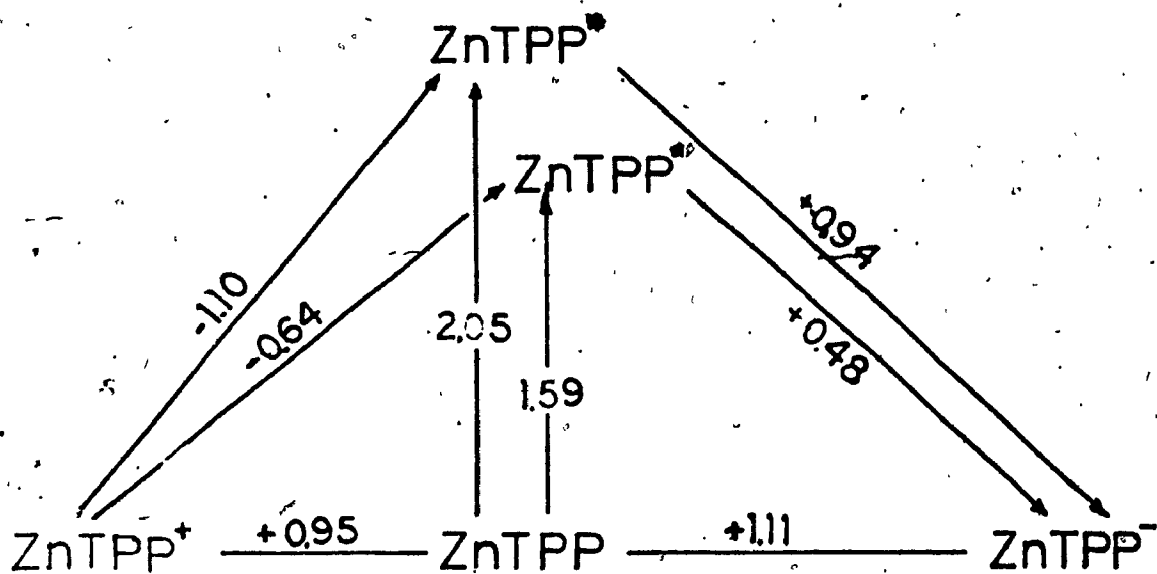


Figure 6.1. Latimer diagrams for ZnTPP and ZnTPPS

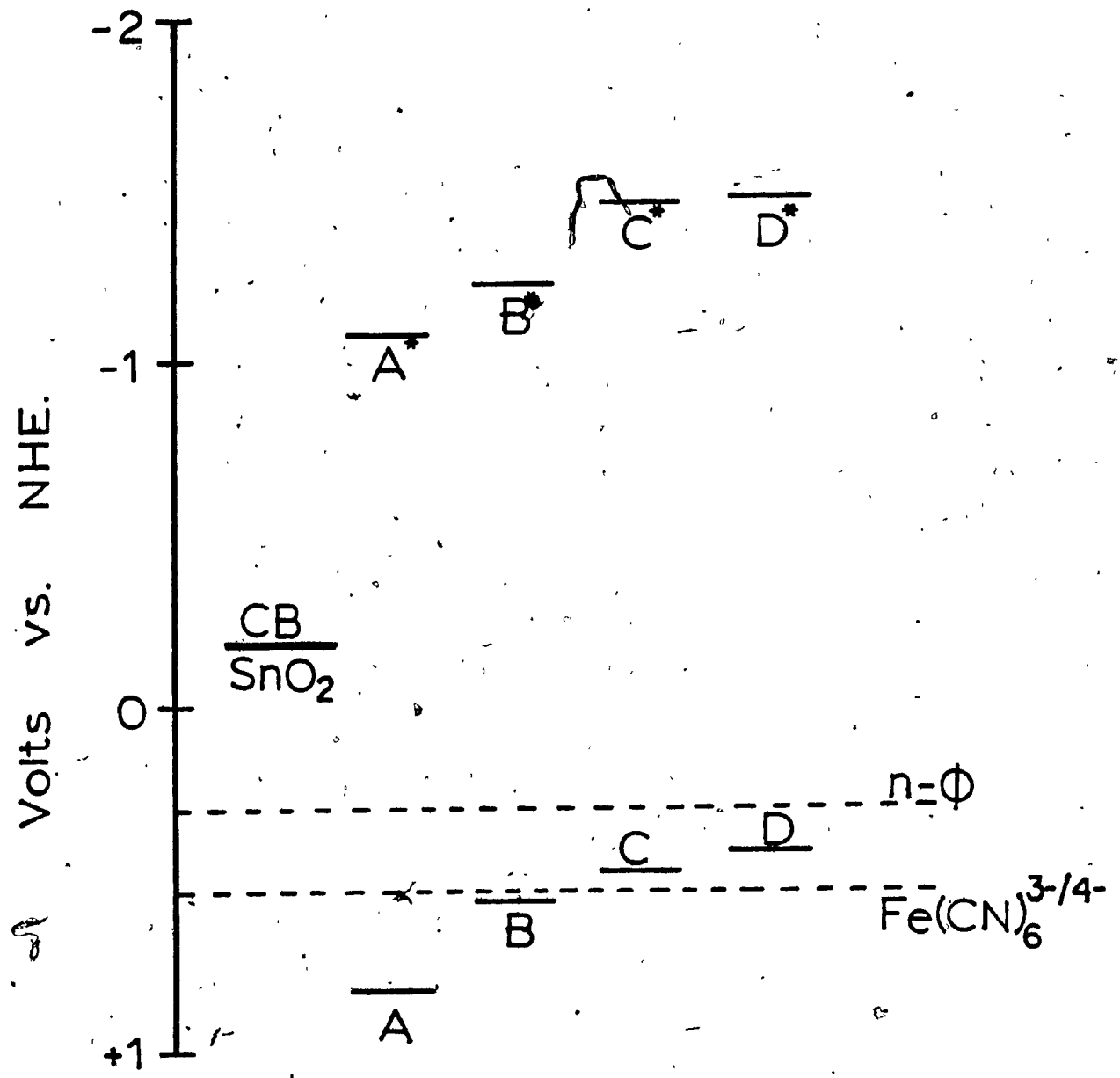


Figure 6.2. Energetics of ZnTPP and axially ligated ZnTPP with respect to the SnO₂ conduction band edge. (A) ZnTPP, (B) ZnTPP-pyridine (C) ZnTPP-triphenylarsine and (D) ZnTPP-PVP.

lies below that of the highly n-doped SnO_2) is brought into contact with the SnO_2 , the Fermi levels will be equilibrated by electron transfer from the SnO_2 to the porphyrin. On the other hand, if the porphyrin film is in contact with a redox couple (such as $\text{Fe}(\text{CN})_6^{3-/4-}$), a similar equilibration will take place between the redox level of the electrolyte and the porphyrin film. Judging from the relative positions of the SnO_2 level, the ZnTPP level and the $\text{Fe}(\text{CN})_6^{3-/4-}$ level in figure 6.2, the "bands" in the porphyrin film will bend upwards. This "band bending" was earlier used to explain the formation of blocking contacts between ZnTPP and ITO (125). The equilibrium (and therefore the relative band bending in the porphyrin film) will be with respect to the electrolyte in solution (131). Band bending for ZnTPP - Triphenylarsine and ZnTPP - PVP films will thus be downwards.

On irradiation of the films of ZnTPP and axially ligated ZnTPP on SnO_2 in contact with the redox couple, the photocurrents observed at short circuit indicate that the "undoped" films, the ZnTPP - pyridine and the ZnTPP - triphenylphosphine films give cathodic photocurrents. This suggests that electron transfer from the porphyrin excited states to the redox couple in solution took place. In this case reduction of photoproduced holes at the SnO_2 /porphyrin interface took place. The energetics of the redox ground and excited states in figure 6.1 suggests that the excited states of the porphyrin is energetic

enough (- 0.64 -- -1.10 V vs NHE) to allow electron transfer to the electrolyte. However, the porphyrin excited state is also energetic enough to act as an electron donor to the conduction band of SnO_2 . The factor which decides the eventual fate of the electron is determined by the potential barrier posed by either the SnO_2 /porphyrin interface or the porphyrin/electrolyte interface. Band bending seems to create a lower barrier at the porphyrin/electrolyte interface for the cases where a cathodic current is observed. The converse is true if anodic currents are observed, as in the case of ZnTPP - Triphenylarsine. Equilibration of the Fermi levels with the electrolyte seems important since the photocurrent direction can be switched from anodic to cathodic in the case of ZnTPP - PVP and ZnTPP - Triphenylarsine films by using nitrophenol, a couple whose redox potential is more cathodic than that of $\text{Fe}(\text{CN})_6^{3-/4-}$. In this case, the band bending occurring in the ZnTPP - Triphenylarsine and ZnTPP - PVP films will be upwards, creating conditions similar to those in the "undoped" ZnTPP films.

The charge transport mechanism within the films take place essentially by photo-generated holes via a "hopping" mechanism (97). Holes may be represented by the localized molecular notation ZnTPP^+ . This mechanism is supported by the indication in the visible spectra immediately after photoelectrochemistry of a significant steady state concentration of $\text{ZnTPP}(\text{X})^+$ (where X denotes a ligand) in the films (figures 3.13 - 3.15(b)). This steady state

concentration of $\text{ZnTPP}(X)^+$ decays back to $\text{ZnTPP}(X)$ after cessation of illumination in a matter of minutes.

Action spectra (figure 3.26) also suggest that the origin of the photocurrents is closely linked to the porphyrin excited states. No difference in photocurrent sign or magnitude was observed when either the porphyrin/electrolyte or SnO_2 /porphyrin interface was irradiated, indicating that the net photocurrent generation depends on the bulk properties of the film.

The magnitude of the photocurrent generated will depend on the efficiency of the transport process in the films and the transfer of the charge at the interfaces. The transport process in turn depends on the resistance of the film, the mobility of the charge and the lifetime of the excited carrier. Dark electrochemistry with the thin films (section 3.4.5) suggest that resistance is not a major problem for thin films. The limiting process in the thin films cannot be attributed to the resistance of the films. Photophysical data listed in table 5.2 suggest that the fluorescence of ZnTPP in solution is decreased on addition of axial ligands. The lifetime of the triplet state is increased by the addition of axial ligands. This effect is more pronounced in thin films of ZnTPP and ZnTPP -pyridine. The excited state lifetimes and the charge separation at the interfaces seems to be the factors controlling the magnitude of the photocurrent. The rate

constants k_e and k_0 for the reactions discussed in section 1.4.1 therefor become important. The effect of the lifetime of the excited porphyrin becomes even more important in the instances of thicker films. The dependence of the photocurrent on film thickness discussed in section 3.5.3 and illustrated in figure 3.27 shows that although pyridine "doped" films show high quantum yields at low film thickness, the yield decreases at larger thickness. This seems to indicate that pyridine in the ZnTPP film had increased the efficiency of charge separation at the interface, but that the lifetimes of the excited states are reduced and exciton transport to the interface is becoming limiting. The efficient formation of the $\text{ZnTPP}^+ - \text{pyridine}^-$ ion pair in solution (section 5.4) after flash photolysis seems to support high charge separation yields.

Dark electrochemistry on $\text{SnO}_2/\text{ZnTPP} - \text{pyridine}$ electrodes (section 3.4.3) also showed enhanced interfacial kinetics for the $\text{Fe}(\text{CN})_6^{3-/4-}$ couple at the ZnTPP - pyridine/electrolyte interface.

The linear slope of the photocurrent - film thickness curve for ZnTPP is typical for an organic molecule undergoing an exciton type transport mechanism (97, 135). In this instance, interfacial electron transfer might be limiting. The ZnTPP film seems to be the best for exciton transport and the ZnTPP - Pyridine film best for charge separation, but the ZnTPP - PVP film seems to combine the worst of both.

6.2. EFFECT OF STRUCTURE OF PENDANT-GROUP POLYMERS: THE ELECTROCHEMICAL AND PHOTOELECTROCHEMICAL CONSEQUENCES.

6.2.1. The role of the polymer.

The pyridine moieties of PVP acts as pendant groups to axially ligate dyes like ZnTPP and ZnTPPS-4. In this way, the favourable mechanical properties of the polymer can be exploited. It was however found that the simple model of pyridine axially ligated to the metal of the dye molecule is not entirely suitable to explain the photoelectrochemical effects observed in polymers. PVP - dye films succeed in increasing the chromophore concentration on the semiconductor, but the PVP film acts as an insulator and at large thickness charge transport throughout the film becomes the limiting factor. This limiting factor can be overcome by introducing an ionically conductive component in the polymer (see fig. 4.3(A)), whilst still retaining the PVP - component by a process of blending. The polymer blend, which was first reported by Anson (90), acts as a polyelectrolyte even when large concentrations of dye molecules are incorporated into films. This is clear from the results presented and discussed in section 4.4.1. This polymer blend also possess most of the essential properties which are required for the use of effective electrode coatings,

ie. strong irreversible binding to electrode surfaces, moderate ion exchange capacities for ions in the electrolyte solution, high retention for multicharged counterions for long periods in solutions which do not contain the counterions, good chemical and mechanical stability, and rapid charge propagation rates of counterions within the films. Most, if not all of these properties have been demonstrated in experiments discussed in Chapter 4.

6.2.2. Diffusion of counterions in the polymer.

The higher than normal diffusion coefficients for $\text{Fe}(\text{CN})_6^{3-/4-}$ observed by Anson (90) and in this work can be explained by the internal morphology of the films. Anson proposed distinct hydrophobic and hydrophylic domains in the copolymer which can be associated with the styrene groups and the quarternary ammonium groups (figure 4.3). It was found that the copolymer I is extremely hygroscopic and that the films swell tremendously on incorporation of solvated counterions. The formation of hydrophilic domains within the polymer, together with the large internal aqueous volume, contribute to the high diffusion coefficients observed. From table 4.1 it is observed that this charge propagation process is little perturbed by the presence of large organometallic chromophores, even if the chromophores themselves are anions such as ZnTPPS-4 . The incorporation of dye

molecules in the films (precast from solution) does decrease the anion concentrations in the films, indicating that there is competition between anionic dye molecules and $\text{Fe}(\text{CN})_6^{3-/4-}$.

6.2.3. Polymer band Structure; A Molecular - ion state approach.

The semiconductor band model described in section 1.4 is used successfully in explaining the behaviour of inorganic crystalline solids and even some organic crystals (97, 136). However, materials as complex as polymeric solids are difficult to fit into the context of the existing band model.

Duke et.al.(127) and Lewis (135) have set forth a model whereby polymer chain ordering, chain length and pendant groups can be taken into account in establishing the states which exist in a random copolymer consisting of crystallites interspersed with amorphous regions. This model, referred to here as the molecular - ion state approach, represents the different states in a polymer matrix as large distributions, each depending on a particular environment, and in most cases associated closely to the pendant groups of the polymer. These molecular - ion states are best represented in figure 6.3. For pendant polymers such as polystyrene or PVP, the positive and negative ion states of the molecules can be

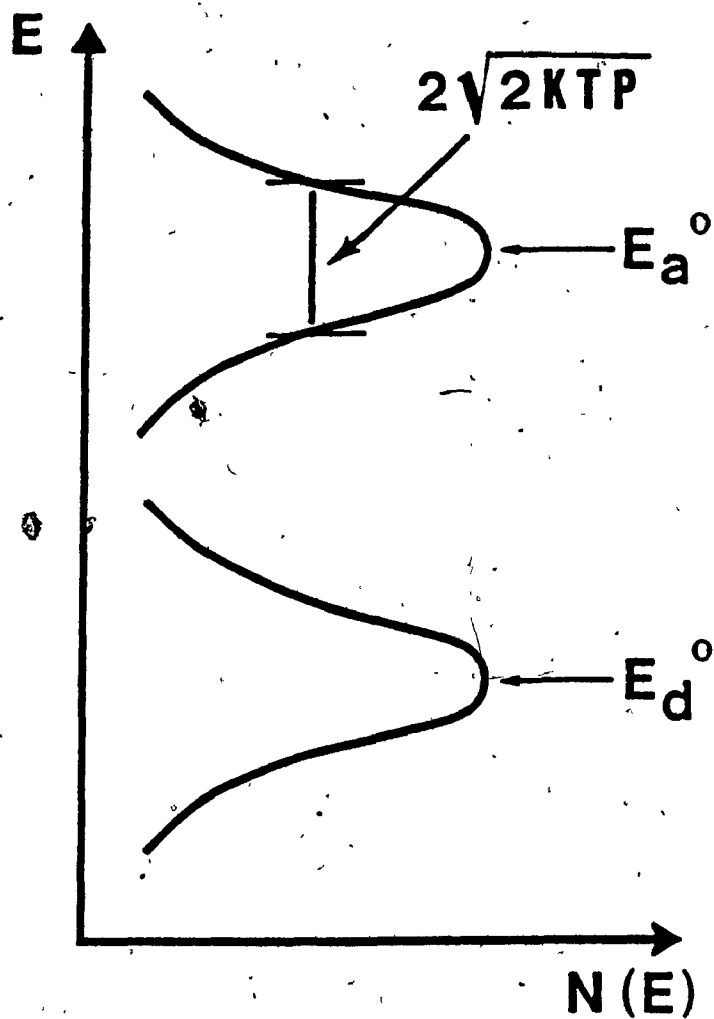


Figure 6.3. Energy distributions of the donor and acceptor states in pendant polymer groups. (from ref. 135.)

characterised by their ionization energy I_g and electron affinity A_g respectively. These energies will become modified in the solid by the induced polarization energies of the surrounding medium. The states E_A and E_D which are the acceptor and donor states respectively, will then have values of $-(A_g + P)$ and $-(I_g - P)$. P , the reorganization energy, will have components due to collective polarization of the surrounding medium and due to inner sphere interaction involving local bond changes. Duke (127) have determined the energy gap between E_A and E_D for PVP by photoemission spectroscopy to be 5.5 eV. Since this "bandgap" is so large, electron transitions do not occur between E_D and E_A of the same molecule, unless the energy input is equal to or larger than the energy of the bandgap. E_D and E_A states are discrete separate ion states which are coupled to the polarization fluctuations of the surrounding medium rather than being localized energy-band states associated with polymer macromolecules. Overlap of E_D and E_A can occur for some polymeric solids since the value of P can be very large (up to 3 eV) (135, 138), resulting in broadening of the Gaussian distributions in figure 6.3.

The values obtained for $N(E)$, E_A and E_D for the saturated backbone pendant - group polymers PVP and polystyrene can be used effectively in the copolymer blend to model the energetics of the polymer molecular - ion states which interact with those of the semiconductor, dye, and electrolyte. If the assumption is made that the electron

energies of the polar pendant groups of styrene and PVP do not change significantly (also shown by theoretical models to be the case (127, 138, 139)), then the other major factor involved i.e. the density of states, will depend on the concentration of the pendant groups in the polymer.

6.3. PHOTOELECTROCHEMICAL AND ELECTROCHEMICAL CONSIDERATIONS FOR DYE-POLYMER FILMS.

An evaluation of the electrochemical and photoelectrochemical properties of the dye - polymer films (chapter 4), the photophysical properties of the porphyrin dyes (chapter 5) and the molecular - ion model set forward in the previous section sets the stage for the mechanistic considerations presented in figure 6.4. The energetics of the semiconductor, the polymer, the dyes and the redox couple are presented with respect to the free electron energy.(eV) or the electrochemical potential.

The valence band and conduction band in the present case is that of n-SnO₂ at pH 7, although in principle any of energy levels of the other semiconductors used in the experiment can be used in a parallel analysis. The energy levels of the dyes are placed according to values obtained for the first oxidation process as well as the value of the flat band potential, the first excited singlet state (from fluorescence maxima) and the lowest lying excited triplet state (from table 1.3). The redox level of the

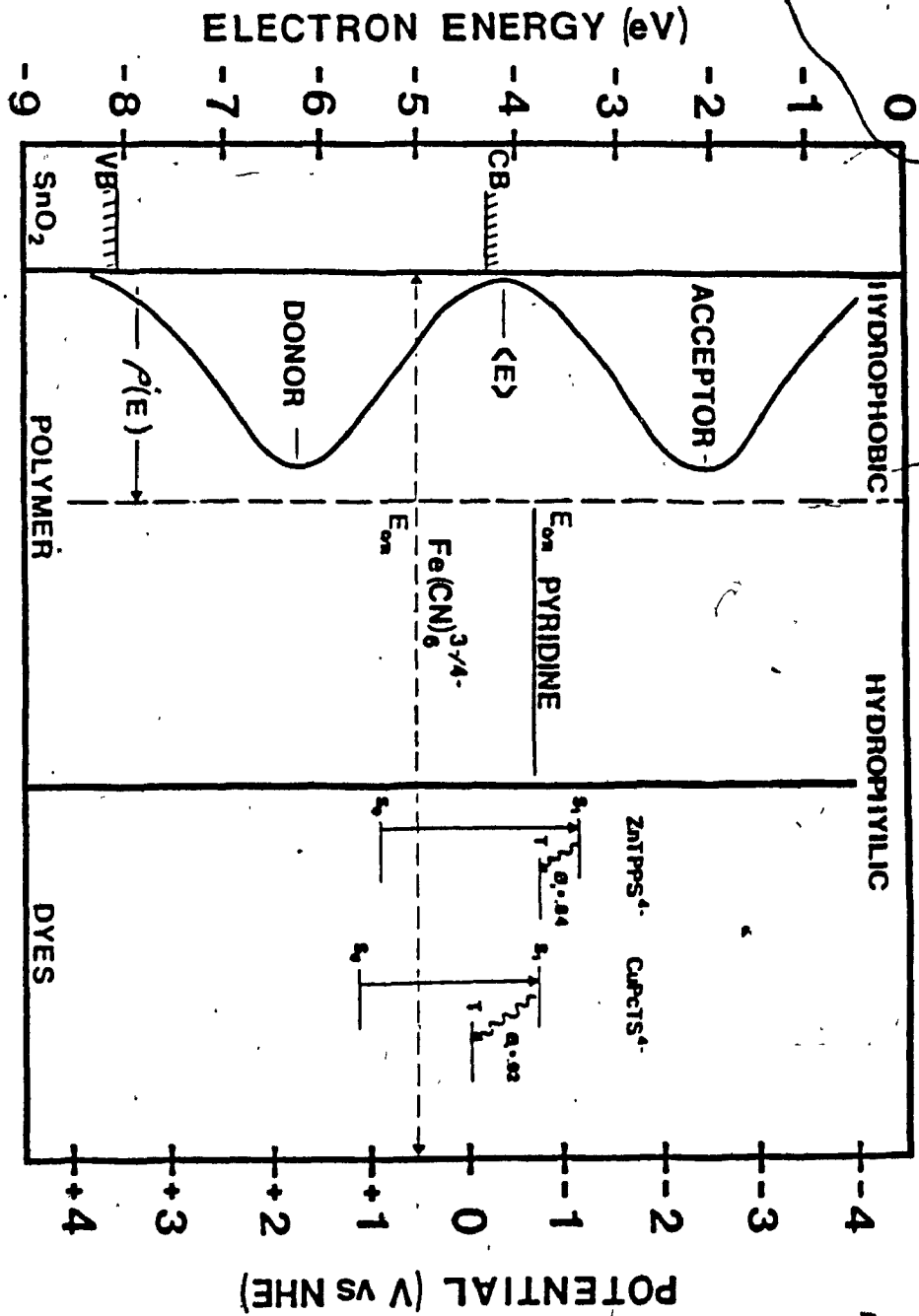


Figure 6.4. Relative positions of energy levels of chromophores with respect to the semiconductor and polymer levels. (From ref. 140.)

electrolyte used is that reported in table 3.6.

The molecular - ion states of the hydrophobic domain of the polymer blend used (ie. PVP - copolymer) were estimated from values obtained in references (127) and (138) and from known quantities of styrene and vinylpyridine in the copolymer. The energy level of the pyridinium groups are obtained from the voltammetric peak height as described in section 4.1.3.

The ZnTPPS-4 dye, which is axially ligated to the pyridine groups of PVP can also be electrostatically bound to the quaternary groups of the copolymer. It will then be reasonable to assume that a large number of the dye molecules find themselves at the interfaces of the hydrophilic and hydrophobic domains. Visual inspection of thick films showed distinctly segregated aggregations of dye within the otherwise homogeneous looking film. Anson has reported (90) that incorporation of $\text{Fe}(\text{CN})_6^{3-/4-}$ into these films induce the similar phenomena.

This property of the environment of the dye within the polymer is important since photoelectrochemical behaviour of films of ZnTPP and ZnTPPS-4 are totally different, although there are not large differences between their energetics and their photophysical properties. The only difference is that ZnTPP will tend to remain in the hydrophobic domain of the polymer blend.

To explain the photochemical behaviour of ZnTPP and ZnTPPS-4 in these films ie. the production of anodic photocurrents under irradiation in the presence of a redox

couple like $\text{Fe}(\text{CN})_6^{3-/4-}$, it is important for the longest living lowest lying excited state of the porphyrin to be at least more energetic than the pyridine acceptor levels, the molecular - ion acceptors and the conduction band of the semiconductor. Anodic photocurrents signifies an electron transfer from the redox couple in solution to the polymer - dye film at the polymer - porphyrin/solution interface and an electron transfer to the semiconductor at the semiconductor/polymer - porphyrin interface. Taking into account that the primary photoprocess which occurs is the excitation of the dye molecules in the polymer film, and that the photocurrent generation was directly linked to porphyrin excited states (section 4.5.3), it is conceivable that electron transfer from the redox couple takes place to the photogenerated cation radical of the porphyrin. The porphyrin excited state can decay to the long - lived triplet state after which it transfers an electron to the pyridine to which it is ligated. This process was described and supported by spectroscopy in section 5.4. The electron on the reduced pyridine can be trapped within the molecular - ion acceptor states of the polymer. The localized nature of the trap states encourages charge storage and a low effective mobility for charge transport. Efficient transport within the molecular ion acceptor states will only occur when sufficient traps have been filled to overcome the potential barrier for charge hopping from one state to the next (134, 135). From

figure 6.4, it can be seen that these molecular - ion acceptor states should be energetic enough to transfer negative charge to the conduction band of the semiconductor.

This charge trapping by the polymer, a phenomenon which has been analysed by Lewis (135) and Schmidlin (128) explains the photocurrent transients observed for the films on SnO₂ and ITO as seen in figure 4.17(a) and (b). The slow rise in photocurrent can be associated with the filling of molecular - ion traps in the polymer. The slow decay is associated with the emptying of these traps. This process is similar to one described by Seanor (136) for polymers such as polymethylene and polyacetylene where defects in the polymer chains lead to localized trap sites.

The relative density of states $N(E)$ also plays a significant role. A large enough hydrophobic domain is necessary for molecular - ion conduction. This is seen in figure 4.21, where at low film thickness (<1 μm) the photocurrent produced is low. Thin films will have low densities of states for the molecular - ions. A similar behaviour is observed for the ZnTPP - polymer films in figure 4.20.

The schematic presentation of figure 6.5 completes the circle of the origin of the anodic photocurrents observed for these films. Electroneutrality is maintained by a continuous in - and out - diffusion of the redox couple at the polymer - solution interface. Because of the high

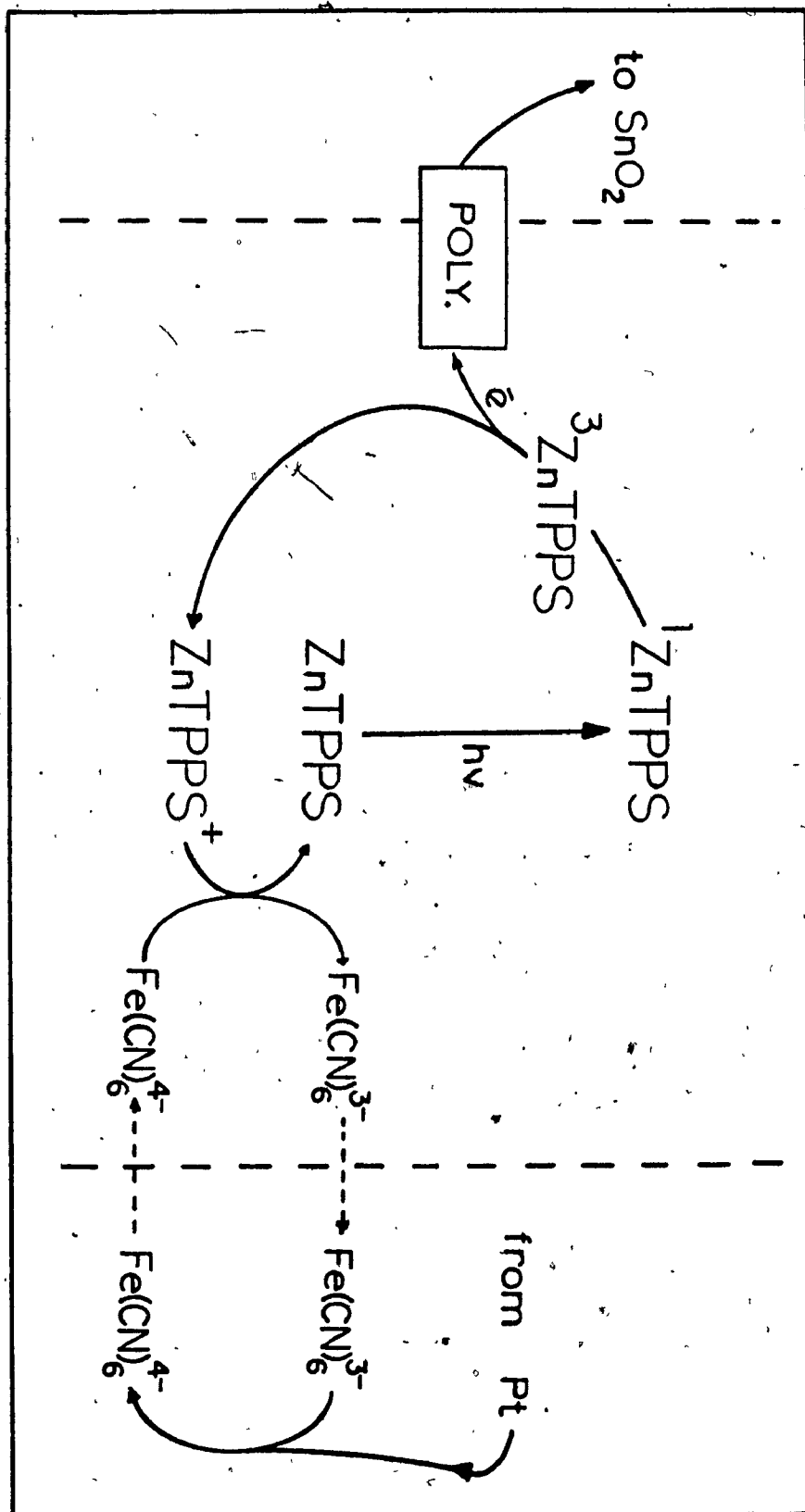


Figure 6.5. Schematic presentation of the reaction mechanism in the photoelectrochemical cell.

diffusion coefficients measured for $\text{Fe}(\text{CN})_6^{3-/4-}$ in these films, this latter process does not seem to be rate limiting.

Further evidence that the energetics of the dye dispersed in the polymer should have the appropriate energy to transfer an electron to the molecular - ion states is seen for the case of copper phthalocyanine (CuPcTS-4) (140). The excited singlet state is energetic enough but is short-lived. The excited triplet state lies below the energy state for the reduction of pyridine. Consequently very low photocurrents are observed which can be attributed to electron transfer from dye molecules adsorbed on the SnO_2 surface.

6.4. CATALYTIC EFFECTS OF PORPHYRIN FILMS ON DIFFERENT SEMICONDUCTING SURFACES.

The mechanistic consideration put forward for the porphyrin films in PVP - copolymer suggest that sensitization of the wide - bandgap semiconductors like SnO_2 , ITO and TiO_2 take place preferentially via an oxidative cycle. Photocurrent behaviour support this. In cases where both the thin porphyrin - polymer film and the semiconductor are excited, such as with CdS and CdSe electrodes (section 4.5.1), the currents are again anodic. These anodic currents were attributable to the n - type character of the semiconductor, so that we have a

situation where minority carriers from the semiconductor are injected into the film. The oxidizing power of the photoelectrodes in all cases are limited by the oxidizing power of the porphyrin in the film. The photoelectrodes tested for photocatalytic behaviour (SnO_2 , TiO_2 , CdS) shows that the intermediates observed during photolysis of a $\text{K}_3\text{Fe}(\text{CN})_6$ solution in 0.01 M NaOH are the same as those that are observed for the semiconductor powder catalysts tested and reported in the annex. This relationship shows that the processes occurring at macroelectrodes can in some instances be used to explain redox processes in microsystems.

CONCLUSIONS.

The general objectives of sensitization of wide bandgap semiconductors and a strategy for photocatalysis design have been attained to a certain degree. The simplistic approach of axial ligation has shown that the electrochemical and photoelectrochemical properties in the solid state are adversely affected. The redox properties of the ZnTPP is affected, and surface kinetics of a simple redox couple like $\text{Fe}(\text{CN})_6^{3-/4-}$ is increased on axial ligation. The solid state flat - band potentials are shifted and the excited state lifetime properties are changed. The fluorescence lifetimes are decreased and the triplet lifetimes are increased by axial ligation.

The study showed that thin film sensitization with porphyrin films will be inefficient since not enough sensitizer can be coated on the semiconductor without introducing other negative effects like film resistance. The alternative approach of sensitization by incorporating the porphyrin molecule in a suitable conductive polymer was much more successful.

The redox and photophysical properties of the porphyrin were not adversely changed by the polymer host at suitable loadings. Larger concentrations of sensitizer could be put on semiconductor surfaces without some of the limiting effects observed for the thin solid state films. The use of the conductive polymer enhanced the charge carrier

properties of the films.

The mechanisms for the photocatalytic behaviour of the films were elucidated for both the thin films and the polymer films. The proposed mechanism for the polymer films involving proper tuning of the dye, polymer, semiconductor and electrolyte levels could serve as a model for the design of better and more efficient photocatalysts.

Particulate photocatalysts based on the respective photoelectrodes have shown catalytic behaviour for complexed cyanide degradation and also degradation of other refractory waste (146) suggesting a direct relationship between the macro - and microsystems.

REFERENCES

1. M. Gratzel, (Ed.), "Energy Resources through Photochemistry and Catalysis", Academic Press, New York, 1983.
2. M. Schiavello, (Ed), "Photoelectrochemistry, Photocatalysis and Photoreactors", D. Reidel Pub. Company, 1985.
3. J.W. Buchler in D. Dolphin, (Ed). "The Porphyrins Vol. 1", Academic Press, New York, 1977, Chap. 10.
4. P. Hambright in K.M. Smith, (Ed), "Porphyrins and Metalloporphyrins", Elsevier, New York, 1976, Chap.6
5. H. Brockmann in D. Dolphin, (Ed), "The Porphyrins Vol. 2", Academic Press, New York, 1978, Chap. 9.
6. J.H. Fuhrhop in K.M. Smith (Ed), "Porphyrins and Metalloporphyrins", Elsevier, New York, 1976, Ch. 14.
7. D. Ostfield, M. Tsutsui, Acc. Chem. Res., 7, 52 (1974).
8. J. L. Hoard, Science, 174, 1295 (1971).
9. H. Bahar, P. Hambright, L. Wagner, J. Amer. Chem. Soc., 95, 5942 (1973).
10. W.R. Scheidt, M.E. Kastner, K. Hatano, Inorg. Chem., 17, 706 (1978).
11. H. Kobayashi, Y. Yanagawa, Bull. Chem. Soc. Jap., 45, 450 (1972).
12. B.R. James, D.V. Stynes, J. Amer. Chem. Soc., 94, 6225 (1972).

13. M.P. Gouterman in D. Dolphin (Ed), "The Porphyrins Vol. 3", Academic Press, New York, 1978, Chap. 1.
14. W.D. Edwards, M.C. Zerner, *Can. J. Chem.*, 63, 1763 (1985).
15. M.P. Gouterman, *J. Mol. Spectrosc.*, 6, 138 (1961).
16. J.R. Darwent, P. Douglas, A. Harriman, G. Porter, M. C. Richoux, *Coord. Chem. Rev.*, 44, 83 (1982).
17. A. Harriman, *J. Chem. Soc. Farraday Trans.*, 2, 72, 1281 (1981).
18. E. Amonyal, P. Keller, A. Moradpour, *Nouv. J. Chim.*, 2, 547 (1978).
19. J. Kiwi, M. Gratzel, *J. Amer. Chem. Soc.*, 101, 724 (1979).
20. J. Kiwi, M. Gratzel, *Nature (London)*, 281, 657 (1979).
21. M.P. Pileni, A.M. Braun, M. Gratzel, *Photo. Chem. Photobiol.*, 31, 423 (1980).
22. M. Nappa, J.S. Valentine, *J. Amer. Chem. Soc.*, 101, 5075, (1978).
23. F. Hopf, T.P. O'Brien, W.R. Scheidt, D. Whitten, *J. Am. Chem. Soc.*, 99, 277 (1975).
24. A. Antipas, J. Buchler, M. Gouterman, P. Smith, *J. Am. Chem. Soc.*, 102, 138 (1980).
25. K. Yamamoto, *Inorg. Chem. Acta.*, 113, 181 (1986).
26. C.K. Schauer, O.P. Anderson, S.S. Eaton, G.R. Eaton, *Inorg. Chem.*, 24, 4082 (1985).
27. S. Ariel, D. Dolphin, G. Domazetis, B. James, T.W.

- Leung, S.J. Rettig, *Can. J. Chem.*, 62, 755 (1984).
28. S.J. Cole, G.C. Curthoys, E.A. Magnusson, J.N. Phillips, *Inorg. Chem.*, 11, 1024 (1977).
 29. H. Callet, A. Graudeau, M. Gross, *J. Chem. Soc. Perkin II*, 1321 (1975).
 30. C.H. Langford, S. Seto, *Inorg. Chem. Acta*, 221 (1984).
 31. A.M. Crouch, C.H. Langford, *J. Electroanal. Chem.*, 221, 83 (1987).
 32. H. Kido, C.H. Langford, *J. Chem. Soc. Chem. Comm.*, 350 (1983).
 33. A. Harriman, M.C. Richoux, P. Neta, *J. Phys. Chem.*, 87, 4937 (1983).
 34. D.G. Davis in D. Dolphin (Ed), "The Porphyrins Vol. V", Academic Press, New York, 1978, 139.
 35. K.M. Kadish, L.R. Shine, R.K. Rhodes, L.A. Bottomley, *Inorg. Chem.*, 20, 1274 (1981).
 36. K.M. Kadish, R.K. Rhodes, *Inorg. Chem.*, 20, 2961 (1981).
 37. A. Wolberg, J. Manassen, *J. Am. Chem. Soc.* 92, 2982 (1970).
 38. H. Kabayashi, T. Hara, Y. Kaizu, *Bull. Chem. Soc. Jpn.*, 5, 2148 (1972).
 39. P. Gans, J.C. Marchon, C.A. Reed, J.R. Regnard, *Nouv. J. Chim.*, 5, 203 (1981).
 40. H. Levanoz, P. Neta, *Chem. Phys. Lett.*, 70, 100 (1980).
 41. N. Carnieri, A. Harriman, *Inorg. Chem. Acta.*, 62, 103, (1982).

42. J. Fajer, D. Borg, A. Forman, D. Dolphin, R.H. Felton, J. Am. Chem. Soc., 92, 3451 (1970).
43. J. Fuhrhop, D. Mauzerall, J. Amer. Chem. Soc., 91, 4174 (1969).
44. A. Forman, D.C. Borg, R.H. Felton, J. Fajer, J. Am. Chem. Soc., 93, 2790 (1971).
45. W.R. Browett, M.J. Stillman, Inorg. Chim. Acta., 49, 69 (1981).
46. C.E. Castro in D. Dolphin (Ed), "The Porphyrins Vol. V", Academic Press, New York, 1978, 2.
47. F. Basolo, R. Johnson, "Coordination Chemistry", Benjamin Inc., New York, 1964, 164.
48. D. Dolphin, D.J. Halko, E.C. Johnson, K. Rousseau in F.R.Longo (Ed), "Porphyrin Chemistry Advances", Ann Arbor Science, Mich., 1979, 119.
49. A.G. Padilla, S. Wu, H.J. Shine, J. Chem. Soc. Chem. Comm., 236 (1976).
50. L. El Kahef, M. El Meray, M. Gross, A. Giraudeau, J. Chem. Soc. Chem. Comm., 621 (1986).
51. H.J. Shine, A.G. Padilla, S. Wu, J. Org. Chem., 44, 4069 (1979).
52. K. Kalyanasundaran, M. Neumann - Spallart, J. Phys. Chem., 86, 5163 (1982).
53. F.R. Hopf, D.G. Whitten in D. Dolphin (Ed), "The Porphyrins VII", Academic Press, New York, 1978, 162.
54. A. Harriman in ref. 1., 163
55. A. Harriman, J. Chem. Soc. Faraday Trans. I, 76,

- 1978 (1980).
56. A. Harriman, J. Chem. Soc. Faraday Trans. I, 77, 369 (1981).
57. A. Harriman, J. Chem. Soc. Faraday Trans. 2, 77, 1281 (1981).
58. A. Harriman, G. Porter, P. Walters, J. Chem. Soc. Faraday Trans. I, 79, 1335 (1983).
59. D. Le Roux, J.C. Mialocq, O. Anitoff, G. Folcher, J. Chem. Soc. Faraday Trans. 2, 80, 909 (1984).
60. P.D. Wildes, D.G. Whitten, J. Am. Chem. Soc. 92, 7609 (1970).
61. D.G. Whitten, P.D. Wildes, C.A. de Rosier, J. Am. Chem. Soc., 94, 7811 (1972).
62. R.W. Murray, Acc. Chem. Res. 13, 135 (1980).
63. R.W. Murray in A.J. Bard (Ed), "Electroanalytical Chemistry Vol. 13", Marcel Dekker, New York, 1984, 191.
64. R.W. Murray, Ann. Rev. Mater. Sci., 14, 145 (1984).
65. G.H. Fricke, Anal. Chem., 52, 529R (1980).
66. C.E.D. Chidsey, R.W. Murray, Science, 231, 25 (1986).
67. A.F. Diaz, F.A. Rosales, J.R. Rosales, K.K. Kanazawa J. Electroanal. Chem., 103, 233 (1979)
68. J. Facci, R.W. Murray, J. Phys. Chem. 85, 2870 (1981).
69. D.C. Bookbinder, N.S. Lewis, M.G. Bradley, A.B. Bocarsley, M.S. Wrighton, J. Am. Chem. Soc., 101, 7721 (1979).

70. K.W. Willman, R.W. Murray, J. Electroanal. Chem., 133, 211 (1982).
71. A.H. Schroeder, F.B. Kaufman, V. Patel, E.M. Engler, J. Electroanal. Chem., 113, 193 (1980).
72. C.H. Langford, B.R. Hollebone, D. Nadezhdin, Can. J. Chem., 59, 652 (1981).
73. P. Ghosh, T.G. Spiro, J. Am. Chem. Soc., 102, 5543 (1980).
74. Y.S. Lipatov and L.M. Sergeeva, "Absorption on Polymers", Wiley, New York, 1974.
75. M. Okano, K. Itoh, A. Fujishima, J. Electrochem. Soc., 134, 837, (1987).
76. O. Niwa, T. Tamamura, J. Chem. Soc. Chem. Commun., 817 (1984).
77. T. Ohsaka, O. Takeyoshi, N. Oyama, J. Electroanal. Chem., 200, 159 (1986).
78. H.D. Abruna, P. Derisevich, M. Umana, T.J. Meyer, R.W. Murray, J. Am. Chem. Soc., 103, 1 (1981).
79. L. Faulkner, L.R. Majda, J. Electroanal. Chem., 137, 149 (1982).
80. J. Leddy, A.J. Bard, J. Electroanal. Chem., 114, 89 (1980).
81. S. Nakahama, R.W. Murray, J. Electroanal. Chem., 158, 323 (1983).
82. J.M. Calvert, T.J. Meyer, Inorg. Chem., 20, 27 (1981).
83. L.D. Margerum, T.J. Meyer, R.W. Murray, J. Phys.

- Chem., 90, 2696 (1986).
84. R. Shigehara, N. Oyama, F.C. Anson, J. Am. Chem. Soc., 103, 2552 (1981).
 85. A. Bettelheim, R.J.H. Chan, T. Kuwana, J. Electroanal. Chem., 110, 93 (1980).
 86. N. Oyama, F.C. Anson, J. Electrochem. Soc., 127, 247, (1980).
 87. N. Oyama, S. Yamaguchi, Y. Nishiki, K. Tokuda, H. Matsuda, F. Anson, J. Electroanal. Chem., 139, 371 (1982).
 88. H. Braun, F. Decker, K. Doblhofer, H. Sotobayashi, Ber. Bunsenges. Phys. Chem., 88, 345 (1984).
 89. D.D. Montgomery, K. Shigehara, E. Tsuchida, F.C. Anson, J. Am. Chem. Soc., 106, 7991 (1984).
 90. D.D. Montgomery, F.C. Anson, J. Am. Chem. Soc., 107, 3431 (1985).
 91. D.A. Buttry, F.C. Anson, J. Am. Chem. Soc., 105, 685 (1983).
 92. Y. Tsou, F.C. Anson, J. Phys. Chem., 89, 3818 (1985).
 93. B.J. Feldman, P. Burgmayer, R.W. Murray, J. Am. Chem. Soc., 107, 872 (1985).
 94. F.F. Fan, A.J. Bard, J. Electrochem. Soc., 133, 301 (1986).
 95. Y.W. Park, A.J. Heeger, M.A. Druy, A.G. MacDiarmid, J. Chem. Phys., 73, 946 (1980).
 96. S. Yanagida, A. Kabumoto, K. Mizumoto, C. Pac, K. Yoshino, J. Chem. Soc. Chem. Commun., 474 (1985).

97. J. Simon, J.J. Andre, "Molecular Semiconductors", Springer - Verlag, Berlin, 1985, 240.
98. D.A. Upson, D.J. Steklenski, US Patent No. 12690, (1980).
99. F.B. Kaufman, E.M. Engler, J. Am. Chem. Soc., 101, 547 (1979).
100. P. Daum, J.R. Lenhard, D.R. Rolison, R.W. Murray, J. Am. Chem. Soc., 102, 4649 (1980).
101. P.J. Pearce, A.J. Bard, J. Electroanal. Chem., 114, 89 (1980).
102. R.W. Murray, P.G. Pickup, C.R. Leidner, P. Derisevich, J. Electroanal. Chem., 164, 39 (1984).
103. H.S. White, J. Leddy, A.J. Bard, J. Am. Chem. Soc., 104, 4811 (1982).
104. H. Dahms, J. Phys. Chem., 72, 362 (1968).
105. C.G. Bazuin, A. Eisenberg, J. Chem. Ed., 58, 938 (1981)
106. A.J. Bard, L.R. Faulkner, "Electrochemical Methods, Fundamentals and Applications", J. Wiley & Sons, New York, 1980, 143.
107. C. Kittel, "Introduction to Solid State Physics", J. Wiley & Sons, New York, 1976, 210.
108. S. Chandra, "Photoelectrochemical Solar Cells Vol 5", Gordon and Breach Science Publ., New York, 1985, 21.
109. J.B. Goodenough in ref. 2, 3.
110. H. Gerisher in F. Cardon, W.P. Gomes, W. Dekeyser (Ed), "Photovoltaic and Photoelectrochemical Solar

Energy Conversion", Plenum Press, New York, 1981, 199.

111. H. Gerisher, J. Phys. Chem., 88, 6096 (1984).
112. A.J. Bard, J. Phys. Chem., 86, 172 (1982).
113. M.S. Wrighton, Pure & Appl. Chem., 57, 57 (1985).
114. M. Gratzel, A.J. Frank, J. Phys. Chem., 86, 2967 (1982).
115. R. Memming in ref. 109, 144.
116. R. Memming, F. Schroppel, Chem. Phys. Lett., 62, 207, (1979).
117. M. Gleria, R. Memming, Zeitschr. fur. Physikalische Chem., 98, 303 (1975).
118. W.R. Fawcett, A.S. Baranski, J. Electrochem. Soc., 27, 766 (1980).
119. A.S. Baranski, W.R. Fawcett, A.C. McDonald, R.M. de Nobriga, J. Electrochem. Soc., 128, 963 (1981).
120. T. Kuwana, N. Winograd in A.J. Bard (Ed), "Electroanalytical Chemistry Vol. 8", Marcel Dekker, New York, 1973.
121. R.S. Nicholson, I. Shain, Anal. Chem., 36, 706 (1964).
122. R.J. Klinger, J.K. Kochi, J. Phys. Chem., 85, 1731 (1981).
123. R.N. Adams, "Electrochemistry at Solid Electrodes", Marcel Dekker, New York, 1969, 219.
124. H. Gerisher in H. Eyring, D. Henderson and W. Josh (Eds), "Physical Chemistry, An Advanced Treatise, Vol. 9A", Academic Press, New York, 1970, 485.

125. Y. Yamashita, Y. Harima, Y. Matsumura, Bull. Chem. Soc. Jpn., 58, 1761 (1985).
126. H. Gerisher, J. Electroanal. Chem., 150, 553 (1983).
127. C.B. Duke, W.R. Salaneck, T.J. Fabish, J.J. Ritsko, H.R. Thomas, A. Paton, Physical Review B, 18, 57177 (1978).
128. F.W. Schmidlin, Physical Review B, 16, 2362 (1977).
129. H.D. Rubin, D.J. Arent, B.D. Humphrey, A.B. Bocarsly, J. Electrochem. Soc., 134, 93 (1987).
130. M.P. Irvine, R.J. Harrison, M.A. Strahand, G.S. Beddard, Ber. Bunsengesellschaft, 89, 226 (1985).
131. A.M. Crouch, D.K. Sharma, C.H. Langford, - Submitted for Publication, J. Chem. Soc. Chem. Comm., (1987).
132. G.S. Nahor, J. Rabani, J. Phys. Chem., 89, 2468 (1985).
133. S.U.M. Khan, J.O.M. Bockris, J. Phys. Chem., 89, 554 (1985).
134. H. Inokuchi, Y. Manyama in J. Mort and D.M. Pai (Eds), "Photoconductivity and Related Phenomena", -Elsevier, Amsterdam, 1976, 156.
135. T.J. Lewis, IEEE Trans. Elec. Ins., Vol. E 1 - E 21, 289 (1986).
136. D.A. Seanor, "Electrical Properties of Polymers", New York, 1982,
137. M. Ieda, IEEE Trans. Elec. Ins., E1-19, 289 (1984).
138. T.J. Fabish, C.B. Duke, J. Appl. Phys., 48, 4256 (1977).

139. H. Scher, E.W. Montroll, Physical Rev. B., 12, 2455
(1975)
140. I. Ordonez, A.M. Crouch, M.F. Lawrence, C.H.
Langford, Submitted for Publication, (1987).
141. V. Balzani, V. Carassity, "Photochemistry of
Coordination Compounds", Academic Press, New York,
1970.
142. S.N. Frank, A.J. Bard, J. Phys. Chem., 81, 1484
(1977).
143. S.N. Frank, A.J. Bard, J. Am. Chem. Soc., 99, 303
(1977).
144. N.M. Dimitrijevic, D. Savic, O.I. Miric, A.J. Nozik,
J. Phys. Chem., 88, 4278 (1984).
145. G. Hodes, M. Gratzel, Nouv. J. Chim., 8, 509 (1984).
146. C.H. Langford, M.K.S. Mak, A.M. Crouch, Canadian
Patent Application, 1986.

ANNEX

PHOTOCHEMICAL TREATMENT OF COMPLEXED CYANIDES BY PORPHYRIN-POLYMER COATED SEMICONDUCTING POWDERS.

The photoelectrochemical nature of photocatalytic and photoconversion reactions described in section 1.4.2 and the results of photoelectrochemistry at semiconductor electrodes discussed in chapters 3 - 5 forms the basis for the testing of the catalytic power of the porphyrin films in a micro photocatalytic environment.

The test solution chosen was the complex cyanide $K_3Fe(CN)_6$.

A.1. Monitoring of reaction and intermediate products.

The experiments were carried out as described in section 2.3.2. The reaction during photolysis of the catalyst - slurry was monitored in four ways.

- (i) By measuring the absorption at 300 nm for the disappearance of $K_3Fe(CN)_6$.
- (ii) Measuring the absorption at 578 nm for the appearance of CN^- as described in section 2.3.2.
- (iii) Monitoring the pH of the test solution.
- (iv) Qualitative detection of Fe (III) by thiocyanate.

A.2. Effect of irradiating complexed cyanide solutions in semiconductor slurries.

Figure 7.1 depicts the results of irradiating the naked TiO_2 and porphyrin - polymer coated TiO_2 and particles in $\text{K}_3\text{Fe}(\text{CN})_6$ for four hours. The compound $\text{K}_3\text{Fe}(\text{CN})_6$ is photoactive by itself (141), and a blank run figure 7.1 (a) containing no catalyst indicates that 75 - 80% of the original $\text{K}_3\text{Fe}(\text{CN})_6$ is still present after a period of four hours of irradiation. The end product of irradiation is a mixture of complexed cyanides of the type $[\text{Fe}(\text{CN})_5\text{H}_2\text{O}]^{2-}$ and $\text{Fe}(\text{OH})_3$.

This reaction has been described in Balzani and Garassiti (141).

Figure 7.1 (b - d) shows the degradation of $\text{K}_3\text{Fe}(\text{CN})_6$ in 0.1 M NaOH when the photocatalysts used were TiO_2 and coated TiO_2 . For the coated TiO_2 , both UV and visible irradiation was used. For TiO_2 , only UV - irradiation was used. It can be seen that the coated TiO_2 acts as a better catalyst than the naked TiO_2 . This is also true for all the other semiconductor particles tested. Table 7.1 lists the efficiencies of the different powders in terms of their t_{60} ie. the amount of cyanide degraded after 60 minutes. As is apparent from the table, the composite photocatalyst is significantly more effective than the corresponding base semiconductor. Two other semiconductors tested (not shown in the table) ie. CdTe and Fe_2O_3 do not

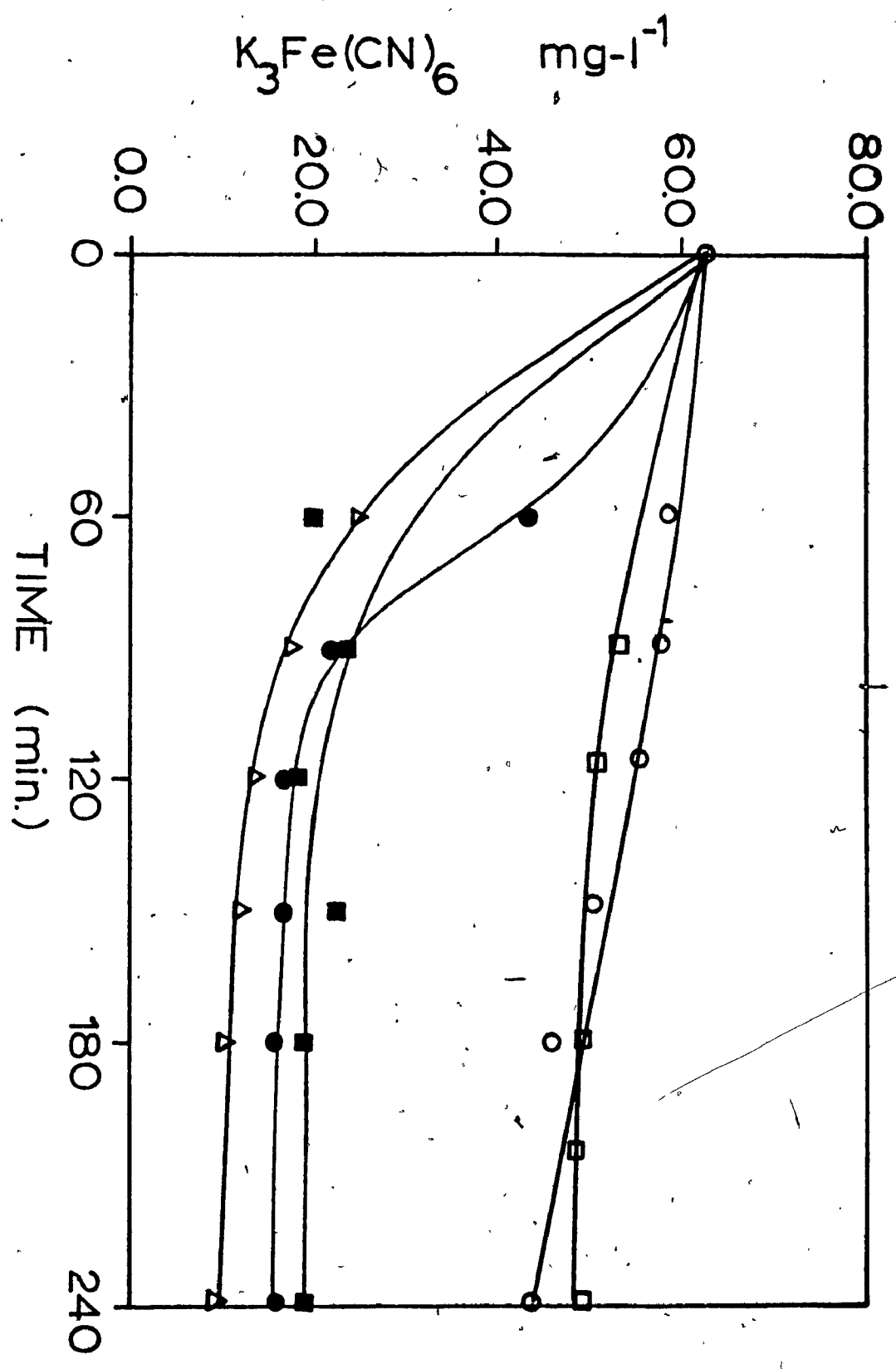


Figure 7.1. Decay of the ferricyanide concentration in the presence of different irradiated TiO_2 based catalysts. (O) No catalyst, (□) TiO_2/X dark control (●) TiO_2 , (■) TiO_2/X irradiated with hv 400nm and (Δ) TiO_2/X irradiated with UV and visible light. (X = ZnTPPS-PVP-copolymer.)

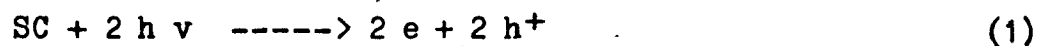
show significant degradation for ferricyanide, whether they are bare or coated.

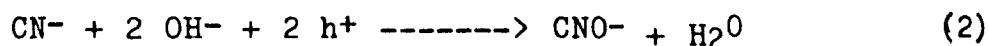
In all the above cases, dark controls show decreases of ferricyanide of between 5% and 8% after a four hour period. This can be attributed to the exchange of $\text{Fe}(\text{CN})_6^{3-}$ in the ion exchange polymer.

Photocatalysis was performed with test solutions at two pH values. Photocatalysis of the test solution $\text{K}_3\text{Fe}(\text{CN})_6$ in 0.1 M NaOH showed no appreciable changes in pH over the four hour period and minimal detectable free cyanide. In all cases tests for Fe(III) hydroxides were positive. Monitoring of small pH changes at pH 12 can be difficult due to adsorption on the pH electrode.

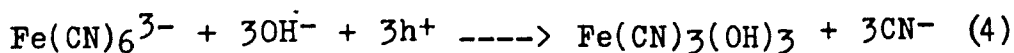
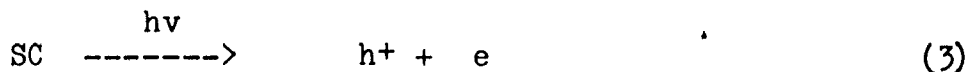
The test solution $\text{K}_3\text{Fe}(\text{CN})_6$ in 0.01 M NaOH show more appreciable pH changes. Free cyanide was also detected. Tables 7.2 - 7.7 summarize the results obtained for this test solution with different photocatalysts. In all cases, there is no quantitative relationship between the $\text{Fe}(\text{CN})_6^{3-}$ degradation, the free CN^- concentration and the pH changes. In all cases, Fe(III) is detected by thiocyanate. No attempt will be made here to try and elucidate the mechanism by persuance of detection of intermediates since the principle objective is to show the photocatalytic nature of the porphyrin polymer film.

Bard and Frank (142, 143) have proposed a mechanism for CN^- oxidation on semiconductor particles (SC).





Present experimental data suggest that a similar mechanism for $\text{Fe}(\text{CN})_6^{3-}$ oxidation can take place i.e.



Although free cyanide detected in our experiments is not quantitative, it is possible that reactions 2 and 4 take place simultaneously. The presence of mixed cyanide complexes in the irradiated solutions after a 24 hour period seems to suggest reaction 4.

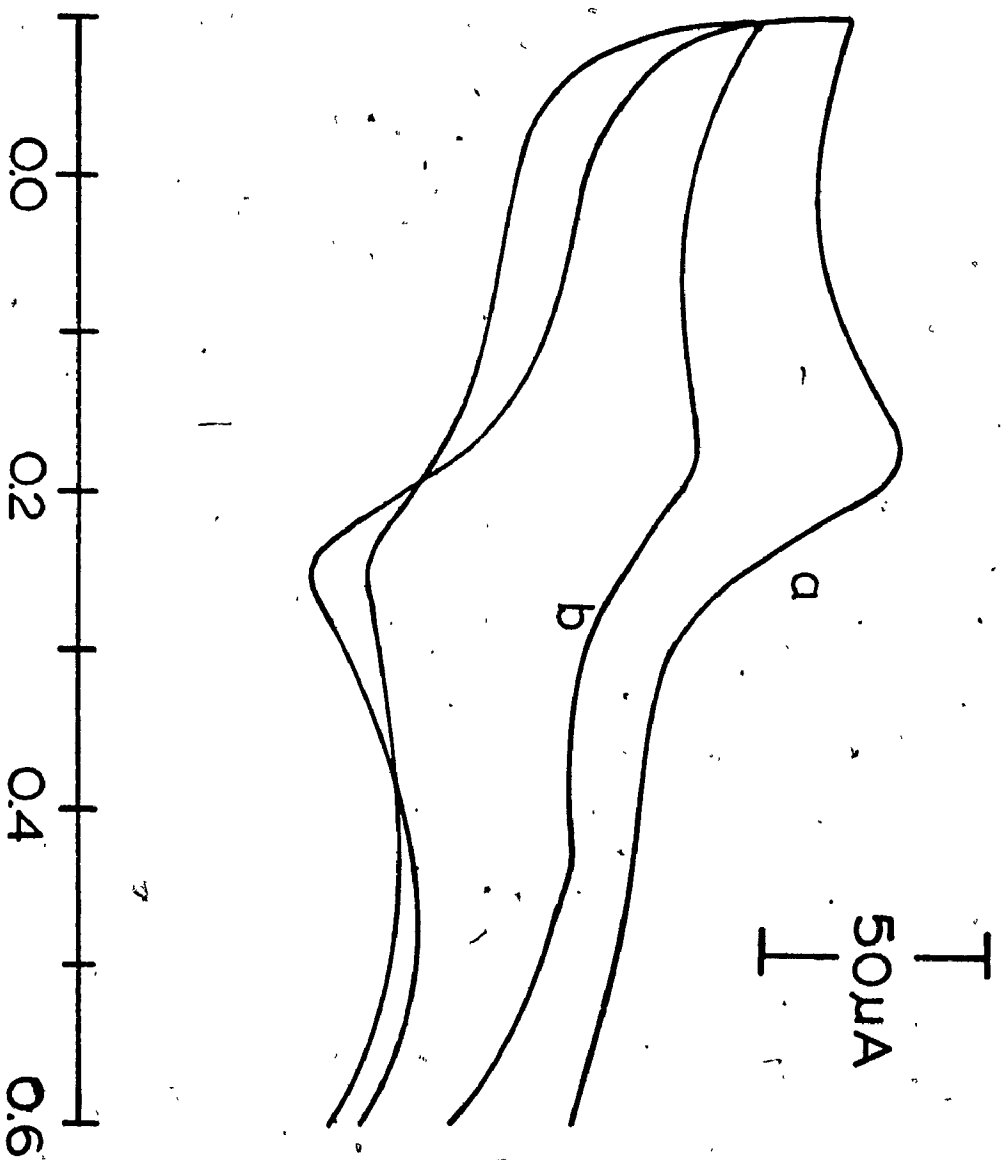
A photoelectrochemical experiment on the cell $\text{ITO/CdS} - \text{ZnTPPS-4} - \text{PVP} - \text{Polymer}/\text{K}_3\text{Fe}(\text{CN})_6$ (0.01 M NaOH / Pt (0.01 M KCl), followed by cyclic voltammetry suggest that the decrease in the $\text{Fe}(\text{CN})_6^{3-}$ voltammogram is followed by the appearance of a voltammetric peak at +0.7 V vs Ag/AgCl (figure 7.2) which would correspond to the formation of $\text{Fe}(\text{III})$ hydroxides. There are precedents in the literature (144, 145) that reactions at macroelectrodes can be extrapolated to microsystems as long as the particles are larger than the dimensions of the space charge layer (145).

An absorption spectrum of the changes in the $\text{K}_3\text{Fe}(\text{CN})_6$ spectrum is seen in figure 7.3 for the photocatalyst TiO_2 .

TABLE 7.1

EXTENT OF DEGRADATION OF FERRICYANIDE AFTER 60 MIN.

Photocatalyst	Ferricyanide remaining after 60 mins. irradiation. (ppm)
Base TiO ₂	58
Coated TiO ₂	37
Base CdS	43
Coated CdS	24
Base CdSe	50
Coated CdSe	31



V vs Ag/AgCl

Figure 7.2. Cyclic voltammograms of 2 mM $K_3Fe(CN)_6$ in 0.01 M NaOH before (a) and after (b) irradiation at a Cds/ZnTPPS-PVP-copolymer electrode.

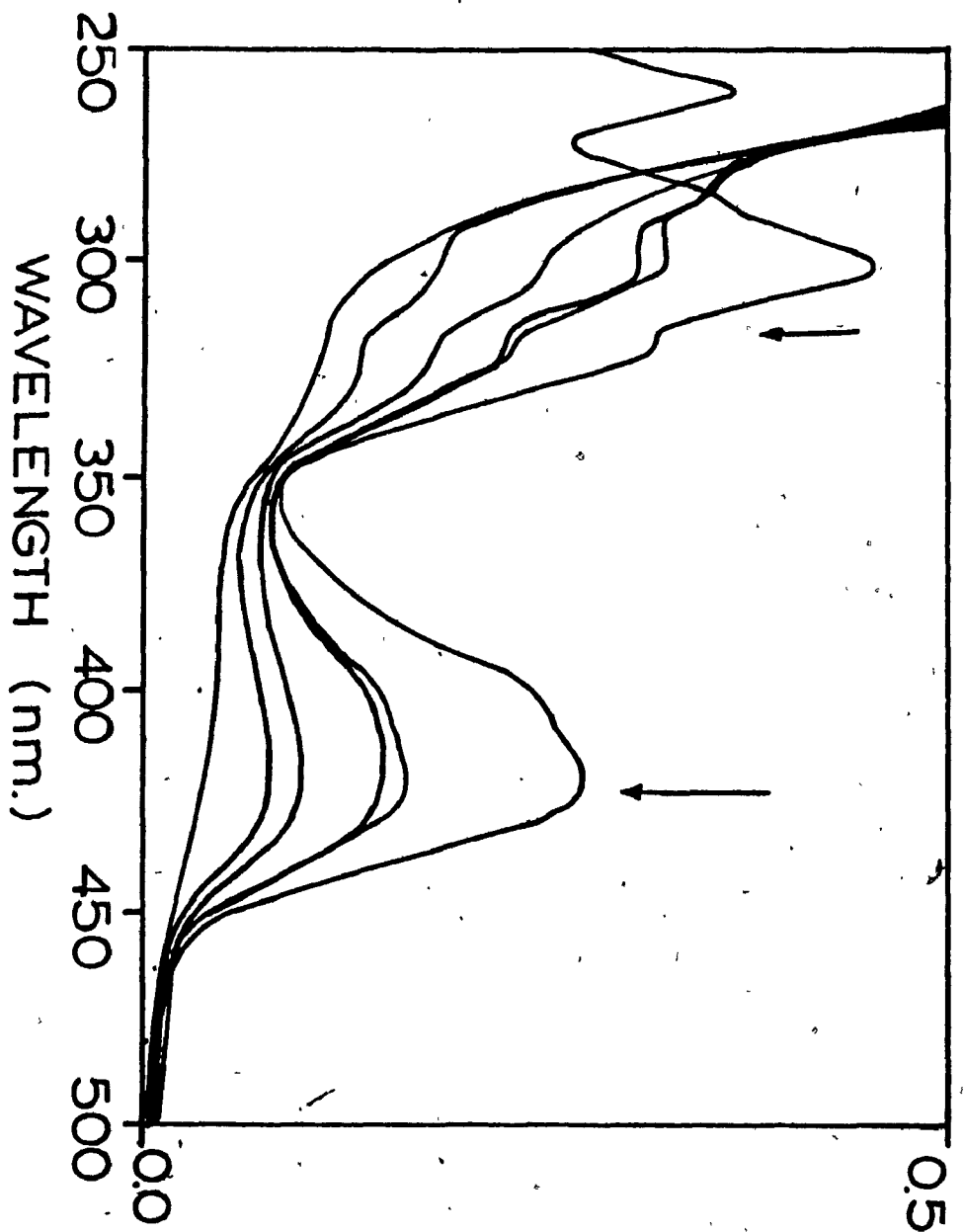


Figure 7.3. Absorption spectra showing the visible bands decreasing on irradiation. The solution is 95 ppm $K_3Fe(GW)_6$.

A.3. Photochemical treatment of other refractory waste.

The coated photocatalysts in table 7.1 have been shown to be effective for the degradation of PCB's (146) in organic - water media. A similar catalyst based on the ZnTPP - PVP film on TiO_2 was effective for the degradation of HCB in oil (146).

TABLE 7.2

Time min.	[K ₃ Fe(CN) ₆] ppm	pH	[CN ⁻] mg/l
0	95	11.3	0
30	65.7	11.07	0.54
60	61.2	10.88	1.4
90	49.6	10.78	2.78
120	39.6	10.73	4.59
150	27.4	10.68	6.55
270	35.8	10.67	23.72

Catalyst = 0.1 g TiO₂
 Electrolyte = 93 mg Ferricyanide in 0.01 M NaOH
 Irradiation = UV with IR cutoff (water filter)

TABLE 7.3

Time min.	[K ₃ Fe(CN) ₆] ppm	pH	[CN ⁻] mg/l
0	91.6	11.22	0
45	37.6	11.04	2.81
60	37.6	11	4.31
120	30.6	10.91	10.5
180	30.6	10.87	14.4
240	28.2	10.86	12.27

Catalyst = 0.12 g TiO₂/X
 Electrolyte = 93 mg Ferricyanide in 0.01 M NaOH
 Irradiation = UV with IR cutoff (water filter)

TABLE 7.4

Time min.	[K ₃ Fe(CN) ₆] ppm	pH	[CN ⁻] mg/l
0	99.6	11.41	0
30	80.4	11.09	4.21
60	79.2	11.01	3.65
90	73.6	10.94	1.56
150	75.8	10.89	6.18
180	73.4	10.91	7.08

Catalyst = 0.1122 g CdS
 Electrolyte = 93 mg Ferricyanide in 0.01 M NaOH
 Irradiation = UV with IR cutoff (water filter)

TABLE 7.5

Time min.	[K ₃ Fe(CN) ₆] ppm	pH	[CN ⁻] mg/l
0	96	11.44	0
30	60	11.09	9.64
60	56	10.94	12.25
120	48	10.8	10.09
180	46.2	10.73	18.34
240	46	10.7	22.43

Catalyst = .1303 g CdS/X.
 Electrolyte = 93 mg Ferricyanide in 0.01 M NaOH
 Irradiation = UV with IR cutoff (water filter)
 cutoff = 400nm

TABLE 7.6

Time min.	[K ₃ Fe(CN) ₆] ppm	pH	[CN ⁻] mg/l
0	100	10.66	0
30	79.8	10.73	2.69
60	75.8	10.82	2.64
150	70.2	10.85	1.59
180	67.8	10.87	2.49
240	46.0	10.7	2.3

Catalyst = .1102 g CdSe
 Electrolyte = 93 mg Ferricyanide in 0.01 M NaOH
 Irradiation = UV with IR cutoff (water filter)
 cutoff = 400nm

TABLE 7.7

Time min.	[K ₃ Fe(CN) ₆] ppm	pH	[CN ⁻] mg/l
0	100.2	11.43	0
40	65.0	11.07	1.09
60	55.8	10.96	1.56
120	38.0	10.82	1.89
180	28.0	10.84	2.57
240	56.0	10.83	2.9

Catalyst = .1412 g CdSe/X
 Electrolyte = 93 mg Ferricyanide in 0.01 M NaOH
 Irradiation = UV with IR cutoff (water filter)
 cutoff = 400nm